ORBITAL INTERACTIONS IN GROUP 6 IMIDO DIAMIDO COMPLEXES

By

ELON AYINDE ISON

A DISSERTATION PRESENTED TO THE GRADUATE SCHOOL
OF THE UNIVERSITY OF FLORIDA IN PARTIAL FULFILLMENT
OF THE REQUIREMENTS FOR THE DEGREE OF
DOCTOR OF PHILOSOPHY

UNIVERSITY OF FLORIDA

2004

Dedicated to my grandparents, John and Lucille McNeil.

ACKNOWLEDGMENTS

There are inevitably more people who have contributed to my experiences at the University of Florida than there is time or space to enumerate. However, I must acknowledge a few people without whom this work would not be possible. First and foremost, I must acknowledge my advisor, Dr. James Boncella, whose hands off but steady guidance was ideal in allowing me to learn and develop as an organometallic chemist.

The patience and guidance of two men, Dr. Khalil Abboud who performed all the crystallographic experiments, and Dr. Ion Ghiviriga for his help in NMR, cannot go unnoticed. In fact, this thesis would not be possible if not for their efforts, I must also acknowledge Dr. Adrian Roitberg and Dr. Stephen Fau, at the University of Florida QTP facility for the help with computational chemistry and for giving us access to their facilities.

I would be remiss if I did not acknowledge my past and "present" group members. In particular I would like to, acknowledge Alison Knefely, the last of the Boncella clan at the University of Florida. In the short time we worked together, she surely provided a pleasant working environment. She is a great lab-mate and friend, even though she is frequently on the wrong side of political issues. Her friendship and personality have surely been missed.

Finally, I would like to thank my family. My parents Patsy, and Walter, have been supportive throughout this entire experience. My work ethic and values are almost totally

attributable to their parenting. I would also like to acknowledge my little sister Aysha. I would not have made it through this experience if it were not for my wife Ana. In fact, if it were not for her I would literally never have figured out this template. She has been an absolute "rock" throughout this entire experience and most importantly has remained my best friend. There have been times throughout this experience when I thought that the struggle was not worth it. It was at these times that my daughter Mya has helped me "keep it in perspective."

TABLE OF CONTENTS

page

ACKNOWLEDGMENTS iii

LIST OF TABLES viii

LIST OF FIGURES ix

ABSTRACT xii

CHAPTER

1 INTRODUCTION AND BACKGROUND 1

Theoretical Calculations and Methodology 3
ONIOM Calculations 4
Organoimido Chemistry and the Concept of π Loading 5
Bonding in π Loaded Imido Complexes 6
Early Examples of π loaded complexes. 9
Group 6 Imido Diamido Complexes 10
Molybdenum and Tungsten Alkyl and Alkylidene Complexes 12
Complexes of Mo and W Imido Diamido Complexes Containing π donor Ligands 16
Scope of the Dissertation 18

2 STRUCTURE REACTIVITY AND BONDING OF MOLYBDENUM IMIDO DIAMIDO COMPLEXES 20

Introduction 20
Structure Dynamics and Bonding of Imido Diamido Alkyne Complexes 21
Summary 33
Dynamics and Bonding of Molybdenum Imido Diamido Olefin Complexes 33
Diamide Ligand Folding in d^2 vs d^0 Group 6 Imido Complexes 39
Conclusions 44

3 SYNTHESIS AND REACTIVITY OF GROUP 6 IMIDO DIAMIDO METALLACYCLES 45

Introduction 45

Synthesis and Reactivity of Mo Imido Diamido Metallacyclopentenes and Metallacyclopentadienes....46
Synthesis of metallacyclopentene complexes....47
Kinetics and Mechanism of the Thermal Rerrangement of **25**....51
Computational Studies on the Thermal Rearrangement of **25**....55
Synthesis and reactivity of a metallacyclopentadiene complex....65
Summary and Conclusions....68

4 SYNTHESIS AND REACTIVITY OF Mo(VI) COMPLEXES WITH ALKYL AND ARYL ISOCYANIDES....70

Introduction....70
Synthesis of Isocyanide Complexes and Insertion into the Metal-Diamide Bond....70
Synthesis, Structure and Dynamics of a Chelating Imino Carbamoyl Complex....83
[2+2+1] Cycloaddition reactions of metallacycles with alkyl isocyanides RNC....89
Summary and Conclusions....91

5 ALKYL ALUMINUM INDUCED DIAMIDE TRANSFER FROM GROUP 6 IMIDO DIAMIDO COMPLEXES....92

Introduction....92
Reactions of Mo Dialkyl Complexes with Trimethyl Aluminum (TMA)....93
Reactivity of Alkyl Aluminum Halides with Group 6 Imido Diamido Olefin Complexes....98
Reaction of metallacyclopentanes with alkyl aluminum halides....100
Reactivity of alkyl aluminum reagents with styrene complexes....104
Reactivity with alkyl aluminum halides....108
Reactivity of an isobutylene complex with $EtAlCl_2$....109
Summary....114
Implications of Aluminum Induced Diamide Transfer to Olefin Dimerization Catalysis....114
Reactions of W complexes with alkyl aluminum reagents....116
Diamide transfer to other W complexes....117
Conclusions....119

6 EXPERIMENTAL....121

General Methods....121
Synthesis of η^2–alkyne complexes....121
Synthesis of *bis*-Isocyanide Complexes....126
Synthesis of a Chelating Imino Carbamoyl Complex, **(33)**....127
Reactions with alkyl aluminum reagents....128
Synthesis of $[(\eta^2\text{-ethylene})(Et)Mo(NPh)\eta^4\text{-}(o\text{-}(SiMe_3N)_2C_6H_4)Al(CH_3)_2]$, **(42b)**....130
Synthesis of $[(\eta^2\text{-styrene})(Me)Mo(NPh)\eta^4\text{-}(o\text{-}(SiMe_3N)_2C_6H_4))Al(CH_3)_2]$, **(39)**....131
Synthesis of $[(\eta^2\text{-styrene})(Me)Mo(NPh)\eta^4\text{-}(o\text{-}(SiMe_3N)_2C_6H_4)\}Al(Cl)_2]$, **(40)**....131
Synthesis of $[(\mu^2\ NPh)Mo(Cl)(\eta^4\text{-}(Cl_2Al((o\text{-}(Me_3SiN)_2\text{-}C_6H_4))]_2$, **(41)**....133
Kinetic Study....134

Computational Studies. 135
X-ray Experimental 137
X-ray Experimental for Complex **26b** 137
X-ray Experimental for Complex **29** 140
X-ray Experimental for Complex **25** 142
X-ray Experimental for Complex **30b** 144
X-ray Experimental for Complex **33** 146
X-ray Experimental for Complex **34** 148
X-ray Experimental for Complex **36** 150
X-ray Experimental for Complex **41** 152

LIST OF REFERENCES 155

BIOGRAPHICAL SKETCH 163

LIST OF TABLES

Tables page

2-1 ^{1}H and ^{13}C NMR data for alkyne complexes 22

2-2 Comparison of selected bond lengths and angles between model compounds **22** and **23** and the reported crystal structure for **21f**[b] 27

2-3 NLMO analysis of alkyne π bond 31

2-4 NBO analysis of Mo—N(imido) bonds 31

2-5 NBO analysis of the Mo—N(Imido) bond in **20c** 39

2-6 Fold angles for some Mo Imido Diamido Complexes 40

2-7 NLMO analysis of Mo—N(Imido) and Mo—N(Diamide) bonds in **23** and **24** 43

3-1 Dependence of DEAD on the formation of **26c** 54

3-2 Selected bond lengths (Å) and angles (^{0}) for ONIOM optimized structures for the thermal rearrangement of **25** 60

4-1 Selected bond Lengths(Å) and Angles(^{0}) for **31** and **32** 78

6-1 Kinetic analysis for the reaction of DEAD with **25** 135

6-2 Crystal data and structure refinement for **26b** 139

6-3 Crystal data and structure refinement for **29** 141

6-4 Crystal data and structure refinement for **29** 143

6-5 Crystal data and structure refinement for **30b** 145

6-6 Crystal data and structure refinement for **33** 147

6-7 Crystal data and structure refinement for **34** 149

6-8 Crystal data and structure refinement for **36** 151

LIST OF FIGURES

Figures page

1-1 The ONIOM extrapolation scheme 4

1-2 Limiting VB description of a metal – imido linkage 7

1-3 Π perpendicular set of N(p) orbitals in threefold symmetry 10

2-1 Thermal ellipsoid plot of **21e**. 24

2-2 Variable temperature ^{1}H NMR spectrum of the $SiMe_3$ region for **21b** 25

2-3 B3LYP optimized models for alkyne complexes **22** and **23** and their transition states 27

2-4 Bonding interactions in between Mo, imido, and the alkyne fragment 30

2-5 NLMO plots (isocontour 0.04) of Mo—N(imido) bond in **22** and **TS 22** 32

2-6 Optimized ONIOM structures for **20c** 37

2-7 HOMO of **23** and **20c** showing π backbonding of the metal fragment to the olefin in **23** or acetylene in **20c** 37

2-8 HOMO of **TS23** and **TS20c** showing π backbonding of the metal fragment to the olefin. 38

2-9 Occupied molecular orbitals of **24** 43

3-1 Thermal ellipsoid plot of **26b** 52

3-2 First order kinetics for the formation of **26c** 54

3-3 Eyring plot for the reaction of **25** with DEAD 55

3-4 Thermal ellipsoid plot of **25** 56

3-5 Optimized structures (mPW1K/LANL2DZ) for the thermal rearrangement of **25** ..58

3-6 Reaction profile ΔG^{0}_{298} (K) for the thermal rearrangement of **25** at the mPW1k/SDD-Aug-cc-pVDZ level of theory 58

3-7 ONIOM (mPW1K/LANL2DZ:mPW1K/LANL2MB) optimized structures for the thermal rearrangement of **25** 59

3-8 Occupied molecular orbitals(B3LYP/LANL2DZ) for **25** 62

3-9 Occupied molecular orbitals (B3LYP/LANL2DZ) for **25b** 63

3-10 Occupied molecular orbitals (B3LYP/LANL2DZ) for **25c** 63

3-11 Thermal ellipsoid plot of **29**. 67

4-1 Thermal ellipsoid plot of **30b** (30% ellipsoids) 74

4-2 Thermal ellipsoid plot of **31** 76

4-3 Optimized structure (ONIOM B3LYP/LANL2DZ:B3LYP/LANL2MB) for **31** and **32** 79

4-4 3-Center-4-electron bonding between the diamide lone pair electrons the metal d orbitals and the π* orbitals of a π acceptor ligand 79

4-5 Interaction of diamide lone pairs and isocyanide ligand with metal d_{xy} orbital. 81

4-6 Interaction of diamide lone pairs and CO ligand with metal d_{xy} orbital. 81

4-7 Thermal ellipsoid plot of **33** 85

4-8 Space filling diagram generated from the crystal structure of **33** 87

4-9 Variable temperature ^{1}H NMR spectrum (C_7D_8) of **33** 88

5-1 Thermal ellipsoid plot of **34** 95

5-2 Thermal ellipsoid plot of **36**. 96

5-3 Optimized B3LYP structures for model complexes $Me_2Al((o\text{-}(Me_3N)_2\text{-pda})^{-1}$, **37,** and $(CH_2)_4Mo(CH_3)(NH)(o\text{-}(Me_3N)_2C_6H_4)Al(CH_3)_2$, **38** and their molecular orbitals. 98

5-4 ^{1}H NMR spectrum of **42a**, (η^2-ethylene)Mo(Me)(NPh) η^4-($Cl_2Al((o\text{-}(Me_3SiN)_2\text{-}C_6H_4))$ in C_6D_6. 102

5-5 Proposed structure for **42b** showing selected carbon and (parentheses) and proton chemical shifts assigned by NMR spectroscopy....102

5-6 X-ray structure determination of **39a** 105

5-7 Proposed structure for **39a** showing selected carbon and (parentheses) and proton chemical shifts assigned by NMR spectroscopy....107

5-8 ^{1}H NOESY spectrum of **39a** 107

5-9 Proposed structure for **39b** showing selected carbon and (parentheses) and proton chemical shifts as assigned by NMR spectroscopy. 108

5-10 ^{1}H NOESY spectrum of **39b** 108

5-11 Thermal ellipsoid plot of **41**. 112

5-12 ^{1}H NMR spectrum of W metallacyclopentane methyl complex 117

5-13 ^{1}H NMR spectrum for the reaction of **12**, with TMA 120

Abstract of Dissertation Presented to the Graduate School
of the University of Florida in Partial Fulfillment of the
Requirements for the Degree of Doctor of Philosophy

ORBITAL INTERACTIONS IN GROUP 6 IMIDO DIAMIDO COMPLEXES

By

Elon Ayinde Ison

August 2004

Chair: James M. Boncella
Major Department: Chemistry

The orbital interactions of group 6 imido diamido complexes have been investigated. The synthesis of alkyne complexes, **21**, (η^2-alkyne)Mo(NPh)(*o*-($Me_3SiN)_2C_6H_4$) by the reaction of alkynes with **20a**, (η^2-isobutylene)Mo(NPh)(*o*-($Me_3SiN)_2C_6H_4$), has been reported, along with the X-ray crystal structure of **21e**, and the dynamic solution behavior of these complexes via low temperature. DFT calculations have been used to study the bonding in these complexes and an NBO analysis was used to determine the extent of π donation by the alkyne ligand. DFT calculations were also performed on **20c** and **24**.

The synthesis of metallacyclopentene complexes, **26**, [(NPh)Mo(C(R)C(R)CH_2CH_2)(*o*-$(Me_3SiN)_2C_6H_4$)], by the sequential π ligand exchange of ethylene from **25** and an alkyne is reported. An X-ray structure of the metallcyclopentene complex **26b**, [(NPh)Mo(C(H)C(Ph)CH_2CH_2){*o*-$(Me_3SiN)_2C_6H_4$}], is reported. The synthesis of the metallacyclopentadiene complex

[(NPh)Mo(C(Ph)CHC(Ph)){o-$(Me_3SiN)_2C_6H_4$}], **29**, a by the [2+2] cycloaddition reactions of two alkynes is reported. The thermal rearrangements of **25**, was examined by kinetics and DFT.

The synthesis and characterization of *bis*-isocyanide complexes, $(RNC)_2Mo(NPh)$(*o*-$(Me_3SiN)_2C_6H_4$), **30** of Mo and the subsequent reactivity of these complexes with excess isocyanide yielding *tris*-isocyanide complexes in the case of ^tBuNC and an unusual chelating iminocarbamoyl *bis*-isocyanide complex in the case of 2,6 – dimethyl phenyl isocyanide are reported. X-ray structures of the *bis*-isocyanide complex **30a** and the iminocarbamoyl *bis*-isocyanide complex are also reported.

The reactivity of alkyl aluminum reagents with alkyl, olefin and alkynes has been demonstrated. Treatment of an orange solution of Mo(NPh)(*o*-$(Me_3SiN)_2C_6H_4)(CH_2)_4$, **25**, in toluene, with 1 equivalent of trimethyl aluminum (TMA) yields the metallacyclopentane methyl complex, $(CH_2)_4Mo(NPh)$-η^4-[(*o*-$(SiMe_3N)_2C_6H_4)$}$Al(CH_3)_2$, **34**. A similar reaction occurs when an orange solution of the diphenyl acetylene complex, **35,** is treated with 1 equivalent of TMA and yields the diphenyl acetylene methyl complex, (η^2-diphenyl acetylene)$(CH_3)Mo(NPh)\eta^4$-[(*o*$(SiMe_3N)_2C_6H_4)$}$Al(CH_3)_2$ **36**. The metallacyclopentane complex **25**, reacts with alkyl aluminum halides to yield the olefin alkyl complexes (η^2-ethylene)(R)$Mo(NPh)\eta^4$-[(*o*-$(SiMe_3N)_2C_6H_4)$}$Al(CH_3)_2$, **42**.

The reaction of the styrene complex **20c**, with ethyl aluminum dichloride or trimethyl aluminum results in the formation of complexes **39**, (η^2-styrene)$Mo(Et)(NPh)\eta^4$-(Cl_2Al((*o*-$(Me_3SiN)_2$-$C_6H_4)$) or **40**,(η^2-styrene)$Mo(CH_3)(NPh)\eta^4$-(($(CH_3)_2Al$((*o*-$(Me_3SiN)_2$-$C_6H_4)$)), respectively. In contrast, the

reaction of ethyl aluminum dichloride with **20a**, results in the the displacement of isobutylene and the formation of the briging imido dimer $[(\mu^2\ NPh)Mo(Cl)(\eta^4\text{-}(Cl_2Al((o\text{-}(Me_3SiN)_2\text{-}C_6H_4))]_2$, **41**. The X-ray crystal structure of **41** was determined.

CHAPTER 1
INTRODUCTION AND BACKGROUND

The transition metal series of the periodic table enables chemists to have access to a wide variety of compounds and chemical reactions that are otherwise inaccessible in main-group chemistry. Thus, a tremendous amount of research has been devoted to the development of new and interesting organometallic complexes with an emphasis on the understanding of the structure, bonding and reactivity of the transition metal species. These efforts were devoted to the synthesis and structural characterization of new organometallic complexes that are supported by various types of ancillary ligands including cyclopentadienyl, (Cp), trispyrazoyl borate (Tp), amides, alkoxides and imines.[1] Significant advances in the field of catalysis and synthetic organic chemistry have occurred as a result of these studies; the number and type of organometallic catalysts are too innumerable to be discussed here. This pioneering work has provided insight into the bonding and general understanding of organometallic mechanisms. The reactivity observed at a given metal center is highly dependant on the electronic as well as steric requirements of the ancillary ligands that support a particular metal species. Consequently, synthetic organometallic chemists have focused on the derivitization and discovery of new ligands, with the goal of "tuning" the reactivity at a metal-center.

The development of molecular orbital (MO) theory has allowed the structural and reactivity trends to be discussed in terms of specific interactions of molecular orbitals.[2,3] The accuracy of these methods depends on the way in which interactions between electrons are handled a concept defined as electron correlation. Hartree Fock (HF)

theory, for example, provides a method for converting the many-electron Schrödinger equation, into many simpler one-electron equations that can be solved to yield single electron wavefunctions called orbitals. However, significant errors may arise because electron correlation in these methods is treated in an average sense.

Technological advances have allowed for the successful employment of gradient corrected density functional theory (DFT) in calculating molecules, particularly involving transition metals, and in the use of small core relativistic effective core potentials (ECP's). DFT offers an advantage over traditional HF methods because it implicitly treats electron correlation. This has set the stage for the calculation of geometries, bond energies, vibrational spectra, activation energies for chemical reactions and other important properties of transition metal complexes.[4-7] These achievements have truly enhanced the understanding of the nature of the bonding seen in transition metal complexes and have allowed researchers to accurately make predictions about the existence of intermediates, the stabilities of species and the accessibility of kinetic pathways in reaction mechanisms.

In this dissertation we describe our latest efforts in an ongoing study of group 6 imido complexes supported by a chelating ancillary ligand. To study these complexes we employ the techniques of X-ray crystallography, NMR spectroscopy and computational chemistry(DFT), in order to properly assess the effects of ligand π donation on the properties and reactivity of these complexes. This chapter begins with a brief overview of the computational methods used to study these complexes and then proceeds to describe bonding in transition metal imido species and the concept of π loading. A brief

account of the group 6 imido diamido complexes previously synthesized in the Boncella lab along with an outline for the dissertation is also presented.

Theoretical Calculations and Methodology

Unlike Hartree-Fock calculations, density functional theory (DFT) implicitly treats electron correlation by utilizing an energy functional, some with empirically adjusted parameters[4-6]: $E^{xc}(\rho) = E^{x}(\rho) + E^{c}(\rho)$ where

E^{xc} is the exchange correlation functional

E^{x} is the exchange functional

E^{c} is the correlation functional

Modern functionals such as the generalized gradient approximation (GGA) or gradient corrected functionals and the so called hybrid functionals employ an admixture of exact Hartree-Fock (HF) exchange functionals and correlational exchange functionals, and have been shown to provide accurate geometries and reasonable energetics for a wide variety of systems at a computational cost similar to HF theory. DFT has a distinct advantage over traditional wave-function based techniques (*ab initio*) because the explicit addition of electron correlation to these techniques becomes quite computationally expensive.

In performing calculations on complex systems involving transition metals it is sometimes necessary to simplify the ligands of a given system not only to expedite the calculations but also to perform the number of calculations necessary to appropriately describe the system under study. However, these simplifications can and sometimes do lead to problematic interpretations and predictions of molecular systems as the steric and/or electronic consequences of ligand trimming must be considered. The electronic

consequences of ligand trimming are separate from and can compound with an incomplete basis set and an imperfect energy functional.

ONIOM Calculations

An obvious solution for the treatment of complex molecular systems is the partitioning of the system into two or more parts or layers, where the interesting or difficult part of the system (inner layer) is treated at a high level of theory and the rest of the system with a computationally less demanding method.

The ONIOM (Our owN n-layered Integrated molecular Orbital + molecular mechanics Method) developed by Morokuma and co-workers is a hybrid method designed to enable different levels of theory to be applied to different parts of a molecule/system and combined to produce a consistent energy expression.[8-12] The basic idea behind the ONIOM approach can be explained as an extrapolation scheme in a two dimensional space with the size of the system on the x-axis and the level of theory on the y-axis (Figure 1-1).

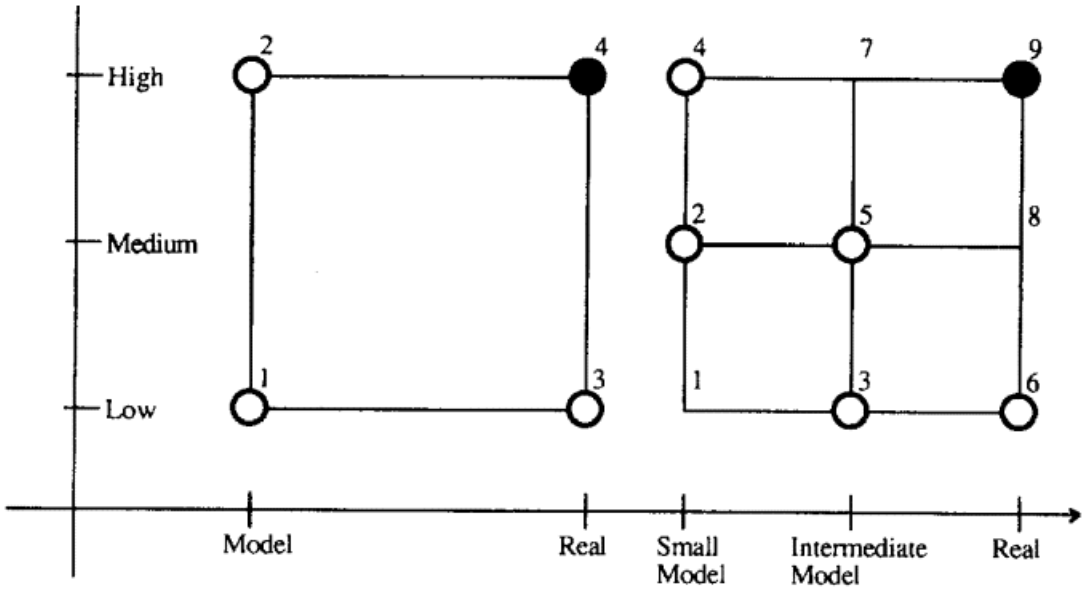

Figure 1-1. The ONIOM extrapolation scheme for a molecular system portioned into two (left) and three (right) layers

In order to describe the real system at the highest level of theory, point 4 in a system partitioned in two layers and point 9 in a system partitioned in three layers, the extrapolated energy is defined as $E_{ONIOM2} = E_3 - E_1 + E_2$ where E_3 is the energy of the entire (real) system calculated at the low level method and E_1 and E_2 are the energies of the model system determined at the low and high level of theory respectively. E_{ONIOM2} is an approximation to the true energy of the real system E_4: $E_4 = E_{ONIOM2} + D$. If the error, D, of the extrapolation procedure is constant for two different structures their relative energy ΔE_4 will be evaluated correctly by the ONIOM method. The accuracy of the ONIOM method depends on two factors: the choice of the lower level of theory and the model system. Thus the model system and level of theory must be chosen so as to accurately describe the energetics of the real system. Morukuma, Milstein,[13,14] Landis[15,16] and others have successfully employed this method to transition metal systems. We have successfully employed this method throughout this dissertation in describing the consequences of ligand π donation in group 6 imido diamido complexes.

Organoimido Chemistry and the Concept of π Loading

Organoimido transition metal chemistry has received attention in recent years because of its implication in several catalytic processes such as such as propylene ammoxidation and nitrile reduction. Imido complexes have also been shown to function as imido transfer intermediates in the aziridination and amination of olefins. There have been several reviews in recent years; the definitive work on imido chemistry occurs in Nugent and Mayer's *Metal-Ligand Multiple Bonds*,[17] in addition there have been more recent reviews by Wigley[18] and Eikey and Abu-Omar[19] et al.

Recent interest in imido chemistry has focused on the electronic structure and reactivity of imido complexes towards C—H bond activation. This involved repeated coordination of imido ligands to a single metal center, a strategy defined as π loading by Wigley group[20-24]. The premise behind the π loading strategy is that repeated coordination of more than one strongly π-bonding ligand will lead to increased competition for metal dπ acceptor orbitals. This will result in the localizition of charge at one of these π donor ligands and hence weakened π bonding and increased reactivity at this ligand. The Wolczanski and Horton groups have studied d^0 *bis*-imido complexes of Ta and V, and have demonstrated their ability to activate methane. Cundari and co-workers have compared methane activation by three-coordinate group 4, and group 5, and *bis*-imido amido complexes.[25-27] The results of these early studies demonstrate clearly that the strategy of π loading is a potentially useful method for generation of highly reactive organometallic species.

Bonding in π Loaded Imido Complexes

The imido ligand can be considered to bond to a transition metal with one σ bond and either one or two π bonds. The simplest model for bonding in complexes employing these ligands is a simple limiting valence bond (VB) model (Figure 1-2).[18] Figure 1-2 depicts the three limiting structures predicted by the simple VB model. Structure **A** depicts an sp^2 hybridized nitrogen leading to a M=N double bond (1σ, 1π) and a bent M—N—R linkage with the lone pair residing in a N(sp^2) orbital. In this formalism the imido behaves as a $4e^{-1}$ donor. In structure **B**, the M=N (double bond) is maintained if symmetry restrictions or a severe electronic mismatch with the available metal orbitals does not allow lone pair donation.

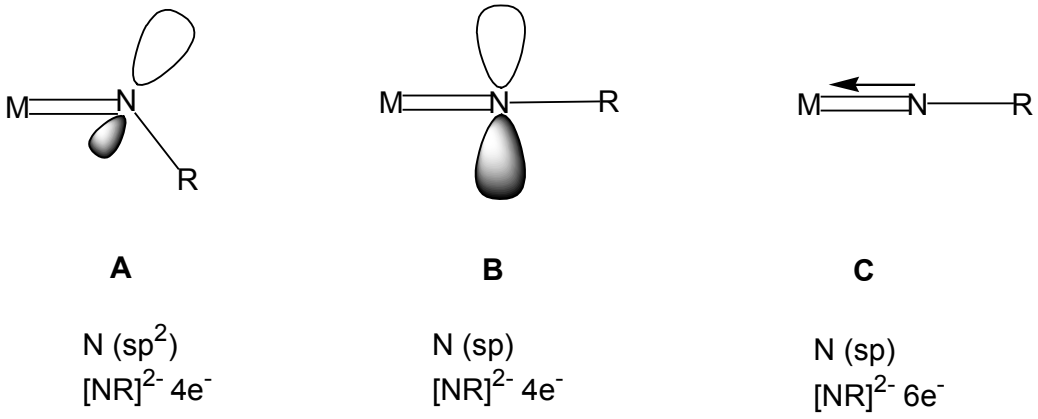

Figure 1-2. Limiting VB description of a metal – imido linkage

Most of the imido complexes described in the literature can be described by Structure **C**, where the imido ligand is formally a six electron donor (1σ, 2π).

There are very few examples of bent imido complexes in the literature. The classic example is found in the bis-imido complex $Mo(NPh)_2(S_2CNEt_2)_2$, **1**,[28] which contains one bent imido (MoNC =139.4(4)^0) and one linear imido (MoNC = 169.4(4)^0) (Scheme 1-1).

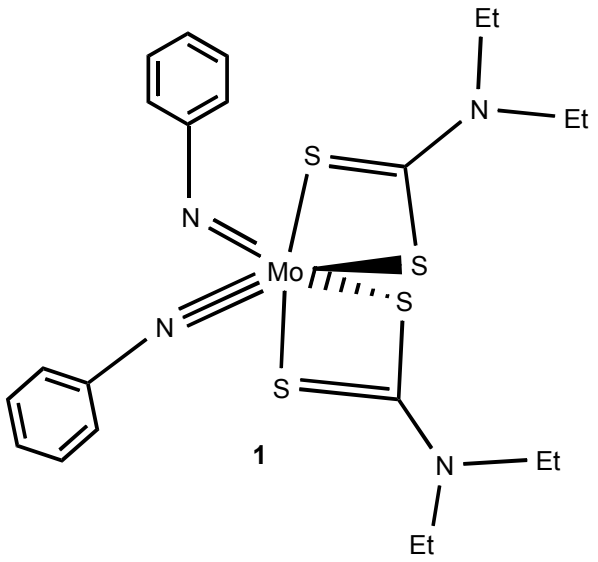

1

Scheme 1-1. $Mo(NPh)_2(S_2CNEt_2)_2$, a classic example of a bent imido complex

The bent imido can be described by the limiting structure **A**, whilst the linear imido can be described by the limiting structure **C**, and this allows the complex to attain an 18-electron configuration.

Several researchers have attempted to use similar VB arguments to describe the bonding in imido complexes and implied that the M—N bond length and MNC bond angles should reflect the limiting structures in Figure 1-2. However, it has been demonstrated by Cundari et al.,[25-27] that the VB description of the metal imido bond is not sufficient to describe the bonding in these complexes. Using *ab initio* calculations on a series of imido complexes these authors have shown that eight different resonance forms may be used to describe the M—N bond (Scheme 1-2). The results of these studies clearly demonstrate that the M—N (imido) bond cannot be described by a single resonance form as suggested by the VB description and a molecular orbital approach is often needed to accurately describe the bonding in metal—imido complexes.

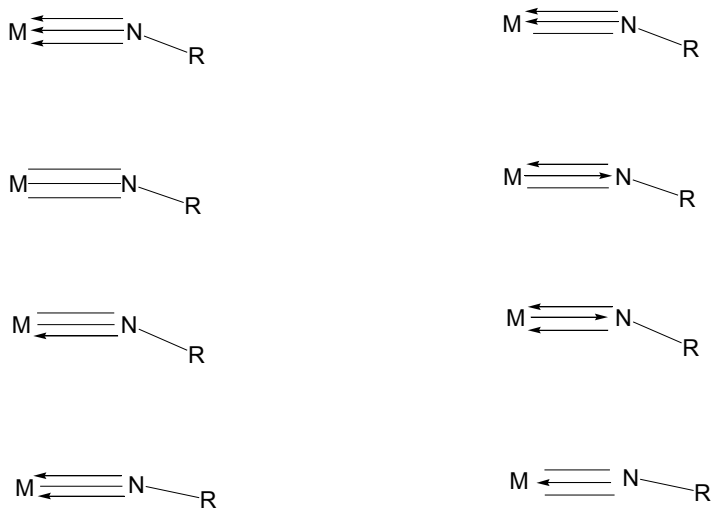

Scheme 1-2. Eight principal resonance contributors for the M—N (imido) bond. In this representation a straight line represents a covalent bond (i.e one electron in a TM-centered AO-like MO and one in the N centered counterpart), an arrow pointing towards the metal represents a dative bond and an arrow pointing towards the N represents a back bond. The bottom line (or arrow) describes the σ bond and the other lines π components of the M—N linkage.

Early Examples of π loaded complexes.

Early examples of heavily π-loaded complexes involve multiple coordination of imido ligands. The three–coordinate complex $Os(N\text{-}2,6\text{-}C_6H_3\text{-}i\text{-}Pr_2)_3$, **2**, by Schrock et al.[29] and the four-coordinate anion $[W(N\text{-}2,6\text{-}C_6H_3\text{-}i\text{-}Pr_2)_3Cl]^-$, **3**,[23] are the classic "20-electron" complexes (Scheme 1-3). Both complexes are characterized by a ligand based, non-bonding MO comprised of a set of ligand π orbitals oriented roughly perpendicular to the molecules C_3 axis which results in these complexes being described as 18-electron complexes. For example, the $[W(N\text{-}2,6\text{-}C_6H_3\text{-}i\text{-}Pr_2)_3Cl]^-$ molecule is best described as an 18-electron complex, as one combination of the imido nitrogen pπ orbitals has a_2 symmetry, and there is no corresponding orbital metal d orbital that can interact with this orbital (Figure 1-3).

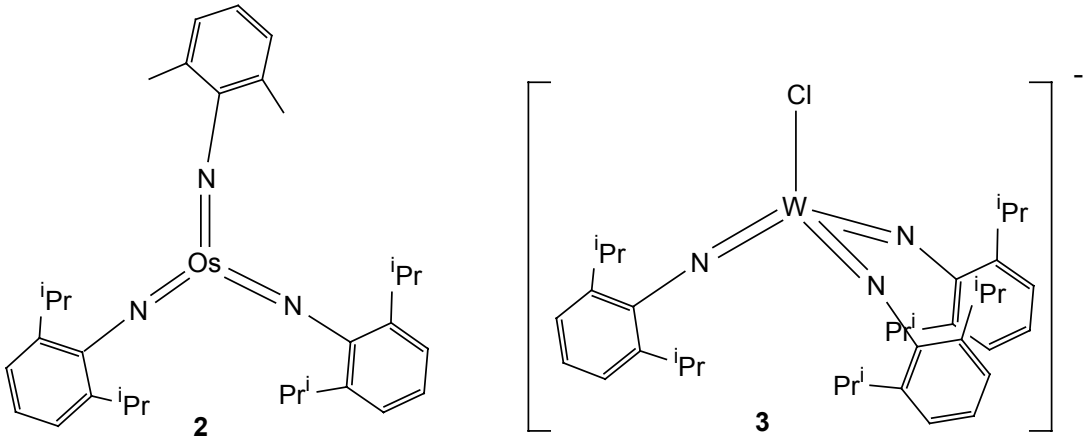

Schrock et.al.
*J . Am. Chem. Soc.***1990**, 112, 1643 - 1645

Wigley et.al.
*J . Am. Chem. Soc.***1991**, 113, 6326 - 6328

Scheme 1-3. Examples of π loaded complexes

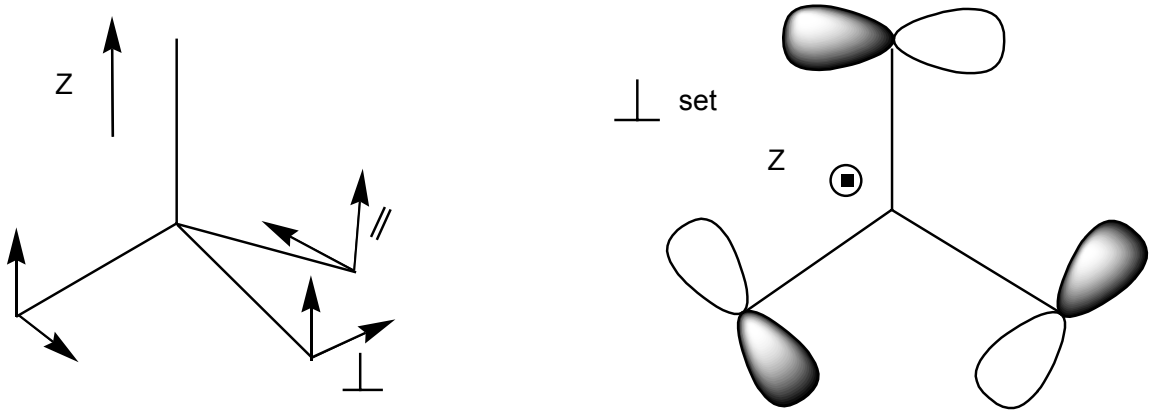

Figure 1-3. Pi perpendicular set of N(p) orbitals in threefold symmetry for **3**

This π loading strategy may be applied to complexes employing ligands other than imido or a combination of imido and another π donor ligand such as alkynes and amides. The Boncella group has employed this π loading strategy in the synthesis of imido diamido complexes. The π conflict that arises because of the presence of several π donor ligands is responsible for the interesting chemistry of these molecules.

Group 6 Imido Diamido Complexes

The Boncella group has developed extensive chemistry in the area of group 6 imido diamido complexes starting from the two metal dichloride species Mo(NPh)(*o*-$(Me_3SiN)_2C_6H_4)Cl_2(THF)$, **4**,[30] and W(NPh)(*o*-$(Me_3SiN)_2C_6H_4)Cl_2$ **5**.[31] Their syntheses are shown in Schemes 1-4 and Scheme 1-5. The Mo dichloride complex **4** is synthesized by treating a suspension of the bisimido complex, $Mo(NPh)_2Cl_2(DME)$ **6**, with a pentane solution of the diamine *o*-$(SiMe_3N)_2(-C_6H_4)$, and allowing the suspension to stir for 24hrs. The aniline complex Mo(NPh)(*o*-$(Me_3SiN)_2C_6H_4)Cl_2$(aniline), **7**, is generated by an apparent transfer of the diamine protons to one of the imido ligands in **6**. Lewis bases readily displace aniline in this complex. Thus stirring **7** in THF readily generates **4** quantatatively.

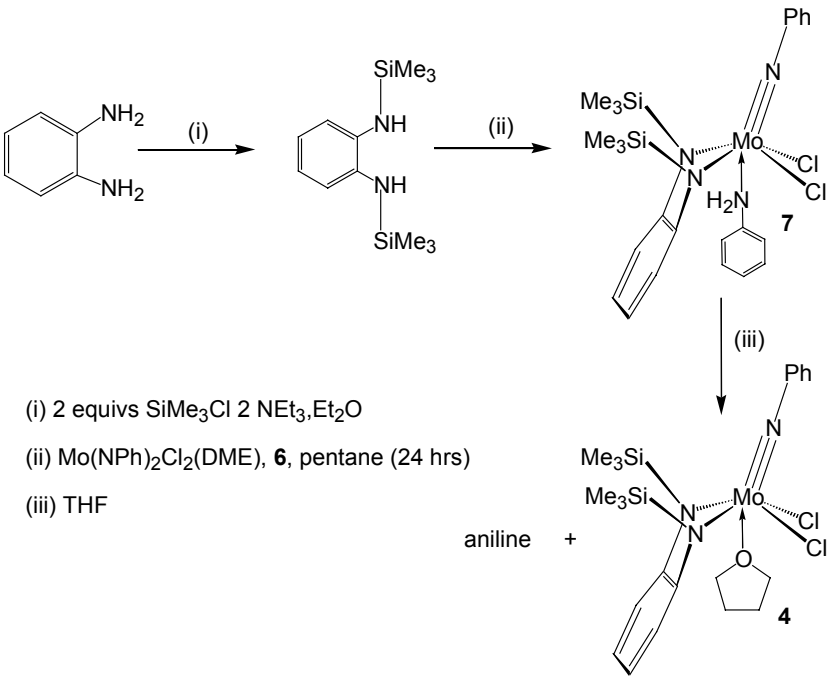

Scheme 1-4. Synthesis of Molybdenum imido-diamido dichloride, (**4**).

The W dichloride complex is synthesized by treating the dilithiated salt of the diamine with a pentane solution of the W tetrachloride complex (NPh)$WCl_4(OEt_2)$, **8** Scheme 1-5.

These complexes serve as starting materials for some extremely rich and diverse chemistry that stems from the electron rich environment provided by the diamide and imido ligands. Molecular orbital calculations have demonstrated that in addition to the imido ligand donating its 6 electrons (1σ, 2π), the diamide ligand could donate its lone pair electrons into a metal d orbital of appropriate symmetry.[32,33] Thus, all the t_{2g} orbitals on the metal are occupied. The addition of an additional π donor ligand to the metal would result in a competition for available d orbitals ,i.e., a π loaded environment on the metal center.

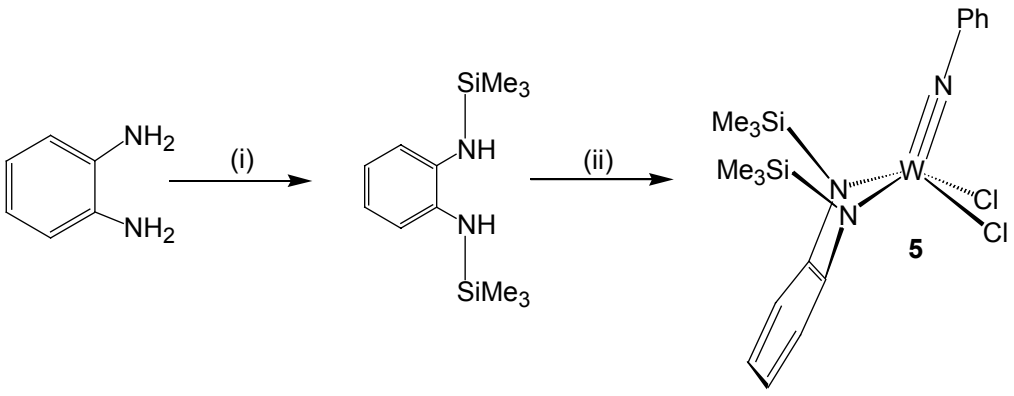

(i) 2 equivs $SiMe_3Cl$ 2 NEt_3,Et_2O

(ii) (a) 1. 2 equivs n-BuLi

(b) $(NPh)WCl_4(OEt_2)$, **8**, pentane

Scheme 1-5. Synthesis of Tungsten imido-diamido dichloride, (**5**).

Molybdenum and Tungsten Alkyl and Alkylidene Complexes

The dichlorides **4** and **5** were easily converted to alkyl complexes, **9**, and **10**, respectively, upon treatment with non- β-hydrogen-containing alkyl magnesium reagents (Scheme 1-6). The generation of the *bis*-neopentyl complexes $M(NPh)(o(Me_3SiN)_2C_6H_4)(CH_2(C(CH_3)_3)_2$ (M = Mo, **9c**; M = W, **10c**) provided an avenue into alkene metathesis chemistry.

When compounds **9c** and **10c**, were heated in the presence of PMe_3, the alkylidene species $M(NPh)(CHCMe_3)(PMe_3)(o\text{-}(Me_3SiN)_2C_6H_4)$ (M = Mo, **11**; M = W **12**) are generated via α abstraction (Scheme 1-7). Compound **12** has been shown to be an active catalyst for the methathesis of terminal olefins but competing decomposition processes drastically limit the catalyst's lifetime.[34]

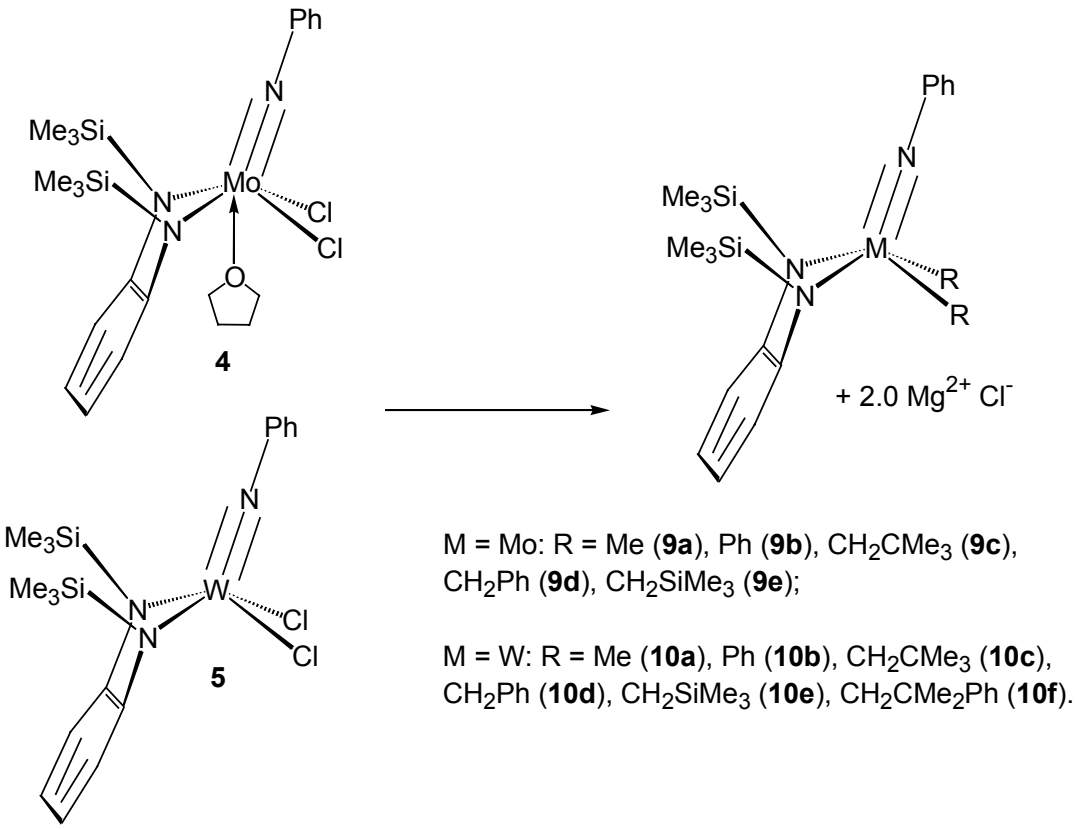

Scheme 1-6. Synthesis of molybdenum and tungsten dialkyl complexes.

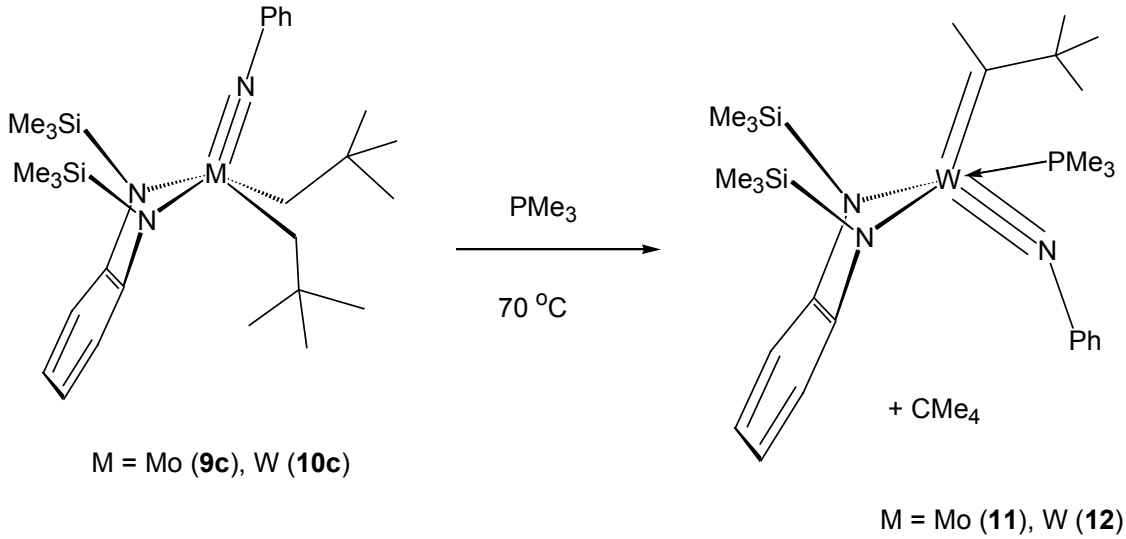

Scheme 1-7. Formation of molybdenum and tungsten alkylidene adducts.

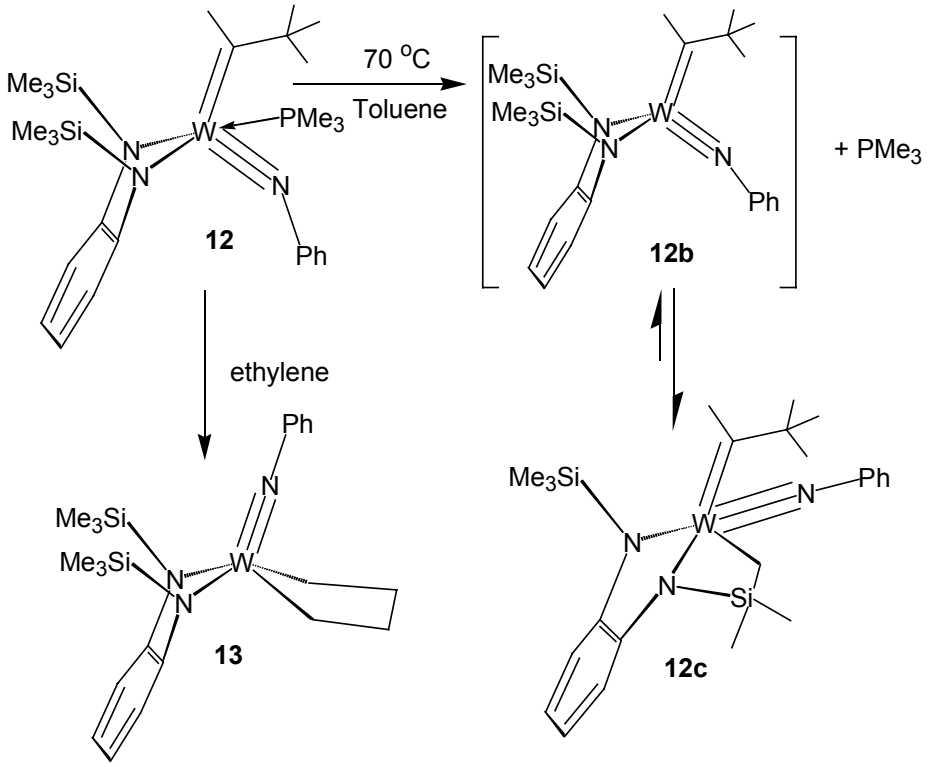

Scheme 1-8. Reversible metallation of **12** in the absence of PMe_3 and the formation of **13** in the presence of excess ethylene

Removal of PMe_3 from complex **12** results in a reversible metalation of one of the $SiMe_3$ groups of the *o*-$(Me_3SiN)(C_6H_4)$ ligand as shown in Scheme 1-8. When **12** is treated with excess ethylene the metallacyclopentane complex **13**, $W(NPh)(o\text{-}(Me_3SiN)_2C_6H_4)(CH_2)_4$, is formed. The mechanistic details of the formation of **13** from **12** in the presence of excess ethylene have been detailed in the literature and will not be discussed here.[34] For the purposes of this discussion it will suffice to say that the reaction **12** with ethylene to form **13** is a deactivation pathyway when **12** is used as an olefin metathesis catalyst for terminal olefins.

It is noteworthy that the Schrock group has also observed metallacyclopentanes in olefin metathesis reactions.[35-42] However, the metallacycles formed with these species are particularly unstable and decompose via β hydrogen abstraction/transfer mechanisms.

The difference in reactivity between Schrock's complexes (Scheme 1-9) and ours originates from the nature of the ancillary ligands. The *bis*-alkoxide ancillary ligands in Schrock's complexes,[43] **14** and **15**, are not very good at stabilizing the metal center via π donation. In our complexes the diamide ligands have a high propensity to donate nitrogen p electrons to metal orbitals of appropriate symmetry. The implications of these interactions are the primary focus of this dissertation.

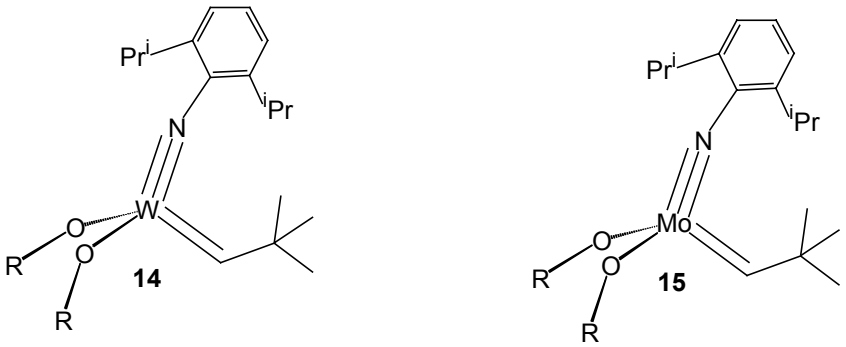

a) R = $CCH_3(CF_3)_2$
b) R= ^tBu

Scheme 1-9. Examples of Schrock's metathesis catalysts

Reaction With Alkyl Isocyanides

The reactivity of tungsten alkyls **10a** and **10c** has been explored with *tert*-butyl isocyanide (Bu^tNC) (Scheme 1-10).[44] Complexes **10a** and **10c** inserted Bu^tNC into each metal alkyl bond, affording the η^2-imino-acyl complexes **16** and **17**. When heated, **16** underwent a carbon-carbon coupling reaction giving **18**. This insertion into metal alkyl bonds and the subsequent coupling chemistry have been well documented for early metals with CO or isocyanides.[45] However, the related insertions of isocyanides into metal amide bonds are less well studied, and given the ligand centered nature of the

highest occupied molecular orbitals in these complexes, isocyanide insertion into the metal diamide bond might be expected.

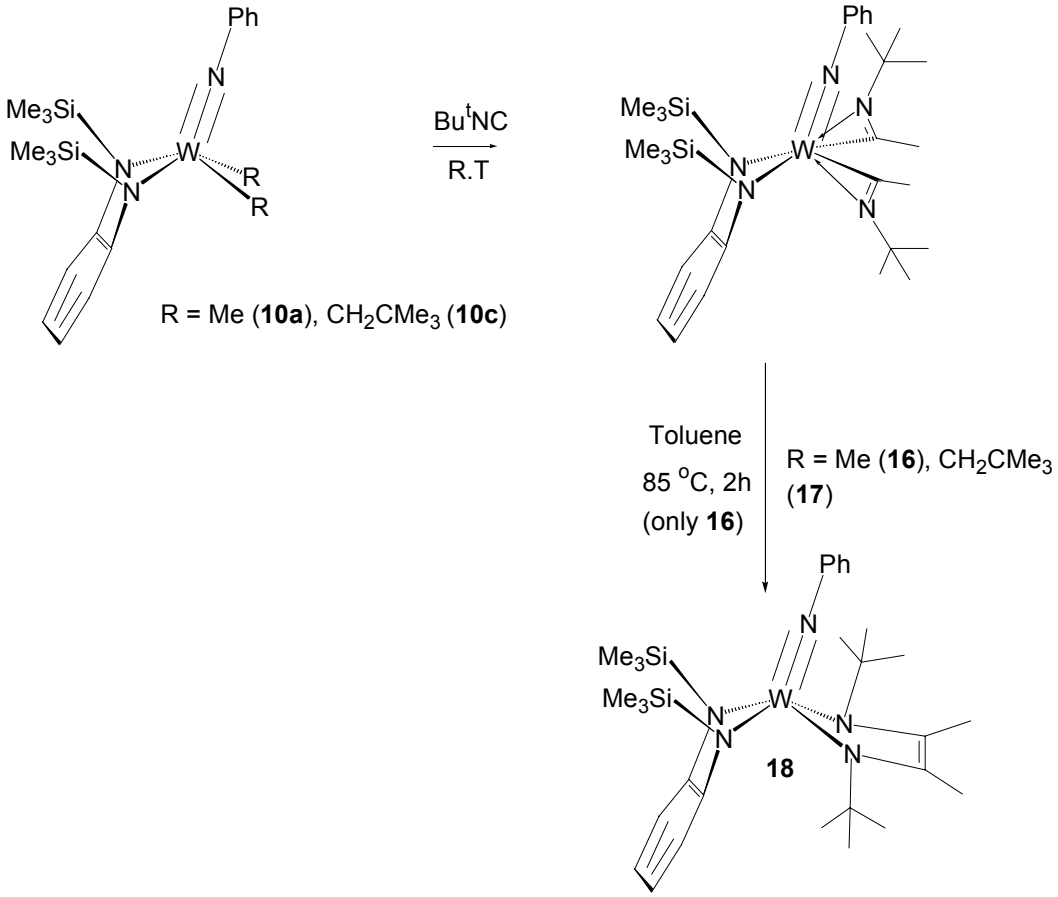

Scheme 1-10. Reactivity of tungsten dialkyls with ^{t}BuNC.

Complexes of Mo and W Imido Diamido Complexes Containing π donor Ligands

Alkyl complexes containing β hydrogens (**10g**, R = Phenethyl; **10h,** R = Ethyl) can be synthesized and isolated with W. These complexes are stable at room temperature, but the treatment of **10g** and **10h** with a Lewis Base (PMe_3) results in the formation of the olefin complexes **19** (Scheme 1-11).[32]

The formation of the olefin complexes **19**, has been showed to proceed by a β-hydrogen transfer from the ethyl and phenethyl groups in **10g** and **10h** respectively. This reaction is unusual as it is promoted by the association of a PMe_3 ligand whereas β-

hydrogen transfer reactions are usually promoted by the dissociation of a ligand. In contrasts, Mo alkyls containing β-hydrogens are not stable and undergo β-hydrogen transfer reactions at -20^0 C resulting in the formation of stable isolable olefin complexes **20** (Scheme 1-12).[46]

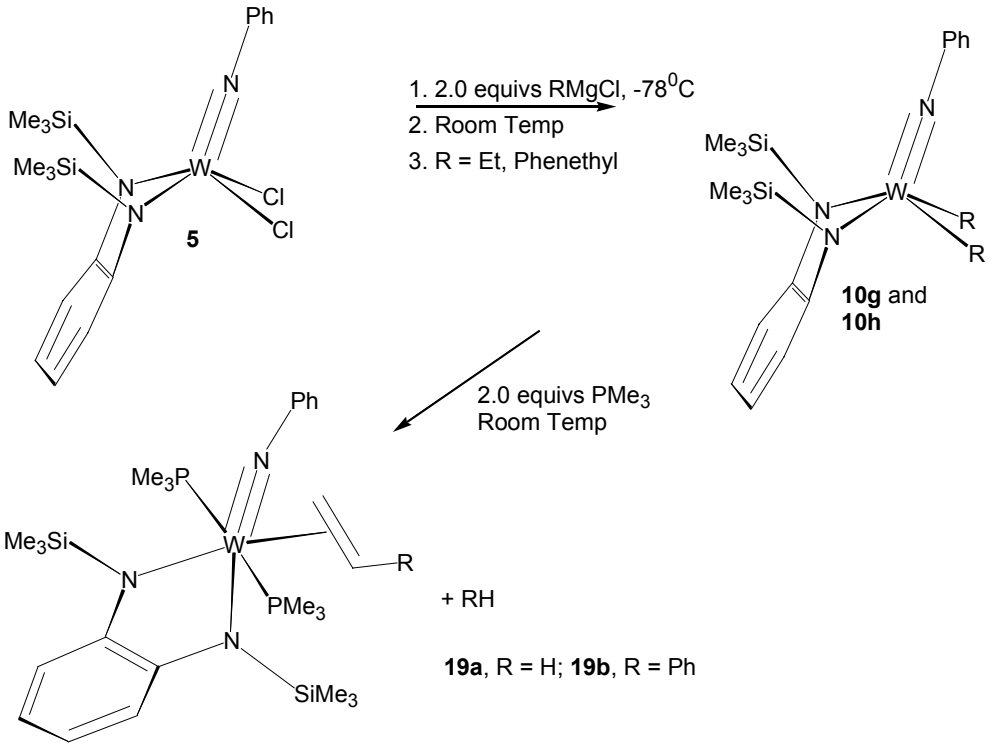

Scheme 1-11. Synthesis of W olefin complexes by PMe_3 promoted β-hydrogen transfer

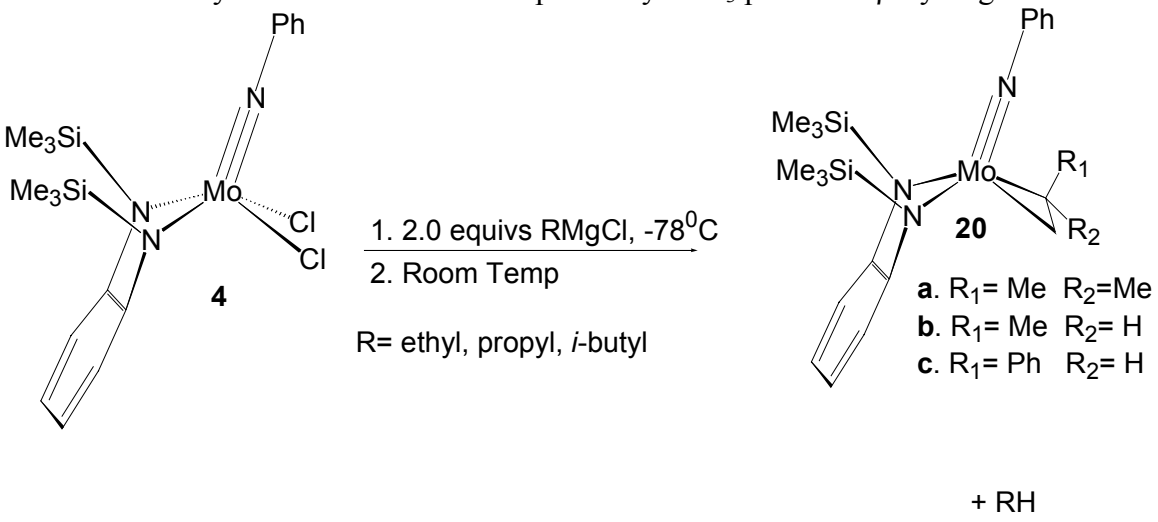

Scheme 1-12. Synthesis of olefin complexes of Mo

The olefin complexes, **20**, have served as useful starting materials for the synthesis of several complexes incorporating π donor ligands. These include arenes, imines,[47] butadienes,[48] alkynes, and pyridine ligands.[49] These complexes all exhibit unusual structural properties as well as interesting chemical reactivity. These properties originate from the electron rich environment at the metal center provided by the diamide and imido ligands. Our interest in studying these complexes stems from a desire to understand the implications of π loading in these complexes, an in so doing, produce species that may be used as catalysts in organic synthesis.

Scope of the Dissertation

The implications of competitive ligand π donation (π loading) in group 6 imido diamido complexes are systematically discussed in this manuscript. We have attempted to do this by utilizing a series of techniques (DFT, X-ray crystallography, NMR spectroscopy, and kinetic and mechanistic studies), in an attempt to attain a deeper understanding of the influence of the diamide and imido ligands on the properties of these complexes. The effects of π loading competition between alkyne and imido ligands, as well as the electronic origins of ligand folding in d^0 and d^2 complexes are discussed in Chapter 2. The synthesis of metallacyclopentenes via π ligand exchange and the kinetics and mechanism of the thermal rearrangement of metallacyclopentanes are studied by DFT and kinetic studies and are presented in Chapter 3. Reactions at the diamide ligand are discussed in Chapters 4 and 5. The synthesis of isocyanide complexes and the isocyanide insertion in the metal diamide bond to form an iminocarbamoyl complex is discussed in Chapter 4, whilst the alkyl aluminum induced diamide transfer from group 6

imido diamido complexes and the implications to olefin dimerization/codimerization catalysis are discussed in Chapter 5.

CHAPTER 2
STRUCTURE REACTIVITY AND BONDING OF MOLYBDENUM IMIDO DIAMIDO COMPLEXES

Introduction

Species containing transition metal to ligand multiple bonds are widespread and play an important role in organometallic chemistry.[17] These species usually contain ligands such as imido, nitrene, oxo and alkylidenes that bind to the metal via overlap of the ligand p π and metal d π orbitals. When there are several π donors on a given metal center, ligand to metal π bonding results in a competition for available unfilled metal d orbitals. The term "π loading" has been used by Wigley and others to describe this phenomenon, and it has been suggested that the competition for metal π orbitals can lead to increased reactivity of organometallic complexes.[20-27]

While the structural and electronic effects of "π loading" is well documented for both tetrahedral and octahedral (bis)imido and mixed oxo-imido complexes,[50-53] there is a sparsity of similar studies on ability of alkyne ligands to compete as π donors on a given metal center in a π loaded environment. Although, it has been demonstrated that alkynes can stabilize high oxidation states of transition metals via donation of their $\pi_{\perp}$ electrons, it is not clear whether these interactions are strong enough to compete with traditional π donors.

Recently, our group has investigated the chemistry of group 6 imido complexes of the form M(NPh)(*o*-$(Me_3SiN)_2C_6H_4$)X_2 (M=Mo and W) which incorporate the *o*-pda (o-phenylenediamine) ligand.[30,31] This work has demonstrated that the diamide ligands are

involved in a multicenter π donor interaction with the metal center via the diamide lone pair electrons. The success in the synthesis of high oxidation state olefin complexes,[34,46] inspired us to pursue the synthesis and reactivity of alkyne complexes, and in so doing answer the question: Can donation of the alkyne $\pi_\perp$ electrons effectively compete with the imido and diamide ligands on the metal center for empty metal d orbitals?

In this chapter, the synthesis of alkyne complexes, **21**, (η^2-alkyne)Mo(NPh)(*o*-($Me_3SiN)_2C_6H_4$), along with the X-ray crystal structure of **21e**, and their solution behavior via low temperature ^{1}H NMR spectroscopy is discussed. DFT calculations (B3LYP) have been used to study the bonding in these complexes and an NBO analysis was used to determine the extent of π donation by the alkyne ligand.

Structure Dynamics and Bonding of Imido Diamido Alkyne Complexes

Synthesis of Alkyne Complexes. Base-free molybdenum alkyne complexes of the type [η^2-(alkyne)Mo(NPh)-*o*-($Me_3SiN)_2C_6H_4$)], **21**, were prepared by treating pentane solutions of **20** with the appropriate alkyne, followed by removal of solvent under reduced pressure (Scheme 2-1). The alkyne reactants displace the bound olefin with complete conversion to products within 15 min at 20 ºC. The ^{1}H NMR spectra of **21** are consistent with monomeric alkyne complexes. As shown in Table 2-1, the ^{13}C NMR resonances of the α carbons of the alkyne fragment are significantly deshielded suggesting the involvement of the alkyne $\pi_\perp$ electrons in the M—alkyne bonding.[54-60] Alkyne complexes **21a-e** are air sensitive, but stable in solution and in the solid-state. In contrast, the alkyne complex **21f** is thermally unstable and decomposes in solution at –40 ºC within *ca.* 12 h.

Table 2-1. ^{1}H and ^{13}C NMR data for alkyne complexes

			^{13}C NMR, ppm		^{1}H NMR, ppm	Tc, K	$\Delta G^{\ddagger}$, Kcal/mol
Complex	**R_1**	**R_2**	**C_1**	**C_2**			
3a	CO_2Me	H	175	177	9.2	257	13.2
3b	Ph	Me	185	180	--	268	13.4
3c	$SiMe_3$	Me	200	181	--	268	13.4
3d	Ph	Ph	180	--	--	--	--
3e	$SiMe_3$	$SiMe_3$	205	--	--	--	--
3f	Me	Me	187	--	--	--	--

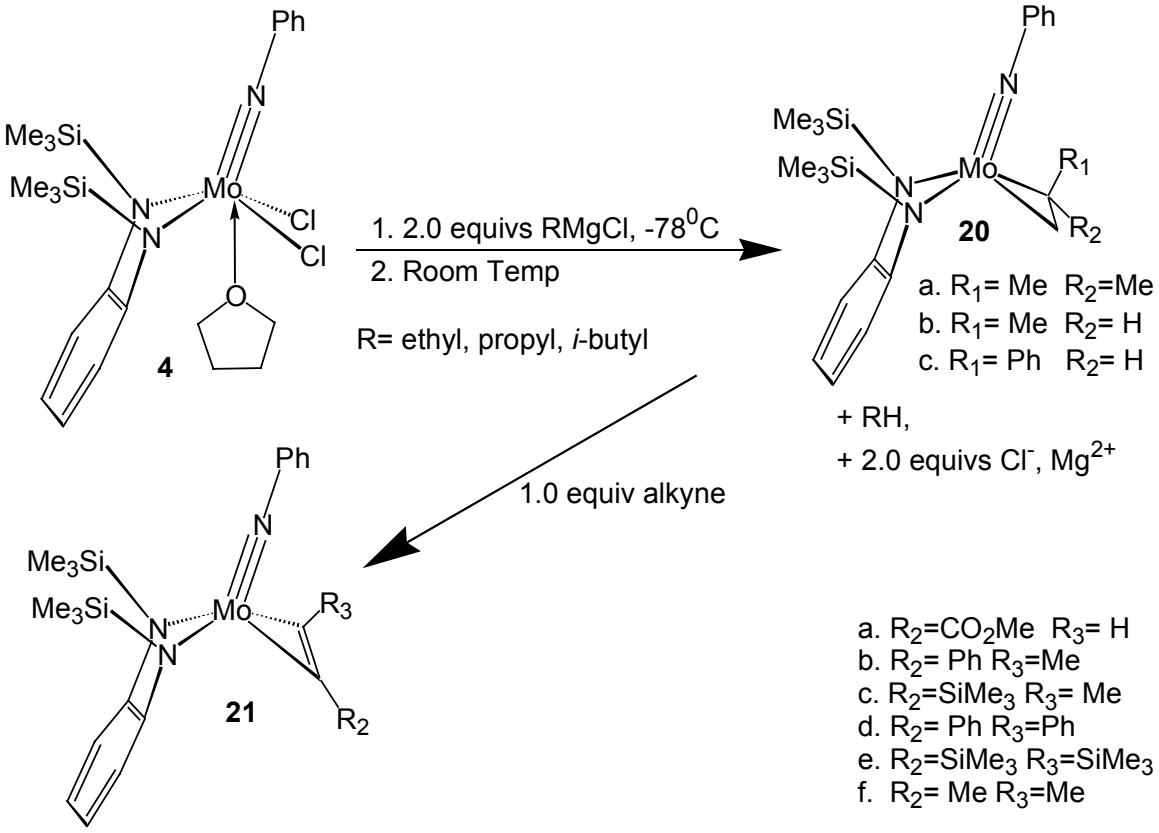

Scheme 2-1. Synthesis of alkyne complexes

A single crystal X-ray analysis was performed on a single crystal of **21e.** This crystal structure was originally reported by a previous graduate student, Tom Cameron,[61] however, it is included here for the purposes of discussion. As shown in the thermal ellipsoid plot in Figure 2-1, the alkyne complex adopts a pseudo square pyramidal structure with the imido ligand occupying the apical position. The alkyne ligand is oriented perpendicular to the Mo=N bond of the *cis* imido ligand and the Mo—C(19) and

Mo—C(20) bond lengths, 2.078 and 2.079 Å respectively, are consistent with Mo—C single bonds. The C(19)—C(20) bond length for **21e**, 1.305 Å, is close to the generally accepted value for C—C double bonds. Pronounced back bonding is responsible for the lengthening of this alkyne bond, and the structure of **21e** is thus best described as having a large contribution from a metallacyclopropene structure. In this resonance form, the alkyne ligand can be considered as a dianionic ligand and the formal oxidation state of the metal would be best described as Mo(VI).

In addition, the diamide ligand is folded through concerted torsion of the NR group about the C—N bond of the pda ring. The fold angle (angle between the N(2) Mo N(3) plane and the plane of the pda ring) is 133^0. This folding has been attributed to donation of the diamide lone pair electrons into the empty metal d_x^2-$_y^2$ orbital.[32,33,62]

In solution, the alkyne complexes exhibit C_s symmetry just as in the solid state. In complexes **21d-f**, the alkyne substituents are the same, and a plane of symmetry bisecting the C—C bond of the alkyne, containing the N=M bond of the imido ligand, and bisecting the *o*-pda ring causes the $SiMe_3$ protons to become chemically equivalent. These protons appear as a broad peak at 0.4-0.6 ppm. However, in complexes **21a-c** where the alkyne substituents are different, there is no longer a plane of symmetry and the $SiMe_3$ protons are no longer equivalent. These protons appear as a broad singlet in the ^{1}H NMR spectra at room temperature. However, cooling a C_7D_8 solution to -50^0C, results in the splitting of this peak into two singlets (Figure 2-2). Using the two site exchange approximation,[63] the activation barrier for this process has been measured to be 13.2 Kcal/mol. Interestingly, the barrier is the same regardless of the alkyne substituent (Table 2-1).

This fluxional process can be explained by rotation of the alkyne fragment about the Mo—alkyne centroid axis. This motion takes the alkyne ligand through a transition state that is also of C_s symmetry (Scheme 2-2) where the alkyne is oriented parallel to the imido ligand.

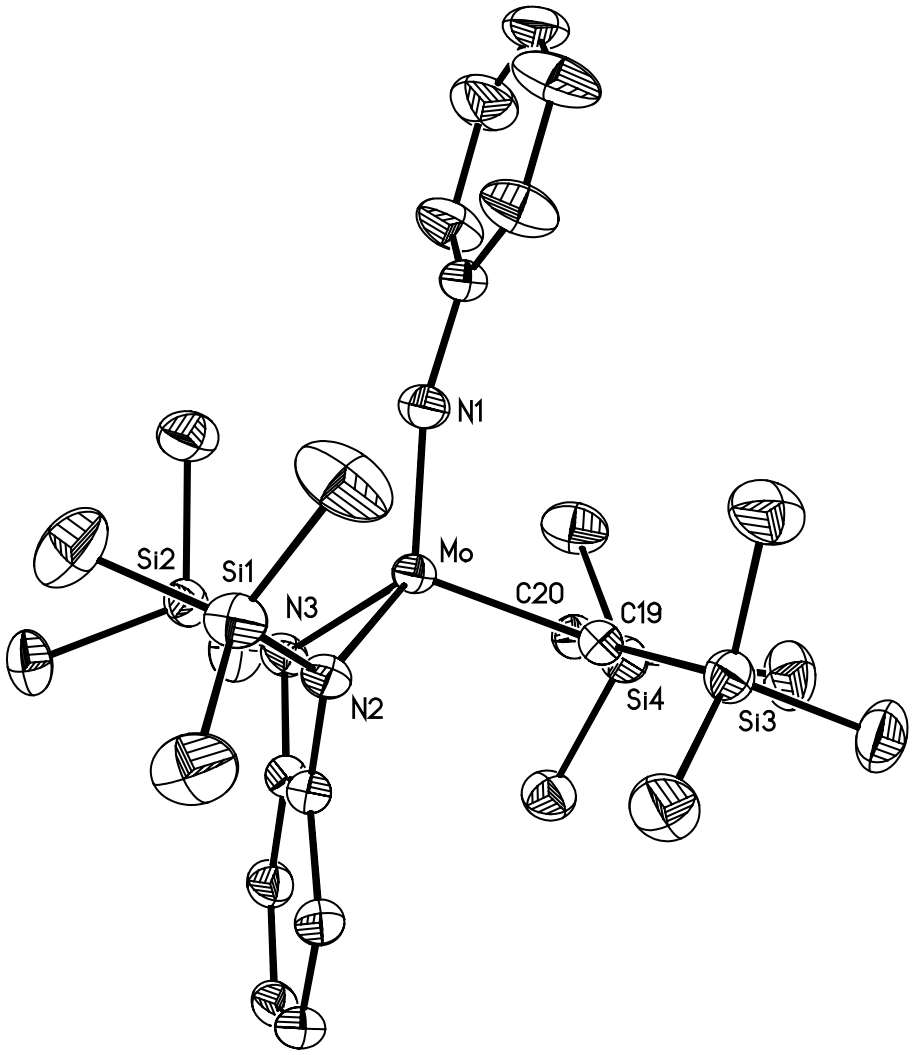

Figure 2-1. Thermal ellipsoid plot of **21e**, [Mo(NPh)(η^2–*bis*-trimethysilylacetylene){o-$(Me_3SiN)_2C_6H_4$}], (40% probability thermal ellipsoids) selected bond lengths (Å): Mo—N(1), 1.745(2); Mo—N(2), 2.023 (2); Mo—N(3), 2.009 (2); Mo—C(19), 2.078 (3); Mo—C(20), 2.079 (3); C(19)—C(20), 1.305, (4).

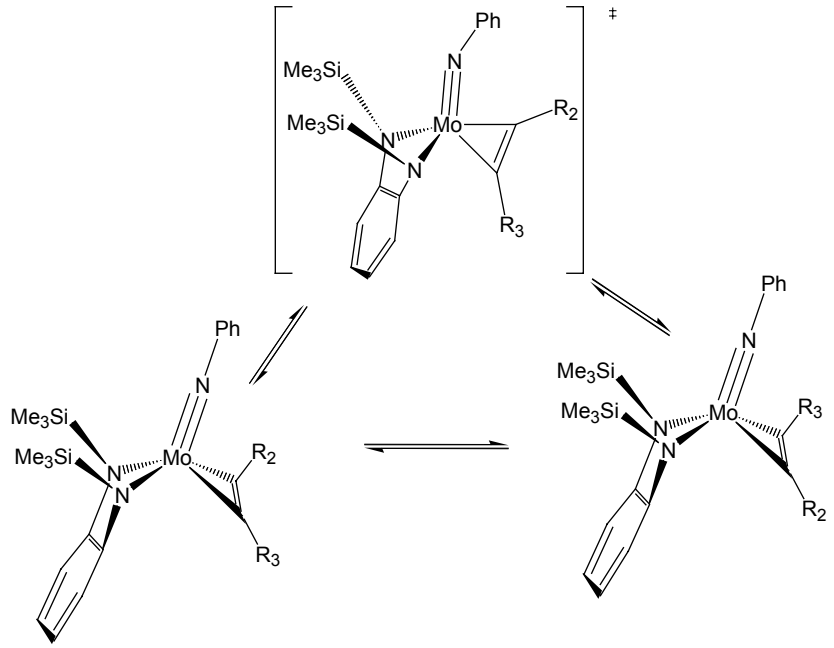

Scheme 2-2. Alkyne rotataion in **21**

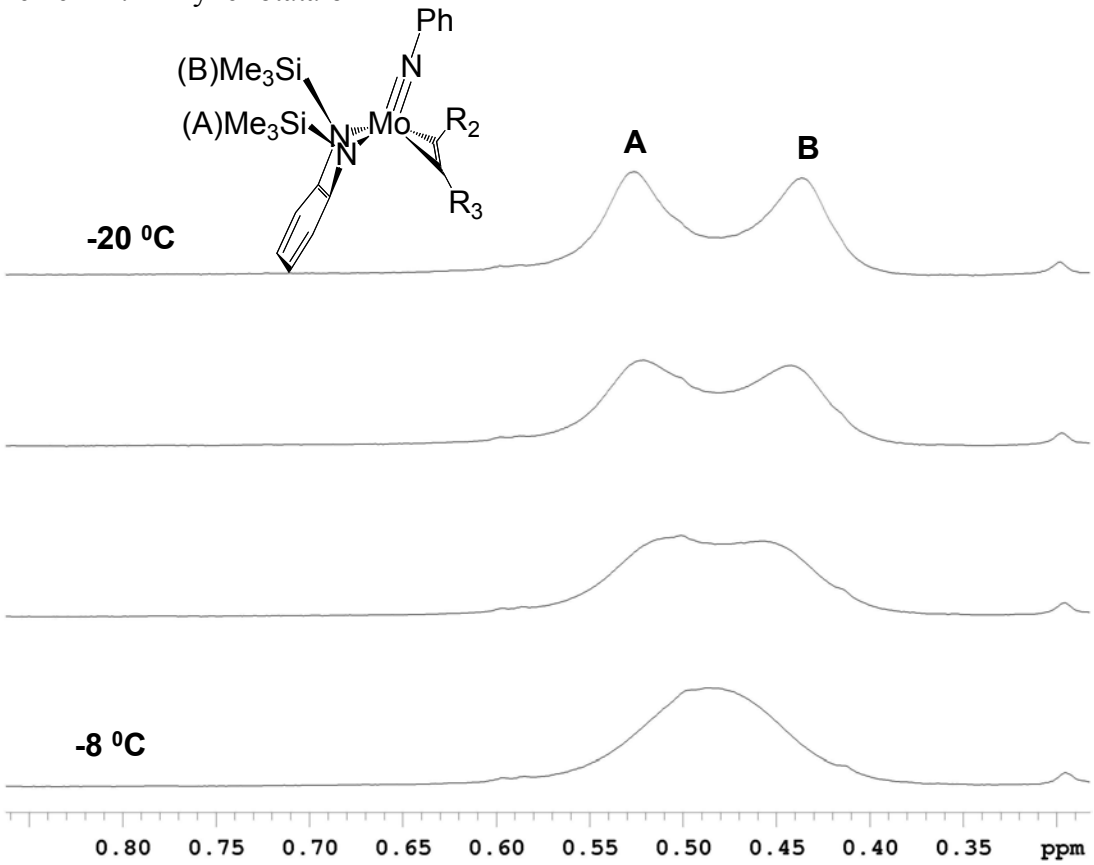

Figure 2-2. Variable temperature ^{1}H NMR spectrum of the $SiMe_3$ region from –20 to –8^{0}C for complex **21b**

Molecular orbital calculations. To elucidate the bonding pattern of the alkyne fragment in these complexes, density functional theory calculations (DFT) were performed. Initial calculations were carried out on model compound **22** (Figure 2-3), which is a simplified version of **21** where the *o*-phenylene group (o-C_6H_4) that links the two N atoms of the diamido ligand was simplified to a –CH=CH- carbon chain. The organic groups on the nitrogen atoms ($SiMe_3$ of the amido and phenyl group of the imido) were replaced by hydrogen atoms for simplicity. Propyne was used as the alkyne fragment in this model. The calculated structure for **22** is generally in good agreement with the X-ray crystal structure data obtained for **21e** and **21f**.[48] The only exception is that the ligand is significantly less folded in this model than in the actual compounds (147^0 vs 133^0). This is due to the inability of the hydrogen atoms on the diamide ligand to successfully model the bulky $SiMe_3$ group. In order to obtain a more accurate model for the alkyne complexes we employed the ONIOM approach (developed by Morokuma[8-12] et.al [9,10,11,12]) to model the complete ligand system with all substituents used in the experiment (Figure 2-3).

We defined a two-layer model, (model compound **23)** for the 2-butyne complex **21f**. The outer layer consisted of the entire complex, including the entire *o*-pda ligand, and phenyl and $SiMe_3$ substituents on the imido and diamide ligand respectively, and the inner layer comprised of **22,** with acetylene as the alkyne fragment. The inner layer was modeled using the B3LYP[64,65]/LANL2DZ[66,67] basis set, whilst the B3LYP/LANL2MB basis set was used to model the substituents. As shown in Table 2-2 below there is excellent agreement between the calculated structure **23**, and the X-ray crystal structure for **21f**.

Table 2-2. Comparison of selected bond lengths and angles between model compounds **22** and **23** and the reported crystal structure for **21f**[b]

Bond Lengths and Angles	**22**	**TS 22**	**23**	**TS 23**	Xray data **21f**[b]
Mo—N(1)	1.755	1.798	1.776	1.818	1.745(2)
Mo—N(2)	2.018	2.053	2.003	2.005	2.009(2)
Mo—N(3)	2.018	2.037	2.020	1.991	2.022(2)
Mo—C(19)	2.087	2.089	2.086	2.087	2.078(3)
Mo—C(20)	2.071	2.079	2.083	2.075	2.079(3)
C(19)—C(20)	1.331	1.346	1.333	1.353	1.305(4)
Fold angle[a]	147^0	141^0	137^0	138^0	133^0

a. The fold angle is defined as the angle between the planes made by Mo, N(2), N(3), and the plane defined by the benzenoid portion of the *o*-pda ring.
b. See reference 49 and 61 for crystallographic information.

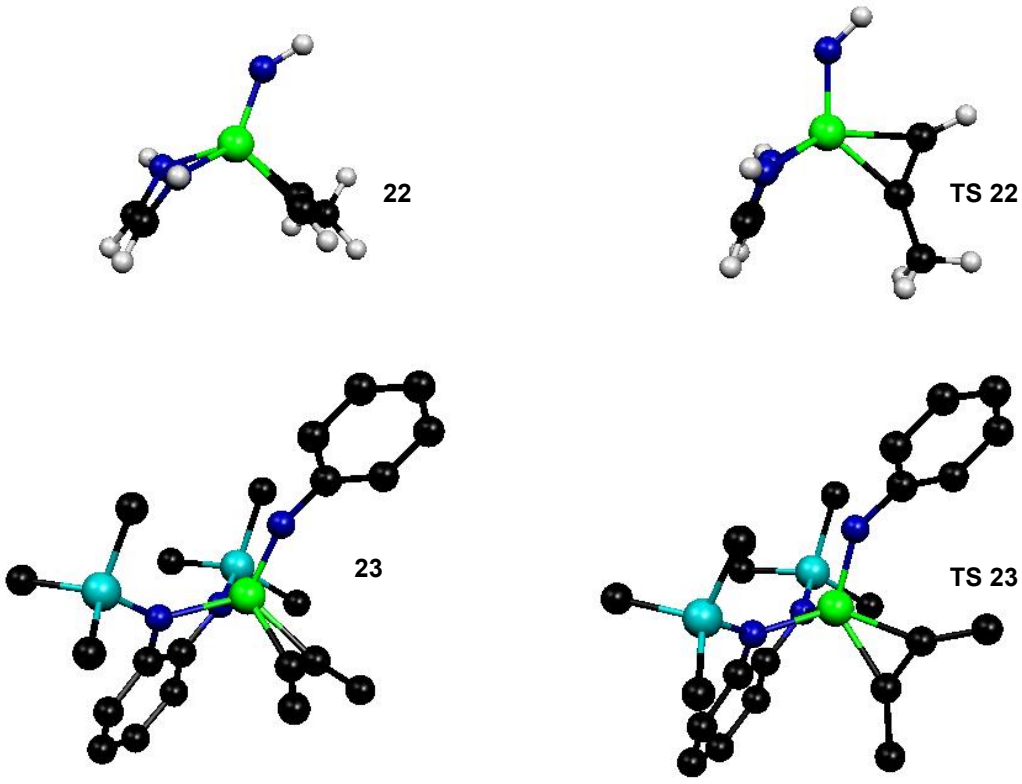

Figure 2-3. B3LYP optimized models for alkyne complexes **22** and **23** and their transition states

The transition states corresponding to alkyne rotation about the Mo –alkyne bond in both **22** and **23** have been located. In both these transition states the alkyne ligand is now oriented parallel to the Mo—N(imido) bond. This involves rotation of the alkyne ligand in **22** and **23** by 90^0 about the Mo-alkyne bond. The activation energy obtained

from these calculations is 16.9 Kcal/mol for the rotation of **22** and 14.4 Kcal/mol for the rotation of **23**. The ONIOM model, in particular, compares favorably to the experimentally obtained activation barrier of 13.2 Kcal/mol.

In order to better understand the nature of the bonding in these complexes, we undertook a qualitative MO analysis and applied Weinhold's Natural bond orbital (NBO)[68-70] method to the complex. Scheme 2-3 shows the most important orbital interactions between a metal L_3M fragment and *o*-$(SiMe_3N)_2C_6H_4^{2-}$ ligand assembled in C_s symmetry, with a mirror plane directly bisecting the *o*-pda ligand and containing the Mo—N(imido) bond. The frontier orbitals of a L_3M fragment have been determined by Albright et al.[71] and are represented on by the left side of Scheme 2-3. The metal t_{2g} orbitals in this non-standard orientation are comprised of one orbital of a'' symmetry primarily d_{xy}, and two orbitals of a' symmetry primarily $d_{x^2-y^2}$, and d_{z^2}. The metal e_g orbitals become a'', primarily d_{yz}, and a' primarily d_{xz}. In the case of Mo, the three t_{2g} derived orbitals lie relatively high in energy and above the chelate's populated π^* orbital. The $d_{x^2-y^2}$ orbital is closest in energy to this orbital and is responsible for the folding of the diamide ligand, seen in these complexes. The two filled orthogonal p_π orbitals on the imido nitrogen, destabilize the metal t_{2g} orbitals of a' (d_{z^2}) and a''(d_{xy}) symmetry.

Donor electrons on the alkyne alter the MO diagram in Scheme 2-3. These electrons compete for empty metal orbitals with the imido ligand i.e. the alkyne $\pi_\perp$ electrons compete with the imido for the metal d_{z^2} orbital in the ground state and the d_{xy} orbital in the transition state, resulting in a 3-center-4-electron bonding interaction between the imido, the metal center and the alkyne ligand. As is typical for three center interactions, three orbitals can be expected for the combination of the three fragments, i.e.

(a bonding, nonbonding, and antibonding combination of the orbitals from the 3 fragments). The bonding combination for the interaction of the alkyne, the imido nitrogen lone pair and the metal d_z^2 orbital is depicted in Figure 2-4.

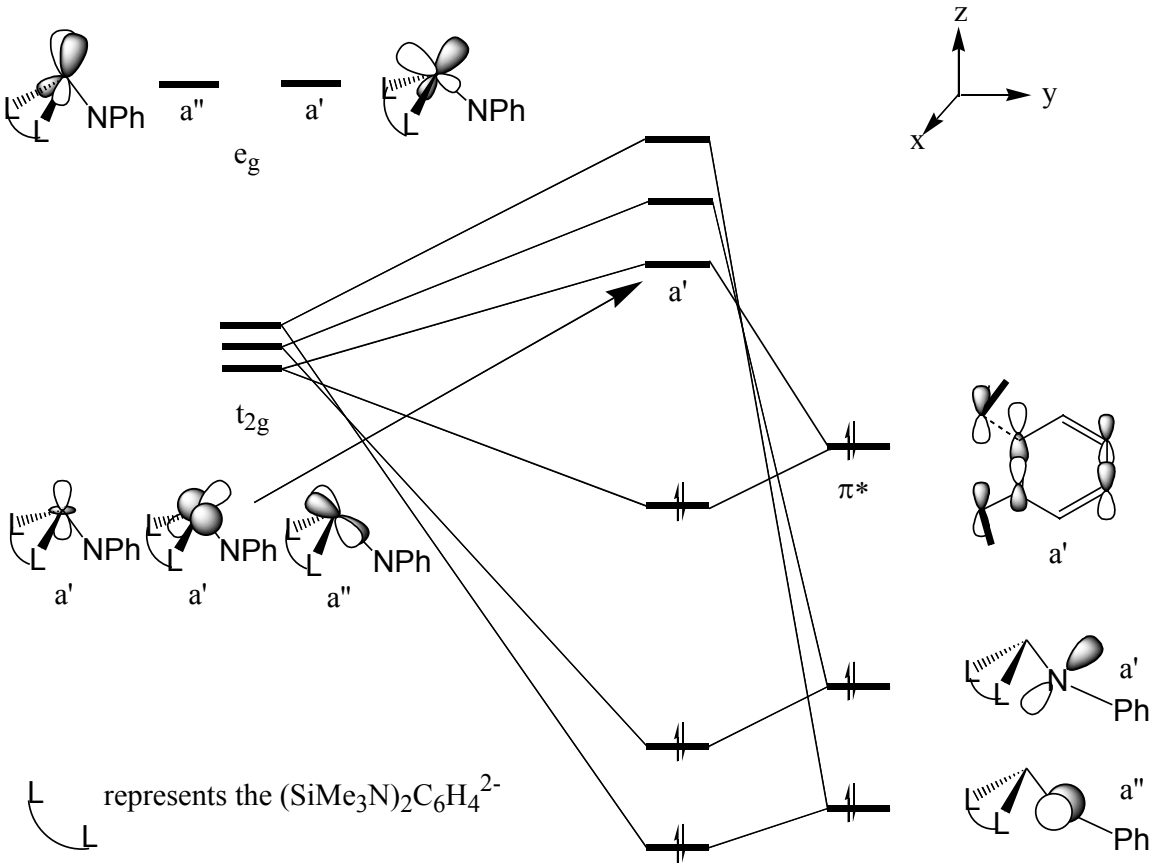

Scheme 2-3. The effects of the consideration of π contributions of the diamide and imido ligands (right side) on a typical ML_3 fragment (left side). In this non-standard orientation the metal d orbitals have a different composition than that usually used for octahedral complexes. This is due to the coordinate system shown in the top right corner of this figure. In a pure ML_3 fragment the z-axis coincides with a threefold rotational axis of an ocatahedron. The atomic composition of of the metal d orbitals, are mixed so that the orbitals are reorientated to lay between the M—L bonds. For example the a' component of the e_g set becomes $\sqrt{1/3}(_{x^2-y^2}) + \sqrt{2/3}\ _{yz}$. For full details on the atomic composition of a pure ML_3 fragment see. Albright et al.[71]

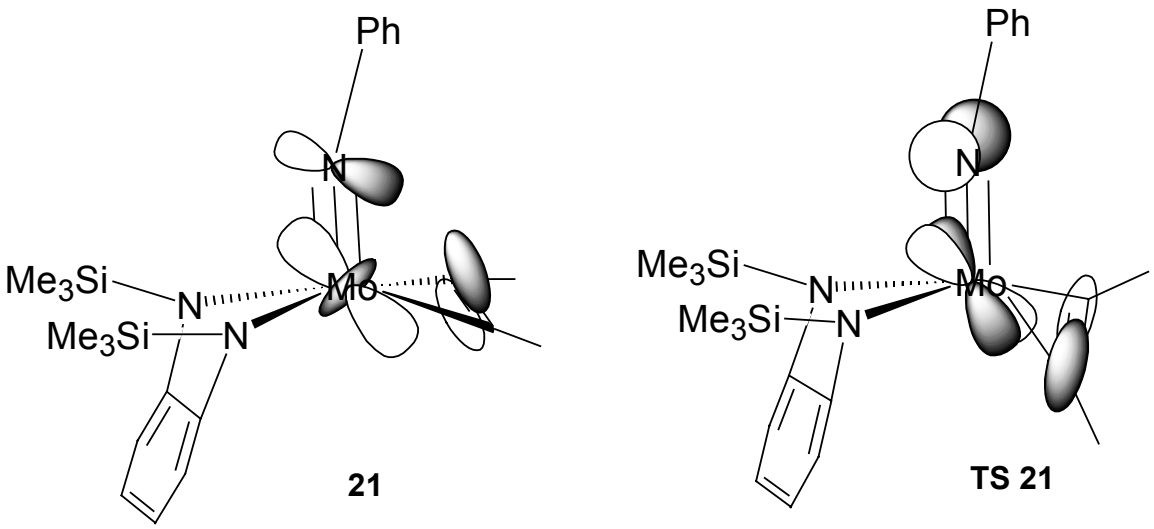

Figure 2-4**.** Bonding interactions in between Mo, imido, and the alkyne fragment

NBO population analysis**.** More detailed information about the alkyne→metal π interactions can be obtained from an NBO population analysis. The NBO[68] program diagonalizes the one and two center blocks of the first order reduced density matrix in such a way that natural bonds are obtained that are said to represent the best Lewis structure of a molecule. This involves a sequence of transformations from a given basis set to various localized sets: natural atomic orbitals (NAOs), natural hybrid orbitals (NHOs), natural bond orbitals (NBOs), and natural localized molecular orbitals (NLMOs). The NLMOs can then be transformed to occupied MOs. Delocalization effects appear as weakly occupied antibonding or Rydberg orbitals.

given basis sets ⟶ NAOs ⟶ NHOs ⟶ NLMOs

Lewis structures obtained from NBO analyses accounted for approximately 97% of the electron density. As shown in Table 2- 4, the NLMO analysis can be used to quantify the delocalization of the alkyne $\pi_{\perp}$ electrons. In the transition states **TS 22** and **TS 23,** a greater proportion of the electron density of the parent NBO of the alkyne C—C π bond

is delocalized onto molybdenum. In addition, the occupancy of this bond is also lower in the transition state.

Table 2-3. NLMO analysis of alkyne π bond

Model	%π C—C	% Mo	Occupancy
22	86.9	9.2	1.738
TS22	80.1	13.8	1.660
23	86.9	8.5	1.738
TS23	78.9	14.0	1.640

Table 2-4, shows the population analysis of the Mo—imido bond. The bond type, percent contribution from each atom and occupancy of each chemical bond are presented. The Mo=N(imido) bond in model complexes **22** and **23,** where the alkyne is aligned in an orthogonal orientation, consists of a σ-bond and two π-bonds as would be expected for a metal—nitrogen triple bond. All bonds are substantially polarized towards nitrogen with contributions from nitrogen (68-77%) and (22-32%) from molybdenum.

Table 2-4. NBO analysis of Mo—N(imido) bonds

Model	Bond Type	%Mo	%N	Occupancy	Covalent Bond order[b]
22	σ	22.9	77.1	1.94	
	π_1	27.3	72.7	1.83	0.960
	π_2	31.7	68.3	1.90	
23	σ	26.2	73.8	1.97	
	π_1	22.1	77.9	1.76	0.949
	π_2	31.6	68.4	1.83	
TS 22	σ	37.9	62.1	1.97	
	π_1	39.3	60.7	1.92	0.928
	n[a]	6.4	89.5	1.80	
TS 23	σ	37.1	62.9	1.92	
	π_1	36.4	63.6	1.88	0.868
	n[a]	6.7	86.5	1.74	

[a] n, lone pair [b] Atom-Atom overlap-weighted NAO bond order

However, this bond in transition state structures **TS 22**, and **TS 23**, consists of one σ-bond and one π-bond, the third π-bond is significantly localized on the nitrogen atom (N contribution 87-90%) and is best described as a lone pair with some delocalization

onto the molybdenum center (6.4-6.8%). This data, in addition to the lower covalent bond orders of the Mo—N bonds for model complexes **22** and **23,** (Table 2-4) suggests a weakening of the Mo—N(imido) bonds in the transition state.

The NLMOs of **22** and **TS 22** are represented pictorially in Figure 2-5. The larger contributions of the Mo d-π orbital in the transition state **TS 22** is evident in Figure 2-5h versus the significantly smaller contributions from these orbitals in Figure 2-5d. Also the localization of the third Mo—N(imido) π bond is evident in Figure 2-5g.

Thus, it is only in the transition state that the alkyne π electrons compete effectively for metal d orbitals. This is evidently a higher energy process, as the stronger metal nitrogen π bonds are replaced by weaker metal carbon π bonds, leading to the observed activation barrier associated with alkyne rotation.

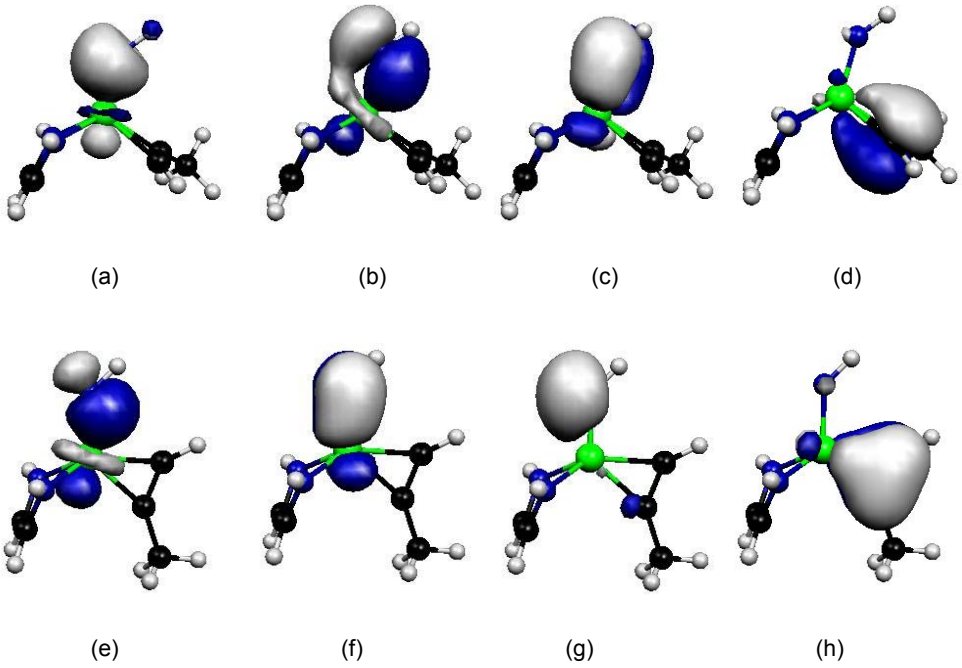

Figure 2-5. NLMO plots (isocontour 0.04) of Mo—N(imido) bond in **22** (a-c): a = imido—Mo dz^2 (σ), b = imido—Mo (dz^2, dyz hybrid, π), c = imido—Mo (dxy, π) and **TS 22** (e-g): e = imido—Mo dz^2 (σ), f = imido—Mo (dxy, π), g = imido lone pair. Plot d = C—C π bond –Mo(dz^2, dyz hybrid) in **22**, h = C—C π bond –Mo (dxz, dxy hybrid) in **TS 22**.

Summary

We have demonstrated the synthesis of novel high oxidation state molybdenum imido alkyne complexes that show significant interactions between the alkyne $\pi_{\perp}$ electrons and the metal center. The implications of this interaction on the structure and dynamics of these complexes have been explored via DFT (B3LYP) and NBO calculations. These calculations reveal that the alkyne π donation in these complexes occurs at the expense of Mo—N(imido) bonding. This is an unfavorable interaction since the stronger Mo—N bonds, are replaced by weaker Mo—C bonds. The perpendicular orientation of the alkyne ligand in the ground state of these complexes arises as the molecule minimizes the alkyne to Mo π donation and maximizes the imido to Mo π donation. It is clear that the interplay of π donor ligands in this class of compounds plays a crucial role in determining their properties and suggests that a judicious choice of the π donors may offer a way to modify the chemistry of these compounds in a desirable fashion.

Dynamics and Bonding of Molybdenum Imido Diamido Olefin Complexes

The chemistry of group 6 metal imido diamido complexes has resulted in the isolation and characterization of a number of olefin complexes of both W and Mo.[32,46] These olefin complexes are formed when a dialkyl complex containing β hydrogen atoms undergoes β hydrogen transfer and the loss of one molecule of an alkane. In the case of W, β hydrogen transfer is induced by the addition of a Lewis base (Scheme 2-4) whilst, in the case of Mo spontaneous β hydrogen transfer occurs at room temperature.

Crystal structures of olefin complexes of both W and Mo have been reported.[72,73] Like the alkyne complexes they are characterized by a significant amount of π back

bonding, a fact that is manifest for these complexes in both the solid-state structural features, and in solution. For example, in the crystal structure of the styrene complex of Mo, (Mo(NPh)(η^2-styrene)(*o*-$(Me_3SiN)_2C_6H_4$), **20c**, a long C—C bond (1.46Å) is observed for the styrene ligand. Further, in both the ^1H and ^{13}C NMR spectra of this compound, the resonances for the styrene ligand are shifted significantly upfield, suggestive of a metallacyclopropane like structure for these olefin complexes.

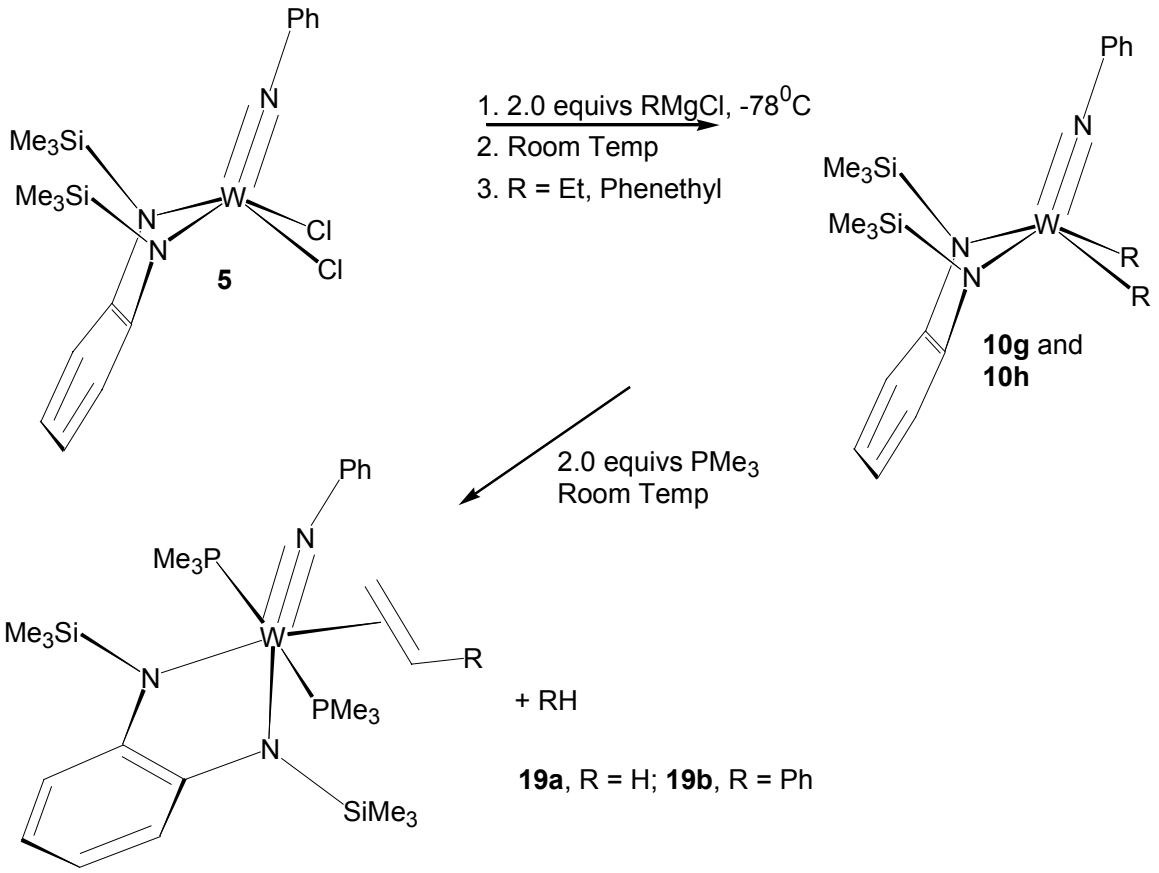

Scheme 2-4. Synthesis of W olefin complexes

Unlike the alkyne complexes, olefin rotation is much slower and is not observed on the NMR timescale. Complex **20c** in particular exists in solution as two isomers; the phenyl substituents of one isomer are *anti* to the imido ligand and while this substituent in the other isomer is *syn* to the imido ligand. No intercoversion of these two isomers were observed even when a C_6D_6 solution of **20c** was heated at 80 ^0C.[74]

In order to investigate the dynamics of olefin rotation in these complexes, ONIOM calculations were performed. For these calculations a two-layer oniom system was employed as has been described earlier in this chapter (Figure 2-6). The core of these calculations consisted of the –CH=CH- carbon chain replacing the *o*-phenylene group (o-C_6H_4) and with hydrogens in place of the organic groups on the nitrogen atoms ($SiMe_3$ of the amido and phenyl group of the imido) as described earlier. Ethylene was used as the olefin fragment in this model. This layer was optimized within the ONIOM program using the B3LYP/LANL2DZ method. The outer layer consisted of the full system and was modeled with the computationally less expensive B3LYP/LANL2MB basis set. There was good agreement between the calculated structure for **20c** and the experimental X-ray structure of this compound.

Using this method we were able to calculate an activation barrier of for olefin rotation of 25.4 Kcal/mol. This is consistent with the experimental observation that olefin rotation is slow on the NMR timescale yet rapid enough on the chemical timescale to give two isomers as the product of the reaction. The energy barrier can also be explained by examining the molecular orbitals, and revisiting the molecular orbital diagram of Scheme 2-3 (Shown again below).

Recall that the fragment orbitals L_3M fragment are comprised of a t_{2g} set that has one a'' symmetry (d_{xy}) orbital and two orbitals of a' symmetry $d_{x^2-y^2}$ and d_{z^2}, whilst the e_g set are composed of a'' (d_{yz}) orbital and a' (d_{xz}) orbital. As the alkyne or olefin fragment approaches the L_3M fragment perpendicular to the M—N bond of the imido ligand the a''(d_{xy} and d_{xz}) orbitals mix, one linear combination of these orbitals directs the lobes of the metal orbital towards the π^* orbital of the incoming ligand, the other linear

combination directs the lobes of the d orbitals towards the imido ligand. The olefinic fragment is thus stabilized by π back bonding from the metal a'' orbitals to the π* orbital of the fragment. This is clearly seen by examining the HOMO of **23** and **20c** (Figure 2-7).

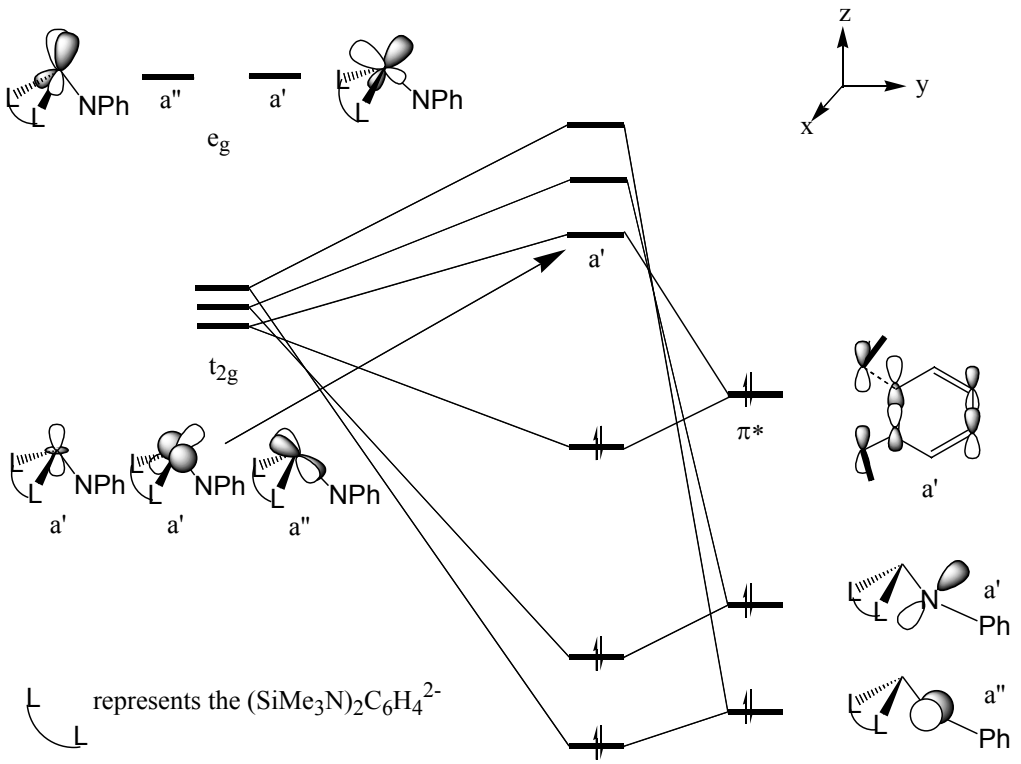

Scheme 2-3. The effects of the consideration of π contributions of the diamide and imido ligands (right side) on a typical ML_3 fragment (left side). In this non-standard orientation the metal d orbitals have a different composition than that usually used for octahedral complexes. This is due to the coordinate system shown in the top right corner of this figure. In a pure ML_3 fragment the z-axis coincides with a threefold rotational axis of an ocatahedron. The atomic composition of of the metal d orbitals, are mixed so that the orbitals are reorientated to lay between the M—L bonds. For example the a' component of the e_g set becomes $\sqrt{1/3}(_{x^2-y^2}) + \sqrt{2/3}\ _{yz}$. For full details on the atomic composition of a pure ML_3 fragment see. Albright et al.[71]

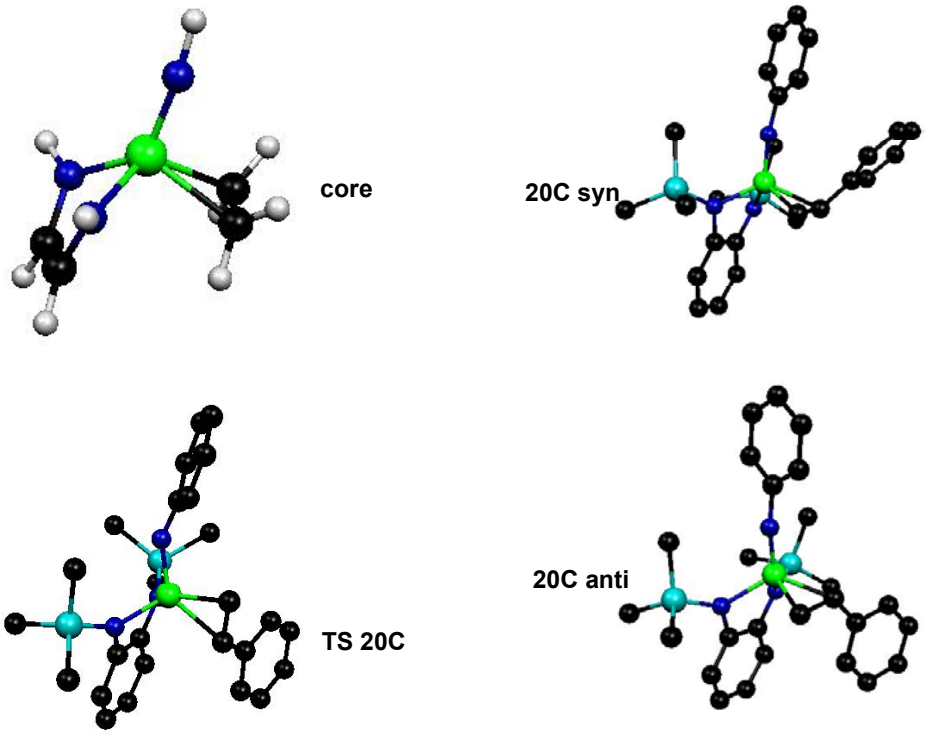

Figure 2-6. Optimized ONIOM structures for **20c**

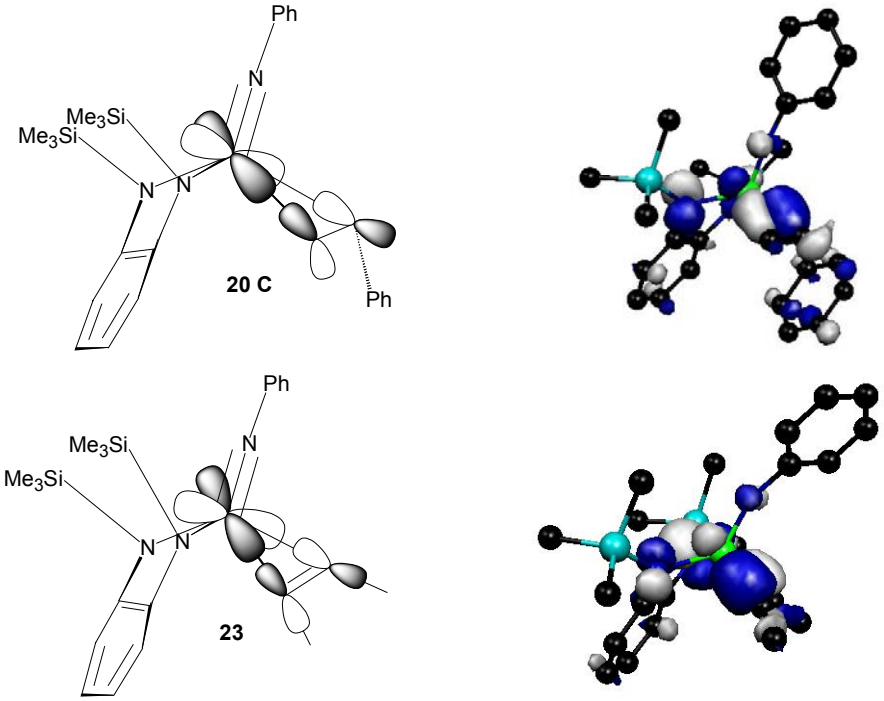

Figure 2-7. HOMO of **23** and **20c** showing π backbonding of the metal fragment to the olefin in **23** or acetylene in **20c**

Rotation of the olefinic fragment by 90^0 results in the symmetry of the π* orbital of this fragment changing from a'' to a' as it is moved into the mirror plane of the molecule. This orbital can now interact with the metal d orbitals of a' symmetry, specifically a linear combination of the d_z^2 and d_{yz} orbitals. Recall however, that the imido lone pair electrons were donated into the d_z^2 orbital. Imido—Mo lone pair donation in this case is made energetically unfavorable by the presence of d electrons in this orbital. This is clearly seen when the HOMO of **TS 20c** and **TS 23** are examined (Figure 2-8). The imido lone pair is clearly non-bonding in **TS 20c** and **TS 23.**

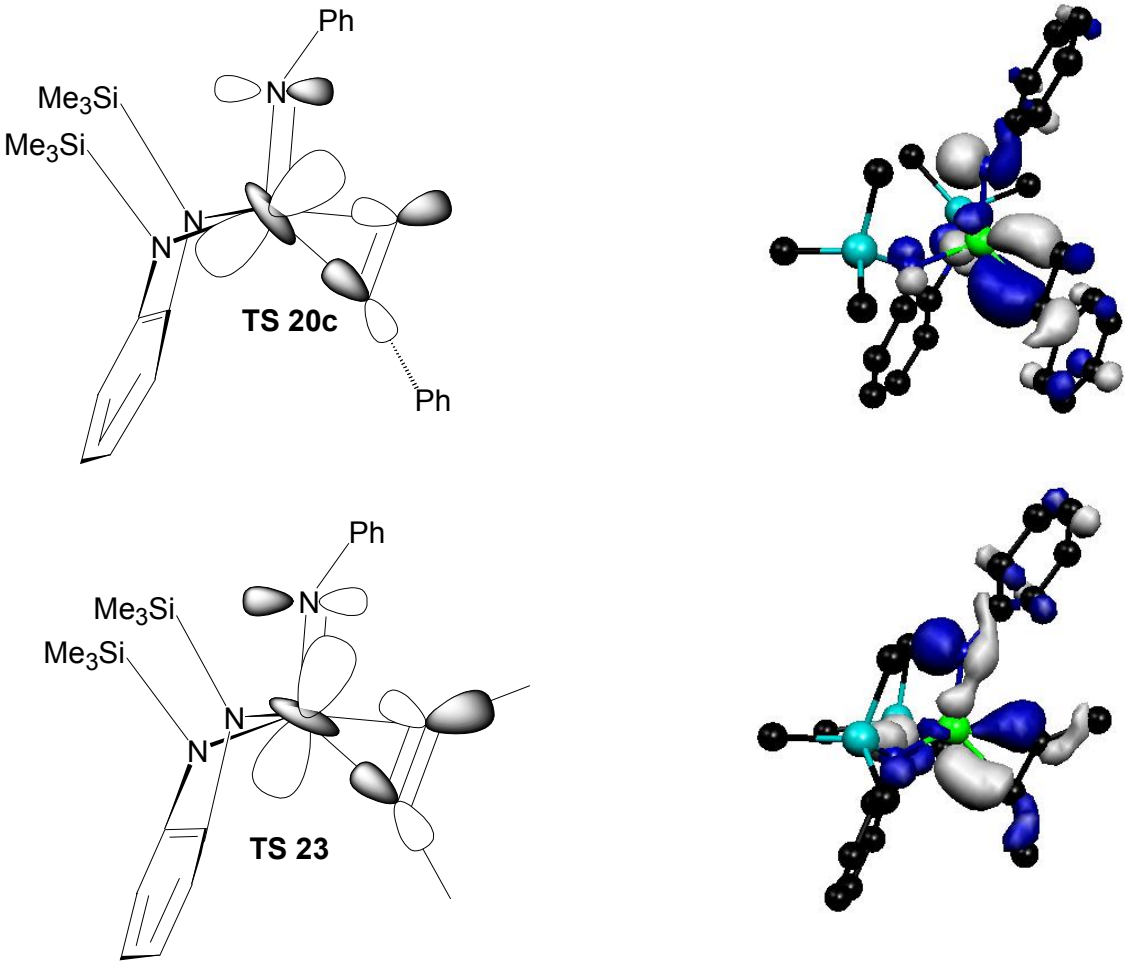

Figure 2-8. HOMO of **TS23** and **TS20c** showing π backbonding of the metal fragment to the olefin.

The weakening of the Mo—N(Imido) bonds is confirmed by an NBO analysis(Table 2-5). The covalent bond orders for the imido bond are clearly smaller in the TS. Further, the NBO representation of the imido bond reveals that the delocalization of π_2 onto Mo is much less in the TS(7.3), than in **6**(18.2), i.e., the lone pair on the imido ligand is more greatly polarized toward the nitrogen atom of the imido ligand when the olefin is oriented parallel to the imido ligand (85.7%) than when the olefin is oriented perpendicular to the imido ligand.

Table 2-5. NBO analysis of the Mo—N(Imido) bond in **20c**

Model	Bond Type	%Mo	%N	Occupancy	Covalent Bond order
20c	σ	34.1	66.0	1.96	
	π_1	35.0	65.3	1.90	0.99
	π_2	18.2	76.2	1.64	
TS 20c	σ	35.2	64.8	1.88	
	π_1	30.6	69.4	1.79	0.88
	π_2	7.3	85.7	1.73	

These results demonstrate that *cis* perpendicular orientation of π ligands is the most stable in these systems as this orientation maximizes the stabilization of the metal center arising from the imido ligand. Orientation of these ligands parallel to this bond generates interactions that result in the weakening of the Mo—Imido bond.

Diamide Ligand Folding in d^2 vs d^0 Group 6 Imido Complexes

Computational and structural studies on d^0 diamide imido complexes have demonstrated the importance of diamide lone pair donation in the bonding in these complexes. In these structures, the diamide lone pair electrons are donated to an empty metal d orbital of appropriate symmetry through concerted torsion of the sp^2 nitrogens in order to achieve effective lone pair p—d overlap. This torsion results in the folding of the *o*-pda ligand as depicted in Table 2-6.

It is evident from Table 2-6 that there is a distinct correlation between the fold angle of the diamide ligand and the oxidation state of the metal. In the d^0 dialkyl complexes like the metallcyclopentane complex **25**, the diamide ligand is considerably folded. As shown in Table 2-6, in the alkyne complex **21f**, and the alkene complex **20c**, the diamide ligand folds to an extent that is comparable to **25**. This occurs because there is significant π back bonding in these complexes, and they are best described as d^0 metallacyclopropene and metallcyclopropane complexes respectively (*vide supra*).

The folding of the diamide ligand is minimized in the d^2 complexes, [*cis*-(pyridine)$_2$Mo(NPh)-*o*-(Me$_3$SiN)$_2$C$_6$H$_4$}, **44**, [*cis*-(2,6-dimethylphenyl isocyanide)$_2$Mo(NPh)-*o*-(Me$_3$SiN)$_2$C$_6$H$_4$}, **30b**, and [η^4-(butadiene)Mo(NPh)-*o*-(Me$_3$SiN)$_2$C$_6$H$_4$}, **24**. The synthesis and characterization of **24** and **44** has been reported whilst the synthesis of **30b** is discussed in chapter 4. However, it is clear from Table 2-6, electronic properties of the metal prevent diamide folding in complexes in the Mo(IV) oxidation state.[30,31,48,49,75,76]

Table 2-6. Fold angles for some Mo Imido Diamido Complexes

Molecule	Fold Angle^0
[η^2-(2-butyne)Mo(NPh)-*o*-(Me$_3$SiN)$_2$C$_6$H$_4$}, **21f**	133.0
[η^2-(styrene)Mo(NPh)-*o*-(Me$_3$SiN)$_2$C$_6$H$_4$}, **20c**	129.2
Mo(NPh)(*o*-(Me$_3$SiN)$_2$C$_6$H$_4$)(CH$_2$)$_4$, **25**	132.5
[η^4-(butadiene)Mo(NPh)-*o*-(Me$_3$SiN)$_2$C$_6$H$_4$}, **24**	167.8
[*cis*-(pyridine)$_2$Mo(NPh)-*o*-(Me$_3$SiN)$_2$C$_6$H$_4$}, **44**	175.5
[*cis*-(2,6-dimethylphenyl isocyanide)$_2$Mo(NPh)-*o*-(Me$_3$SiN)$_2$C$_6$H$_4$}, **30b**	173.7

In order to investigate the electronic origin of this phenomenon we compared the molecular orbitals of the alkyne complex **23** with the model butadiene complex **24**. The model compound **24** was again optimized using the ONIOM method as described earlier.

There was good agreement between the calculated metric parameters of **24** and the reported X-ray crystal structure of **24**.[48]

The structure and bonding of *cis*-butadiene complexes can vary between two extremes, the π^2 and the σ^2, π-designations (Scheme 2-6). The bonding in π^2 complexes is best described by a synergistic model i.e., the ligand acts as a σ donor, as well as a π acceptor, as the metal donates a pair of d electrons in the ligand's π^* orbital. In σ^2, π-type complexes, the butadiene ligand is considered a dianionic dialkyl, a result of considerable back bonding. The oxidation state of the transition metal, as well as, the ancillary ligands of the complex, dictates which structure type will be adopted. In the Boncella labs butadiene complexes of both W and Mo have been synthesized. The butadiene complex of Mo, **24**, may be best described as π^2 d^2 Mo(IV) complex. In contrast, the corresponding complex with W may be described with a σ^2, π designation. This is attributable to the greater tendency of 5d transition metals to π back-bond.

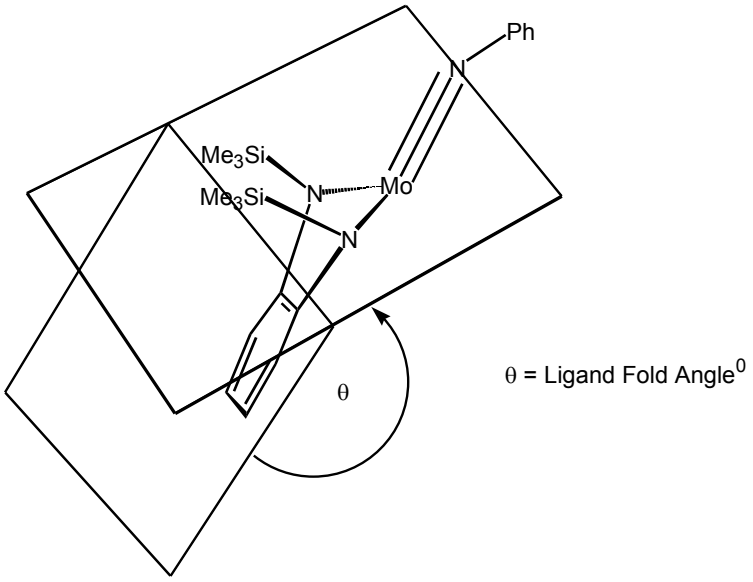

Scheme 2-5. Fold angle in group 6 diamido complexes

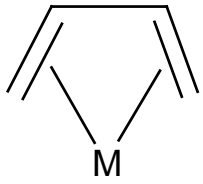

π^2

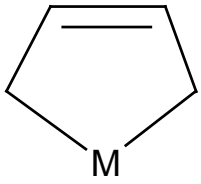

σ^2, π

Scheme 2-6. The π^2 and σ^2, π limiting structures for *cis*-butadiene complexes

Figure 2-9 shows the molecular orbitals for the HOMO and HOMO-2 for **24**. Unlike the d^0 complexes where the diamide lone pair was donated into the $d_{x^2-y^2}$ orbital, this is not possible in this case since this orbital is occupied and is used in π back bonding to the butadiene ligand (HOMO-2). The diamide lone pairs are of the correct symmetry to interact with the d_{z^2} orbital; this is evident in the HOMO. The d_{z^2} orbital is raised in energy by donation from one of the imido lone pair electrons. Therefore, donation by the diamide lone pair electrons into this orbital results in a competition for the available d_{z^2} orbital between the diamide and the imido ligand. This would result in a weakening of the Mo—N(Imido) bond in favor of Mo—N (diamide) bonding. The imido ligand however is a much stronger π donor ligand, thus the Mo—N(Imido) bonding is favored over Mo—N(diamide) bonding. This is clearly evident from the NLMO analysis (Table 2-7). The diamide lone pairs n_1 and n_2 are only slightly delocalized unto Mo (1.81 and 0.99% respectively). In contrast, the delocalization of these lone pair electrons onto Mo in **21** is significantly greater (8.2 and 7.4% respectively). The Mo—N(Imido) bond is slightly weaker in **24** (bond order 0.93) than in **23** (0.95). However the bonds in the imido bond are polarized towards nitrogen to a greater extent than in the d^0 alkyne complex.

Table 2-7.NLMO analysis of Mo—N(Imido) and Mo—N(Diamide) bonds in **23** and **24**

Model	Bond Type	%Mo	%N	Occupancy	Covalent Bond order[b]
24					
Imido	σ	19.3	80.7	1.88	
	π_1	19.7	80.3	1.82	0.93
	n	16.5	78.6	1.64	
Diamide	n_1	1.81	81.4	1.64	0.50
	n_2	0.99	81.8	1.64	
23					
Imido	σ	26.2	73.8	1.97	
	π_1	22.1	77.9	1.76	0.95
	π_2	31.6	68.4	1.83	
Diamide	n_1	8.2	82.7	1.67	0.50
	n_2	7.4	83.3	1.68	

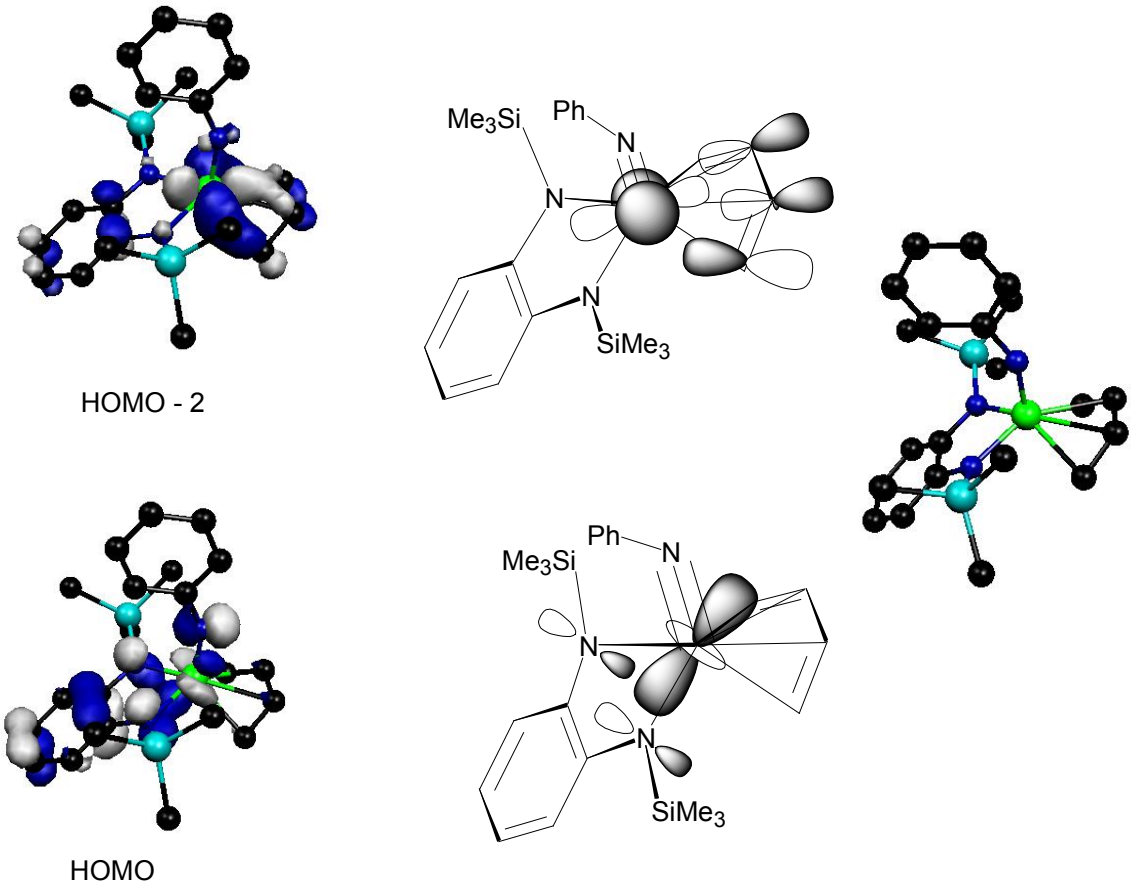

Figure 2-9. Occupied molecular orbitals of **24**

Conclusions

The results presented in this chapter clearly demonstrate the importance of π donor interactions by both the diamide and imido ligands in our complexes. These interactions contribute greatly to the stability of our complexes in that they stabilize the highly electropositive metal centers. Competition for available metal d orbitals can lead to reactivity of these complexes and as is demonstrated in later chapters, this reactivity may either be metal centered or ligand centered. These data suggest that the reactivity of these complexes can be carefully modulated by the judicious choice of ancillary ligands.

CHAPTER 3
SYNTHESIS AND REACTIVITY OF GROUP 6 IMIDO DIAMIDO METALLACYCLES

Introduction

Metallacyclopentane complexes were originally observed in our labs as species that result from the deactivation of W(VI) alkylidenes in olefin metathesis reactions.[34] Since these initial studies we have been able to successfully isolate and characterize metallacyclopentane complexes of W and Mo by more direct methods.[34,46,74] Group 6 imido metallacyclopentane complexes are quite rare, and our complexes are unusual in that their inherent stability towards decomposition by either β hydrogen elimination/abstraction or β carbon-carbon bond cleavage allows them to be readily isolated and characterized.

Schrock and co-workers have also observed group 6 imido metallacyclopentane complexes that resulted from the decompostion of alkylidene species. [73,77] These complexes however lacked the inherent stability of those seen in our group and decompose via β hydrogen transfer resulting in the formation of butene. The fundamental difference in our complexes and the complexes studied in the Schrock group is the chelating ancillary ligand. As discussed in the previous chapter, the diamide ancillary ligand, $\{o\text{-}(Me_3SiN)_2C_6H_4\}^{2-}$, is crucial in stabilizing the high oxidation state of the metal by π donation of the diamide lone pairs. The stabilization via π donation is not afforded by the alkoxide ligands in Schrock's metathesis catalysts, as they possess

electron-withdrawing substituents on the alkoxide ligand in addition to the fact that the more electronegative O atom is less likely to donate its lone pair electrons.[35,36,43 73,78,79]

In this chapter, we examine the chemistry of the metallacyclopentane complex, Mo(NPh)(*o*-$(Me_3SiN)_2C_6H_4$)$(CH_2)_4$**, 25**. We begin examining the synthesis of metallacyclopentene complexes by the sequential π ligand exchange of ethylene from the metallacyclopentane complex with an alkyne. We also examine the synthesis of metallacyclopentadiene complexes by the [2+2] cycloaddition reactions of two alkyne moieties. The thermal rearrangements of **25**, are also examined by kinetics and DFT using small models as well as larger (experimentally exact) systems with quantum (B3LYP) and hybrid methods (ONIOM), respectively. We examine the role that diamide π donation plays in influencing the reactivity of these complexes.

Synthesis and Reactivity of Mo Imido Diamido Metallacyclopentenes and Metallacyclopentadienes

Transition metal metallacycles have been implicated as important species in many catalytic and stoichiometric conversions of organic fragments. One such process is the metal mediated cyclooligomerization reaction of alkynes. In the well-known mechanism for this reaction, metallacyclopentenes, metallacyclopentadienes, as well as alkyne and arene complexes have been cited as key intermediates.[80,55] Recent research in this field has focused on stereoselectively controlling the products of the cyclooligimerization reaction. This has been achieved by developing ligand sets that promote highly selective carbon-carbon bond forming reactions in which low valent transition metals mediate the formation of metallacycles from saturated organic substrates. Takahashi,[72,81-84] and Ladipo[85,86] have utilized this chemistry in the synthesis of substituted arenes, pyridines, and other useful organic molecules. In Takahashi's work, the preparation of

multisubstituted benzene and pyridine derivatives was achieved in a one pot synthesis by the use of unsymmetrical metallacyclopentadienes obtained from the intermolecular cross coupling reaction of two different alkynes, and the subsequent treatment with a third alkyne, or nitrile, in the presence of CuCl or $Ni(PPh_3)_2Cl_2$. The development of methodologies that would afford the stereoselective synthesis of metallacycles is an important area of research and warrants further study.

A method for the synthesis of olefin complexes, from Mo(NPh)(*o*-$(Me_3SiN)_2C_6H_4)Cl_2(THF)$ **4**, was recently developed in our labs[30,31] and the tendency of these complexes to form metallacycles has been demonstrated.[34,46] In exploring the reactivity of these complexes, we became interested in developing the chemistry of group 6 metallacycles containing imido and *bis*-amido chelating ligands because of the potential importance of these compounds in organic synthesis.[87] [81,82,84,88]

Synthesis of metallacyclopentene complexes

Heating a toluene solution of the metallacyclopentane complex **25** at 80^0C with one equiv of an alkyne results in the synthesis of the metallacyclopentene complex **26** (Scheme 3-1). The reaction with phenyl acetylene results in a 1:4 mixture of the two regioisomers **26a** and **26b**. The phenyl substituent in the metallacycle in **26a** is in the α position whilst the phenyl substituent in **26b** is in the β position.

The equilibrium between metallacyclopentanes and *bis*-ethylene complexes has been extensively studied.[89-92] It has been demonstrated in our labs that heating the metallacyclopentane complex **25**, in the presence of a Lewis base (PMe_3) results in the formation of the ethylene complex **27** as a phosphine adduct (Scheme 3-2).[34,46] These

results demonstrate that **25**, is a precusor to the ethylene complex **25a**, and that this complex can be trapped in the presence of Lewis bases.

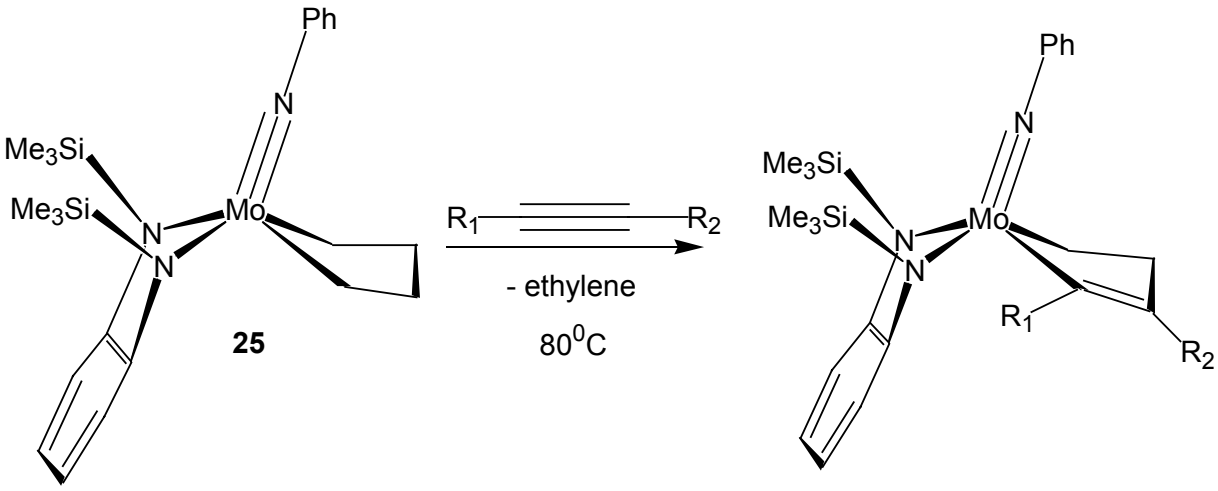

26a. R_1= Ph R_2= H
26b. R_2 = H R_2= Ph
26c. R_1= CO_2Et R_2= CO_2Et

Scheme 3-1. Synthesis of metallacyclopentene complexes

Complex **25a**, can also be generated from the dichloride complex **1**, and ethyl magnesium chloride as outlined in Scheme 3-3. Again this ethylene complex can be trapped in the presence of donor ligands such as PMe_3 and acetylenes. This strategy was employed to synthesize **26b** as a single isomer. The resonances for the metallacycle fragment for this compound were observed as eight line patterns at 3.70, 3.38(2H overlapping) and 1.35ppm in the ^{1}H NMR spectrum. The vinylic proton from the acetylene ligand was observed downfield at 8.47ppm. In addition two peaks were observed for the $SiMe_3$ resonances at 0.43 and 0.40ppm.

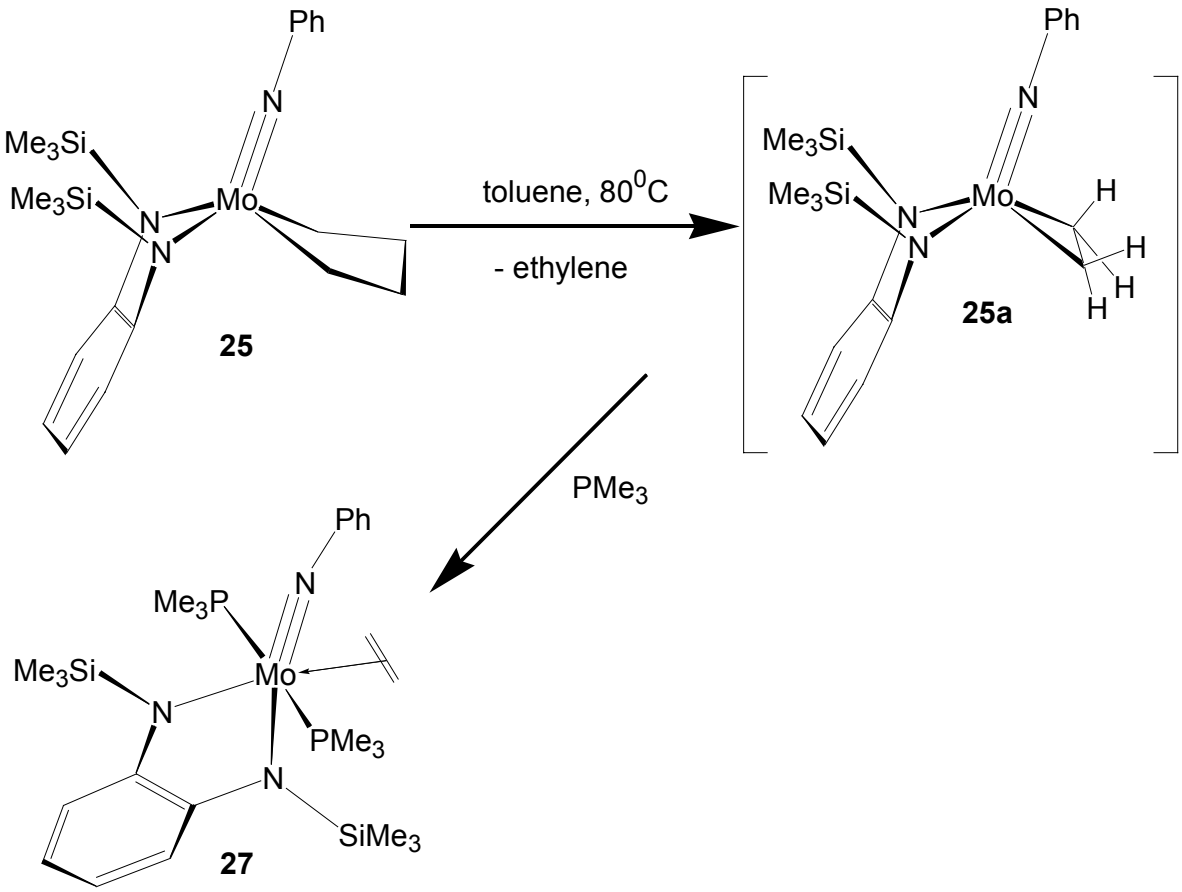

Scheme 3-2. Lewis base generation of olefin *bis*-PMe_3 olefin complex **27**

The strategy employed in Scheme 3-3 takes advantage of the steric environment around the metal central center to promote the stereoselective formation of the metallacycle. Phenyl acetylene adds to **25a**, in a manner that minimizes interaction between the phenyl substituent and the bulky $SiMe_3$ group. This results in the phenyl substituent of the acetylene ligand bonding preferentially β to the Mo center.

Similarly, complex **26a** can be isolated as a single isomer by taking advantage of the steric environment around the metal center. As outlined in Scheme 3-4, exposure of the phenyl acetylene complex, **28**, generated *in situ,* from the isobutylene complex **20a**, to ethylene results in the isolation of **26a**. The resonances for the metallacycle fragment of **26a** are observed at 3.31, 3.06, 3.98 and 1.34 ppm in the ^1H NMR spectrum. The

vinylic proton is observed as a broad singlet at 6.87ppm. Resonances for the $SiMe_3$ protons are observed as singlets at –0.06 and 0.32ppm.

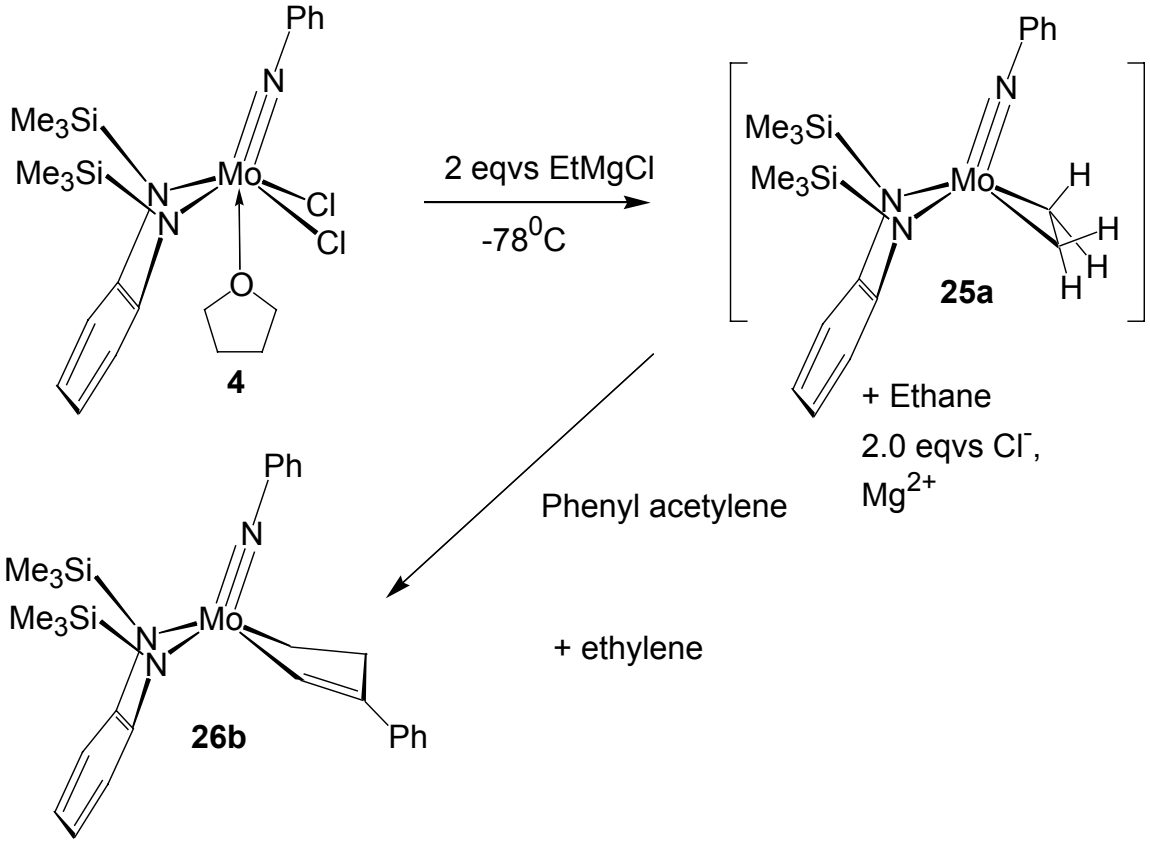

Scheme 3-3. Synthesis of **26b**

X-ray crystal structure of **26b**. The identity of **26b** was also confirmed by X-ray diffraction analysis. X-ray quality crystals were obtained by slow evaporation of a diethyl ether solution of **26b**. Figure 3-1, shows the thermal ellipsoid plot of **26b**. Complex **26b**, exhibits a pseudo square pyramidal structure with the imido ligand occupying the apical position of the square pyramid. The Mo—N(1) bond length of 1.731(2) Å, is comparable to Mo—N lengths in similar complexes. The bond lengths in the metallacycle confirm the predicted arrangement of double and single bonds i.e the arrangement of two long C—C bonds (C(20)—C(21) 1.504(3) Å, and C(21)—C(22) 1.531(3) Å), and one short C—C bond (C(19)—C(20) 1.344(3) Å) confirms the

metallacyclopentene description for this complex. As described for d^0 dialkyl complexes of this type, the diamide ligand is substantially folded (fold angle =135.6^0) and as discussed in the previous chapter, this has been ascribed to donation of the diamide lone pair electrons into a metal d orbital of appropriate symmetry.

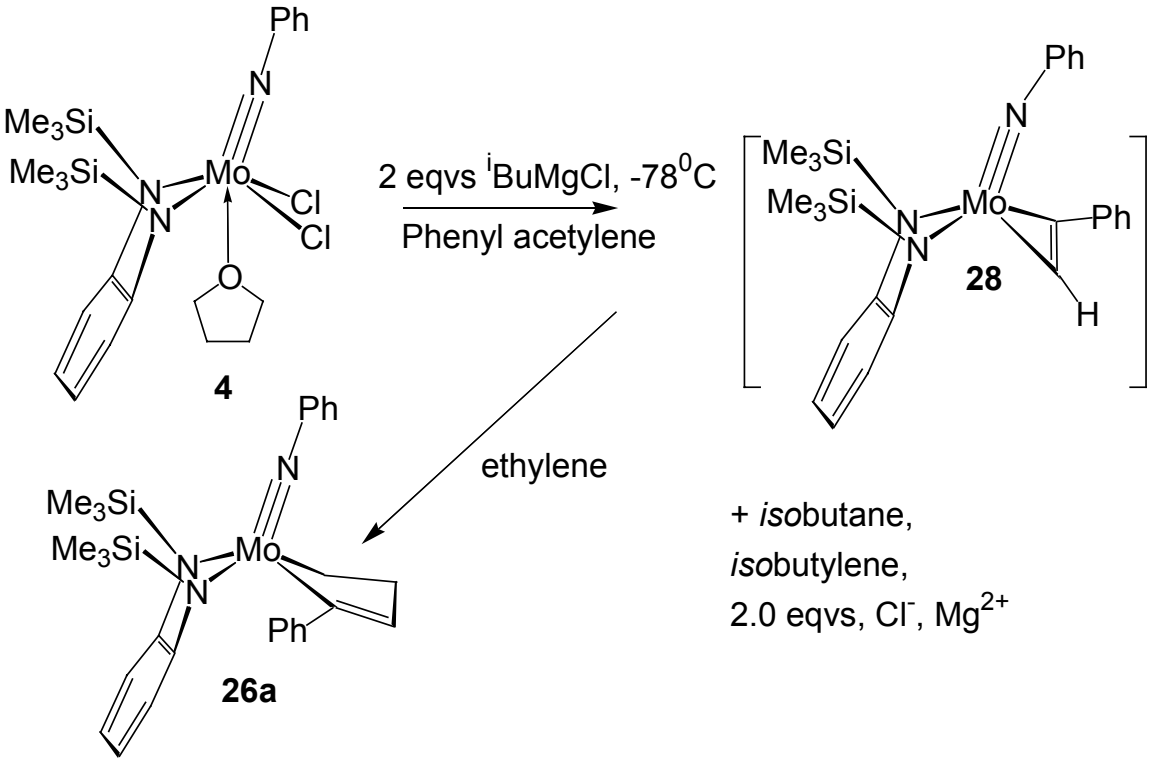

Scheme 3-4. Synthesis of **26a**

Kinetics and Mechanism of the Thermal Rerrangement of **25**

The observation that heating the metallacyclopentane complex, **25**, can induce β C—C bond cleavage of the metallacycle and the elimination of ethylene is consistent with the observation that metallacyclopentane complexes may exist in equilibrium with a *bis*-ethylene species as depicted in Scheme 3-5.

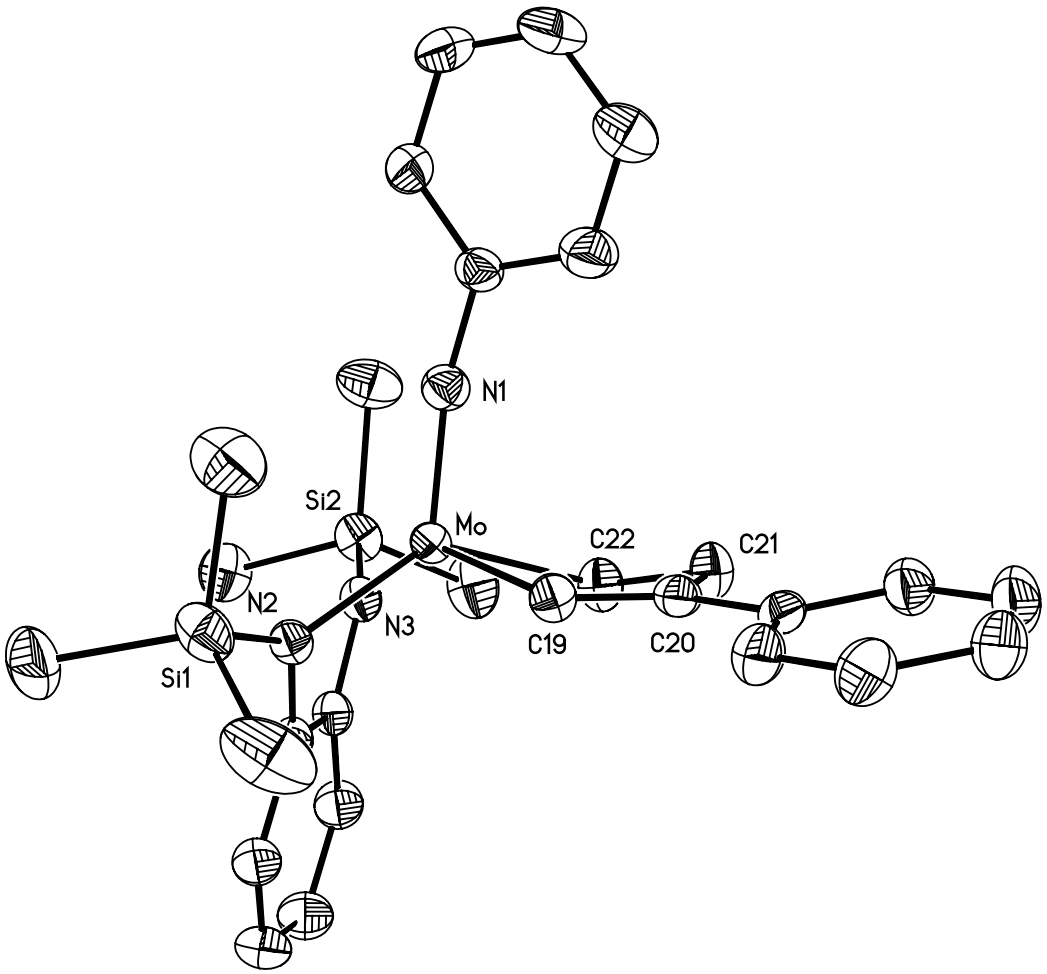

Figure 3-1. Thermal ellipsoid plot of **26b** (50% probability thermal ellipsoids), selected bond lengths (Å): Mo—N (1) 1.7305, Mo—C (19) 2.1520 (2), Mo—C (22) 2.175 (2), C (19)—C (20) 1.344 (3), C (20)—C (21) 1.504(3), C (21)—C (22) 1.531(3).

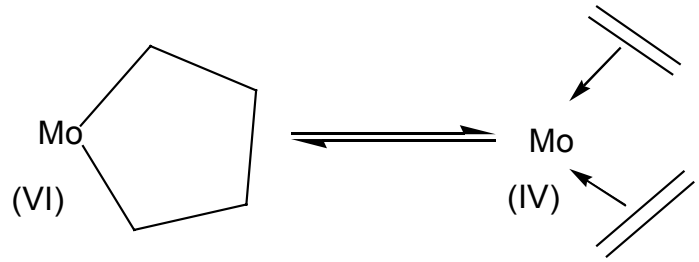

Scheme 3-5. Equilibrium between metallacyclopentane species and *bis*-ethylene species

The reaction depicted in Scheme 3-5 represents a formal reduction of the Mo center by two electrons as β C—C bond cleavage reduces the metal center from Mo(VI) to

Mo(IV). The synthesis of complexes **26** and **27** in Schemes 3-2 to 3-4, suggest that heat is required in order to induce β C—C bond cleavage of the metallacyclopentane. This implies that the equilibrium depicted in Scheme 3-5 lies largely towards the metallacyclopentane species. In order to confirm the existence of this equilibrium, and to clarify the mechanism of π ligand exchange in these metallacyclopentane complexes, we undertook kinetic studies for the reactions of **25** with diethyl acetylene dicarboxylate (DEAD).

The kinetics of the thermal disruption of the metallacycle of **25**, in C_7D_8 were examined by following the disappearance of the $SiMe_3$ peaks of the starting material using ^1H NMR spectroscopy in the presence of excess DEAD. The data points were obtained by plotting the value of the intergral for this peak with respect to time for more than three half-lives.

Activation parameters for the conversion of **25** to **26c** were determined by reacting C_7D_8 solutions (0.020M) of **25** with DEAD (1.40M) in the NMR probe at temperatures between 335 and 356K (three samples at each temperature). The disappearance of **25** follows first order kinetics (Figure 3-2) with a rate constant at 342K of $k = 3.3 \times 10^{-4}\ s^{-1}$ ($t_{1/2} = 2.1 \times 10^3$ s). The reaction rate is independent of the concentration of DEAD (Table 3-1). The energy of activation, $\Delta G^{\ddagger}$, corresponds to17.5 Kcal/mol at 342K. Activation parameters (Figure 3-3) obtained from an Eyring plot($\Delta S^{\ddagger} = R[(\text{intercept}) - 23.76]$; $\Delta H^{\ddagger} = -R(\text{slope})$), for the formation of **26c** from **25** are $\Delta H^{\ddagger} = 20.5(1.0)$ Kcal/mol and $\Delta S^{\ddagger} = -14.7(3.0)$ cal·(mol·K)$^{-1}$.

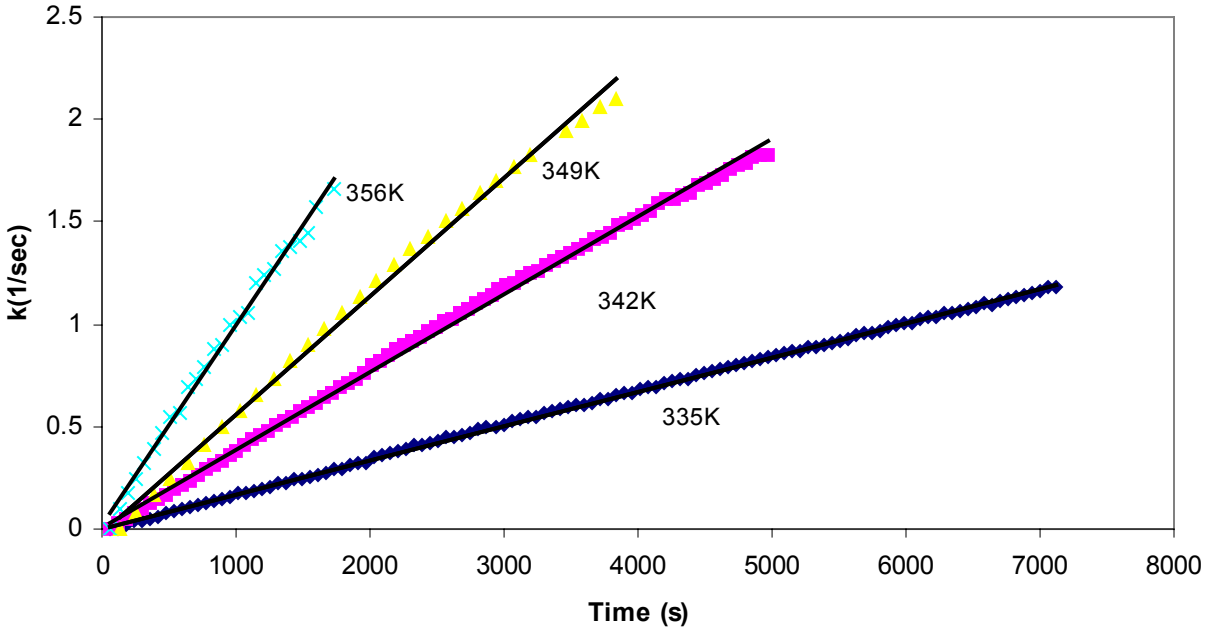

Figure 3-2. First order kinetics for the formation of **26c**

Table 3-1. Dependence of DEAD on the formation of **26c**

[DEAD]/M	Rate k(sec^{-1}) X 10^4
0.974	3.19(4)
1.44	2.86(8)
1.99	2.98(3)
2.60	2.98(11)

The observation that the formation of **26c** does not depend on the concentration of substrate is consistent with the proposed decomposition of the metallacyclopentane fragment via β C—C bond cleavage to a *bis*-ethylene species pior to the rate determining step. The relatively large positive activation barrier $\Delta H^{\ddagger}$, and a negative entropy of activation, $\Delta S^{\ddagger}$, is consistent with a multi-step mechanism, where the metallacyclopentane rearranges and the alkyne binds to this new species (*bis*-ethylene) prior to the loss of ethylene. The observed value for $\Delta S^{\ddagger}$ is a combination of the metallacycle rearrangement steps and the binding of DEAD to the activated complex.

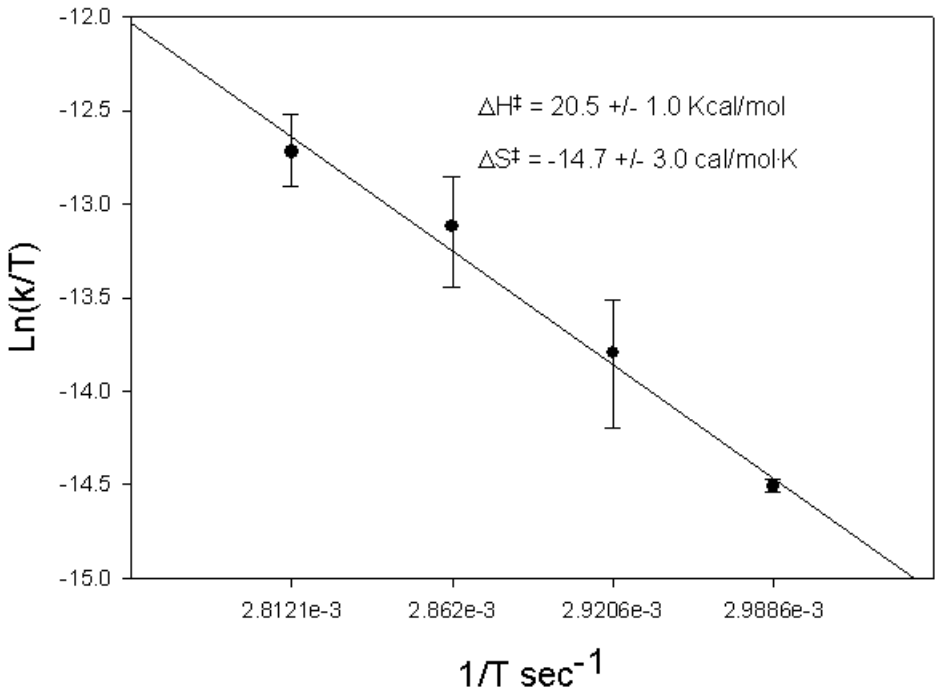

Figure 3-3. Eyring plot for the reaction of **25** with DEAD

Computational Studies on the Thermal Rearrangement of **25**

The synthesis of the metallacyclopentane complex **25**, has been reported, however, X-ray structural studies on this compound were not performed at that time. We were interested in the solid-state structure of this complex and an X-ray study was performed on a single crystal of **25** grown from a concentrated pentane solution at -30^0C. The thermal ellipsoid plot of **25** is depicted in Figure 3-4.

Complex **25**, crystallizes with a pseudo square pyramidal structure with the imido ligand occupying the apical position. The Mo—N(1) bond (1.728Å) is within the normal range for a Mo—N triple bond. The Mo—diamide bonds, Mo—N(2) and Mo—N(3), (2.010 and 2.015Å) are also within the normal range for Mo—C single bonds. The Mo—C(13) and Mo—C(16) bonds (2.187Å and 2.191Å) are typical of Mo—N single bonds.

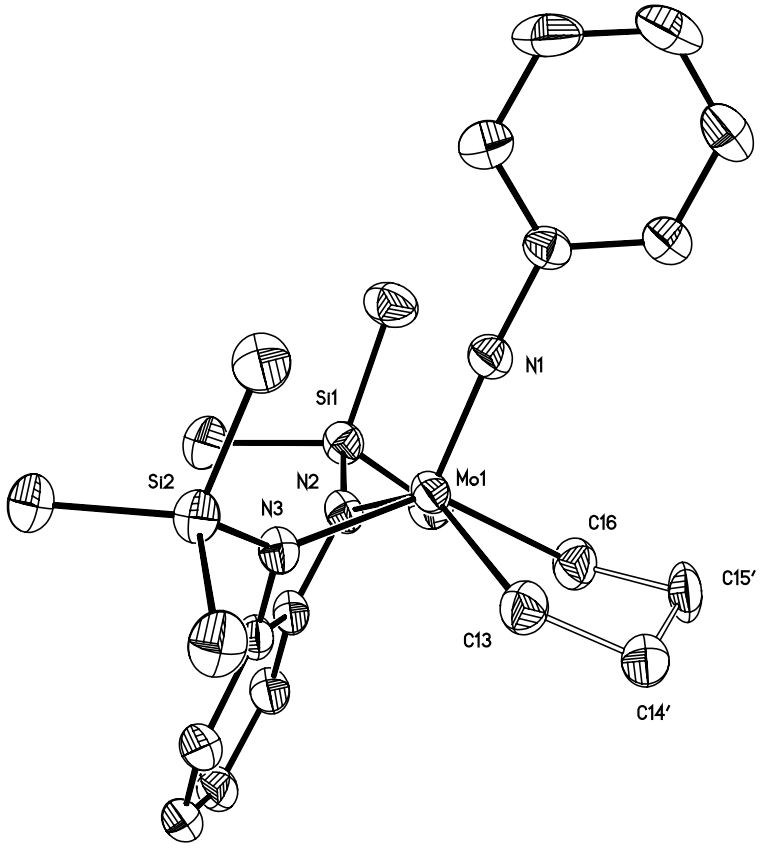

Figure 3-4. Thermal ellipsoid plot of **25**, (50% probability thermal ellipsoids), selected bond lengths (Å): Mo(1)—N(1) 1.728(2), Mo(1)—N(2) 2.010(2), Mo(1)—N(3) 2.015(2), Mo(1)—C(13) 2.187(2), Mo(1)—C(16) 2.191(2)

Although the equilibrium between metallacyclopentanes and *bis*-ethylene species has been observed in the past, we have not, until now, been able to confirm that such a process occurs in our systems since no *bis*-ethylene species has been detected. We therefore turned to computational chemistry in order to investigate the nature of any intermediates that may form during the thermolysis of **25**. For these studies we employed small models as well as larger (experimentally exact) systems.

In the model system, the *o*-phenylene group (o-C_6H_4) that links the two N atoms of the diamido ligand was simplified to a –CH=CH- carbon chain. The organic groups on the nitrogen atoms ($SiMe_3$ of the amido and phenyl group of the imido) were replaced by hydrogen atoms for simplicity. For this model, the recently developed mPW1K

(modified Perdew-Wang 1 parameter for kinetics) exchange correlation functional of Truhlar and coworkers was employed. This functional was recently shown to yield more reliable barrier heights than other exchange-correlation functionals.[93,94] [62,95]

Using this method, three minima were located on the potential energy surface for rerrangement of the metallacycle fragment in **25** (Figure 3-5). Two of these minima (**25b** and **25c**) possess a pseudo trigonal bipyramidal geometry about Mo. One of the diamide nitrogens is oriented *trans* to the imido ligand. The molecule **25b** can best be described as a trigonal bipyramidal (TBP) metallacyclopentane complex whilst complex **25c** can best be described as a trigonal bipyramidal (TBP) *bis*-olefin complex. We were also able to locate the transition states corresponding to the transformations from **25**-**25b** (**TS 25-25b**) and **25b**-**25c** (**TS 25b-25c**). The relative free energies ΔG^0_{298} (relative to **25**), for these transformations are depicted in Figure 3-6.

In order to obtain a more accurate description of the minima during the thermal rearrangement of **25**, ONIOM calculations were performed on larger experimentally exact systems. For these ONIOM calculations a two-layer system was employed, the inner layer consisted of the model complexes described above in Figure 3-5 and were modeled at the mPW1K/LANL2DZ level of theory. The outer layer consisted of the complete system including all substituents on the diamide and imido ligands and was modeled with the mPW1K/LANL2MB basis set. Optimized structures for the minima obtained from these calculations are depicted in Figue 3-7. Unfortunately, all attempts at attaining optimized structures for the transition states for these molecules using the experimentally exact systems failed to converge once the large $SiMe_3$ groups were introduced. However, because we were able to successfully model these transition states

using the small model system and since we are only interested in a qualitative description of the mechanism for β C—C bond cleavage in these systems the TS's obtained using the small model system will suffice for the purposes of this discussion.

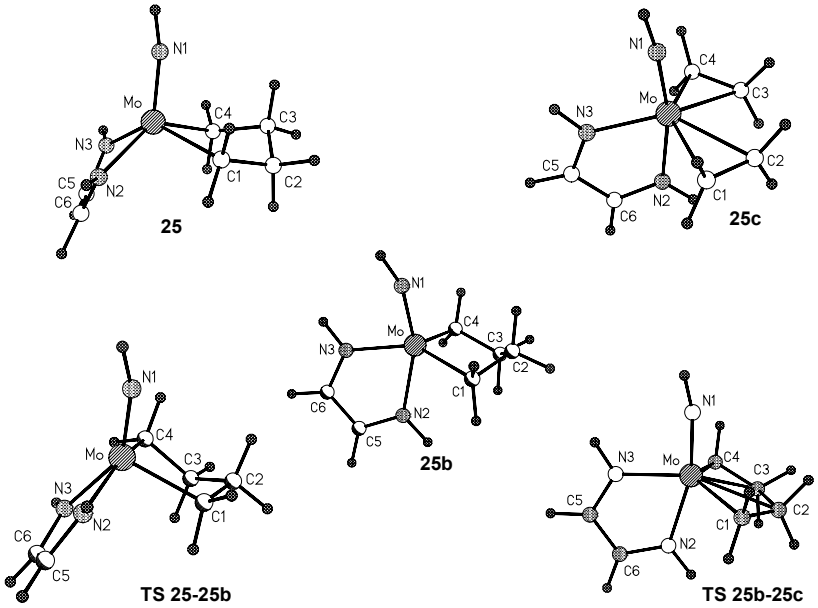

Figure 3-5. Optimized structures (mPW1K/LANL2DZ) for the thermal rearrangement of **25**

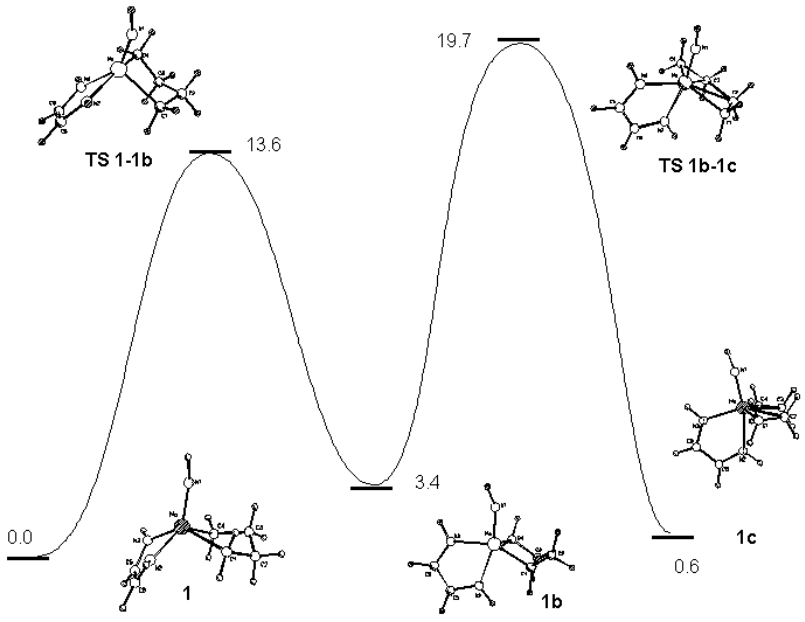

Figure 3-6. Reaction profile ΔG^0_{298} (K) for the thermal rearrangement of **25** at the mPW1k/SDD-Aug-cc-pVDZ level of theory

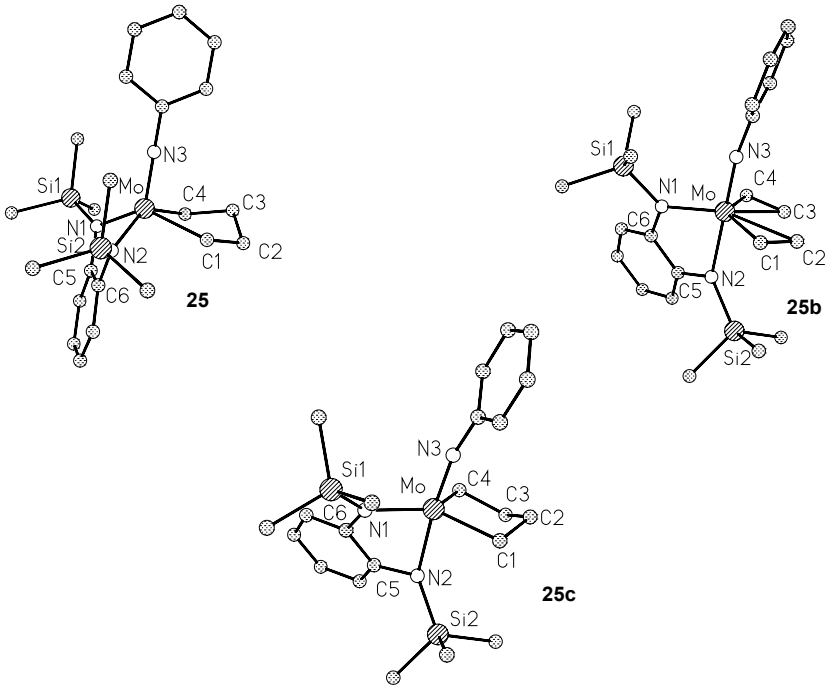

Figure 3-7. ONIOM (mPW1K/LANL2DZ:mPW1K/LANL2MB) optimized structures for the thermal rearrangement of **25**

As shown in Table 3-2 there is good agreement between the calculated structures and the experimentally obtained X-ray structure for **25**. As expected, the ONIOM calculations successfully reproduced the experimentally observed fold angle in **25**. This ligand folding is also seen in the TBP metallacyclopentane complex, **25b** and the TBP *bis*-ethylene complex **25c**. In both TBP species the strong trans influence of the imido ligand results in the lengthening of the Mo—N(2) diamide bond (2.118 and 2.174Å for **25b** and **25c** respectively) relative to the Mo—N(1) bond (1.989 and 2.029Å).

The C—C bond lengths of the ethylene fragment (1.401Å and 1.423Å) in **25c** reflect a significant amount of π back bonding from the metal to the π* orbital of the olefinic fragment. However, these bond distances are shorter than the other olefin complexes seen in our group.[46,74] Further, the M—C (average distance from both carbons of the η^2 ethylene fragment) bond distances of 2.306 and 2.429Å are significantly longer that M—C(olefin) bonds seen in our group. Thus it appears that the

binding of the olefin to the TBP *bis*-ethylene complex **25c** is weaker than other SP olefin complexes seen in our labs. It seems reasonable then, that olefin loss from this molecule will be feasible under the reaction conditions.

Table 3-2. Selected bond lengths (Å) and angles (^{0}) for ONIOM optimized structures for the thermal rearrangement of **25**

Bond	**25**	**25**(X-ray)	**25c**	**25b**
Mo—C(1)	2.213	2.187(2)	2.306*	2.159
Mo—C(4)	2.186	2.191(2)	2.429*	2.132
Mo—N(3)	1.763	1.728(2)	1.798	1.801
Mo—N(2)	2.041	2.015(2)	2.174	2.118
Mo—N(1)	2.032	2.010(2)	2.029	1.989
C(1)—C(2)	1.548	1.544(8)	1.401	1.568
C(2)—C(3)	1.541	1.496(2)	NA	1.577
C(3)—C(4)	1.538	1.563(1)	1.423	1.565
Fold Angle	137.6	132.5	152.4	133.3

* Average M—C distance from both carbons of the η^2 –ethylene fragment

Insight into the nature of the metal—carbon bonds within these complexes can be obtained by inspection of the molecular orbitals. For the bis-ethylene complex **25c**, the metal d orbitals are depicted in Scheme 3-6. The in phase combination of the diamide lone pair electrons is also depicted in this Scheme. This molecule possesses pseudo C_s symmetry with a mirror plane that bisects the diamide chelate and the two ethylene fragments.

The linear combination of diamide lone pairs is of a'' symmetry. .These lone pair electrons are of appropriate symmetry to interact with the d_{yz} and d_{xz} orbitals (see coordinates in Scheme 3-6). However, the energy of these orbitals is perturbed by strong donation from the imido (d_{xz}) and the σ orbitals of the ethylene fragment (d_{yz}). Thus the overlap of the diamide lone pairs with the empty metal d orbitals will not be as significant in this case.

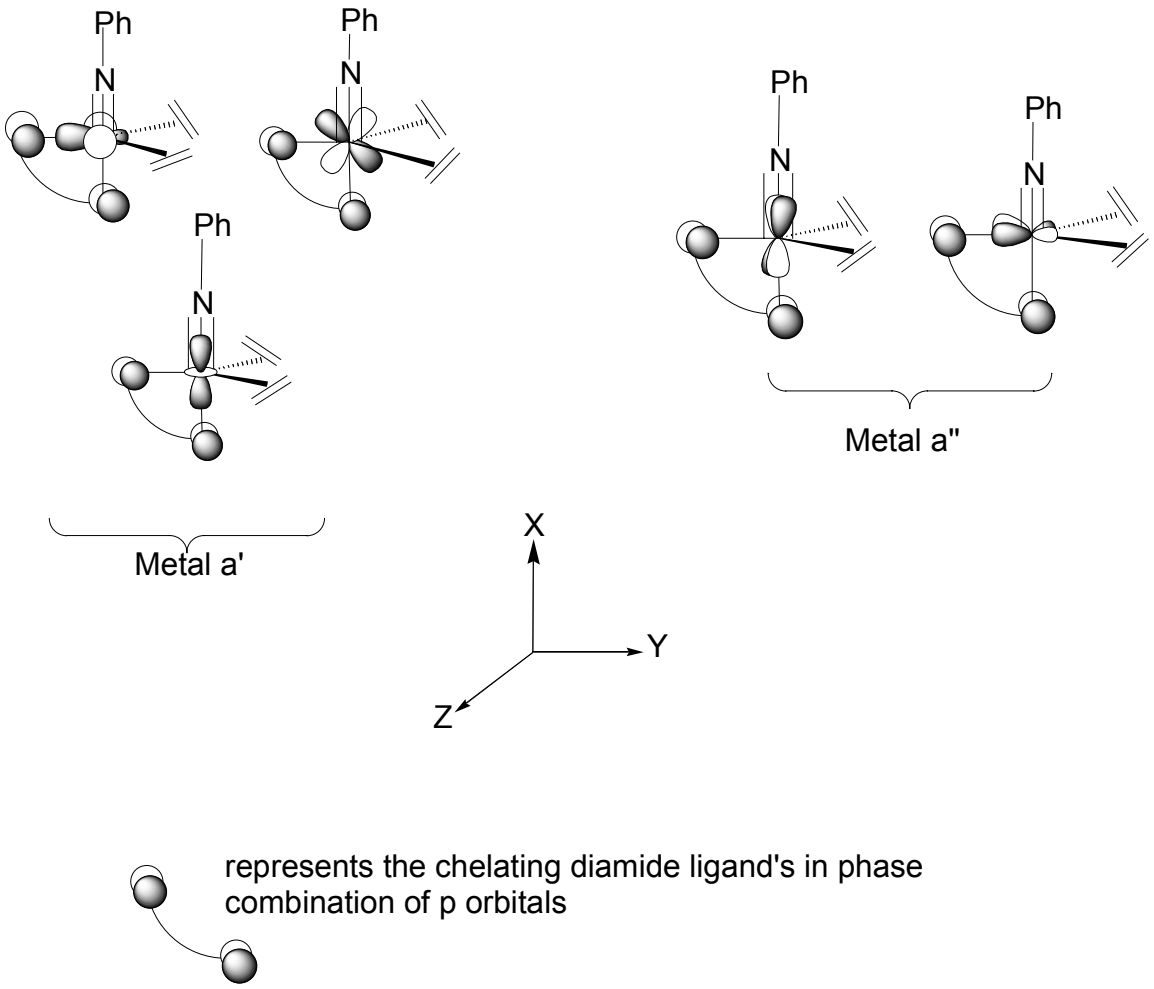

Scheme 3-6. Symmetry adapted orbitals of **25c**.

The diminished importance of diamide π donation is clearly evident by inspection of the occupied molecular orbitals. The highest two occupied molecular orbitals of the SP metallacyclopentane complex **25**, the TBP metallacyclopentane complex **25b**, and the TBP *bis*-ethylene complex **25c**, are depicted in Figures 3-8, 3-9, and 3-10 respectively.

As shown in the HOMO –1 of Figure 3-8, the importance of diamide lone pair donation in the SP metallacyclopentane complex **25**, is clearly evident. As discussed in the previous chapter this π donation is responsible for the folding of the diamide ligand seen in d^0 complexes.

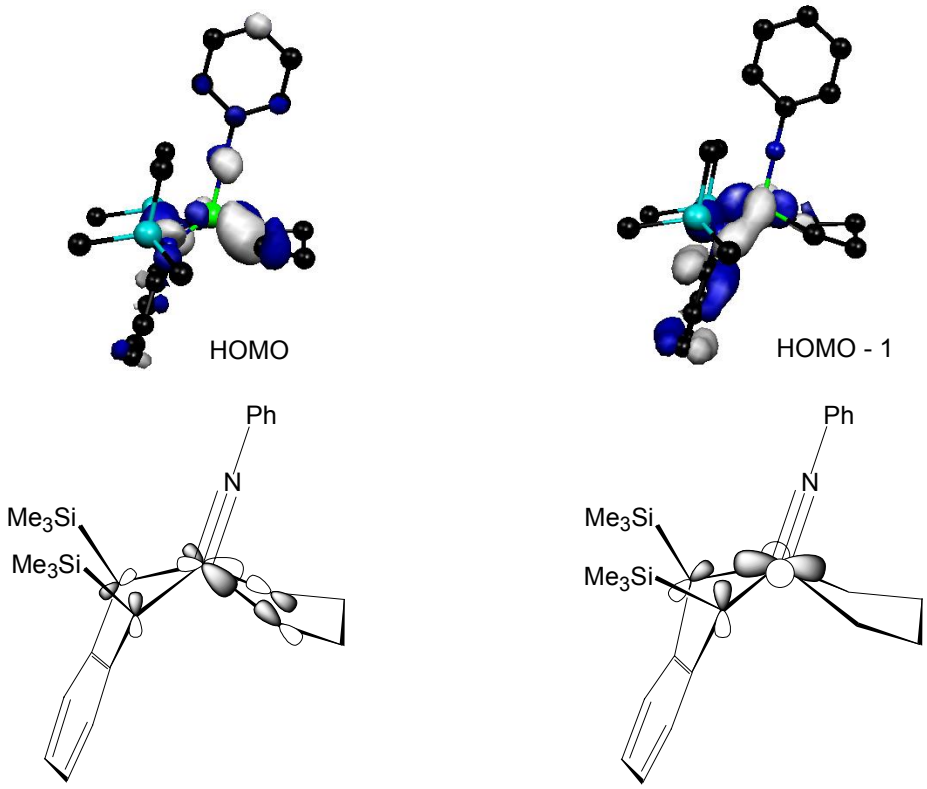

Figure 3-8. Occupied molecular orbitals(B3LYP/LANL2DZ) for **25**

The diminished importance of this interaction is clearly evident in the HOMO and HOMO –1 of the TBP metallacyclopentane complex **25b** (Figure 3-9). The perturbations to the a'' orbitals (d_{xz} and d_{yz} see Scheme 3-6) by the imido and σ orbitals of the metallacyclopentane fragment raises the energy of these orbitals and results in a weaker interaction between the diamide lone pair electrons and the metal d orbitals. The diamide lone pairs remain primarily ligand centered in the HOMO and HOMO-1 orbitals. The fact that the ligand folds quite significantly, (fold angle 133.3^0) suggests that this interaction is not negligible in these complexes, however, the energetics of the interaction are clearly more important in **25** than in **25b**.

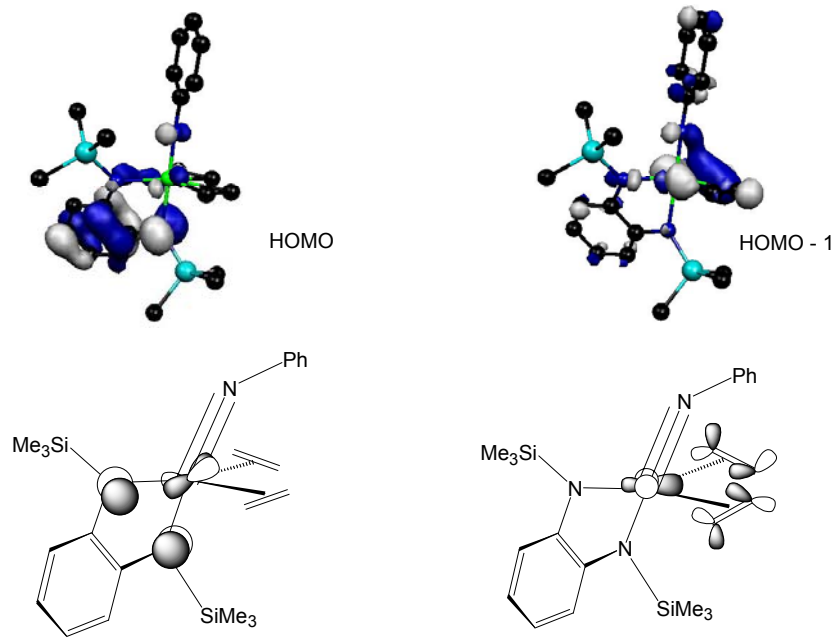

Figure 3-9. Occupied molecular orbitals (B3LYP/LANL2DZ) for **25b**

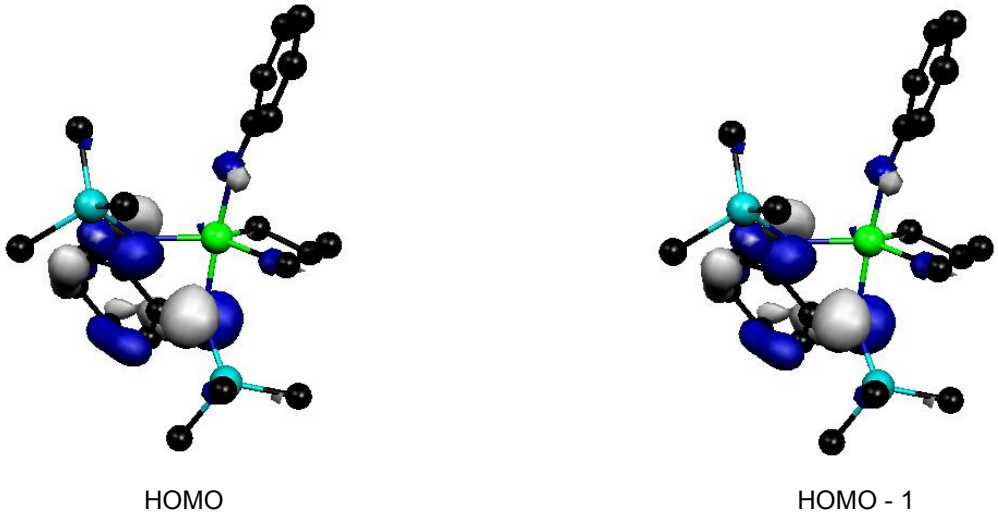

Figure 3-10. Occupied molecular orbitals (B3LYP/LANL2DZ) for **25c**

The diminished importance of diamide lone pair donation is also evident in the HOMO of **25c**. In addition the HOMO –2 shows the ethylene fragments stabilized by π back bonding from the metal to the a linear combination of the π* orbitals of two ethylene fragments (see Scheme 3-6). As mentioned above, **25c** shows lengthened Mo—

C (ethylene) bonds relative to other SP Mo olefin complexes synthesized in our group and is suggestive of a weaker interaction between the metal and ethylene. Decreased π donation by the diamide ligand in these complexes reduces the amount of electron density on the metal that is available for π back bonding and thus there is a reduction in the stabilization of the ethylene ligands in these complexes, in addition to the fact that two ethylene molecules require electron density. Ethylene ligand exchange from **25c**, is therefore possible as the complex can now readily lose a molecule of ethylene as it is less tightly bound in this complex.

These results demonstrate the importance of π ligand donation in stabilizing the high oxidation state of Mo in these complexes. The metallacyclopentane complexes seen in our labs are stable to decomposition by both β-hyrdogen elimination/ transfer reactions and β C—C cleavage of the metallacyclopentane complexes. Rearrangement of the metallcyclopentane from a SP structure to a TBP structure diminishes the M—N(diamide) interactions; as a result β C—C bond cleavage is induced and the complex can react via ethylene exchange.

It is noteworthy that these π ligand exchange reactions are significantly slower for the reactions of the W analogue of **25** with σ and π donors. For example, the reaction of the W metallacyclopentane complex W(NPh)(*o*-$(Me_3SiN)_2C_6H_4$)$(CH_2)_4$, **13,** with PMe_3 proceeds to only 90% completion in 90 days,[34] this is slow in contrast to the facile cleavage of metallacyclopentanes with PMe_3(1 hr) for the Mo complex.[46,74] These results suggests that the barrier for the β C—C bond cleavage and the thermal rearrangement of the W metallacyclopentanes is significantly higher.

Synthesis and reactivity of a metallacyclopentadiene complex.

Our success in synthesizing metallacyclopentenes inspired us to pursue the subsequent synthesis of metallacyclopentadiene complexes. One can envision the formation of metallacyclopentadienes from metallacyclopentenes by the sequential π ligand exchange of an ethylene molecule from a metallacyclopentene as outlined in Scheme 3-7. However, no β C—C bond cleavage of metallacyclopentenes can be induced when **26** is heated at 80^0C in the presence an alkyne for weeks.

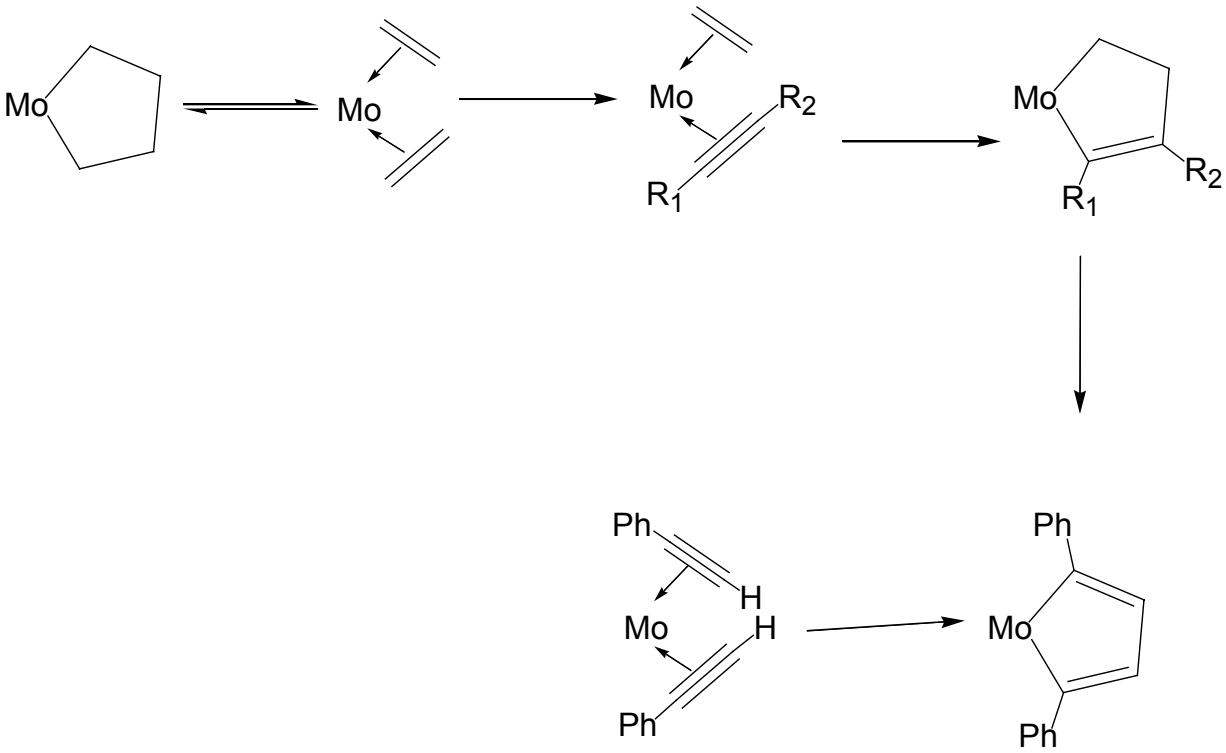

Scheme 3-7. Proposed formation of metallacyclopentadienes from metallacyclopentene complexes. Ancillary ligands have been removed for clarity.

Metallacyclopentadienes can be synthesized however, from the [2+2] coupling reactions of terminal acetylenes. Thus, treatment of a pentane solution of the isobutylene complex, (η^2-isobutylene)Mo(NPh)(*o*-$(SiMe_3N)_2C_6H_4$), **20a** with two equivalents of phenyl acetylene afforded the metallacyclopentadiene complex 2**9**, [(NPh)Mo(C(Ph)CHCHC(Ph))$\{o$-$(Me_3SiN)_2C_6H_4\}$] in 40% yield (Scheme 3-8). The ^{1}H

NMR spectrum of 2**9**, showed a singlet (-0.07ppm, 18H) for the $SiMe_3$ protons. A sharp singlet (6.46ppm, 2H) assigned to the β protons of the metallacycle characterizes the α,α' orientation of the phenyl substituents. An examination of the reaction mixture revealed that small amounts of the α,β and β,β' isomers may also form during the course of this reaction however we were not able to isolate any of these isomers from the reaction mixture and the low yield of these complexes in this reaction prevented their complete spectroscopic characterization.

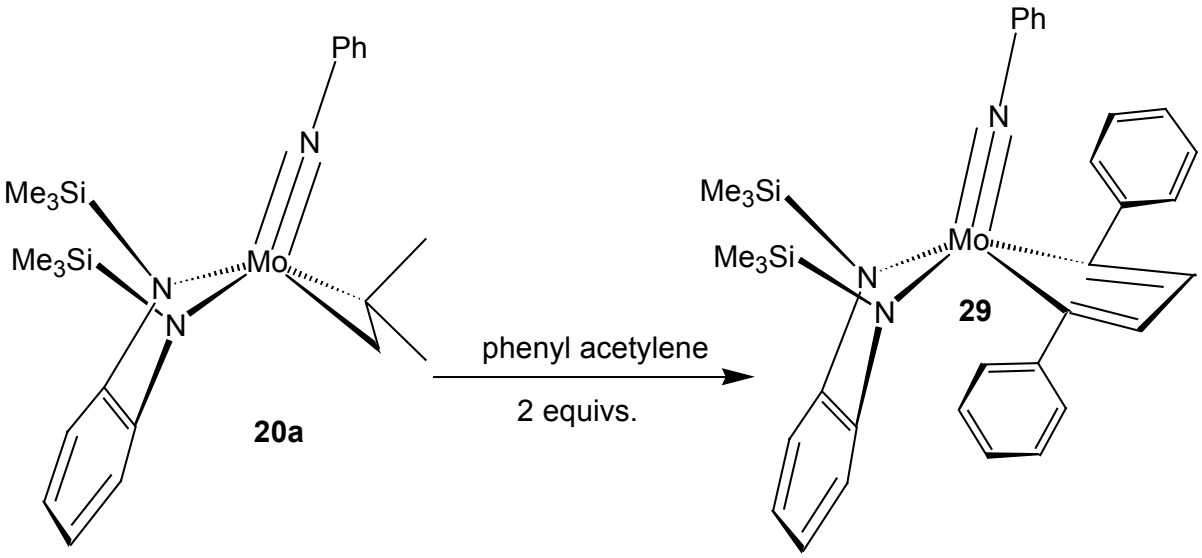

Scheme 3-8. Formation of the metallacyclopentadiene complex **29**

Single crystals of **29**, were obtained from slow evaporation of a concentrated diethyl ether solution (Figure 3-11). Complex **29** was found to have a pseudo square pyramidal geometry in which the imido group occupies an apical position.
The Mo—N(1) bond length is 1.731 Å, is consistent with a metal nitrogen triple bond. The Mo—N(2) and Mo—N(3) bonds (2.008 and 2.004Å) are consistent with Mo—N(diamide) bonds. The Mo—C(22) and Mo—C(19) bonds are with range for Mo—C(sp) bonds. The bond lengths within the metallacycle reflect the localization expected for a metallacyclopentadiene fragment, i.e. two short C—C bonds

(C(19)—C(20) 1.335Å and C(21)—C(22) 1.339Å) and one long C—C bond C(20)—C(21) 1.455Å.

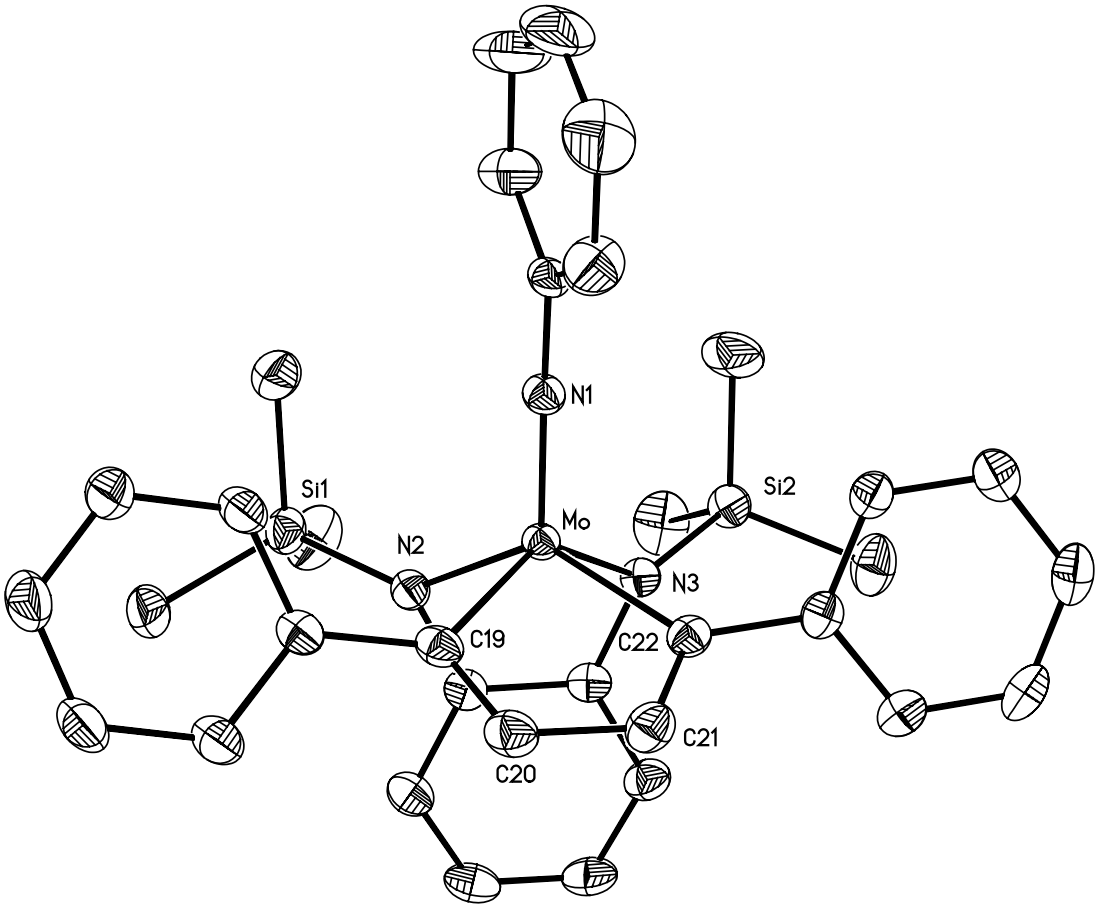

Figure 3-11. Thermal ellipsoid plot of **29**, (50% probability thermal ellipsoids), selected bond lengths (Å): Mo—N (1), 1.731(2), Mo—N(2) 2.008(2), Mo—N(3) 2.002(2), Mo—C (19), 2.197(3), Mo—C (22), 2.188(3), C (19)—C (20), 1.335(4), C (20)—C (21), 1.455(4), C (21)—C (22), 1.339(4).

Metallacyclopentadiene complexes have been implicated as important intermediates in the cyclotrimerization of acetylenes.[81] [78,85,86]When **29** (0.008 mmol) was allowed to react in an NMR tube with excess phenyl acetylene(1.56mmol) at 80^0C for 24hrs, a 50:50 mixture of two cyclotrimerized products, 1,2,4 triphenyl acetylene, and 1,3,5 triphenyl acetylene were produced (Scheme 3-9). We are currently investigating the utility of **29** as a potential cyclotrimerization catalyst.

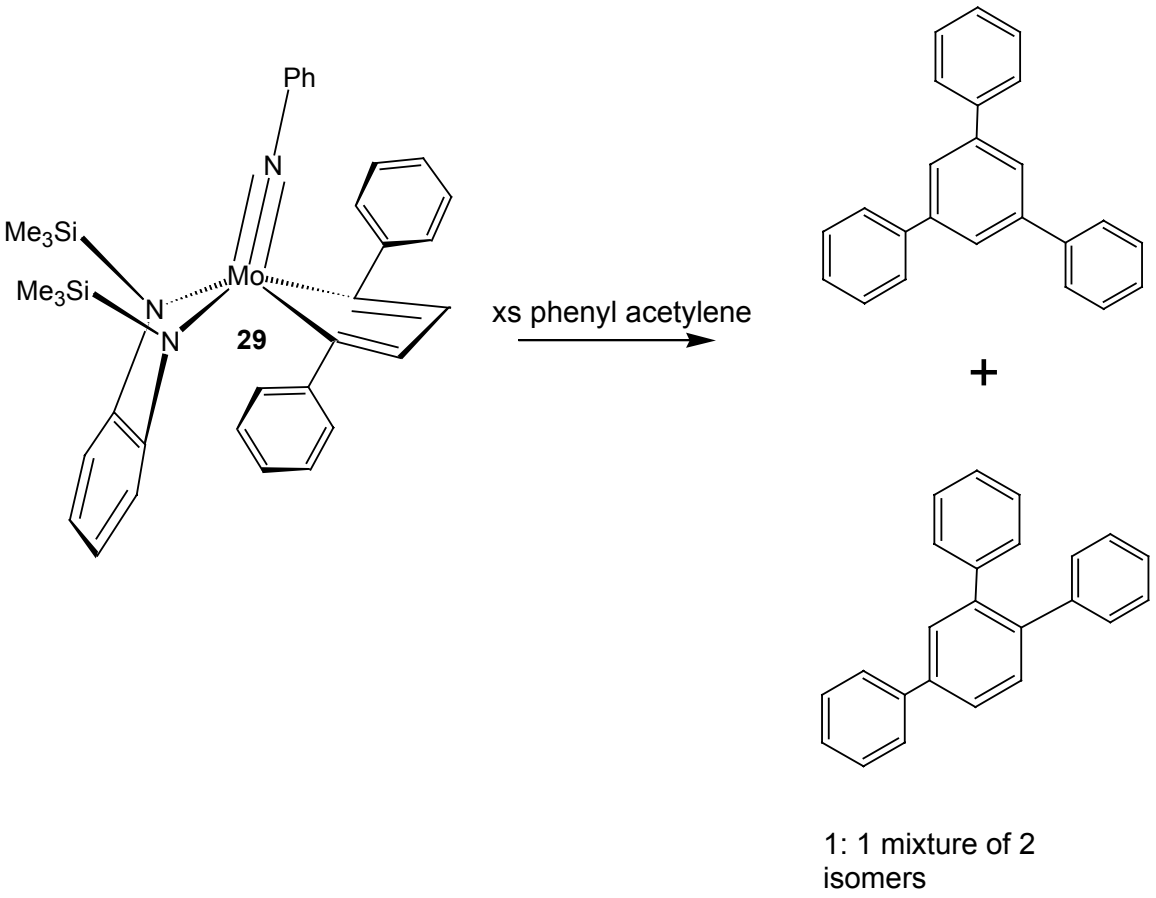

Scheme 3-9. Cyclotrimerization reactions of **29**

Summary and Conclusions

In the previous chapter the structural consequences of π ligand competition on Mo imido diamido complexes were highlighted. We revisited this theme here and have emphasized the importance of diamide donation in the stabiliztion of metallacyclopentane species. Any structural pertubation of the molecule that leads to a reduction in the donor ability of the diamide ligands can lead to increased reactivity. This suggests that more active metallacyclopentane complexes may be synthesized by carefully modulating the substituents on the diamide ligand so as to decrease its π donor ability.

The frontier molecular orbitals of the complexes seen in this chapter and the previous one are all largely ligand centered. It should come as no surprise then that

reactivity at the ligand in these complexes may also be induced. This is the subject of the next two chapters.

CHAPTER 4
SYNTHESIS AND REACTIVITY OF MO(VI) COMPLEXES WITH ALKYL AND ARYL ISOCYANIDES

Introduction

In the previous chapters the importance of ligand π donation in stabilizing the high oxidation state of the metals has been emphasized. We have shown that the competition for available d orbitals on the metal results in interesting structural features as well as reactivity. The highest occupied orbitals in these complexes are primarily ligand centered; therefore, it should come as no surprise that reactivity at the ancillary ligands may be induced. In this and the subsequent chapter, we examine the reactivity of the diamide ligands with isocyanides, and in chapter 5, with alkyl aluminum reagents. We also revisit here the concept of π loading but in this case with a d^2 six coordinate isocyanide complex.

Synthesis of Isocyanide Complexes and Insertion into the Metal-Diamide Bond

Compared to the well-known insertion of CO and isocyanides, RNC, into metal alkyl bonds there are fewer examples of the insertion reaction into metal amide bonds.[96-99] The resulting metal-iminocarbamoyl derivatives that are formed are important in the general context of amination of organic substrates.[87] Alkyl isocyanides (RNC) can be regarded as being isoelectronic with CO, and their increased ability to act as Lewis bases makes them good candidates to interact with electrophillic metal centers.

Recent work in our group has focused on the use of the chelating disubstituted phenylenediamide group $\{o\text{-}(Me_3SiN)_2C_6H_4\}^{2-}$ [$(TMS)_2$pda]. The facile high yield

synthesis of several group(VI) dialkyl complexes of Mo and W has allowed us to investigate the properties of these metal complexes and determine the influence the ancillary ligands have on their structure, stability and reactivity.[30,31] We have demonstrated that π donation by these ligands is important in stabilizing the metal center and influencing the reactivity of these complexes.[32,48,49,100] Alkyl isocyanide insertion into W alkyl bonds has been shown to occur readily at room temperature affording η^2 imino-acyl complexes that subsequently react via C—C coupling reactions of the η^2-imino-acyl group resulting in the formation of diamide ligands.[44]

Until now we have not seen any evidence for isocyanide insertion into the metal diamide bonds. Isocyanide insertion has been shown to occur preferentially at metal alkyl bonds as opposed to metal amide bonds presuamably because of the stronger metal amide bond.[77,83] In this chapter, we report the synthesis and characterization of *bis*-isocyanide complexes of Mo and the subsequent reactivity of these complexes with excess isocyanide yielding *tris*-isocyanide complexes in the case of ^{t}BuNC and an unusual chelating iminocarbamoyl *bis*-isocyanide complex in the case of 2,6 – dimethyl phenyl isocyanide. X-ray structures of a *bis*-isocyanide complex and the iminocarbamoyl *bis*-isocyanide complex are reported. We also examine the effects on π loading in d^2 six coordinate complexes and also attempt to determine the nature of the M—C (isocyanide) bond.

Synthesis of *bis*-Isocyanide Complexes. Treatment of a pentane solution of **20a**, (η^2-isobutylene)Mo(NPh)(*o*-($Me_3SiN)_2C_6H_4$), with two equivalents of *tert*-butyl isocyanide resulted in the precipitation of **30a**, as green microcrystals (Scheme 4-1). The structure of **30a** has been assigned by ^{1}H, ^{13}C, and IR spectroscopy and is consistent with

a square pyramidal structure with the imido occupying the apical position as depicted in Scheme 4-1. Resonances for the $SiMe_3$ protons are observed at (0.75ppm, 18H), whilst, the ^tBuNC protons are observed at (1.06ppm, 18H). The phenyl imido protons are observed at 7.48(dd, 2H, 7.33, 1.47Hz), 6.93(t, 1H, 7.33Hz) and 6.81(tt, 2H, 7.33, 1.47Hz). The *o*-pda ligand protons are observed as a pair of doublet of doublets (5.57, 3.3Hz) at 7.33 and 7.05ppm, respectively.

Similarly, treatment of **20a** with two equivalents of 2,6-dimethyl phenyl isocyanide, afforded **30b** as a dark red crystalline material. Resonances for the $SiMe_3$ protons are observed at 0.73ppm (18H) whilst the RNC (R = 2,6- dimethyl phenyl isocyanide) protons are observed at 2.11ppm (12H). The phenyl imido protons are observed at 7.43ppm(d, 2H), 6.99ppm(t, 2H, 7.24Hz) and 6.88ppm(t, 1H, 7.28Hz). Protons for the RNC phenyl group are observed as a multiplet at 6.63ppm. The *o*-pda ligand protons are observed as a pair of doublets of doublets at (5.65, 3.3Hz) at 7.51 and 7.06ppm.

Two isocyanide stretches in the IR spectrum of **30a** are observed at 2122 (CN symmetric stretch) and 2082 (CN asymmetric stretch). The appearance of these stretches at a lower frequency than the free isocyanide ligand ($\Delta\nu$(CN) = -9 and -50 cm^{-1} respectively) where $\Delta\nu$ (CN) = (stretching frequency of free isocyanide) – (stretching frequency of complex)) is indicative of back bonding from the metal to the isocyanide ligand. By comparison, the isocyanide stretches for **30b** are observed at 2083 cm^{-1} and 2022 cm^{-1} ($\Delta\nu$(CN) = -31 and –92 respectively). The larger $\Delta\nu$(CN) values observed for **30b** is reflective of the greater propensity for 2,6–dimethylphenylisocyanide to act as a π

acceptor ligand. This is in agreement with the observation that aryl isocyanides are better π acceptor ligands than alkyl isocyanides.

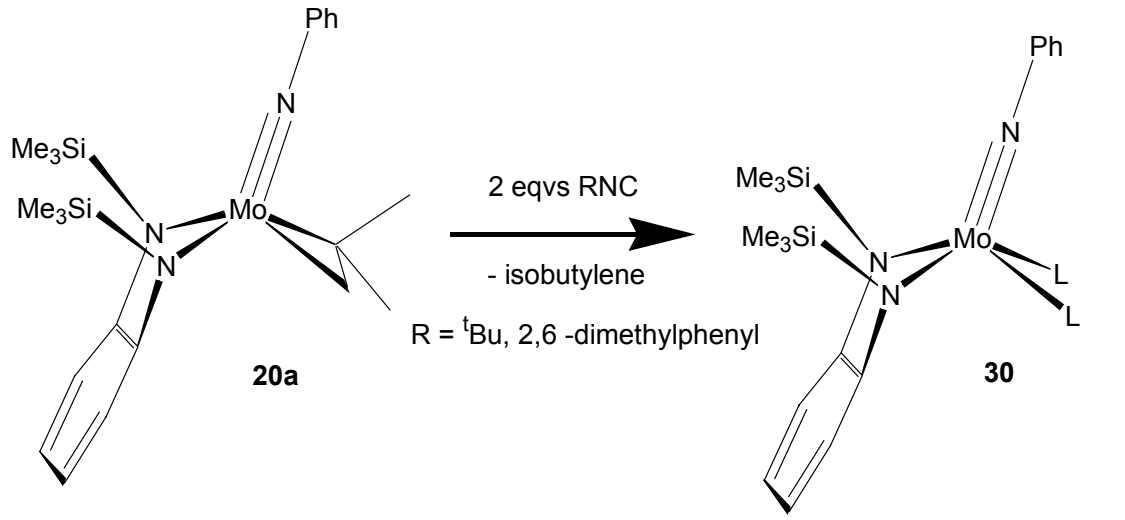

a. L = ^{t}Bu isocyanide

b. L = 2,6-dimethylphenyl isocyanide

Scheme 4-1. Synthesis of *bis*-^{t}BuNC complex

X-ray crystal structure of **30b**. Single crystals of **30b** were obtained by slow diffusion of pentane into a toluene solution of the complex. In addition to the complex, the asymmetric unit has one half of a toluene molecule located on an inversion center. The thermal ellipsoid plot of **30b** is depicted in Figure 4-1.

The geometry of **30b** is best described as a distorted square pyramidal structure with the phenyl imido ligand occupying the axial position. The Mo—N(Imido) bond (1.746Å) is in the normal range for a Mo—N triple bond and the Mo—N (amido) bonds (2.064Å and 2.093Å) are typical Mo-N bond lengths. The Mo—C(isocyanide) bonds (2.088Å and 2.093Å) are shorter than typical Mo—C(sp) (2.2Å) bonds in related complexes suggestive of π back bonding from the metal to the π* orbital of the isocyanide ligand. The isocyanide ligand is linear with C-N-C angles of (173^{0} and 177^{0}).

As has been reported for other terminal isocyanide complexes, there is no significant increase in the C≡N bond distance (Average 1.17Å). Like the previously reported d^2 complexes, the diamide ligand in this complex is flat (fold angle 173.7^0).[49] As discussed in chapter 2, this fold angle results from the fact that π donation of the diamide lone pair electrons into the metal d_{xy} is prevented because this orbital is occupied in these complexes.

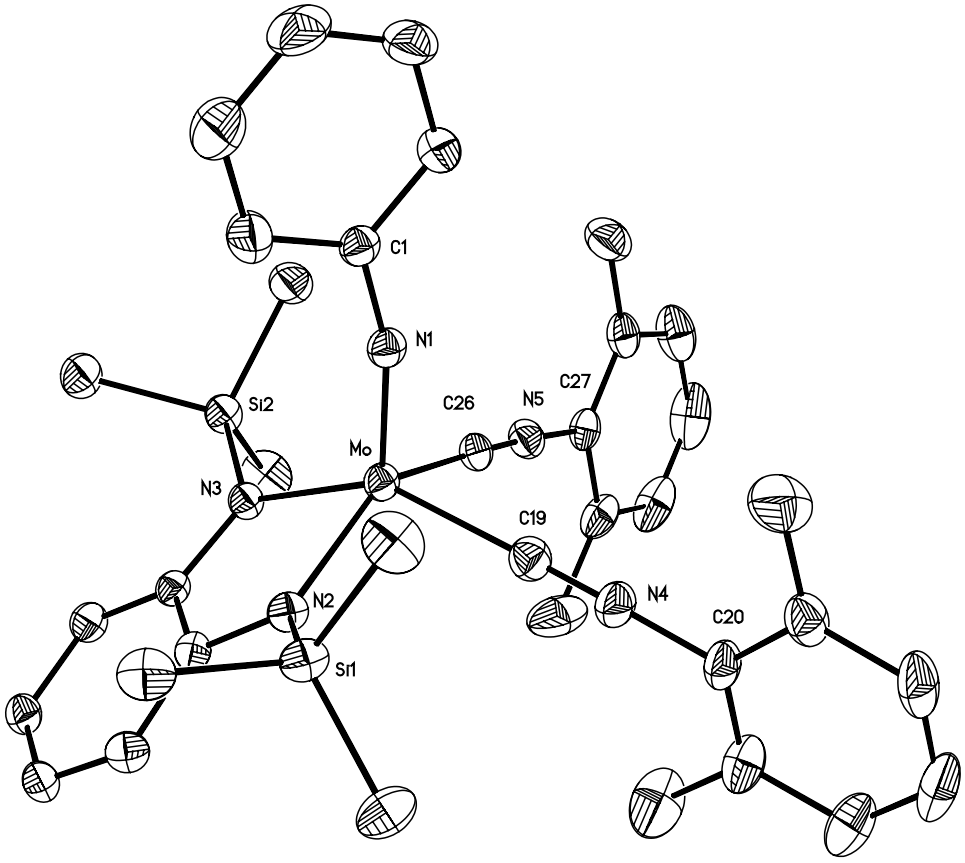

Figure 4-1. Thermal ellipsoid plot of **30b** (30% ellipsoids). Selected bond lengths (Å) and degrees (^{0}): Mo—N(1) 1.746(2), Mo—N(2) 2.064(2), Mo—N(3) 2.093(2), Mo—C(19) 2.088(3), Mo—C(26) 2.085(3), C(19)—N(4) 1.160(3), C(26)—N(5) 1.166(3), C(19)N(4)C(20) 173.4(3), C(27)N(5)C(26) 176.9(2)

Synthesis of *tris*-Isocyanide Complex. The tris-isocyanide complex, $(^tBuNC)_3Mo(NPh)(o\text{-}(Me_3SiN)_2C_6H_4)$, **31**, was previously synthesized and reported in our labs.[74] It is included in this chapter because of its relevance to the subsequent

discussion. When **20a**, was allowed to react with 4 equivs of C≡N(*t*-Bu), a fast color change from green to purple occurred, and purple microcrystals of **31** precipitated from solution and were easily isolated by filtration.

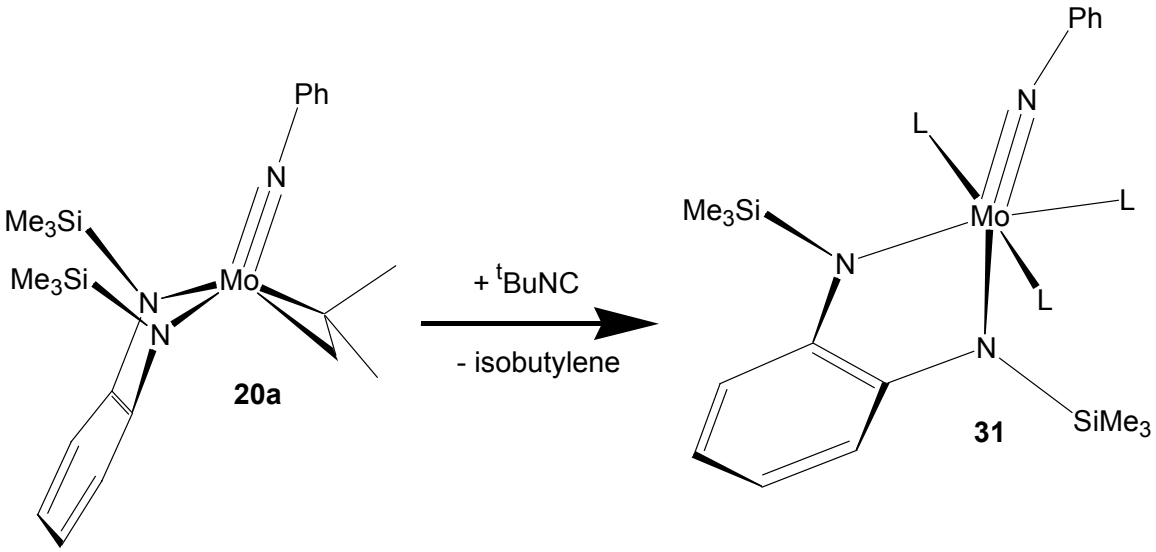

Scheme 4-2. Synthesis of *tris*-^{t}BuNC complex **31**

The pseudo-octahedral structure of **31** is shown in Scheme 4-2, was proposed on the basis of the observed NMR data and confirmed by X-ray crystallography. Resonances corresponding to inequivalent $SiMe_3$ protons were observed at 0.58ppm (br s, 9H) and 0.77ppm (br s, 9H). Broad singlets at 0.93 and 1.17ppm were assigned to inequivalent *tert*-butyl isocyanide peaks. A plane of symmetry containing the imido nitrogen, *o*-pda nitrogens, and one isocyanide ligand makes the remaining isocyanide ligands chemically equivalent.

The broadening observed in the ^{1}H NMR spectrum of **31** has been correlated to an equilibrium involving fast, reversible ligand dissociation. As shown in Scheme 4-3, loss of one RNC ligand induces a plane of symmetry in the *bis*-isocyanide complex, **30a**, that is formed. Thus the remaining isocyanide ligands and the $SiMe_3$ ligands become

equivalent in **30a**. Using the two-site exchange approximation, an activation barrier of $\Delta G^{\ddagger}$ = 15.0 Kcal/mol for the ligand dissociation was calculated.

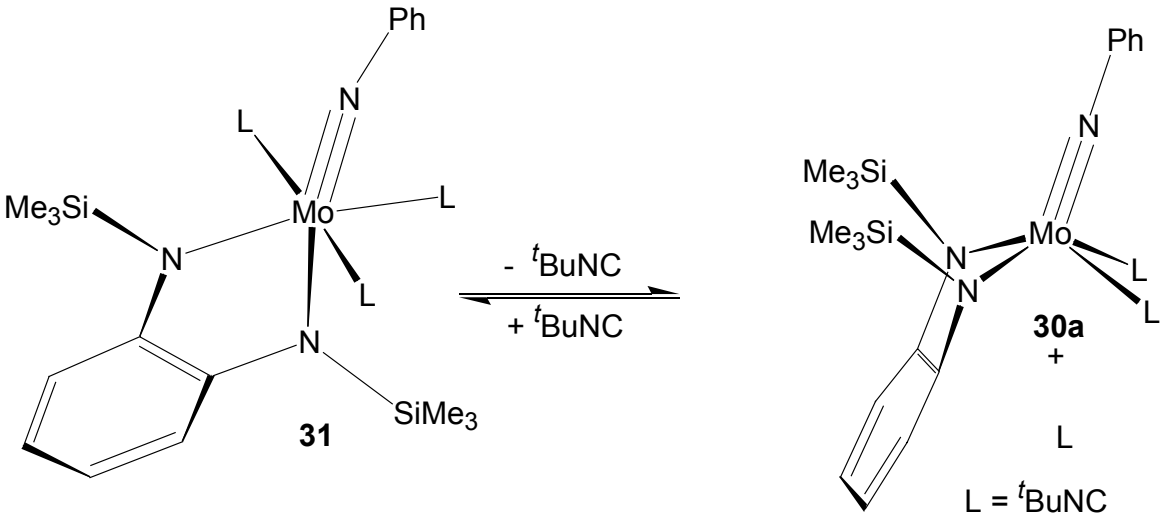

Scheme 4-3. Dissociative equilibrium observed for **31**

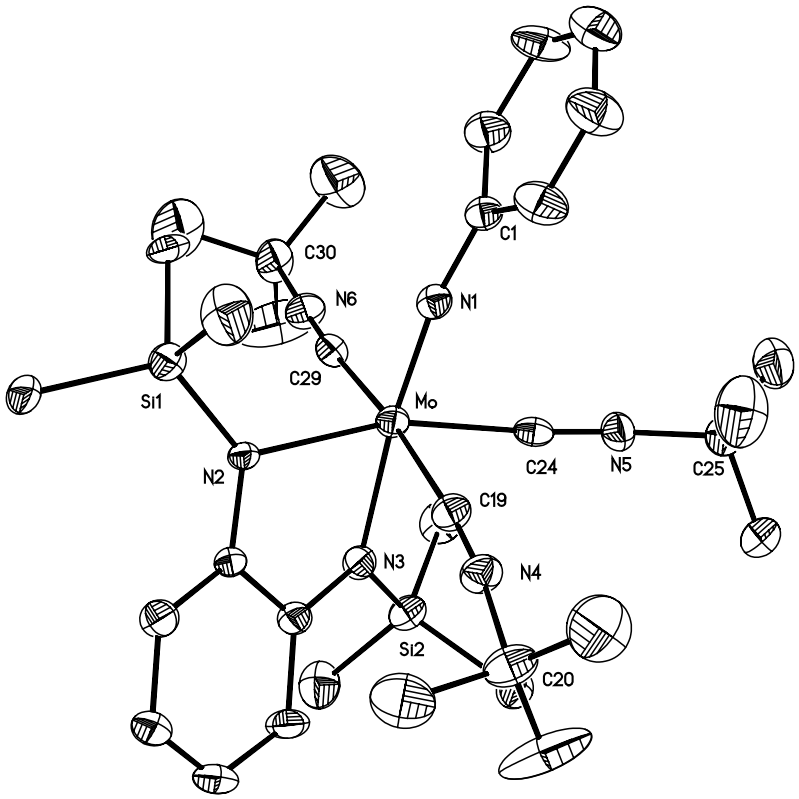

Figure 4-2. Thermal ellipsoid plot of **31**, (30% probability thermal ellipsoids), selected bond lengths (Å) and angles^{0}: Mo—N (1) 1.804(4), Mo—N (2) 2.166 (5), Mo—N (3) 2.130 (5), Mo—C (24) 2.067 (5), Mo—C (29) 2.158 (5), Mo—C (19) 2.137 (2)—N (2) 1.182 (3), C(2)N(2)C(8) 152.8(5).

X-ray crystal structure of **31**. As shown in Figure 4-2, **31** was found to have a distorted octahedral geometry. Three isocyanide ligands were found to occupy meridianal positions. The imido-nitrogen was found to be *trans* to one of the isocyanide groups. The shorter bond length of the Mo—C(2) and longer bond length of the C(2)—N(2) is attributed to π backbonding from the metal d orbitals to the isocyanide ligands.

Molecular orbital calculations. We were interested in describing the bonding of the isocyanide ligand in our complexes and comparing the π acceptor capabilities of RNC with carbonyls. Therefore, DFT calculations were performed on **31** and the previously reported carbonyl complex [Mo(NPh)(PMe_3)$_2$(CO)(*o*-(Me_3SiN)$_2C_6H_4$)], **32**[61] (Figure 4-3). For these calculations a two-layer ONIOM method was employed. For the inner layer the *o*-phenylene group (o-C_6H_4) that links the two N atoms of the diamido ligand was simplified to a –CH=CH- carbon chain. The organic groups on the nitrogen atoms ($SiMe_3$ of the amido and phenyl group of the imido) were replaced by hydrogen atoms for simplicity; and the subsitituents on the phosphine ligand in **32**, and the isocyanide ligand in **31** were replaced by hydrogen atoms. For this layer the B3LYP/LANL2DZ method was employed. The outer layer consisted of the entire complex including all substituents on the imido, phenylene diamide, isocyanide and phosphine ligand and was modeled B3LYP/LANL2MB method.

As shown in Figure 4-3, and Table 4-1, there is good agreement between the calculated geometries and the crystal structure of **31**. The crystal structure of **32** has not been reported but the structure was confirmed as a minimum by a frequency calculation (number of imaginary frequencies=0).

Table 4-1. Selected bond Lengths(Å) and Angles(^{0}) for **31** and **32**

31			**32**	
Bond	ONIOM	X-ray	Bond	ONIOM
Mo—N(1)	1.824	1.805(3)	Mo—N(1)	1.833
Mo—N(2)	2.178	2.166(3)	Mo—N(2)	2.186
Mo—N(3)	2.141	2.130(3)	Mo—N(3)	2.137
Mo—C(1)	2.149	2.137(5)	Mo—C(1)	1.998
Mo—C(2)	2.013	2.067(5)	Mo—P(1)	2.479
Mo—C(3)	2.131	2.158(5)	Mo—P(2)	2.477
C(4)N(5)C(2)	175.5	153.0(4)		

Our interest in the bonding in **31** and **32** stemmed from some interesting features in the structures of these molecules. In addition to the six electrons that can be donated by the imido ligand (one σ and two π), six electrons may also be donated by the diamide ligand through the lone pair electrons on nitrogen (two σ and one π as has been mentioned before for d^0 and d^2 five coordinate complexes in previous chapters). However, a conflict arises because these complexes are Mo(IV) and one of the metal d orbitals is occupied. Thus donation of the diamide lone pair electrons into this orbital would result in an energetically unfavorable filled-filled interaction. The presence of a strong π acceptor ligand *trans* to the diamide lone pair electrons may stabilize this situation as the diamide ligand, the metal orbital (d_{xy}), and the π* orbital of the π acceptor ligand (CNR in **31** or CO in **32**) can engage in 3 center-four-electron bonding as shown in Figure 4-4.

Molecules **31** and **32** possess pseudo C_s symmetry, thus, there are two sets of metal t_{2g} orbitals one with a'' symmetry (d_{xy} and d_{yz}) and another with a' symmetry (Scheme 4-4). A linear combination of the diamide lone pair electrons results in two orbitals of a'' symmetry (π_3 and π_2) and these orbitals can interact with orbitals on the metal of appropriate symmetry i.e. the d_{xy} and d_{yz} orbital. The metal orbitals may also interact via π back bonding to the π acceptor ligand (carbonyl or isocyanide) that is arranged *trans* to

the one of the diamide nitrogen lone pairs. The occupied molecular orbitals generated by DFT(B3LYP) are a good illustration of these interactions Figures (4-5) and (4-6).

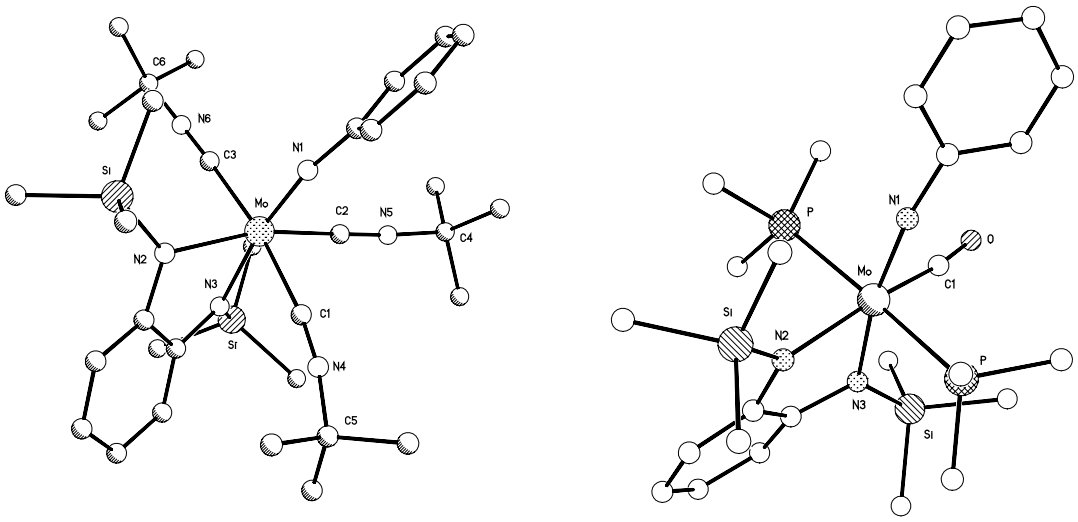

31 **32**

Figure 4-3. Optimized structure (ONIOM B3LYP/LANL2DZ:B3LYP/LANL2MB) for **31** and **32**

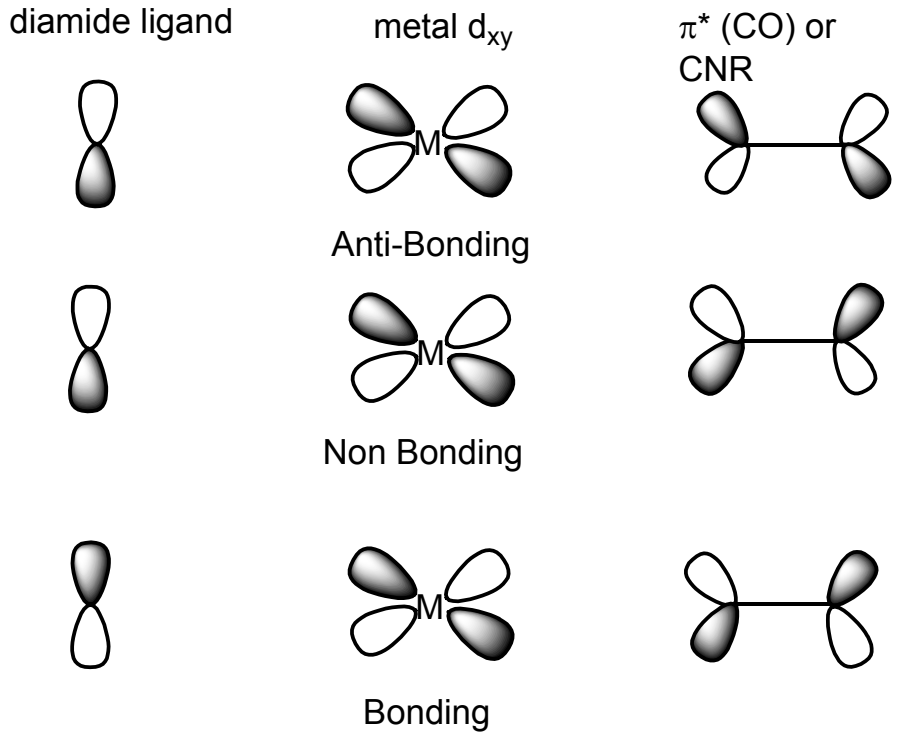

Figure 4-4. 3-Center-4-electron bonding between the diamide lone pair electrons the metal d orbitals and the π* orbitals of a π acceptor ligand

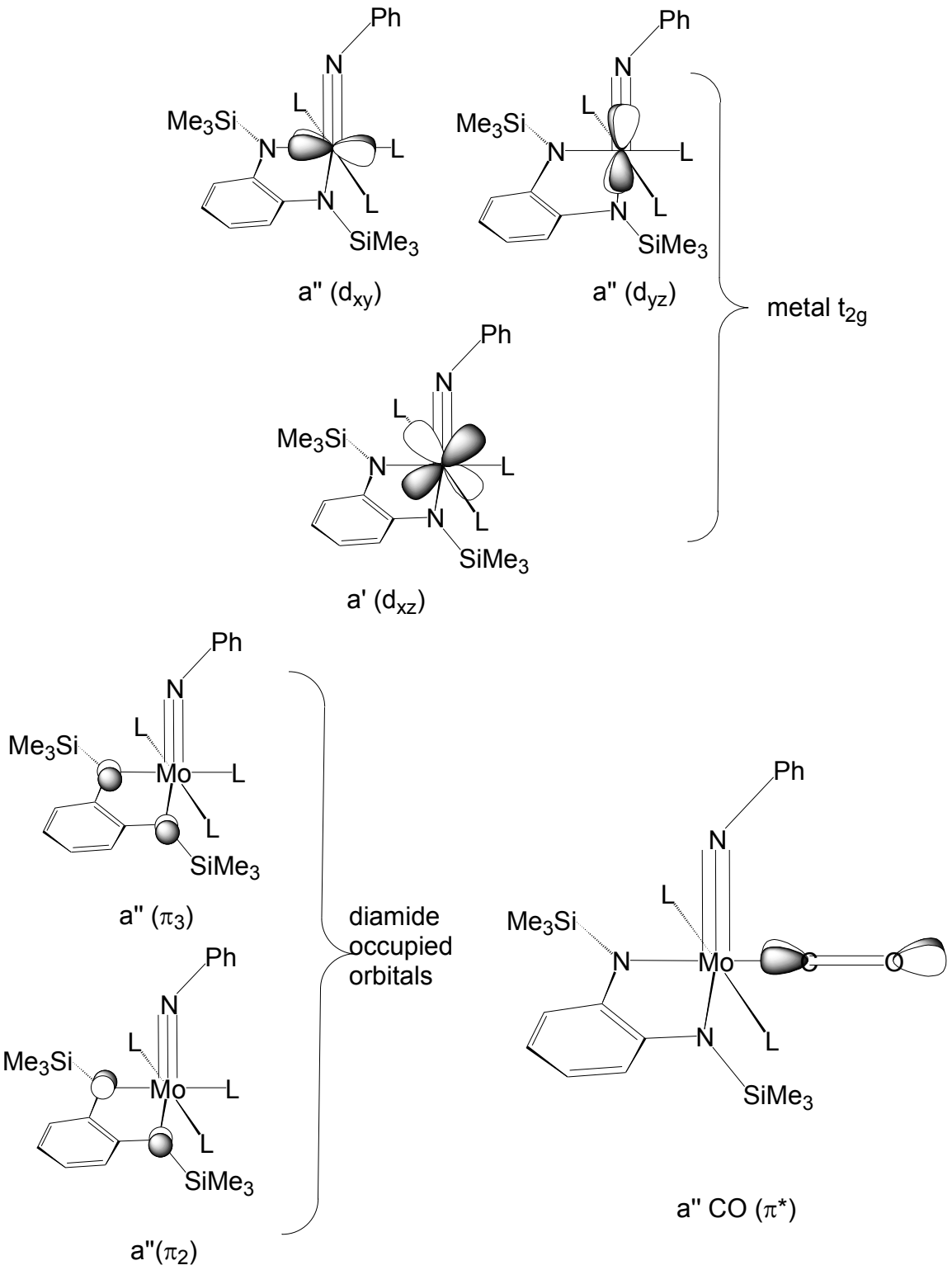

Scheme 4-4. Group orbitals for π interactions in **31** and **32**, CO is used as the π acceptor ligand in this example

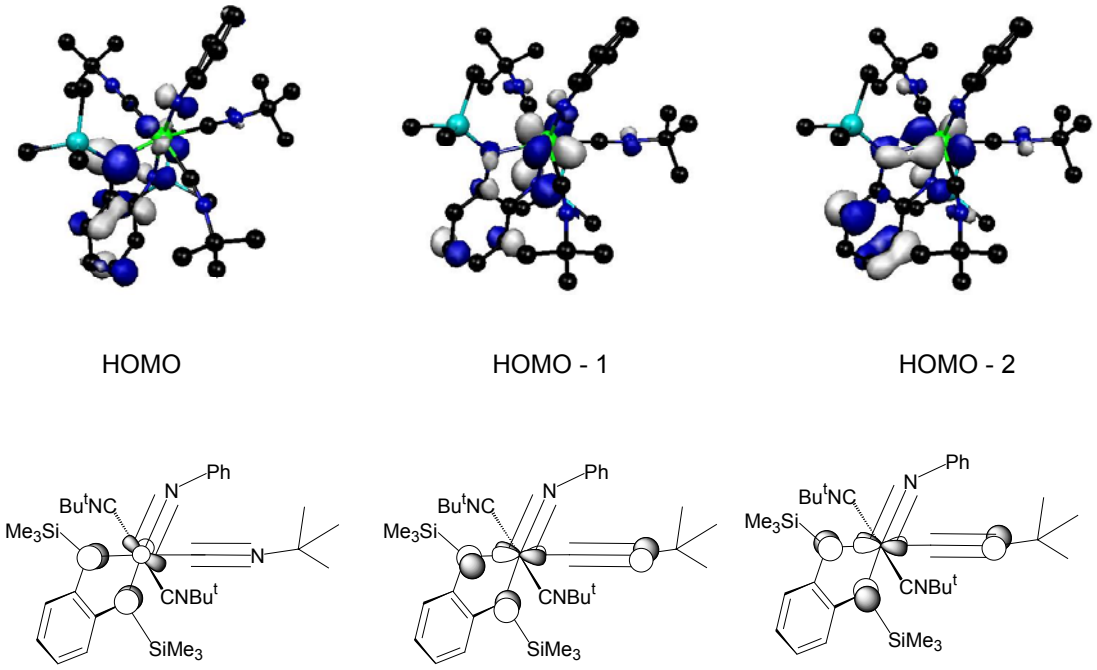

Figure 4-5. Interaction of diamide lone pairs and isocyanide ligand with metal d_{xy} orbital. (Orbitals are displayed at the 0.05 au isocontour level)

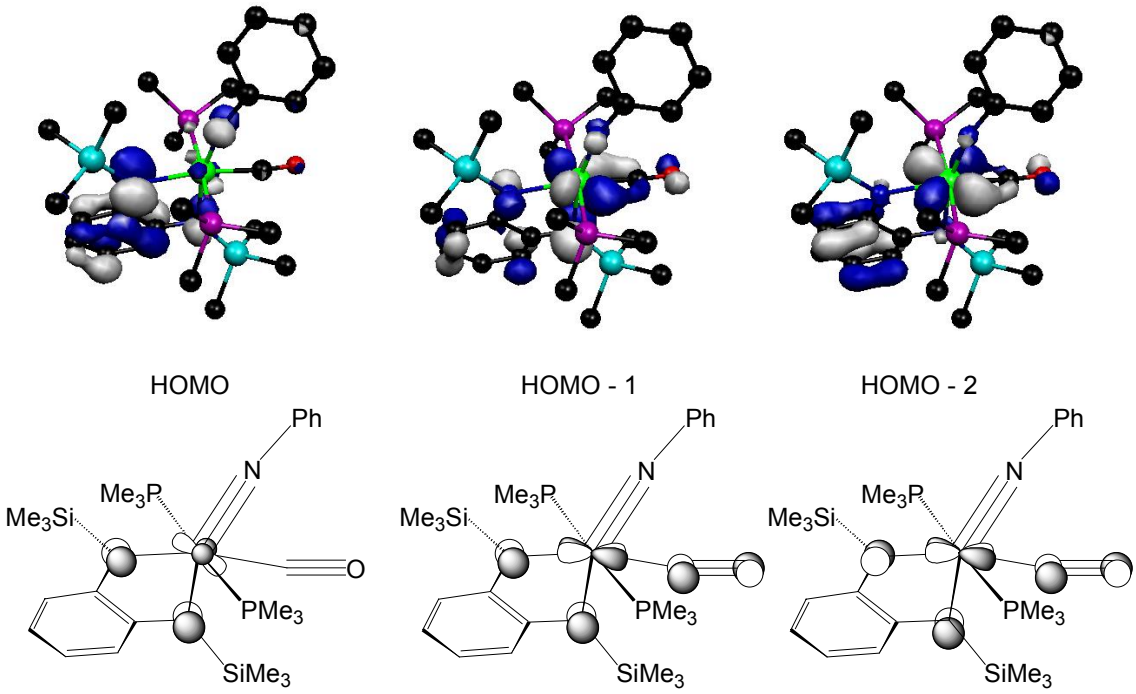

Figure 4-6. Interaction of diamide lone pairs and CO ligand with metal d_{xy} orbital. (Orbitals are displayed at the 0.05 au isocontour level)

The presence of a lone pair electron on the metal limits the π orbital donation by the diamide ligand, thus in the HOMO for both **31** and **32** the diamide lone pairs are primarily ligand centered. The occupied orbitals HOMO –1 and HOMO –2 represent the aforementioned 3-center-4-electron interaction between the diamide lone pairs, the metal, and the π* orbital of the isocyanide or carbonyl ligand. Bonding between the diamide ligand and the metal d_{xy} orbital in HOMO-2 is negated by antibonding to this ligand in HOMO – 1. Thus, the net effect is that the diamide lone pair electrons remain ligand centered in the HOMO and the metal dxy orbital remains largely metal centered.

Also evident from the molecular orbital diagrams are the differing π acceptor capabilities of CO versus the CNR ligand. The coefficient at the isocyanide carbon in **31** is very small suggesting very little contribution from this carbon in the metal—isocyanide π back bond. In bonding to a π acceptor ligand like CO or CNR the metal d orbitals are perturbed by both the π and π* orbitals of the acceptor ligand (Scheme 4-5) and the net result shows cancellation of the electron density at the carbon and reinforcement at the heteroatom (N or O).[101]

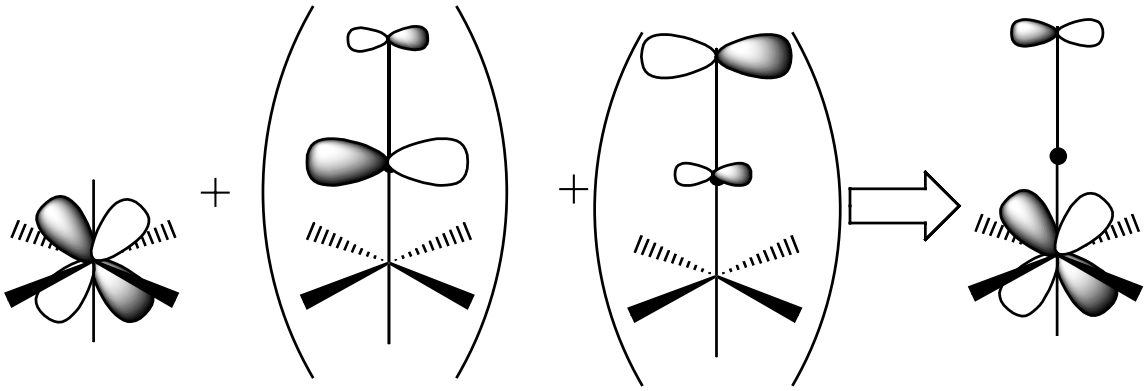

Scheme 4-5. Interaction of a metal d-orbital with a π acceptor ligand

In the case of CO the contribution from π* is greater than the contribution from the π orbital, (because of the difference in electronegativity between carbon and oxygen there

is a larger coefficient at carbon in π*) and CO is an overall π acceptor. The difference in electronegativity is smaller in between carbon and nitrogen thus there is a smaller coefficient on carbon in the π* orbital and this results in cancellation of most of the electron density at this atom in the bonding MO. These differences are clearly evident in the HOMO -1 and HOMO – 2 orbitals in Figures 4-5 and 4-6. The contribution at the carbon in CO in **32**, is significantly greater than in the isocyanide ligand in **31**.

Synthesis, Structure and Dynamics of a Chelating Imino Carbamoyl Complex

Treatment of a C_7D_8 solution of **30b** with two equivalents of 2,6-dimethyl phenyl isocyanide results in the slow conversion (24 hrs) to the imino carbamoyl complex, **33** (Scheme 4-6). Chemical shifts for the $SiMe_3$ protons occur at the (0.44 ppm, s, 9H) and (0.59 ppm, bs 9H). Signals for the 2,6 –dimethyl phenyl isocyanide ligands are observed at (1.94 ppm, s 12H) and two signals were observed for the 2,6-dimethyl phenyl protons at (2.45 ppm, s, 6H) and (1.86 pp s 6H). As shown in Scheme 4-6 the imino carbamoyl ligand is coordinated in η^1 and η^2 fashion to Mo. The chemical shifts for the quaternary carbons of the iminocarbamoyl ligands are observed at (208.2 ppm) and (181.4 ppm) for the η^2 and η^1 carbons respectively.

One peak was observed in the IR spectrum for the asymmetric CN stretch (2088 cm^{-1}) that occurred at a lower frequency than the free isocyanide ($\Delta\nu = 25$ cm^{-1}) again, suggestive of net π back bonding in these complexes.

Isocyanide insertion into metal amide bonds is less extensively studied than the related insertion reactions of metal alkyl bonds. In recent years, studies of isocyanide insertions into Ta amide bonds have been reported. We propose that the formation of **33** occurs by initial coordination of the of two isocyanide ligands followed by the rapid

insertion of the isocyanides into the metal amide bond. A 1,3 siltropic shift then follows and the resulting iminocarbamoyl species is rapidly trapped by two molecules of 2,6-dimethyl isocyanide (Scheme 4-7).

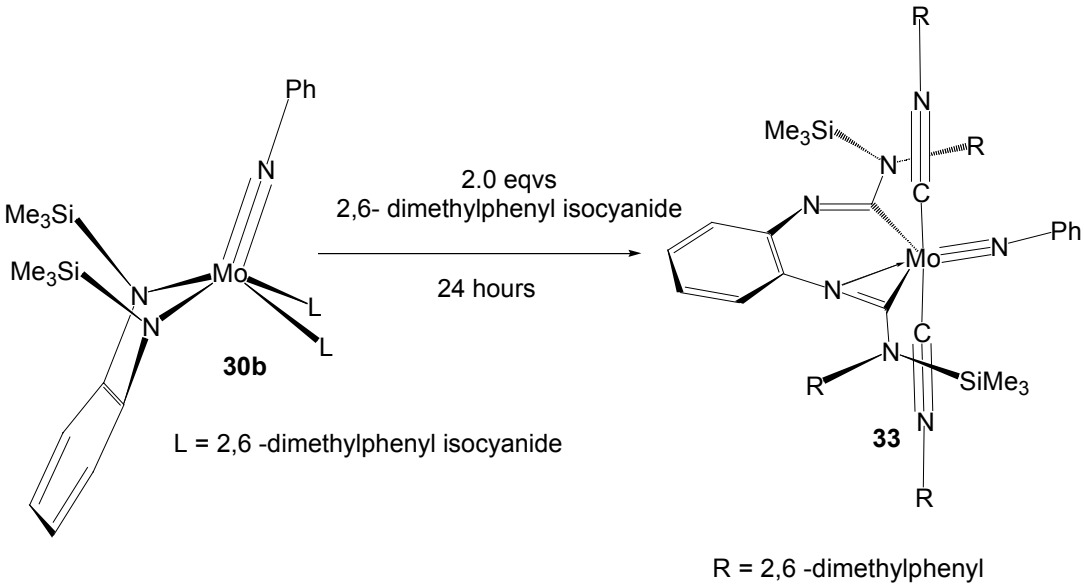

Scheme 4-6. Synthesis of iminocarbamoyl complex, **33**

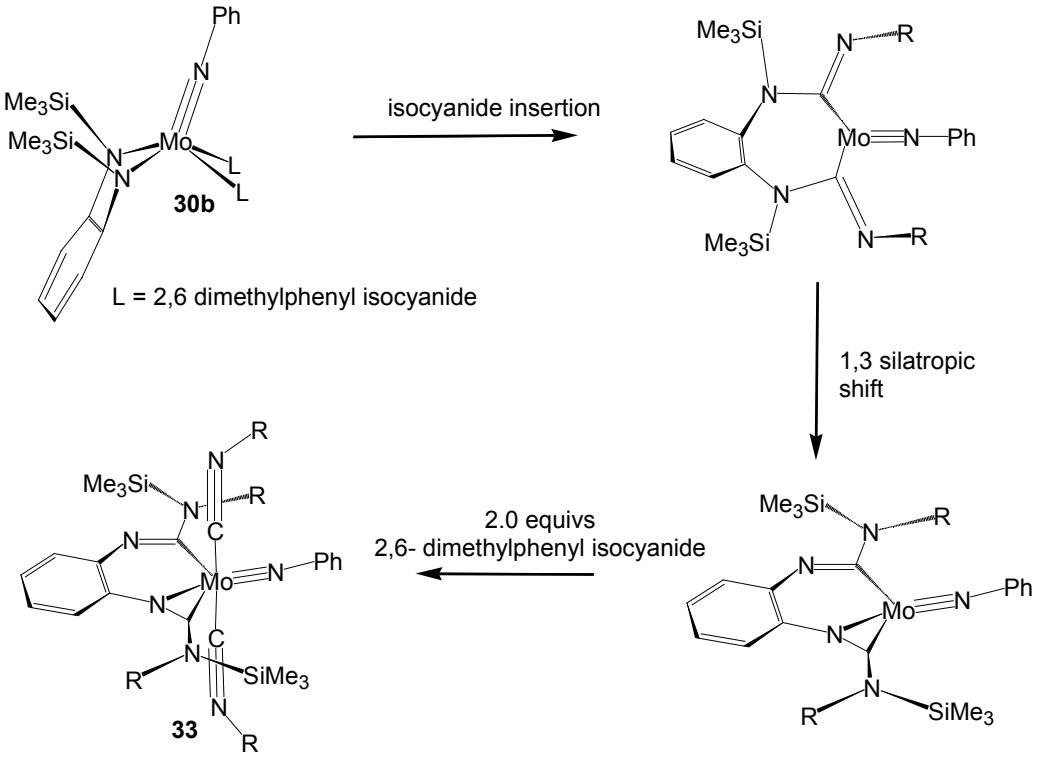

Scheme 4-7. Proposed mechanism for the formation of **33**

X-ray Crystal Structure of **33**. Single crystals of **33** were obtained by a cooling a concentrated pentane solution of this molecule (Figure 4-7). The geometry about Mo may best be described as a distorted trigonal bipyramid with the isocyanide ligands occupying the axial position and the imino carbamoyl fragments and the imido ligand occupying the equatorial plane. A plane of symmetry bisects the two *trans* isocyanide ligands and passes through the imido and iminocarbamoyl fragments. The imino carbamoyl fragment is flat (rms = 0.02), consequently the substituents on the amido nitrogens (N(5) and N(4)) are sterically encumbered (vide infra).

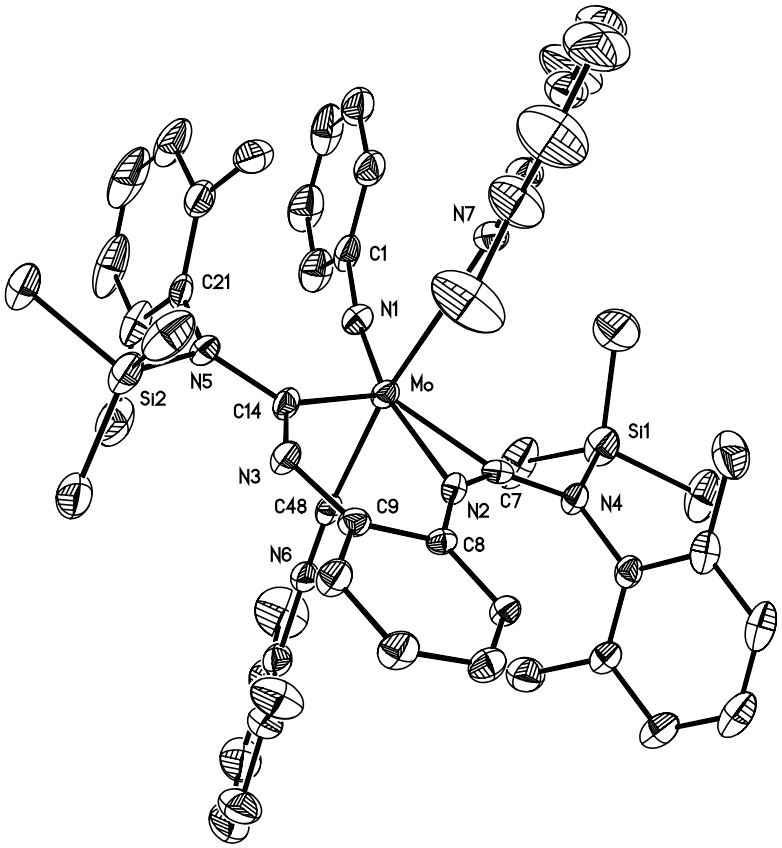

Figure 4-7. Thermal ellipsoid plot of **33**, (30% ellipsoids). Selected bond lengths (Å) and angles(^{0}) Mo—N(1) 1.767(2), Mo—N(2) 2.108(2), Mo—C(57) 2.110(3), Mo—C(48) 2.131(3), Mo—C(14) 2.147(3), Mo—C(7) 2.052(3), N(2)—C(7) 1.274(3), N(3)—C(14) 1.318(4), N(4)—C(7) 1.365(3), N(4)—C(15) 1.454(3), C(21)N(5)C(14) 124.4(3), C(14)N(5)Si(2) 113.4(2), Si(2)N(5)C(21) 122.1, C(57)N(7)C(58) 166.9, C(48)N(6)C(49) 171.8(3)

The Mo—N(1) bond length (1.767 Å) is within normal range for a molybdenum nitrogen triple bond. One imino carbamoyl fragment binds η^1 to the Mo center and shows localized C—N bonds i.e., one short C=N bond, C(14)—N(3), (1.318 Å) and one C—N single bond (C(14)—N(5), (1.403Å). The η^2 imino carbamoyl fragment exhibits a very short C—N bond (C(7)—N(2), (1.274Å)) and a long C(7)—N(4) (1.365Å). Both amido nitrogens N(4) and N(5) are sp^2 hybridized with carbon nitrogen bond lengths shorter than typically seen for C—N single bonds (1.48Å) and the sum of the angles around each nitrogen is equal to 359.9^0. This suggests delocalization within the CNC framework of the imino carbamoyl. The bond lengths for the isocyanide ligands (Average 2.12Å) are shorter than typical Mo—C (sp^2) bonds suggestive of π back bonding to isocyanide in these complexes. The CNC isocyanide bond angles deviate only slightly from linearity (Average 169.4^0).

The space-filling model of **33**, generated from the X-ray study, reveals a very sterically congested region in the plane of the imino carbamoyl fragment (Figure 4-8). This suggests that a free rotation about the carbon nitrogen bonds C(7)—N(4) and C(14)—N(5) is restricted because of steric hindrance around the nitrogen atoms. For this same reason free rotation of the xylyl fragments about N(4) and N(5) are restricted because of steric interactions. Silicon atom Si(2), is located close to two nitogens; this atom is directly bond to N(5) (bond length = 1.78Å), but is also close to N(3) (2.53Å) this distance is less than the sum of the Van der Waals radii of the a nitrogen atom (3.60Å) and as is evident from the space filling diagram Si(2) interacts with both N(3) and N(5). These close contacts are responsible for the fluxionality of these molecules in solution (*vide infra*).

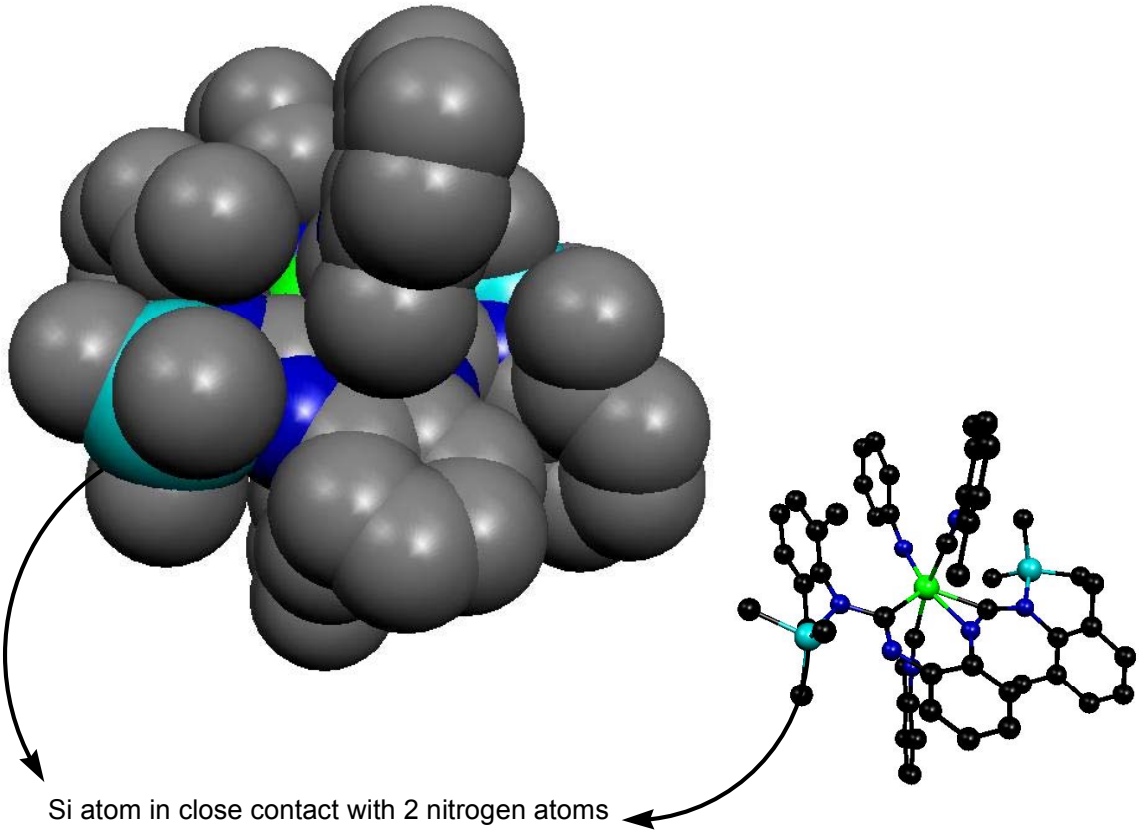

Figure 4-8. Space filling diagram generated from the crystal structure of **33**. The Si—N bond distances (1.78Å) and (2.53Å) are within the sum of the Van der Waals radii of a N and Si atoms (3.60Å)

Dynamic behavior of **33** in solution. Complex **33** is fluxional in solution. At room temperature two $SiMe_3$ protons can be observed at (0.44 ppm, s, 9H) and (0.59 ppm, bs, 9H). When a C_7D_8 solution of is heated to 348K the broad singlet sharpens and grows in intensity. The resonance observed at 0.59 ppm broadens into the baseline as this sample is cooled (Figure 4-9). Below the coalesence temperature (218K) two peaks reemerge at 1.13 ppm and 0.09 ppm in a 5:1 ratio. This fluxionality can be explained by a 1,3 silatropic rearrangement of the $SiMe_3$ group that has close contacts to two nitrogen atoms (Scheme 4-8).

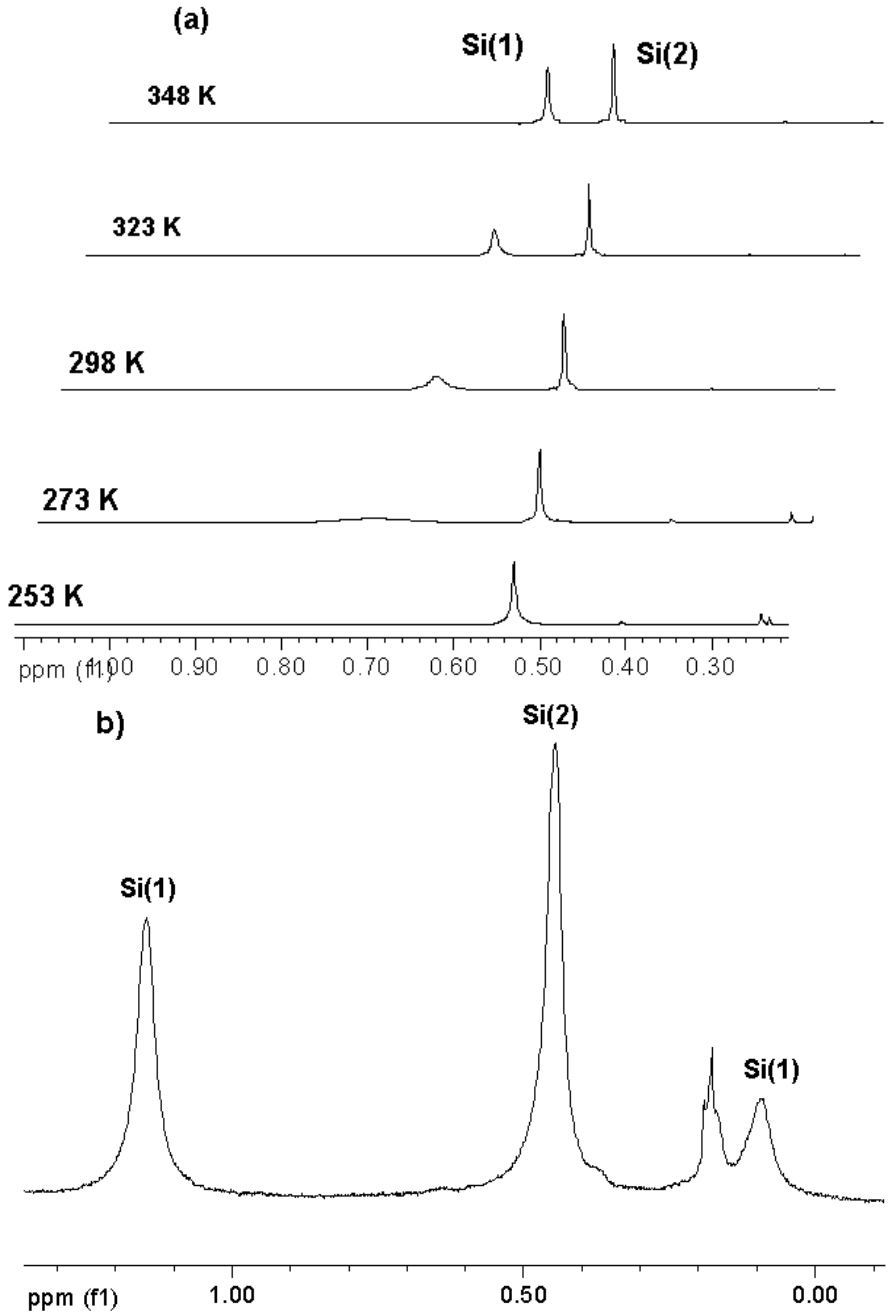

Figure 4-9. Variable temperature ^{1}H NMR spectrum (C_7D_8) of **33**.

a) Broadening of the $SiMe_3$ protons as temperature is cooled. At 348K two peaks are observed for the $SiMe_3$ protons labeled Si(1) and Si(2) Upon cooling the sample the protons for Si(1), broadens into the baseline.

b) ^{1}H NMR spectrum (C_7D_8) of **33** at the low temperature limit (188K). Below the coalasence temperature, two peaks are observed for the Si(1) protons at 1.13 and 0.09 ppm in 5:1 ratio.

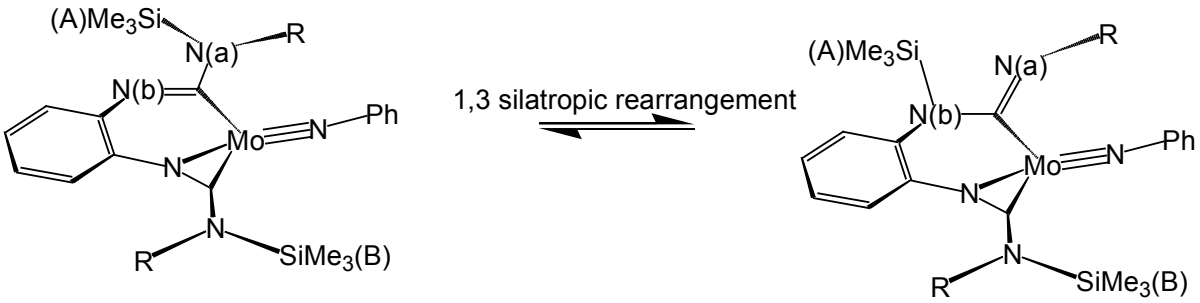

Scheme 4-8. 1,3 silatropic rearrangement in imino carbamoyl ligand. The axial isocyanide ligands have been removed for clarity

Recall, from Figure 4-8 that the group Si(2) has close contacts between both N(a) and N(b). Below the coalescence temperature the equilibrium shown in Scheme 4-8 will be frozen in solution and two species will be detected that differ in the position of $SiMe_3$(A). In one position the group $SiMe_3$(A) is bonded to N(a) and in the other position it is bonded to N(b). The population of these sites are not equal thus the ratio of the two site populations N(a):N(b) is 5:1. Above the coalescence temperature the chemical shifts for the $SiMe_3$ are observed as an average of the two sites i.e. above T_c the $SiMe_3$ group feels both N(a) and N(b). The exchange of unequally populated doublets has been described in more detail by Sandstrom in *Dynamic NMR Spectroscopy*.[102]

[2+2+1] Cycloaddition reactions of metallacycles with alkyl isocyanides RNC.

Our previous work with W alkyls and ^{t}BuNC seemed to suggest that isocyanide insertion in the case of W, proceeded selectively into W alkyl bonds over the W diamide bond.[44] We were interested in investigating whether isocyanide insertion was also competitive in the case of Mo alkyl complexes so we pursued the reactions of the Mo metallacyclopentane complex **25** with isocyanides. Addition of 4.0 equivalents of ^{t}BuNC to **25** results in the formation of **30a** and the iminocyclopentane molecule, **44** (Scheme 4-9). Whilst the addition of 5.0 equivalents of 2,6 – dimethyl phenyl isocyanide to **25,** results in the formation of **44**, and **30b**. Thus, the insertion of isocyanides into metal

amide bonds seems to occur at a rate that is competitive with metal alkyl insertion in these complexes.

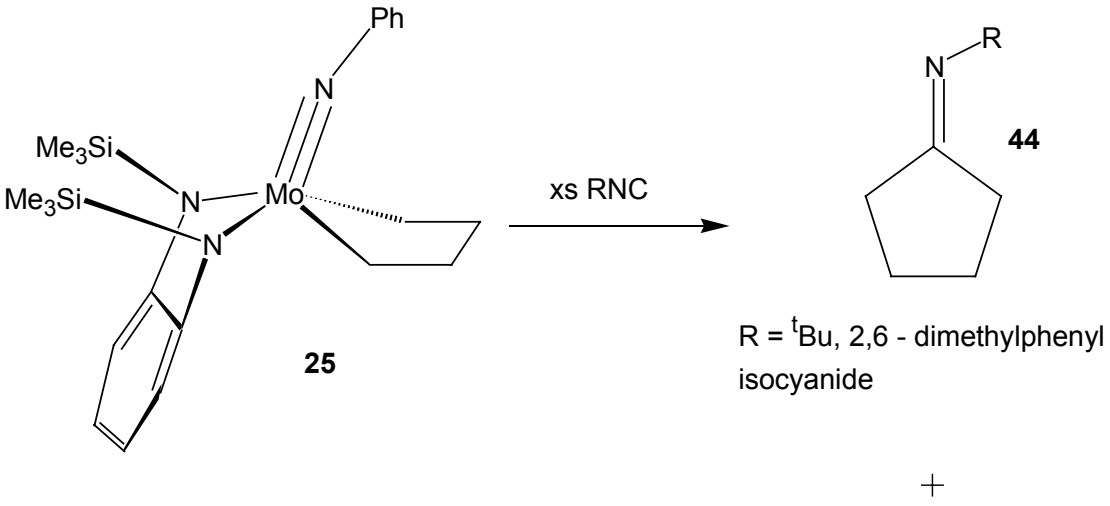

Scheme 4-9. Isocyanide insertion into the metallacyclopentane complex **25**

The reactions outlined in Scheme 4-9, presents a rare example of the metal mediated intermolecular [2+2+1] cycloaddtion reactions of alkenes and alkynes with alkyl isocyanides. Compared with the related carbonylative cyclization, reports of related isocyanide-inserted cyclization is quite rare.[54,59,103] Tamoa et al. published the pioneering work of the Ni(0) induced cyclizations of diynes in 1989.[72] Since then isocyanide insertion into zirconacyclopentadiene, has been demonstrated by Takahashi et al..[56] The Buchwald group[52,104-108] and the Shibata group[55] have demonstrated the only two examples of catalytic coupling of alkynes and alkenes with alkyl isocyanides. We are currently exploring the catalytic possibilities of our complexes in the [2+2+1] cyclization of alkynes, alkenes, dienes and diynes with alkyl isocyanides.

Summary and Conclusions

In this chapter, the role of the chelating diamide fragment has been expanded from that of ancillary ligand to that of a ligand that can take part in the chemistry in these complexes. Again we have emphasized the importance of π ligand interactions and there role influencing the outcome of chemical reactivity.

The insertion reactions seen between 2,6- dimethyl phenyl isocyanide and the diamide ligand results from the π conflict that arises between the diamide nitrogen lone pairs and an occupied d orbital that results in the weakening of the Mo—N (diamide) bond and ultimately a lowering of the barrier to insertion. These results are promising because they suggest that these insertion reactions may lead to the development of a catalyst for the carbonylation of amines. These species have been shown useful as synthetic organic precursors. We are currently investing the potential catalytic abilities of our complexes.

CHAPTER 5
ALKYL ALUMINUM INDUCED DIAMIDE TRANSFER FROM GROUP 6 IMIDO DIAMIDO COMPLEXES.

Introduction

In the previous chapters, the importance of the diamide donation in group 6 imido diamido complexes has been emphasized. The highest occupied molecular orbitals (HOMO) of these complexes are primarily ligand centered and can interact with Lewis Acids. In this chapter, we examine the reactivity of these complexes with alkyl aluminum reagents. Species derived from these interactions are potentially useful as olefin dimerization/oligomerization catalysts.

Neutral aluminum complexes of the form AlX_3 (x=halide, alkyl etc.) have been extensively utilized in organic synthesis as Lewis acid reagents and as catalysts and co-catalysts in organotransition metal mediated polymerizations or oligimerizations.[109] Examples of this include Ziegler-Natta and metallocene based polymerization systems wherein a transition metal complex is treated with an aluminum reagent e.g. $EtAlCl_2$ or MAO(methyl aluminoxane) in the presence of olefin at high pressure. In these cases, the aluminum reagent acts as an alkylating agent, however, the exact nature of the catalytic species that arise from the interaction of the transition metal with the aluminum reagent are still under some debate.[110]

In our labs we have had success in synthesizing high oxidation state imido complexes of the form $M(NPh)(o\text{-}(Me_3SiN)_2C_6H_4)X_2$ (M=Mo and W)[30,31 31] incorporating the ((*o*-$(Me_3Si)_2$-pda) (pda = phenylene diamide) ligand. We have shown

that this ligand stabilizes the metal center via π donation of the diamide lone pair electrons and we have been able to synthesize complexes incorporating various functional groups e.g. metallacycles,[30,46,100 31] alkyls, olefins,[46] and alkynes with both Mo and W.

In an attempt to produce a catalyst that selectively generates 1-hexene from propylene, Exxon[111] revisited a catalytic system first developed by Lawson[112] and Menapace[88,113,114] involving an aniline/WCl_6/Al mixture with a low Al to W ratio (5:1). Their observation that metallacyclopentanes were formed during this catalysis inspired us to examine the reaction of our metallacyclopentane complexes with aluminum reagents to investigate the catalytic activity of the resultant products.

Reactions of Mo Dialkyl Complexes with Trimethyl Aluminum (TMA)

Treatment of an orange solution of Mo(NPh)(*o*-$(Me_3SiN)_2C_6H_4$)$(CH_2)_4$, **25**, in toluene, with 1 equivalent of trimethyl aluminum (TMA) results in a green solution after 15 minutes. Concentration of the solution and subsequent crystallization from pentane (at -78^0C) results in the isolation of green crystals of **34**, a metallacyclopentane methyl complex (Scheme 5-1). A similar reaction occurs when an orange solution of the diphenyl acetylene complex, **35,** is treated with 1 equivalent of TMA. The resultant yellow diphenyl acetylene methyl complex, **36**, precipitates from pentane after stirring for 24hrs.

This transformation is similar to the reaction between alkyl aluminum reagents and lanthanide or early transition metal amides which produce aluminate[115-120] or hydride[121] complexes. The reaction is driven by the formation of the Al-N bond of the aluminum amide complex that is also formed in the reaction. There are apparently no examples of

such an exchange reaction involving an alkyl aluminum reagent and a diamide ligand bound to a transition metal or lanthanide. As shown in (Scheme 5-1) the $R_2Al((o\text{-}(Me_3SiN)_2\text{-pda})$ anion that is formed in the reaction is trapped by coordination of its arene ring to the molybdenum center.

The ^1H NMR spectra of **34** and **36** reveal the presence of highly shielded aromatic protons (4.7-5.5ppm), suggesting π coordination of the aromatic ring to the Mo center. The metallacyclopentane ring protons in **34** appear as multiplets (1.8-3.2ppm). Three different methyl groups and two signals for the protons of the $SiMe_3$ groups are also observed, while the phenyl imido protons appear as a multiplet at 6-8ppm. The proton NMR spectrum of **36** is also consistent with the presence of a π coordinated arene ring and a Mo methyl group. These structures were confirmed with single crystal X-ray diffraction studies.

The thermal ellipsoid plots of **34** and **36** are presented in Figures 5-1 and 5-2. A distorted square pyramid with the *o*-pda ring occupying the apical position best describes the coordination geometry about molybdenum. The aluminum nitrogen bond lengths are typical of Al—N single bonds (1.925 Å). The pda phenyl ring binds to the metal in an η^4-fashion in both complexes but this bonding is not symmetrical. The metal carbon bond distances Mo—C10 (**34**) and Mo—C24 (**36**) are significantly shorter (2.334Å and 2.348Å respectively), than the adjacent metal carbon bonds Mo—C9 and Mo—C11 (2.414Å and 2.464Å respectively) in **34** and Mo—C23 and Mo—C25 (2.463Å and 2.392Å) in **36**. The 4th metal carbon bond Mo—C12(**34**) and Mo—C26(**36**) of this butadienyl fragment is significantly longer (2.605Å and 2.549, respectively).

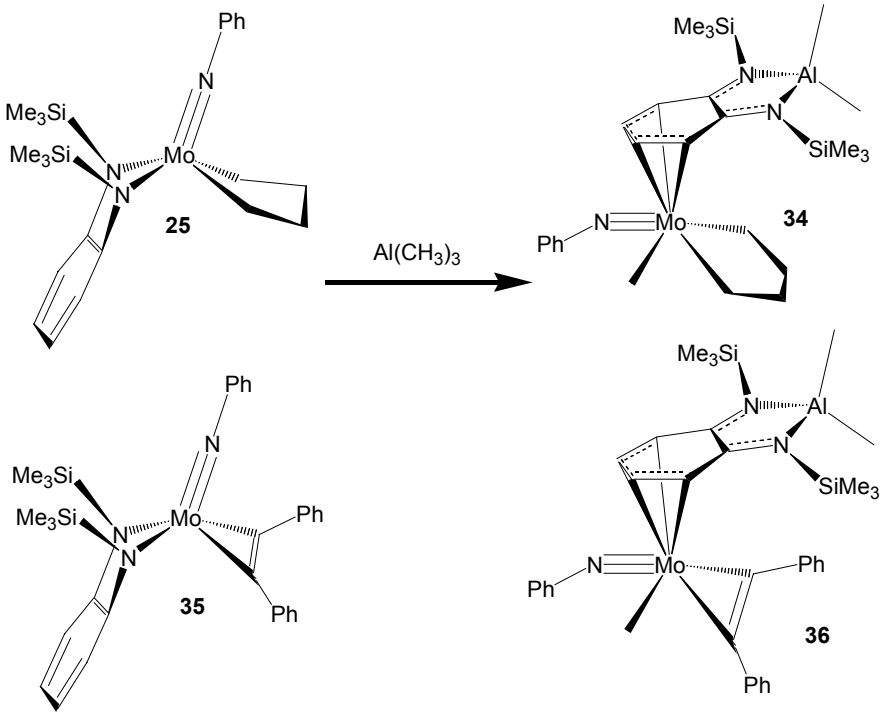

Scheme 5-1. Reaction of metacyclopentane complex with trimethyl aluminum

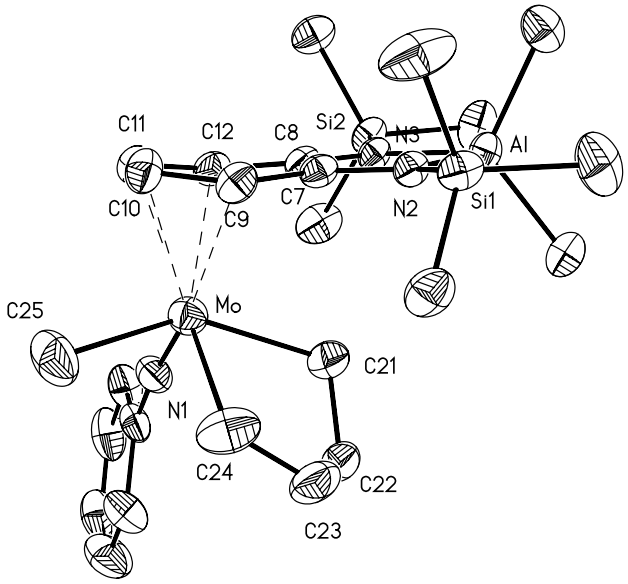

Figure 5-1. Thermal ellipsoid plot of **34** (40% ellipsoids) The hydrogen atoms have been omitted for clarity. Selected bond lengths Å: Mo—N(1) 1.725(3), C(7)—C(8) 1.469(4), C(8)—C(9) 1.421(4), C(9)—C(10) 1.408(4), C(10)—C(11) 1.384(5), C(11)—C(12) 1.400(4), C(12)—C(7) 1.418(4), N(2)—C(8) 1.335(4), N(3)—C(7) 1.346(4), Al—N(2) 1.925(2), Al—N(3) 1.926(2).

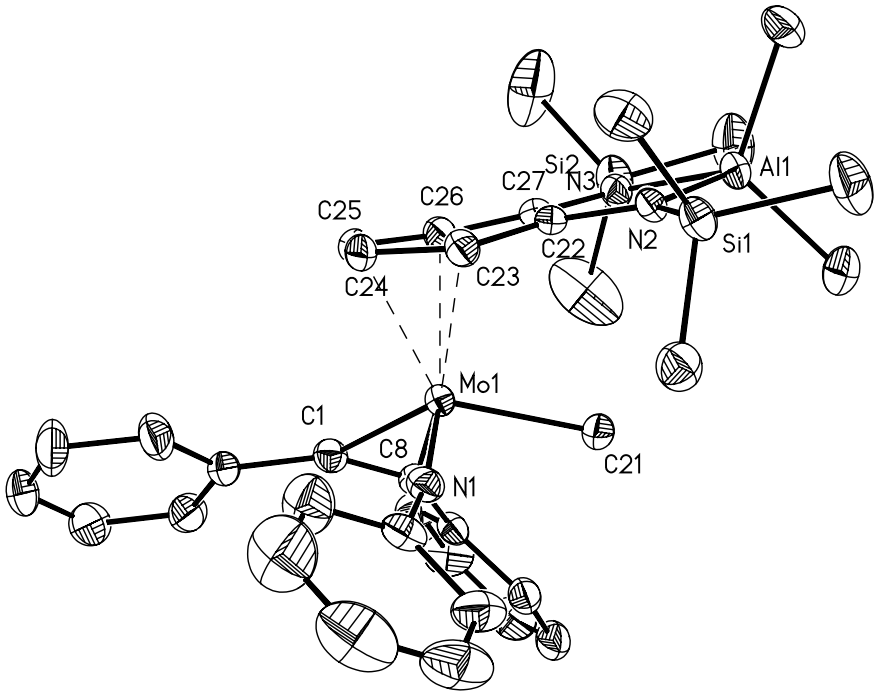

Figure 5-2. Thermal ellipsoid plot of **36** (40% ellipsoids). Hydrogens have been omitted for clarity. Selected bond lengths Å: Mo (1)—N(1) 1.752(2), C(22)—C(23) 1.403(4), C(23)—C(24) 1.405(4), C(24)—C(25) 1.398(4), C(25)---C(26) 1.404(4), C(26)—C(27) 1.416(4), C(22)—C(27) 1.478(4), C(22)—N(3) 1.349(3), C(27)—N(2) 1.339(3), Al(1)—N(3) 1.923(2), Al(1)—N(2) 1.926(2).

The carbon nitrogen bond lengths (average 1.341Å and 1.344Å for **34** and **36** respectively) are slightly shorter than typical for diamide (1.38Å-1.42Å)[122] complexes but longer than diimine complexes (1.28Å).[123] Also, the carbon-carbon bonds of the benzenoid framework are characterized by long Cα—Cα' bonds (1.469Å and 1.478Å).

These data suggest that contributions from the two resonance forms **A** and **B** shown below describe the interaction between the arene fragment and the Mo center. These resonance structures account for the shortened C-N bonds (relative to a diamide structure) and the relatively long Cα—Cα' bonds that are consistent with a single bond between two sp^2 carbon atoms.

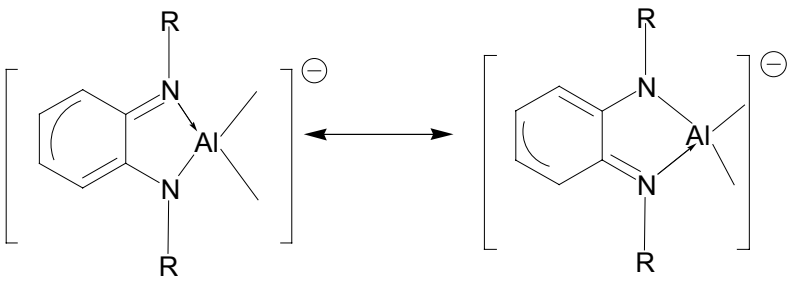

A **B**

DFT calculations[124] were performed on the model compounds $[Me_2Al((o\text{-}(Me_3N)_2\text{-}pda)]^-$, **37** and $(CH_2)_4Mo(CH_3)(NH)(o\text{-}(Me_3N)_2C_6H_4)Al(CH_3)_2$, **38**, in order to understand the structure and bonding in these new complexes. Optimized structures for these models are depicted in Figure 5-3 along with the molecular orbital plot of the HOMO (Figure 5-3c) of this anion. The benzenoid portion of the HOMO is of π symmetry, ideal, for interaction with the empty metal dπ orbitals. The metal center being asymmetric binds strongly with three atoms in **38** while the 4th carbon is less strongly bound due to the *trans* influence of the imido ligand as is observed in the structures of **34** and **36** (Figure 5-3d).

In summary, we have demonstrated the first example of a diamide transfer reaction between trimethyl aluminum and an early transition metal. This transformation involves the formation of a very unusual aluminum anion that stabilizes the molybdenum via π donor interactions. Transfer of carbon to aluminum is known to be an important chain transfer process in aluminum activated α-olefin polymerization reactions. The similar transfer of other ligands, to Al such as diamides has not been investigated[125] These results show the N—Al transfer is possible in early transition metal complexes and suggests that such processes may be possible in diamide containing polymerization catalysis.[126] Preliminary results show that **34** catalyzes the dimerization of ethylene

giving 1-butene at room temperature and 1atm of ethylene pressure. We are currently investigating the utility of these complexes as olefin dimerization catalysts and their relevance to group 4 non-metallocene[125,127] polymerization systems.

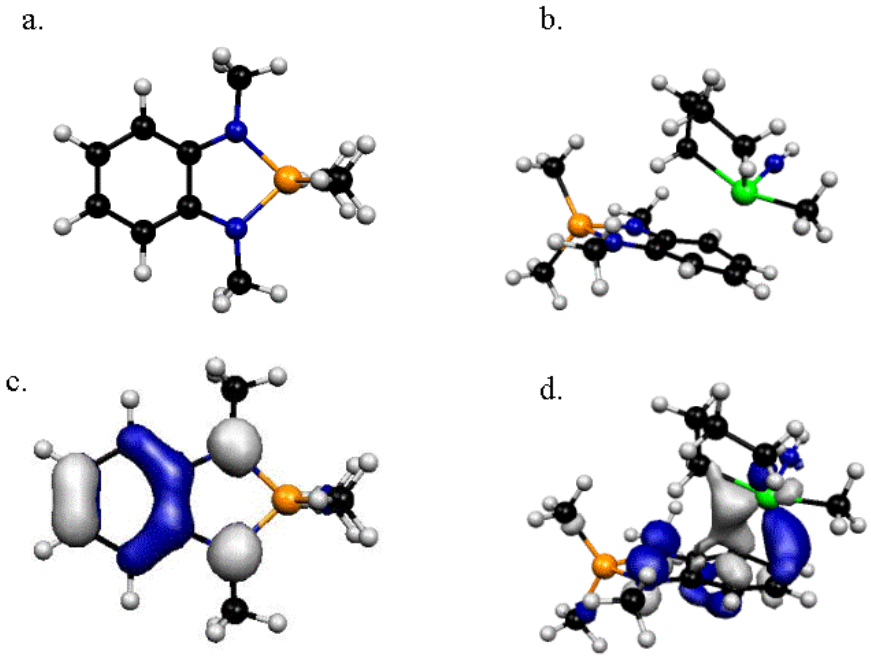

Figure 5-3. Optimized B3LYP structures for model complexes $Me_2Al((o\text{-}(Me_3N)_2\text{-pda})^{-1}$, **37,** and $(CH_2)_4Mo(CH_3)(NH)(o\text{-}(Me_3N)_2C_6H_4)Al(CH_3)_2$, **38** and their molecular orbitals.

Reactivity of Alkyl Aluminum Halides with Group 6 Imido Diamido Olefin Complexes

Alkyl olefin complexes are believed to be intermediates in the Cosseé mechanism[128-130] where an alkene ultimately inserts into a metal carbon σ bond. This mechanism predicts that the type of carbon-carbon bond forming process that may follow olefin insertion i.e. olefin polymerization, oligomerization or dimerization, depends on the rate of chain growth (k_g), versus chain termination via β- elimination (k_t). There are innumerable examples of compounds that appear to catalyze olefin polymerization[101,110,125,127,131] and follow the the Cosseé mechanism, however, the

isolation of d^0 alkyl/alkene complexes has been rare because the absence of dπ electrons prevents stabilization of the olefin and leads to rapid insertion of the olefin into the metal—alkyl bond.[128,129,132]

During the last decade there has been considerable interest in the development of new non-metallocene catalysts in order to harness the potential of other metals to polymerize ethylene. [125,133]This research has led to the development of a wide array of catalysts virtually spanning the entire transition metal series and encompassing a plethora of non-Cp based ligands, including chelating diamides, imido, diketiminates, alkoxides and others.

Chemistry in our group in recent years has focused on group 6 imido complexes incorporating the chelating ((*o*-$(Me_3Si)_2$-pda) (pda = phenylene diamide ligand). We have demonstrated the utility of these ligands in the synthesis of stable isolable high oxidation state alkyl,[30,31] olefin,[32,46] and alkyne complexes, and have emphasized the importance of diamide π donation in stabilizing the metal center. In exploring the reactivity of these complexes with Lewis acids, we discovered serendipitously the unusual diamide transfer reaction of Mo dialkyl complexes with trimethyl aluminum (Scheme 5-1).[134] In these reactions, the chelating diamide ligand is transferred to the aluminum center accompanied by alkylation of Mo, resulting in the isolation of an unusual bimetallic complex. Given the prevalence of alkyl aluminum reagents in olefin oligomerization/polymerization catalysis, we were interested in exploring the reactivity of other molybdenum complexes with alkyl aluminum halides in the hope of elucidating the initial stages of early transition metal mediated olefin polymerization/oligomerization catalysis.

Here we report the reactivity of alkyl aluminum reagents with olefin complexes of the form (η^2-olefin)Mo(NPh)(*o*-$(Me_3SiN)_2C_6H_4$). We begin with the reactivity of the metallacyclopentane complex **25**, Mo(NPh)(*o*-$(Me_3SiN)_2C_6H_4)(CH_2)_4$, with alkyl aluminum halides. This metallacyclopentane reacts by initial β C—C bond cleavage to form a putative Mo—*bis*-ethylene complex that then reacts with the alkyl aluminum halide via diamide transfer as outlined in Scheme 5-1.

The reaction of the styrene complex (η^2-styrene)Mo(NPh)(*o*-($Me_3SiN)_2C_6H_4$) **20C**, with ethyl aluminum dichloride or trimethyl aluminum results in the formation of complexes **39**, (η^2-styrene)Mo(Et)(NPh)η^4-(Cl_2Al((*o*-$(Me_3SiN)_2$-C_6H_4)) or **40**,(η^2-styrene)Mo(CH_3)(NPh)η^4-(($CH_3)_2$Al((*o*-$(Me_3SiN)_2$-C_6H_4)), respectively.

In contrast, the reaction of ethyl aluminum dichloride with **20a**, (η^2-isobutylene)Mo(NPh)(*o*-$(Me_3SiN)_2C_6H_4$), that contains the sterically demanding isobutylene ligand results in the the displacement of isobutylene and the formation of the bridging imido dimer [(μ^2 NPh)Mo(Cl)(η^4-(Cl_2Al((*o*-$(Me_3SiN)_2$-C_6H_4))]$_2$, **41**. The structure of **41** was confirmed by a single crystal X-ray diffraction study.

Reaction of metallacyclopentanes with alkyl aluminum halides.

Treatment of a red/orange toluene solution of **25**, with an alkyl aluminum halide results in a color change from red/orange to yellowish brown in 15 minutes. Removal of solvent under reduced pressure followed by washing the brown solid several times with pentane results in the isolation of **42,**

(η^2-ethylene)Mo(R)(NPh) η^4-(Cl_2Al((*o*-$(Me_3SiN)_2$-C_6H_4)) as a brown powder (Scheme 5-2). Several attempts to crystallize **42** from a variety of solvents have resulted in the

isolation of powder. Therefore the structure of **42** was elucidated by the extensive use of NMR spectroscopy (Figure 5-4).

The protons of the *o*-pda ligand are shifted significantly upfield (4.6—5.6 ppm) upon coordination of the anion $Cl_2Al((o\text{-}(Me_3SiN)_2(C_6H_4})$ to molybdenum. Four distinct signals are assigned to the ethylene protons at 1.04, 1.21, 2.84 and 3.05 ppm with coupling constants suggestive of a metallacyclopropane type structure (J = 14, 10, 2 Hz).

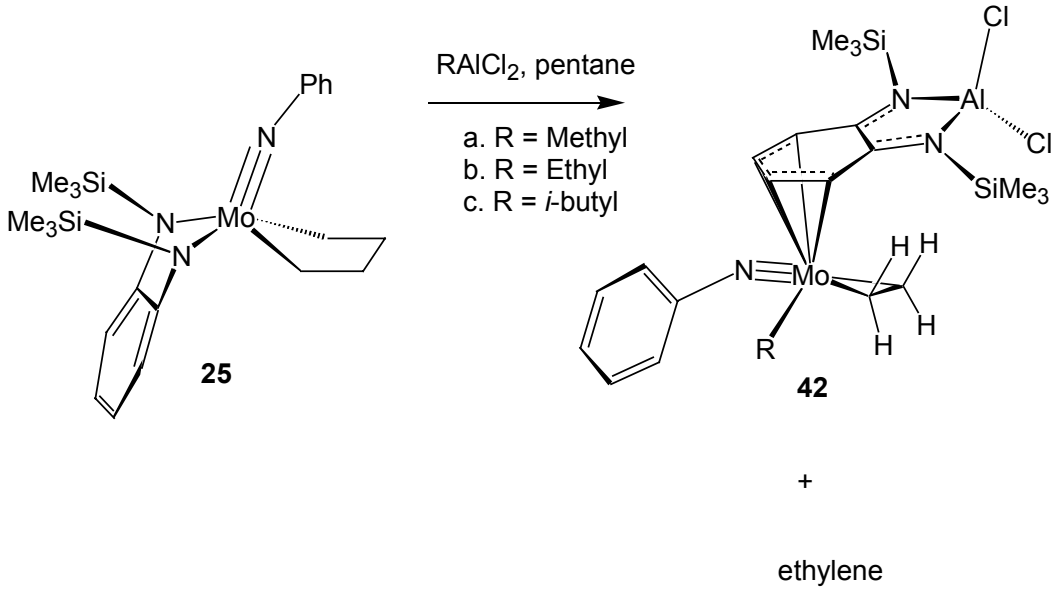

Scheme 5-2. Reaction of metallacyclopentane complex with alkyl aluminum halides

NMR experiments. An array of 2D NMR spectroscopic techniques (gHMQC, gHMBC, NOESY) was utilized to establish the structure of **42b** (η^2-ethylene)Mo(Et)(NPh) η^4 -($Cl_2Al((o\text{-}(Me_3SiN)_2\text{-}C_6H_4))$ (Figure 5-5). The protonated carbons were assigned to their corresponding protons via gHMQC spectra. Long-range coupling of the ethylene carbons (49.0 and 49.7 ppm) to the CH_2 protons of the ethyl fragment (2.22 ppm) were observed in the gHMBC spectrum. Strong NOE's in the 2D ^{1}H NOESY spectrum, places the proton at (5.23ppm) on the same side as SiMe3 protons (0.32ppm) and the proton at (4.70ppm) on the same side as SiMe3 protons (0.26ppm).

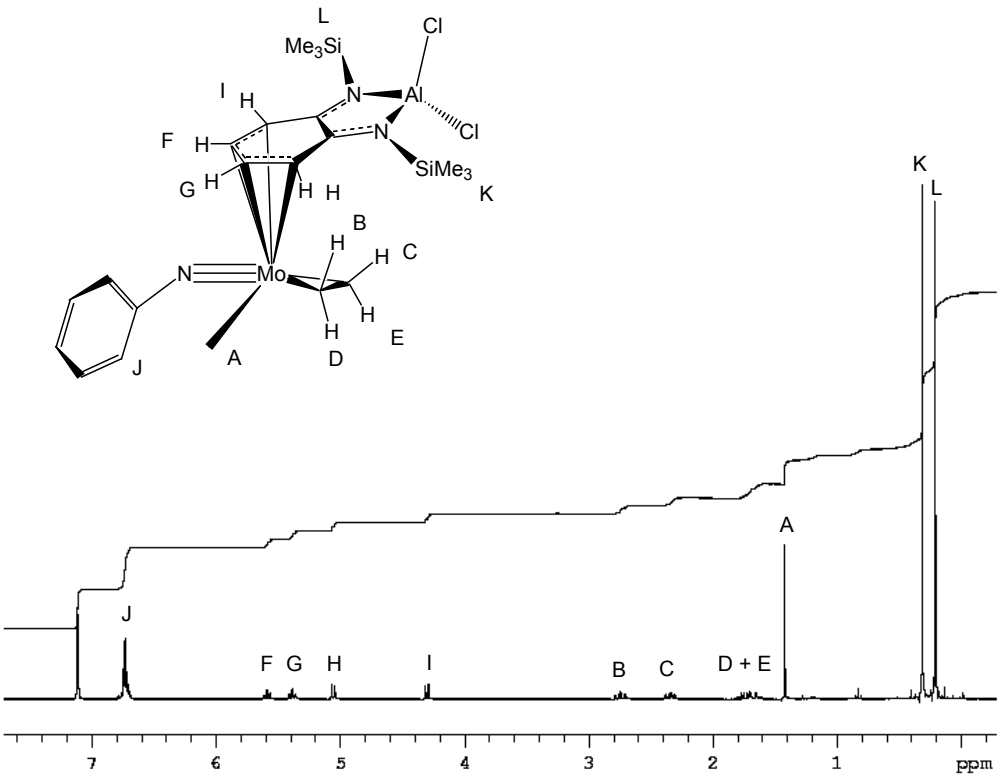

Figure 5-4. ^{1}H NMR spectrum of **42a**, (η^2-ethylene)Mo(Me)(NPh) η^4-(Cl_2Al((*o*-$(Me_3SiN)_2$-C_6H_4)) in C_6D_6.

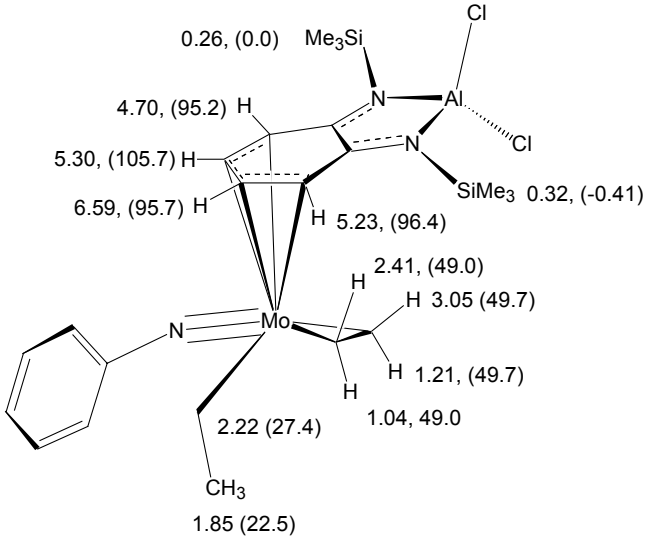

Figure 5-5. Proposed structure for **42b** showing selected carbon and (parentheses) and proton chemical shifts assigned by NMR spectroscopy.

The reactivity of **25** with alkyl aluminum halides differs from the analogous reaction with halide free alkyl aluminum reagents such as trimethyl aluminum. The proposed reaction sequence is shown in Scheme 5-3. The formation of a heterobimetallic

complex by coordination of aluminum to the diamide lone pair electrons is plausible as Lewis acid/base adducts have been isolated and characterized with lanthanide metals.[117,135] However, no intermediates are seen in this reaction even at -60^0C. In the case of alkyl aluminum halides β C—C bond cleavage seems to be induced resulting in the loss of ethylene. This reaction proceeds via prior rearrangement of the metallacycle as shown in path B of Scheme 5-3.

The difference in reactivity seen between alkyl aluminum halides and trialkyl aluminum, results from the accessibility of the diamide lone pair electrons. Computational studies done by Galindo *et al.*,[62] and in our labs,[32] have revealed that the nitrogen lone pairs on the chelating diamide ligand in d^0 complexes are involved in bonding to the metal center via donation into the empty metal $d_{x^2-y^2}$ orbital, and is responsible for the folding of the diamide ligand. This occurs because the HOMO of the chelate is close in energy to the empty metal d – orbitals. As outlined in Scheme 5-3, the square pyramidal (SP) metallacylopentane complex, undergoes a rearrangement to a trigonal bipyramidal metallacyclopentane complex, which then undergoes β C—C bond cleavage to form the *bis*-ethylene complex.

In the (TBP) complexes the $d_{x^2-y^2}$ orbital lies in the node of diamide lone pair electrons and does not interact significantly with this orbital (the linear combination of diamide lone pair electrons is of a'' symmetry compared to the a' $d_{x^2-y^2}$ orbital). Thus there is a greater stabilization of the diamide chelate's HOMO in **25**, than in the TBP intermediates. The diamide lone pair electrons on the metallacyclopentane complex requires the more acidic trialkyl aluminum reagents[109] in order for diamide transfer to be induced.

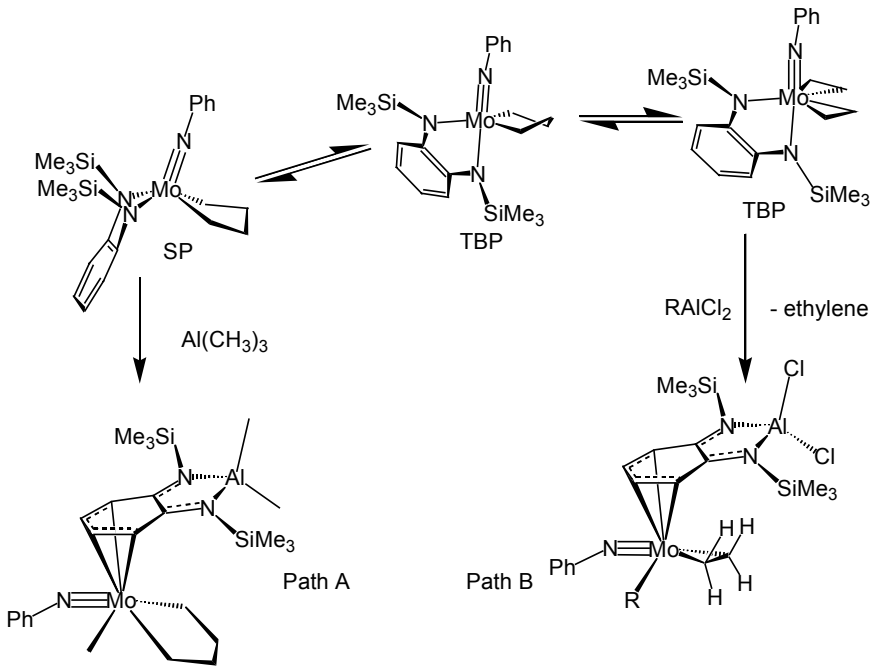

Scheme 5-3. Two pathways for the reaction of metallacyclopentanes with alkyl aluminum reagents

Reactivity of alkyl aluminum reagents with styrene complexes

Inspired by reactivity of alkyl aluminum reagents, with **25**, we investigated the reactivity of olefin complexes with alkyl aluminum reagents. Treatment of a toluene solution of **20C**, (η^2-styrene)Mo(NPh)(*o*-($Me_3SiN)_2C_6H_4$) with 1.2 molar equivalents of trimethyl aluminum, results in diamide transfer and the bimetallic complex **39** as a mixture of two isomers (Scheme 5-5).

The two isomers differ in the orientation of the methyl group transferred from trimethyl aluminum. In **39a** the methyl group is oriented on the same side as the phenyl substituent of the styrene ligand, whilst the methyl group is on the same side of the methylene fragment of the styrene ligand in **39b**. The two isomers can be separated by crystallization from pentane. An X-ray crystal structure determination of **39a**, was obtained and confirms the stereochemistry of **39a**. However we were not able to obtain

crystals of a quality necessary for an accurate structure refinement, therefore, **39a** is depicted in Figure 5-6 for the purposes of confirming the stereochemistry.

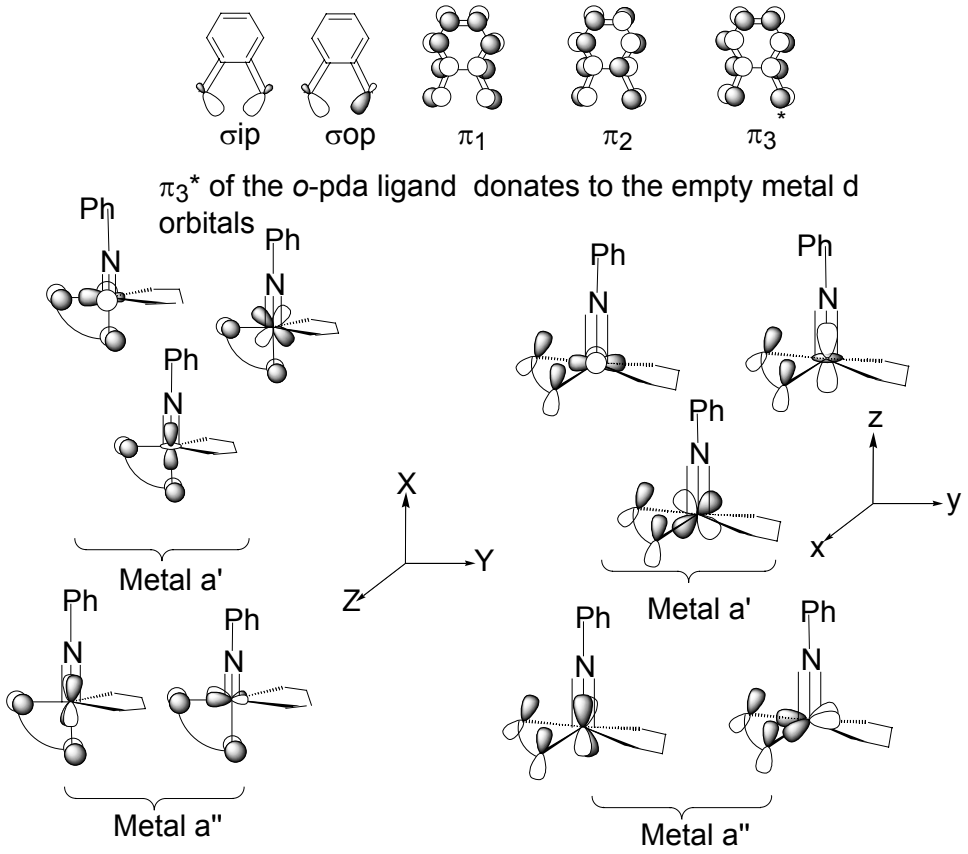

Scheme 5-4. Orbital interactions in square pyramidal (SP) metallacyclopentane complex and trigonal bipyramidal metallacyclopentane complex

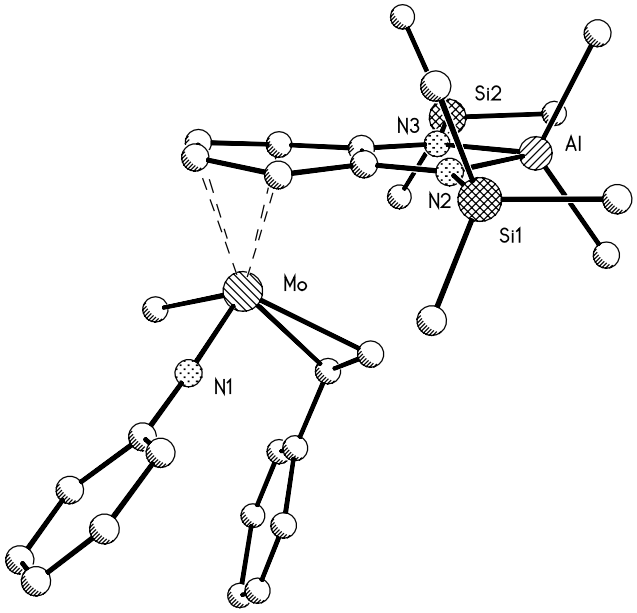

Figure 5-6. X-ray structure determination of **39a**

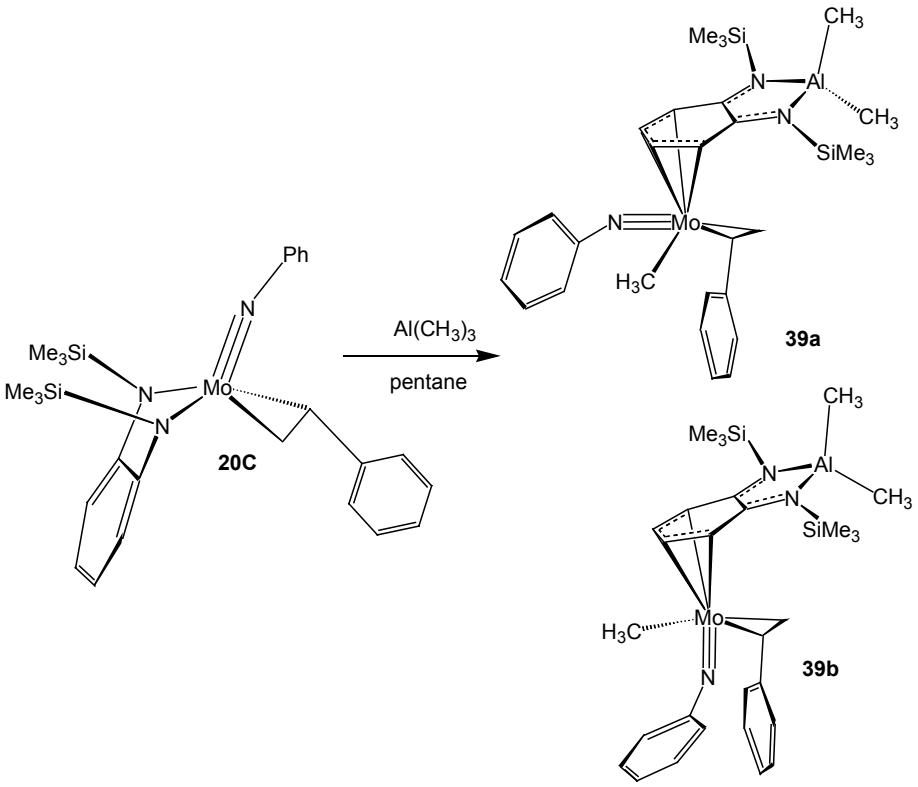

Scheme 5-5. Reactivity of styrene complex with trimethyl aluminum

2D ^{1}H NMR studies. The stereochemistry of **39** was also determined by ^{1}H NMR spectroscopy. Structures for **39a** and **39b** as determined by gHMQC, gHMBC, and NOESY spectroscopy are depicted in Figures 5-7 and 5-9.

The methyl proton in **39a** (1.29ppm), displays NOe's to two phenyl ortho protons (6.55 and 7.00 ppm), two protons from the *o*-pda ligand (4.71 and 5.51 ppm) and one proton from the styrene fragment (2.84 ppm) (Figure 5-8). In contrast, the NOESY spectrum of **39b** the methyl proton (1.32 ppm) showed NOe's to an ortho phenyl proton (6.20), two *o*-pda ring protons (4.96, 5.48ppm), and the two methylene protons (2.99, and 1.97ppm) (Figure 5-10). These results confirm the assignment of the methyl group *cis* to the methylene group in **39b**, and *cis* to the phenyl group in **39a**. The NOESY spectrum did not display any chemical exchange peaks between **39a** and **39b** at 25^{0}C.

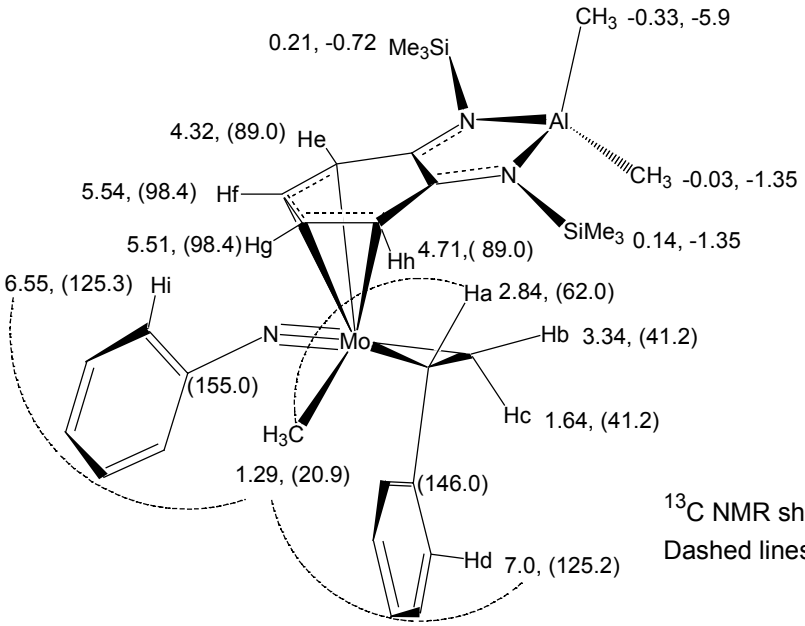

gHMBC
Methyl proton (1.29 ppm) shows 3 bond correlations to the methylene carbon at 41.2 ppm
Metallcycle proton 2.84 shows 2-bond correlations to the methylene carbon at 41.2 and to the phenylene carbon at 146.0ppm

Figure 5-7. Proposed structure for **39a** showing selected carbon and (parentheses) and proton chemical shifts assigned by NMR spectroscopy.

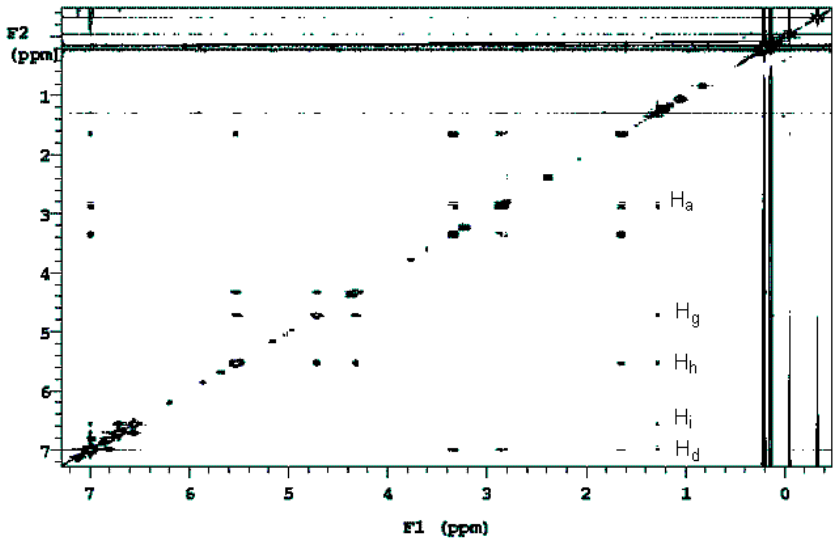

Figure 5-8. ^{1}H NOESY spectrum of **39a**

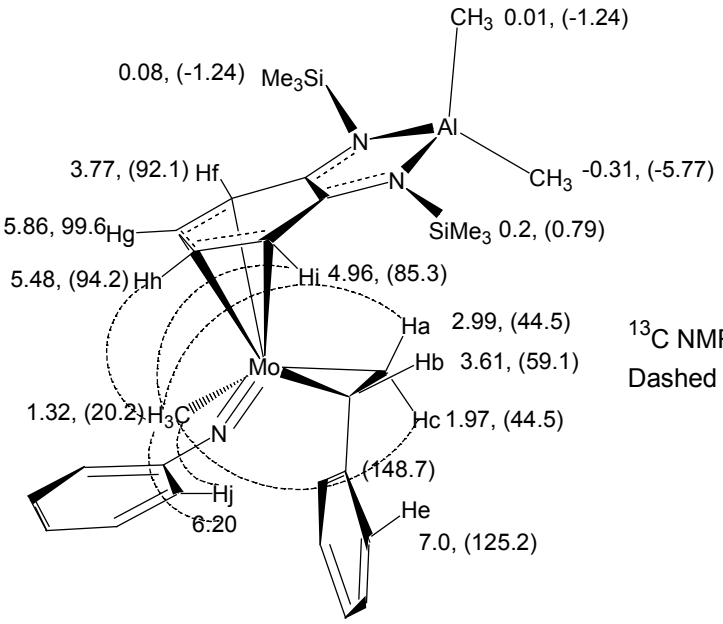

^{13}C NMR shifts are in parentheses
Dashed lines represent NOE's

gHMBC
Methyl proton (1.32ppm) shows 3 bond correlations to the methylene carbon at 44.5ppm
Metallcycle proton 3.61 shows 2-bond correlations to the methylene carbon at 44.5 the phenylene carbon at 148.7ppm

Figure 5-9. Proposed structure for **39b** showing selected carbon and (parentheses) and proton chemical shifts as assigned by NMR spectroscopy.

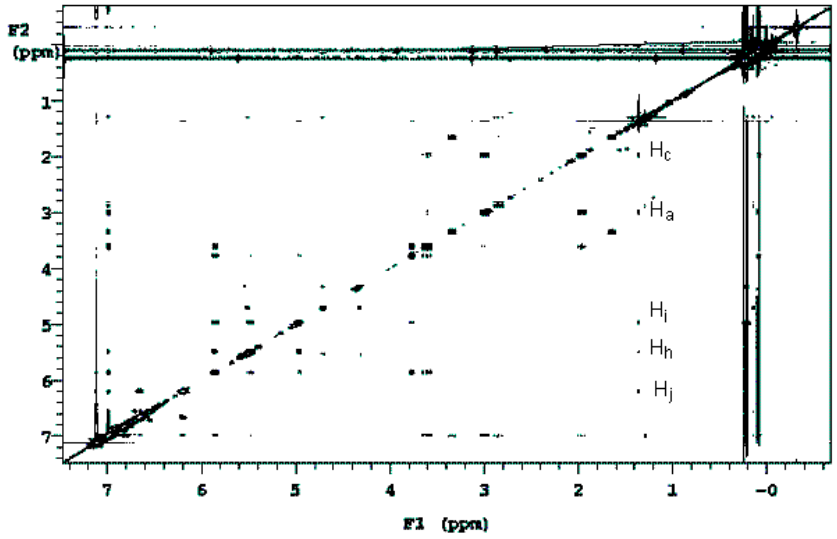

Figure 5-10. ^{1}H NOESY spectrum of **39b**

Reactivity with alkyl aluminum halides.

Treatment of **20c** with 1.2 equivalents of methyl aluminum dichloride, results in the bimetallic complexes **40a** and **40b**. In this case we were not able to separate the two

isomers but there structures were confirmed by NMR spectroscopy. Again, the methyl group in **40a** was oriented *cis* to the phenyl group of the styrene ligand, whilst this group is oriented *cis* two the methylene fragment in **40b**.

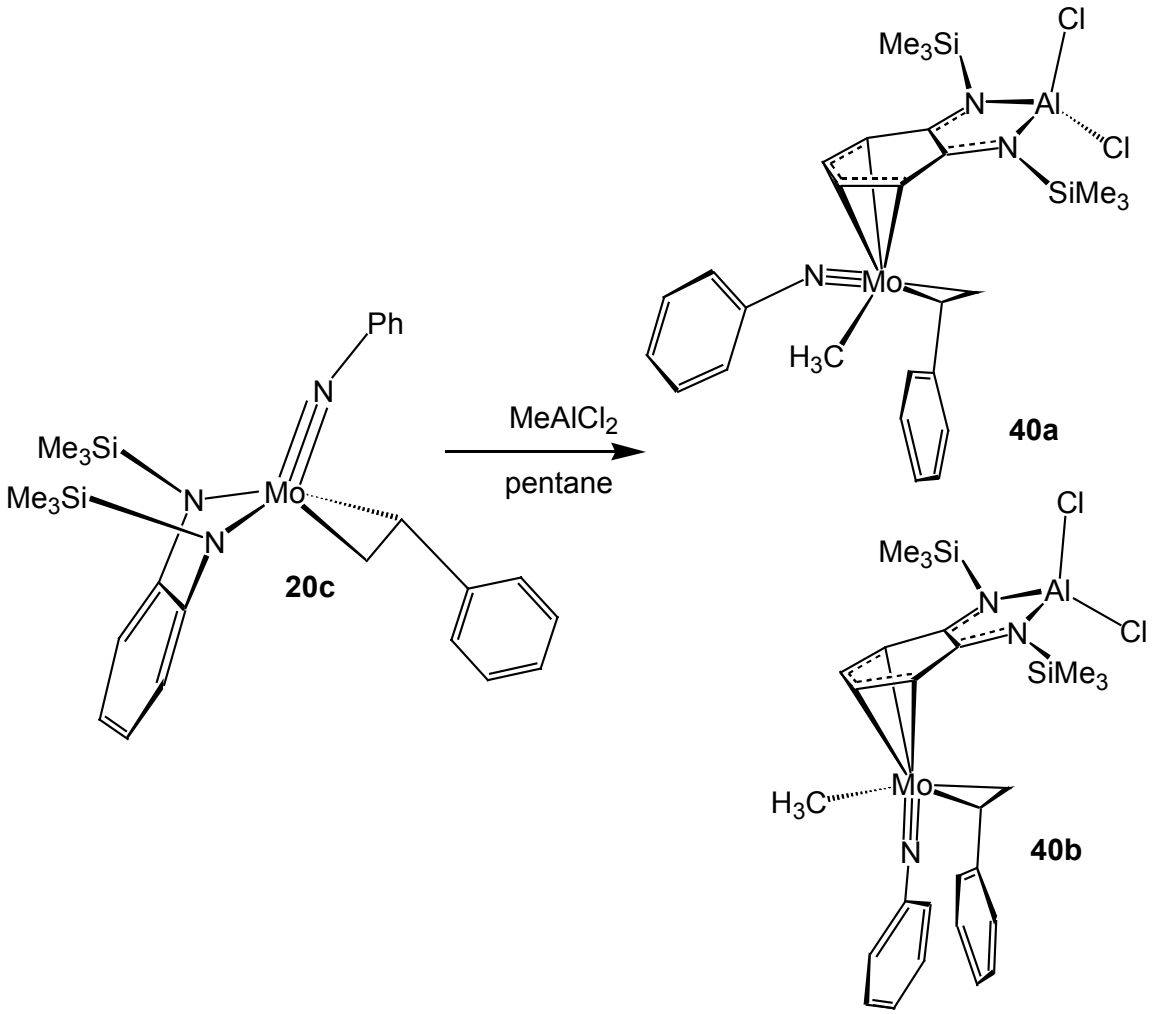

Scheme 5-6. Reaction of styrene complex with methyl aluminum chloride

Reactivity of an isobutylene complex with $EtAlCl_2$

When the isobutylene complex **20a**, (η^2-isobutylene)Mo(NPh)(*o*-($Me_3SiN)_2C_6H_4$), is treated with one equivalent of ethyl alumnum dichloride in pentane. The dimeric complex **41**, [(μ^2 NPh)Mo(Cl)(η^4-(Cl_2Al((*o*-($Me_3SiN)_2$-C_6H_4))]$_2$, precipitates as a green powder (Scheme 5-7).

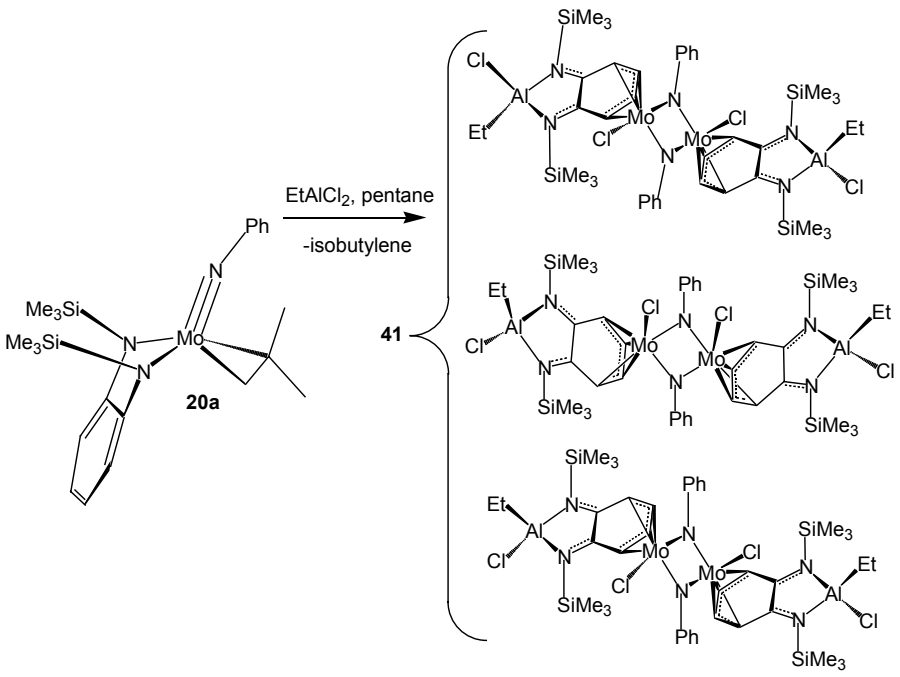

Scheme 5-7. Reaction of isobutylene complex with ethyl aluminum chloride

Complex **41** exists as a mixture of three isomers that are not resolved at 25^0C in the 300 MHz ^{1}H NMR spectrum. However, the spectrum taken on a 500 MHz instrument revealed the presence of three molecules. The 2D ^{1}H NOESY spectrum of **41**, revealed consisted of three dimeric complexes. Three distinct resonances for three different $SiMe_3$ groups are detected (0.28, 0.29, 0.30 ppm). These protons show NOe's in the 2D NOESY (Scheme 5-8) to three distinct aluminate anion $[EtAl(Cl)((o\text{-}(Me_3N)_2\text{-}o\text{-pda})]^{-1}$ rings (Scheme 5-8).

The sterically demanding isobutylene ligand in **20a** is easily displaced by the by the $EtAlCl_2$. After undergoing diamide transfer, the molecule dimerizes through the imido groups as shown in Scheme 5-9. The relative dispositions of the chloride ligands on the Mo and the Cl and Et groups on Al give rise to 4 possible isomers. Three of these isomers are seen in our system; however, because of extensive overlap between the

proton resonances of these isomers it was not possible to assign unambiguously the absolute configuration for each isomer.

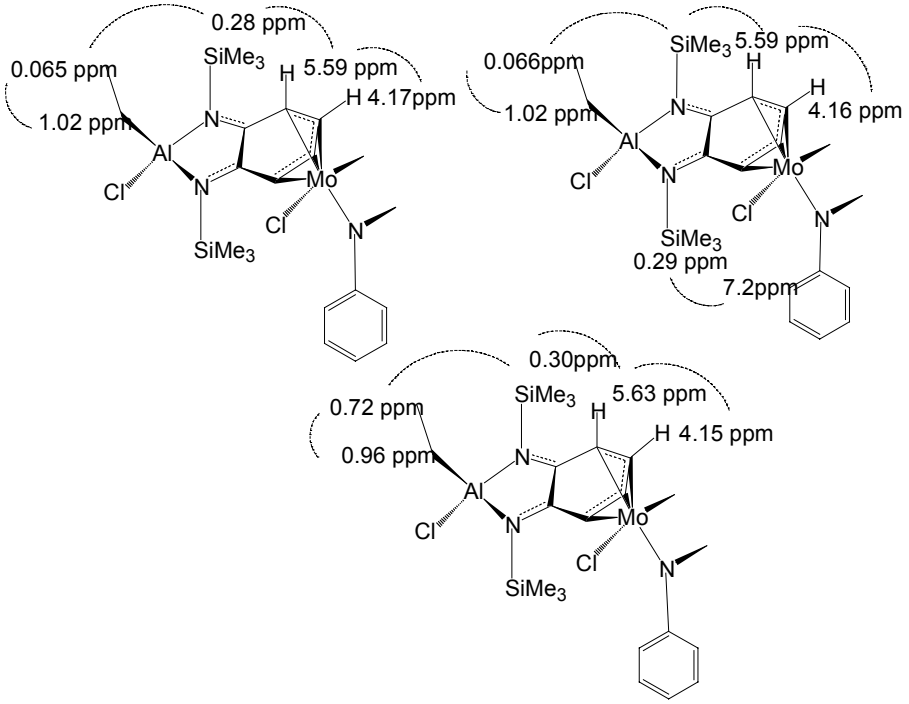

Scheme 5-8. NOE's of isomers of **41**

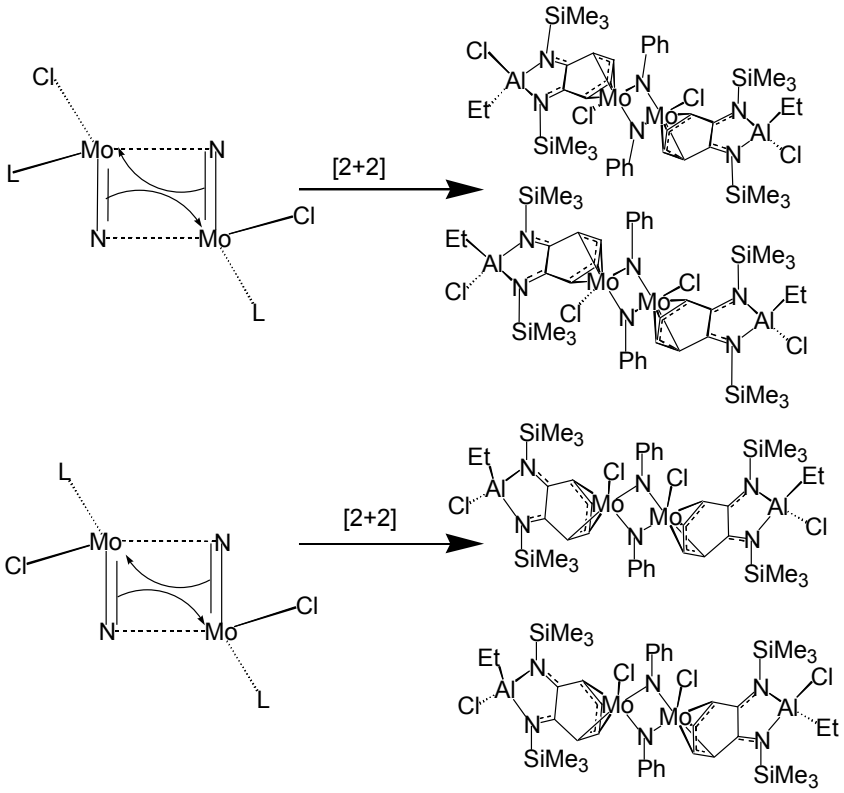

Scheme 5-9. [2+2] cycloaddition reaction of the imido ligand

Crystal Structure of **41**. X-ray quality crystals of **41** were obtained by slow diffusion of pentane into a concentrated toluene solution of **41** (Figure 5-11). The asymmetric unit of **41** consists of ¼ of the dimer. The molecule possesses a C_2 axis and a mirror plane. The $Al(Cl)(C_2H_5)$ moiety is disordered and is refined in two parts. Their site occupation factors were dependently refined to 0.29(1) for the major part, and consequently 0.21(1) for the minor part. These moieties lay on the mirror plane thus the site occupation factors site above add up to 50%.

The coordination geometry about each molybdenum atom is best described as a distorted square pyramid, with the chloride ligands occupying the apical position and the η^4 aluminate anion occupying two coordination sites.

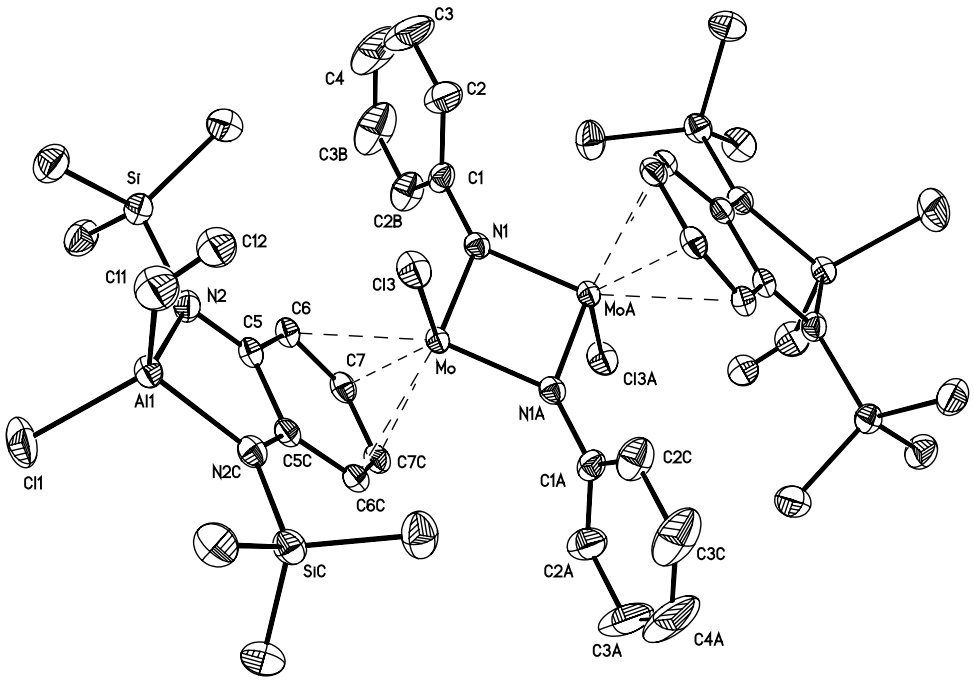

Figure 5-11**.** Thermal ellipsoid plot of **41**, (40% ellipsoids). Selected Bond Lengths (Å): Mo—Cl (3), 2.337; Mo—C (7), 2.269; Mo—N (1), 1.931; Mo—C (6), 2.487; C(5)—N(2), 1.335; C(7)—C(7C), 1.409; C(5)—C(5C), 1.501.

The bonding of the aluminate anion, $[EtAl(Cl)((o\text{-}(Me_3N)_2\text{-}o\text{-pda})]^-$, to molybdenum in **41**, is similar to other Mo complexes synthesized in our group where an alkyl aluminum reagent induces transfer of the diamide ligand. The crystal structure of **41** suggests that there is localization of the charge in the benzenoid portion of the *o*-pda ring (compare the C(5)—C(5C) bondlength (1.501Å) with the C(7)—C(7C) bond length (1.409). Also the C(5)—N(2) (1.335Å) bond length is more closely associated with a semibenzoquinone diimine type structure than a diamide structure.[136-140]

There has been a tremendous amount of research on the unsubstituted *o*-phenylenediamido, $[C_6H_4(NH)_2\text{-}o]^{2-}$, ligand and its "non-innocence" when encountered in transition metal chemistry. In addition to the dianionic diamido form, complexes possessing the monoanionic semibenzoquinone diimine, and neutral benzoquinone diimine ligands have all been observed.

In all complexes involving these ligands the diamide lone pair electrons are intimately involved in the stabilization of the metal center. In group 6 complexes for example, the diamide lone pair electrons are donated into the empty metal d orbitals and the ligand subsequently folds, whereas in group 8 metal complexes the metal d orbitals π back bond into the ligand C—N π^* orbital and subsequently the ligand is flat.[136,141]

Unlike the case with transition metals, aluminum does not posess d orbitals that are low enough in energy to interact with the diamide orbitals. Furthermore, the trivalent nature of the aluminum ion results in an overall negative charge on the newly formed aluminate anion. The excess charge density in this anion is localized onto the benzenoid portion of the *o*-pda ring which subsequently interacts with the molybdenum center through its π electrons. This type of bonding interaction has been observed in DFT

calculations (B3LYP/LANL2DZ) on the model complex $(CH_2)_4Mo(CH_3)(NH)(o\text{-}(Me_3N)_2C_6H_4)Al(CH_3)_2$.[134]

Summary

We have extended the unique diamide transfer reactivity of Mo dialkyls with trimethyl aluminum to other aluminum reagents (alkyl aluminum halides) and olefin complexes. The observed difference in reactivity between alkyl aluminum reagents and alkyl aluminum halides in their reactions with metallacyclopentanes results from the decreased availability of the diamide lone pair electrons in the square pyramidal metallacyclopentane complex. This reactivity leads to the synthesis of stable isolatable alkyl olefin complexes. The alkyl aluminum induced diamide transfer reaction is quite general for molybdenum and we are currently exploring the implications of this reaction in olefin dimerization/oligomerization reactions.

Implications of Aluminum Induced Diamide Transfer to Olefin Dimerization Catalysis

Previous work from our group showed that exposure of a mixture of $W(CH_2)_4(NPh)(o\text{-}(Me_3SiN)_2)$, **13**, and $EtAlCl_2$ to a positive pressure of ethylene resulted in the dimerization and codimerization of the olefin to form a mixture of C_6 products (Scheme 5-10).[142] This olefinic product distribution shown in Scheme 5-10 is not consistent with the well-known Cossee mechanism of olefin polymerization; instead a metallacyclic mechanism must be invoked to explain the observed product selectivity (Scheme 5-11).

The exact nature of the catalytic species is still not known for this process. Therefore, the preceeding work on Mo was attempted in order to attain some insight into the mechanism of these dimerization reactions. In the case of Mo, it seems clear that diamide transfer is an important step in the interaction of the metallacyclopentane with

alkyl aluminum reagents. However, unlike Mo, treatment of the W metallacyclopentane with an alkyl aluminum halide does not result in the disruption of the metallacycle and the liberation of ethylene but instead proceeds with the liberation of 1-butene i.e β C—C bond cleavage was not induced in the case of W. We investigated stoichiometric reactions between various aluminum reagents and W metallacyclopentanes in order determine the nature of any intermediates in this catalysis and in order to investigate their catalytic activity.

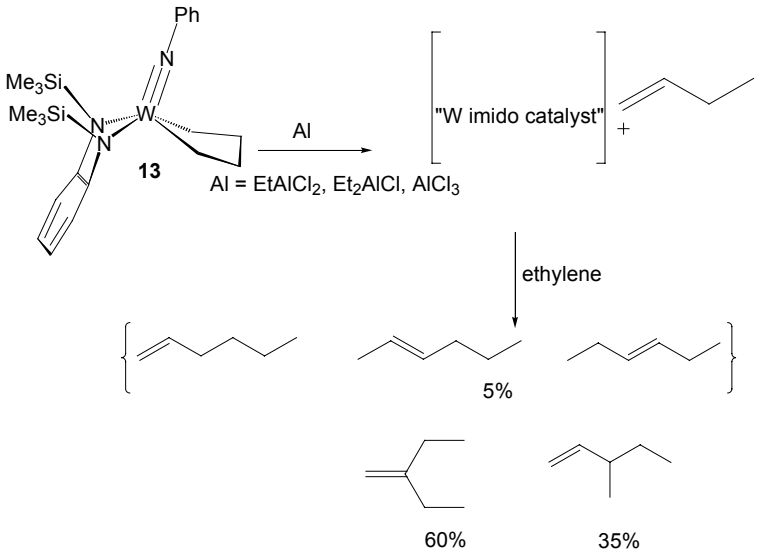

Scheme 5-10. Lewis acid promoted dimerization of ethylene

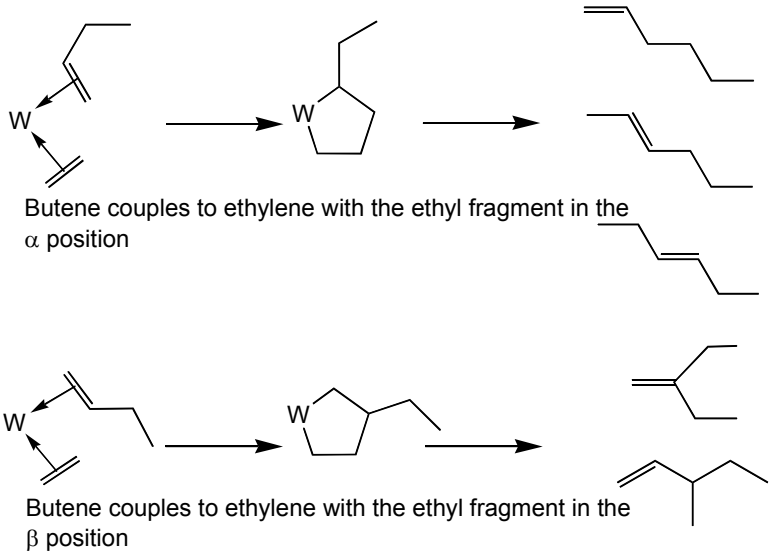

Scheme 5-11. Olefin dimerization based on metallacycle mechanism

Reactions of W complexes with alkyl aluminum reagents

Synthesis of metallacyclopentane methyl complex **42**. In a resealable NMR tube, treatment of a C_6D_6 solution of the metallacyclopentane complex **13**, with 1.2 equivalents of trimethyl aluminum slowly results in the formation of the metallacyclopentane complex **42** after two days (Scheme 5-12).

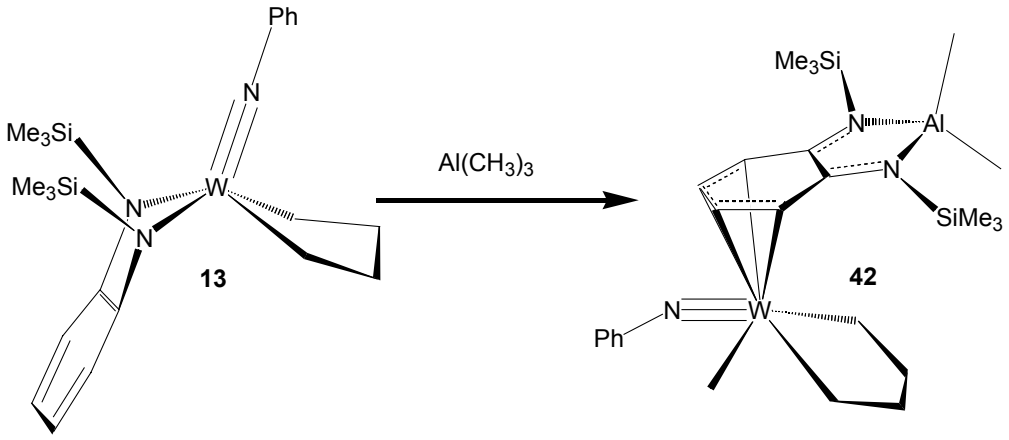

Scheme 5-12. Reaction of W metallacyclopentane with trimethyl aluminum

Attempts to isolate **42** on a preparative scale gave an oil that was difficult to purify. However an examination of the proton spectrum of **42** reveals that it is very similar to the metallacyclopentane methyl complex obtained for Mo (Figure 5-12). The benzenoid protons of the aluminate anion are clearly evident (4.6-5.5 ppm). Three methyl groups (1.2, 0.08, -0.2ppm) and two $SiMe_3$ protons(0.19, 0.17ppm) are also observed.

Reaction with $EtAlCl_2$. Treatment of a C_6D_6 solution of **13** with 1.2 equivalents of $EtAlCl_2$ results in the transfer of the *o*-pda ligand (Scheme 5-13). The exact nature of the species formed could not be determined because the new species quickly decomposes (overnight) in solution. It is clear that an aluminate type species very similar to those seen with Mo is formed during this reaction because of the appearance of peaks between 5.4-6.6 ppm as in the proton NMR spectrum, which are characteristic of the η^4 arene coordination observed in these compounds. Also significant, is the observation that

unlike the reaction of alkyl aluminum halides with the Mo metallacyclopentane which undergoes β C—C cleavage, the reaction between alkyl aluminum halide and **13** retains the metallacycle framework and no ethylene is released during this reaction. Interestingly, treatment of **13**, with two equivalents of $EtAlCl_2$ results in the liberation of butene and a material is formed that then goes on to catalyze the formation of the C6 products identified in the catalysis.

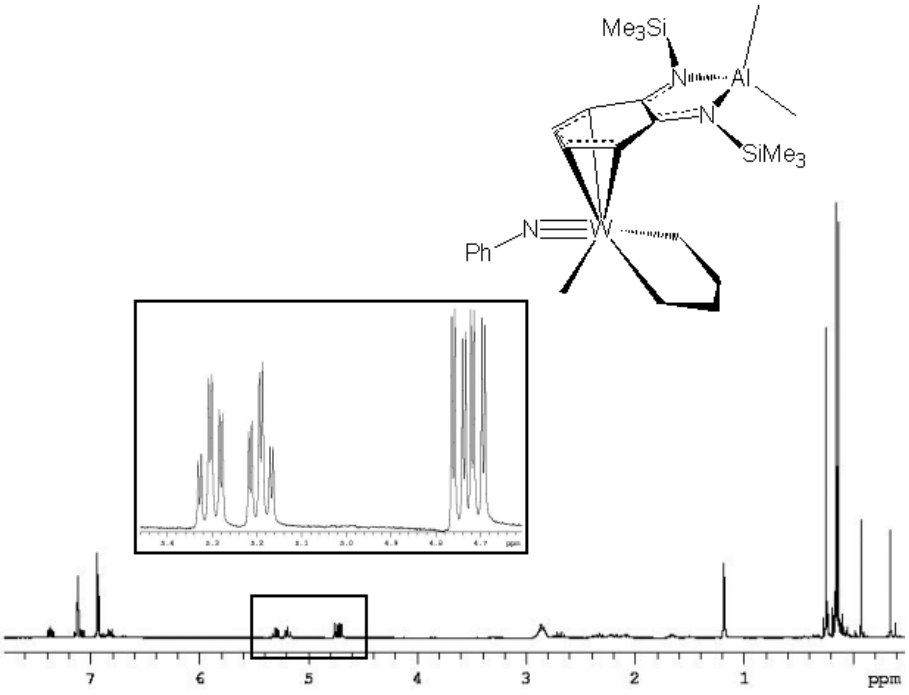

Figure 5-12. ^{1}H NMR spectrum of W metallacyclopentane methyl complex

Diamide transfer to other W complexes.

Diamide transfer to aluminum from other W complexes can also be observed. Treatment of the diphenyl acetylene complex **43**, and the neopentylidene complex **12** with 2 equivalents of trimethyl aluminum also results in the transfer of the diamide ligand (Scheme 5-13). The exact nature of the species formed in these reactions is still unclear as these compounds have not been isolated. However, in the case of **12**, it is clear that two new alkylidene species are formed as two new resonances for the alkylidene protons

(9.3 and 9.1ppm) are observed in the ^{1}H NMR spectrum along with the peaks for the aluminate anion, $[Al(CH_3)_2((o\text{-}(Me_3N)_2\text{-}o\text{-pda})]^-$ (Figure 5-13)

These results demonstrate that the transfer of the diamide group to alkyl aluminum reagents is a general reaction pathway in this class of group 6 imido diamide complex. The generality of this reaction may have important implications on the function of other early transition metal amide complexes that function as α–olefin polymerization catalysts when they are activated by alkyl aluminum reagents. The transfer of a diamide ligand to aluminum has never been considered as a part of the catalyst activation process in these materials.

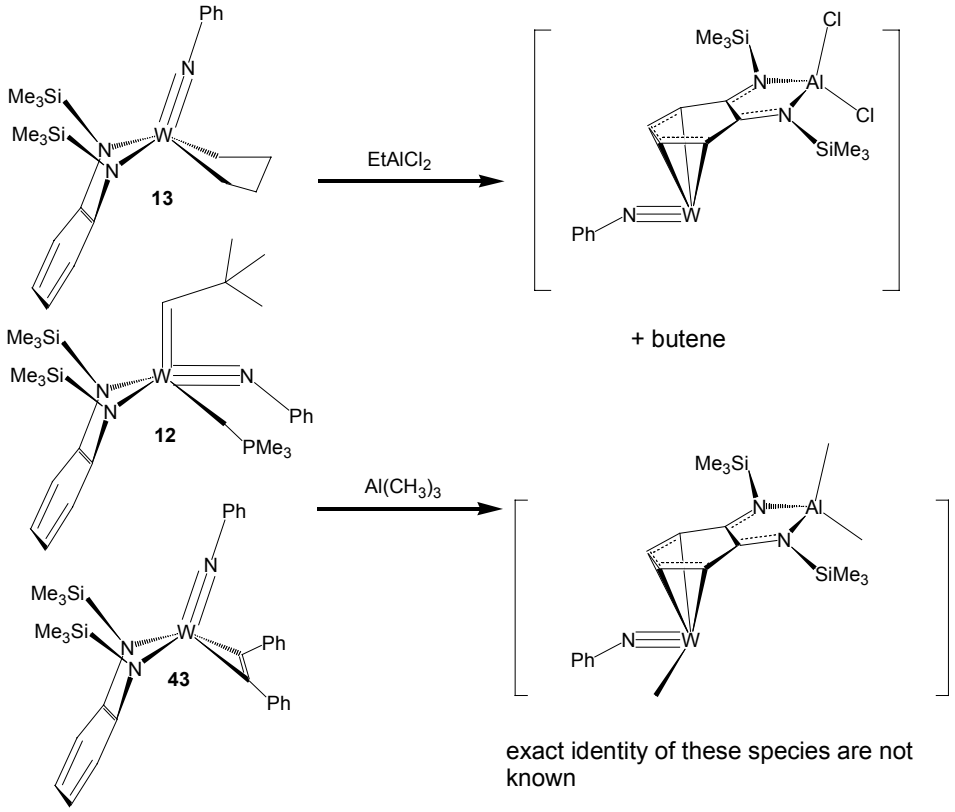

Scheme 5-13. Diamide transfer reactions of W complexes

Conclusions

We have demonstrated in this chapter the novel diamide transfer of the *o*-pda ligand in group 6 metals induced by alkyl aluminum halides. These findings have the potential to be of great interests to a significant portion of the organometallic chemistry community not only because of the possibilities of discovering new catalytic systems but also because they may provide insight into the mechanisms of traditional catalysis i.e. Ziegler Natta and/or metallocene olefin polymerization that use high concentrations of aluminum reagents as cocatalysts in there systems.

The discovery that the diamide transfer is also induced in W is significant as it offers the potential of elucidating the reaction mechanisms of the olefin dimerization/codimerization of ethylene seen in our group. Work is currently underway attempting to isolate some of the species derived from the stoichiometric reaction of W complexes with alkyl aluminum reagents.

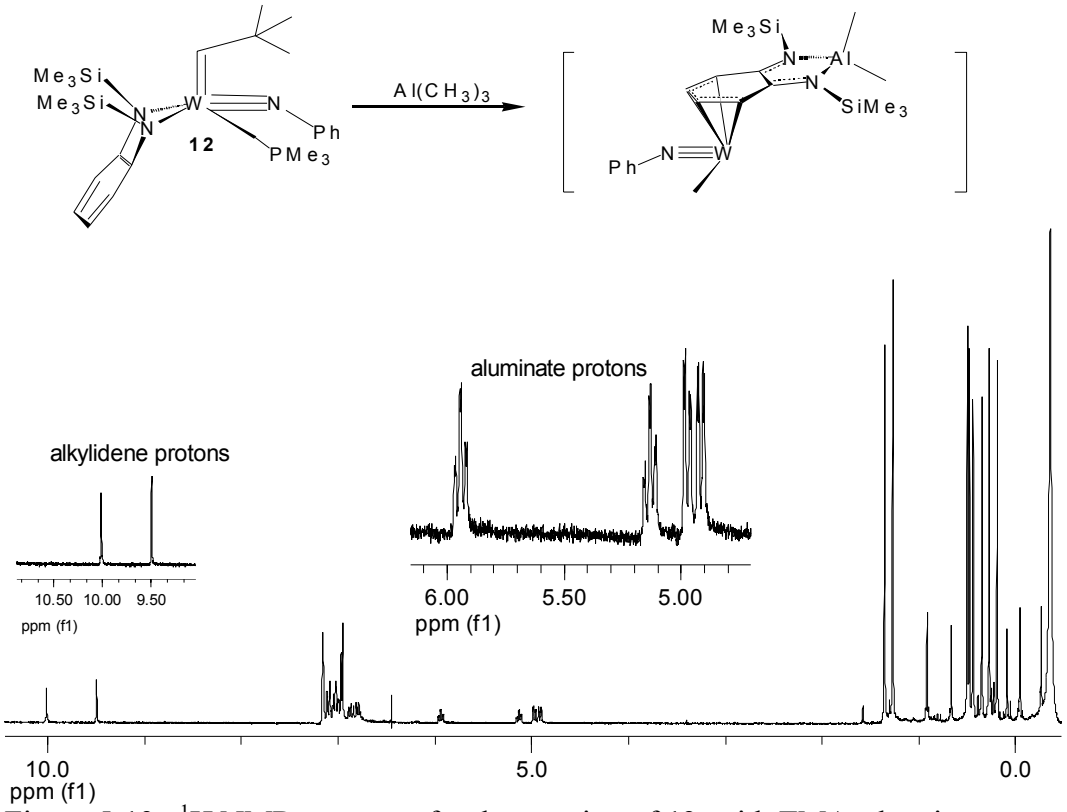

Figure 5-13. ^{1}H NMR spectrum for the reaction of **12**, with TMA, showing resonances for the aluminate anion, $[Al(CH_3)_2((o\text{-}(Me_3N)_2\text{-}o\text{-pda})]^{-1}$, (right inset), and two alkilidene species (left inset).

CHAPTER 6
EXPERIMENTAL

General Methods

All reactions were conducted under a dry argon atmosphere using standard Schlenk techniques and all compounds were handled in a nitrogen-filled dry box. All solvents were distilled under nitrogen from sodium or sodium benzophenone ketyl or passed over activated alumina, stored over molecular sieves, and degassed prior to use. Compounds **4**, **20a**, **20c**, and **25** were synthesized according to published procedures.[30,46,74] All aluminum reagents were purchased from Aldrich and used without further purification.

NMR spectra were obtained on Varian Gemini 300, VXR 300, or Mercury 300 instruments with C_6D_6, C_7D_8, or $CDCl_3$ as solvents, as noted, and referenced to residual solvent peaks. A Varian Inova 500 or a Mercury 300bb equipped with an indirect detection probe was used as indicated for the GHMQC, GHMBC, and NOESY experiments.

The full X-ray diffraction data for all compounds are stored on a database that can be accessed at http://xray.chem.ufl.edu/chemIndex.htm. Contact Dr. Khalil A. Abboud at 352-392-5948 for more information.

Synthesis of η^2 –alkyne complexes

R_1 = H, R_2 = CO_2Me, (**21a**) Methyl propiolate 0.17ml(1.94mmol) was added drop-wise with stirring to a pentane solution of **20a** 0.959g (1.94 mmol). An immediate color change from green to orange occurred. The reaction mixture was allowed to stir for ½ hour after which the solution was concentrated by removal of the solvent *in vacuo*. The

pentane solution was reduced to *ca.* 10ml and then cooled to –78^{0}C for two hours. Orange crystals appeared and after filtration [Mo (NPh)(η^2–methyl propiolate)(*o*-($Me_3SiN)_2C_6H_4$)], **21a** was obtained in 82% yield. Recrystallization from concentrated pentane solutions of **21a** allowed for further purification. ^{1}H NMR (C_7D_8 20^0 C): δ 9.13 (s 1H alkyne proton) 7.33 (d 2H J = 8.1 Hz phenyl imido *ortho* protons) 7.20 (bs 2H *o*-pda ring protons) 6.80 (t 1H phenyl imido *para* proton J = 7.7 Hz) 3.44 (s 3H CO_2Me protons) 0.48 (s 18H $SiMe_3$ protons). One *o*-pda and one phenyl imido resonance is overlapping with sovent. ^{1}H NMR (C_7D_8 -50^0 C): δ 9.08 (s 1H alkyne proton) 7.42 (d, 2H J = 7.2 Hz phenyl imido *ortho* protons) 7.27 (d 2H J = 7.8 Hz *o*-pda ring protons) 6.93 (t 1H J = 7.5 Hz phenyl imido *meta* proton) 6.80 (t 1H J = 7.5 Hz phenyl imido *para* proton) 3.42 (s 3H CO_2Me protons) 0.49 (s 9H $SiMe_3$ protons) 0.45 (s 9H $SiMe_3$ protons). One *o*-pda resonance is overlapping with solvent. ^{13}C NMR (C_6D_6 20^0 C): δ 1.8, 51.8, 122.9, 124.1, 125.7, 126.2, 129.3, 133.4, 138.3, 157.6, 173.8, 176.8. Anal. Calcd for $C_{22}H_{33}MoN_3O_2Si_2$: C, 50.66; H, 6.35; N, 8.02; Found C, 51.40; H, 6.20; N, 7.98.

R_1 = Ph, R_2 = Me (**21b**) 1-Phenyl-1-propyne (0.31ml, 2.48mmol) was added drop-wise with stirring to a pentane solution of **20a** (1.00g, 2.03mmol). An immediate color change from green to orange occurred. The reaction mixture was allowed to stir for ½ hour after which the solution was concentrated by removal of the solvent *in vacuo*. The pentane solution was reduced to *ca*. 10ml and then cooled to –78^{0}C for two hours. Orange crystals appeared and after filtration [Mo(NPh)(η^2–1-phenyl-1propyne)(*o*-($Me_3SiN)_2C_6H_4$)], **21b** was obtained in 84% yield. Recrystallization from concentrated pentane solutions of **21b** allowed for further

purification. ^{1}H NMR (C_6D_6 20^{0}C): δ 7.36 (d 2H phenyl imido *ortho* protons) 7.35 (d 2 H alkyne phenyl *ortho* proton J = 8.1 Hz, 4.9 Hz) 7.24 (bs 2H *o*-pda ring protons) 7.14 (t 2H phenyl imido *meta* proton J = 6.6 Hz) 7.04 (t 2H alkyne phenyl *meta* proton J = 7.5 Hz) 7.00 (t 1H phenyl imido para proton J = 6.3 Hz) 6.91 (s o-pda ring protons) 6.80 (t 1H J = 7.4 Hz alkyne phenyl *para* proton) 2.41 (s 3H CH_3CCPh protons) 0.48 (s 18H $SiMe_3$ protons). ^{1}H NMR (C_7D_8 -40^{0}C) δ 7.38 (d 2H J = 9.0 Hz phenyl imido *ortho* proton) 7.35 (d 2H J = 8.0 Hz alkyne phenyl *ortho* protons) 7.11 (t 2H J = 8.2 Hz alkyne phenyl *meta* protons) 6.88 (dd 2H J = 6.4 Hz, 2.4 Hz *o*-pda ring protons) 6.83 (t 1H J = 8.2 Hz alkyne phenyl *para* proton) 6.77 (t 1H J = 7.2 Hz phenyl imido *para* proton) 2.40 (s 3H PhCCMe proton) 0.52 (s 9H $SiMe_3$) 0.43 (s 9H $SiMe_3$) ^{13}C NMR (C_6D_6 20^0 C): δ 2.4, 18.9, 122.9, 123.8, 124.5, 127.9, 128.8, 129.2, 129.8, 139.5, 158.2, 179.9, 185.4. Anal. Calcd for $C_{27}H_{35}MoN_3Si_2$: C, 58.57; H, 6.37; N, 7.59; Found C, 58.44; H, 6.35; N, 7.52.

R_1 = $SiMe_3$, R_2 =Me, **(21c)** One equivalent of trimethylsilyl propyne (0.141, 0.95mmol) was added drop-wise with stirring to a pentane solution of **20a** (0.47g, 0.95mmol) of. The reaction mixture was allowed to stir for ½ hour after which the solution was concentrated by removal of the solvent *in vacuo*. The pentane solution was reduced to dryness and [Mo(NPh)(η^2–trimethylsilyl propyne)(*o*-$(Me_3SiN)_2C_6H_4$)], **21c** was obtained as a green oil in 95% yield. Further attempts to crystallize this compound were unsuccessful. ^{1}H NMR (C_6D_6 20^{0}C): δ0.44 (s, 9H, $SiMe_3$), 0.46 (s, 18H, $SiMe_3$), 2.44 (s, 3H, Me), 6.82-7.33 (aromatics), 10.11 (s, 1H, alkyne), ^{1}H NMR (C_6D_6 –50^{0}C) 7.33 (d 2H J = 7.8 Hz phenyl imido *ortho* protons) 7.22 (m 2H *o*-pda ring protons) 7.04 (t 2H J = 8.2 Hz phenyl imido *meta* protons) 6.91 (dd 2H J = 7.8 Hz, 3.6 Hz *o*-pda ring

protons) 6.80 (t 1H J = 7.5 Hz phenyl imido *para* proton) 2.45 (s 3H $SiMe_3CCMe$ protons) 0.51 (s 9H $SiMe_3$ protons) 0.48 (s 9H $SiMe_3$ protons) 0.23 (s 9H $SiMe_3$ protons). ^{13}C NMR δ 0.2, 2.03, 20.7, 123.4, 124.0, 128.7, 157.8, 180.7, 199.6

[(NPh)Mo(C(Ph)C(H)CH_2CH_2)(*o*-$(Me_3SiN)_2C_6H_4$)], (**26a**). In a sealed ampule, a pentane solution of **20a** (0.500g, 1.013 mmol) was frozen and evacuated. The vessel was then cooled and the mixture thawed. The neck of the vessel was flushed with dry ethylene for three minutes. Ethylene gas was then added (15psi) to the solution and the mixture was stirred for 12 hrs. The volume was reduced *in vacuo* and cooled to -78^0C. Orange crystals of **26a** quickly precipitated from solution and were isolated in 80% yield. ^1H NMR (C_6D_6): δ -0.07 (s, 9H, $SiMe_3$), 0.33 (s, 9H, $SiMe_3$), 1.66 (dt, 1H, 11.8Hz, 5.9Hz), 2.74 (dddd, 1H, 17.9Hz, 7.2Hz, 5.1Hz, 2.8Hz), 3.05 (dddd, 1H, 17.6Hz, 7.2Hz, 6.6Hz, 2.3Hz), 3.32 (dddd, 1H, 11.7Hz, 5.4Hz, 2.7Hz, 0.9Hz), 6.84 (t, 1H, 2.4Hz), 6.87-7.55 (aromatic), 7.24 (dd, 1H, phenyl *ortho proton,* 8.5Hz, 1.5Hz), 7.33 (dd, 1H, *o*-phenylene diamine proton, 8.0Hz, 1.6Hz), 7.37 (dd, 1H, *o*-phenylene diamine proton, 8.0Hz, 1.6Hz) 7.54 (dd, 1H, *ortho*-phenyl imido proton, 8.4Hz, 1.3Hz). ^{13}C NMR; 1.1, 1.5, 40.1, 56.5, 122.7, 125.0, 125.4, 122.8, 126.0, 126.5, 127.4, 129.4, 132.6, 135.1, 151.8, 157.2, 158.0, 188.6. Anal. Calcd for $C_{30}H_{42}MoN_3OSi_2$: C, 58.80; H, 6.91; N, 6.86; Found C, 58.24; H, 6.79; N, 7.37.

[(NPh)Mo(C(H)C(Ph)CH_2CH_2)(*o*-$(Me_3SiN)_2C_6H_4$)], **(26b)**. Method 1 A purple Et_2O solution of **4** (3.00g, 5.17mmol) was cooled to -78^0C and treated with of (5.17 ml) $EtMgCl_2$ (2.0M solution in Et_2O). An immediate color change from purple to red occurred and the solution was stirred at -78^0C for ½ hr. Phenyl acetylene (0.52ml, 6.20mmol) was then added and the solution was allowed to warm to room temperature.

The solution was stirred overnight and the solvent was then removed *in vacuo*. Complex **26b** was then extracted with a toluene/ pentane solution. The solvent was then removed *in vacuo* and a red solid was obtained. Washing this solid with cold pentane afforded **26b** in 40% yield.

Method 2 In a sealed ampoule a toluene solution of **25** (0.50g, 1.013 mmol) was heated for 12hrs at 72^0C with phenyl acetylene (0.27ml, 1.21mmol). The vessel was then cooled and the toluene removed *in vacuo* to afford an orange solid that consisted of a mixture of **26b** (20%) and **26a** (80%). The orange solid was then dissolved in pentane and recrystalized at -78^0C to afford **26b**. ^{1}H NMR (C_6D_6): δ 0.40 (s, 9H, $SiMe_3$), 0.43 (s, 9H, $SiMe_3$), 1.34 (dt, 1H, 12.2Hz, 6.1Hz), 3.35 (ddd, 1H, 11.9Hz, 6.1Hz, 1.2Hz), 3.41 (ddd, 1H, 16.8Hz, 7.2Hz, 1.4Hz), 3.70 (dddd, 1H, 17.1Hz, 8.2, Hz, 6.0Hz, 2.3Hz) 6.82 (tt, 1H, phenyl imido *para* proton, 7.4Hz, 1.2Hz), 6.99-7.14 (ov, mult, 7H,) 7.36-7.46 (ov, mult, 4H), 7.54 (dt, 2H, phenyl imido *ortho* proton, 7.2Hz, 1.8Hz,) 8.47 (d, 1H, vinylic proton, 2.5Hz). ^{13}C NMR(C_7D_8): δ1.4, 42.8, 56.0, 122.8, 123.7, 125.9, 125.6, 126.0, 126.2, 126.4, 127.5, 129.2, 135.0, 135.2, 141.2, 147.8, 158.1, 168.5, 172.0. Anal. Calcd for $C_{28}H_{37}MoN_3Si_2$: C, 59.24; H, 6.57; N, 7.40; Found C, 60.68; H, 6.76; N, 6.93.

[(NPh)Mo(C(CO_2Et)C(CO_2Et)CH_2CH_2)(*o*-(Me_3SiN)$_2C_6H_4$)], (**26c)**. In a sealed ampoule a toluene solution of **25** (0.521g, 1.06 mmol) was heated for 12hrs at 72^0C with diethylacetylene dicarboxylate (0.186ml, 1.16mmol). The vessel was then cooled and the toluene removed *in vacuo* to afford an orange solid of **26c**. The orange solid was then dissolved in pentane and recrystalized at -78^0C to afford **26c** as an orange solid in 62% yield. ^{1}H NMR (C_6D_6): δ 0.30 (s, 9H, $SiMe_3$), 0.33 (s, 9H, $SiMe_3$), 0.87 (t, 3H, (CH_3), J = 7.1 Hz),1.17 (m 1H metallacycle proton) 1.27 (t, 3H, (CH_3), J = 7.1 Hz), 3.09 (ddd 1H

J = 15.8 6.1 3.8 Hz metallacycle proton) 6.81 (m 1H phenyl imido *para* proton) 7.00 (overlapping multiplets 4H, o-pda protons and phenyl imido *meta* protons) 7.20 (d 1H J = 7.9 Hz *o*-pda proton) 7.58 (d 1H J =7.4Hz phenyl imido *ortho* proton) 7.67 (d 1H J =8.2 Hz *o*-pda proton) ^{13}C NMR(C_7D_8): δ 184.1, 176.1, 164.2, 157.9, 150.1, 134.3, 130.6, 128.2, 128.9, 127.8, 127.7, 126.4, 125.6, 122.0, 60.3, 60.1, 53.7, 41.2, 14.8, 14.5, 1.43

[(NPh)Mo(C(Ph)CHC(Ph))(*o*-($Me_3SiN)_2C_6H_4$)], **(29)**, To a pentane solution of 1.00g (2.03mmol) of **20a**, phenyl acetylene 0.90ml(4.06mmol) was added drop-wise with stirring. Immediate color change from green to yellowish brown occurred. The reaction mixture was allowed to stir for ½ hour after which the solution was concentrated by removal of the solvent *in vacuo*. Cooling to –78^{0}C resulted in the appearance of brown crystals of **29** in 40% yield. ^{1}H NMR (C_6D_6): δ -0.07 (s, 18H, $SiMe_3$), 6.48 (s, 2H, metallacycle) 6.85-7.78 (aromatic). ^{13}C NMR (C_6D_6): 1.3, 124.7, 125.9, 126.6, 127.4, 129.5, 130.7, 142.2, 154.2, and 192.7. Anal. Calcd for $C_{34}H_{39}MoN_3Si_2$: C, 63.63; H, 6.12; N, 6.55; Found C, 62.74; H, 6.24; N, 6.61.

Synthesis of *bis*-Isocyanide Complexes

[(*cis* –^{t}BuNC)$_2$Mo(NPh)(*o*-($Me_3SiN)_2C_6H_4$)], **(30a)**. A pentane solution of **20a**, (1.00g, 2.03 mmol) was charged with *tert*- Butyl isocyanide (0.24ml, 4.06mmol). Green crystals of **30a** quickly precipitated. The suspension was filtered and washed several times with pentane. Excess solvent was removed *in vacuo* to afford **30a** as a green microcrystalline material in 52% yield. Complex **30a** is unstable in solution and disproportionates to **30a** and an unidentified material at 20^0 overnight. Complex **30a** can be stored as a solid at –30^{0}C. ^{1}H NMR (C_6D_6): δ 0.73(s, 18H, $SiMe_3$), 1.06(s, 18H,

^{t}BuNC), 6.81(tt, 2H, phenyl imido *meta* proton 7.4, 1.2 Hz), 6.93(t, 1H, phenyl imido *para* proton, 7.4 Hz), 7.05 (dd, 2H, *o*-phenylene diamide proton, 5.8, 3.3 Hz), 7.32(dd, 2H, phenyl imido *ortho* proton, 7.5 1.3 Hz), 7.48(dd, 2H, , *o*-phenylene diamide proton, 5.6, 3.4 Hz). ^{13}C NMR(C_7D_8): 234.9, 187.1, 151.7, 128.6, 124.3, 123.7, 117.2, 117.1, 58.7, 30.3, 5.5.

[(*cis* 2-6 –dimethyl phenyl-NC)$_2$Mo(NPh)(*o*-($Me_3SiN)_2C_6H_4$)], **(30b).** A pentane solution of **30b**, (1.00g, 2.03 mmol) was charged with 2-6-dimethyl phenyl isocyanide (0.37g, 2.82mmol). Dark red crystals of **30b** quickly precipitated. The suspension was filtered and washed several times with pentane. Excess solvent was removed *in vacuo* to afford **30b** as a dark red microcrystalline material in 72% yield. ^{1}H NMR (C_6D_6): δ 7.52 (dd, 2H, *o*-phenylene diamide proton 5.7 3.5 Hz), 7.46 (d, 2H, phenyl imido *ortho* proton 7.4 Hz), 7.07 (dd, 2H, *o*-phenylene diamide proton 5.8, 3.4 Hz) 6.99 (t, 2H, phenyl imido *meta* proton 7.2 Hz), 6.89 (t, 1H phenyl imido *para* proton,7.3 Hz), 6.64 (ov multiplet, 6H, isocyanide phenyl protons), 2.12 (s, 12H, (CH_3)), 0.74 (s, 18H, $SiMe_3$), ^{13}C NMR(C_7D_8): δ 200.9, 151.4, 131.5, 128.8, 125.2, 124.3, 117.8, 117.5, 18.8, 5.5. Anal. Complex **30b** loses a molecule of 2-6-dimethyl phenyl isocyanide during the elemental analysis. Calcd $C_{27}H_{36}MoN_4Si_2$ C, 57.02; H, 6.38; N, 9.85. Found C,57.20; H, 6.00; N, 9.80.

Synthesis of a Chelating Imino Carbamoyl Complex, **(33)**

A pentane solution of **25** (1.00g, 2.03mmol) was treated with 2,6-dimethyl phenyl isocyanide (1.16g, 8.92mmol) and the solution was allowed to stir overnight and a yellowish brown powder precipitated. Washing this powder several times with cold pentane followed by recrystalization of the solids from pentane, afforded **33** as red

crystals in 46% yield. . ^{1}H NMR (C_6D_6): δ 8.04 (dd, 2H, phenyl imido *ortho* proton, 8.2, 1.6 Hz.), 7.23 (t, 2H, 2,6 dimethyl phenyl isocyanide para proton, 8.4, 1.3 Hz), 7.2-6.5 (overlapping aromatic peaks 16H), 5.43(dd, 1H, phenyl imido *para* proton, 8.2, 1.6Hz) 2.50(s, 6H, (CH_3) (imino carbamoyl), 1.94(s, 12H, (CH_3), 2,6-dimethyl phenyl isocyanide), 1.87(s, 6H, (CH_3), imino carbamoyl), 0.66(bs, 9H, $SiMe_3$), 0.45(s, 9H, $SiMe_3$). ^{13}C NMR (C_7D_8): 203.3, 176.6, 157.7, 146.6, 146.2, 145.3, 137.9, 137.4, 136.4, 133.4, 129.1, 128.8, 127.3, 126.6, 125.3, 125.1, 125.0, 124.7, 124.0, 121.0, 120.8, 119.3, 119.1, 115.3, 20.0, 18.8, 18.2, 5.5, 0.78. Anal. Calcd $C_{54}H_{64}MoN_7Si_2$: C, 67.33; H, 6.70; N, 10.18. Found C, 67.72; H, 6.95, N, 10.07.

Reactions with alkyl aluminum reagents

Synthesis of $(CH_2)_4Mo(NPh)\eta^4$-(*o*-$(SiMe_3N)_2C_6H_4)Al(CH_3)_2$, **(34)** Trimethyl aluminum (2.44mmol, 0.233ml) was added to an orange solution of **25**(1.00g , 2.03mmol) in toluene. The solution turned green after 15 minutes and the solvent was removed *in vacuo.* The green solid was dissolved in pentane and the solution was concentrated. Cooling to –78^{0}C resulted in the isolation of **34**, as green crystals. ^{1}H NMR (C_6D_6): δ –0.26 (s, 3H $Al(CH_3)_2$), 0.00 (s, 3H, $Al(CH_3)_2$), 0.19 (s, 9H, $SiMe_3$), 0.22 (s, 9H, $SiMe_3$), 1.36(s, 3H, $Mo(CH_3)$), 1.96(ddd, J=10.7Hz, 9.7Hz, 4.1Hz, 1H, metallacycle), 2.16(m, 1H, metallacycle), 2.36(m, 2H, metallacycle), 2.61(m, 2H, metallacycle), 2.79(m, 1H, metallacycle), 3.25(m, 1H, metallacycle), 4.79(dd J = 7.7 Hz, 1.6 Hz, 1H, *o*-pda) 4.86(dd J = 7.5 Hz, 1.6 Hz, 1H, *o*-pda), 5.28(td J=7.2Hz, 1.5Hz, 1H, o-pda), 5.40(td J=7.3Hz, 1.5Hz, 1H, *o*-pda), 6.81 (t, J = 7.1 Hz, 1H, imido *para* protons), 6.88 (t J = 7.3 Hz, 1H, imido, meta, protons), 7.00 (d, J = 8.9 Hz, 1H, imido, *ortho*, protons). ^{13}C NMR(C_6D_6) δ -0.80, -0.27, 0.16, 0.18, 35.9, 38.6,51.0, 59.6,

91.0, 93.1, 102.9, 105.5, 124.3, 128.8, 126.6, 155.4, 160.0. Anal. Calcd for $C_{36}H_{51}AlMoN_3Si_2$: C, 61.34; H, 7.29; N, 5.96. Found: C, 61.32; H, 7.03; N, 5.85.

Synthesis of
(η^2-diphenyl acetylene)(CH_3)Mo(NPh)η^4[(*o*($SiMe_3N$)$_2C_6H_4$)}Al(CH_3)$_2$ **(36)**

Trimethyl aluminum (2.03mmol, 0.195ml) was added to an orange solution of **35**(1.04g, 1.69mmol) in pentane. The solution was stirred overnight; during which time a yellow precipitate formed. The mixture was then filtered and the yellow powder was washed several times with pentane. This yellow powder was dried under vacuum and compound **36** was obtained in 40% yield. ^{1}H NMR (C_6D_6): δ -0.27 (s, 3H, Al(CH_3)$_2$), 0.02 (s, 3H, Al(CH_3)$_2$), 0.03 (s, 9H, $SiMe_3$), 0.35 (s, 9H, $SiMe_3$), 1.71 (s, 3H, Mo(CH_3)), 4.03 (dd J = 7.0 Hz, 2.5 Hz, 1H, *o*-pda), 5.51 (dd J = 6.8 Hz, 2.4 Hz, 1H, *o*-pda), 6.07 (td J = 7.0 Hz, 2.1 Hz, 1H, *o*-pda), 6.10 (td J = 6.7 Hz, 2.3 Hz, 1H, *o*-pda), 6.67 (tt J = 7.2 Hz, 1.2 Hz, 1H, imido *para* proton), 6.79 (t J = 7.9 Hz, 2H, imido meta protons), 6.84 (dd J = 8.5 Hz, 1.7 Hz, 2H, imido *ortho* protons), 7.05 (tt J = 7.6 Hz, 1.2 Hz, 1H phenyl *para* proton), 7.14 (tt J = 7.5 Hz, 1.2 Hz, 1H, phenyl *para* proton), 7.20 (t J = 7.7 Hz, 2H, phenyl *meta* proton), 7.27 (t J = 7.7 Hz, 2H, phenyl *meta* proton), 7.44 (dd J = 8.1 Hz, 1.2 Hz, 2H, phenyl *ortho* proton), 7.88 (dd J = 8.2 Hz, 1.2 Hz, 2H, phenyl *ortho* proton). ^{13}C NMR: δ 159.6 , 159.6 , 156.4 , 152.1 , 150.9 , 137.7 , 137.2 , 129.9 , 129.1 , 128.6 , 128.2 , 127.0 , 125.5 , 123.9 ,104.8 , 97.0 , 94.0 , 90.4 , 23.7 , -0.1 , -0.2 , -0.4 , -5.3. Anal. Calcd. $C_{26}H_{46}AlMoN_3Si_2$: C, 53.86; H, 8.00; N, 7.45. Found C, 53.98; H, 7.72; N, 7.45.

Synthesis of [(η^2-ethylene)(CH_3)Mo(NPh)η^4-(*o*-($SiMe_3N)_2C_6H_4$))Al($CH_3)_2$}, **(42a)**

Methyl aluminum dichloride (2.43ml of a 1.0M solution in hexanes)was added to a toluene solution of 25, (1.00g, 2.03mmol). The solution was allowed to stir for one hour and toluene was removed *in vacuo* yielding a red solid. The red solid was washed several times with pentane to yield **42b** in 62.4% yield. ^{1}H NMR (C_6D_6): δ 6.77 (overlapping multiplet, 5H, phenyl imido) 5.62(td, 1H, J = 1.9, 7.2Hz o-pda) 5.42(td, 1H, J =1.9, 7.2Hz o-pda), 5.10(dd, 1H, J =1.9, 7.2 Hz), 4.35 (dd, 1H, J=1.8, 7.3 Hz), 2.78(ddd, 1H, J = 1.8, 10.5, 13.8 Hz η^2-ethylene), 2.38(ddd, 1H, J = 2.0, 7.7, 11.7Hz η^2-ethylene), 1.74(overlapping multiplet, 2H, η^2-ethylene), 1.45(s, 3H, CH_3), 0.35(s, 3H, $SiMe_3$), 0.24(s, 3H, $SiMe_3$). ^{13}C NMR (C_7D_8), δ 156.2, 154.8, 129.2, 127.3, 125.2, 99.0, 98.7, 93.1, 91.4, 48.1, 43.8, 17.6, 0.31, 0.23. Anal. Calcd. $C_{23}H_{39}AlCl_2MoN_3OSi_2$: C, 44.30; H, 6.30; N, 6.74. Found C, 44.57; H, 5.74; N, 7.05

Synthesis of [(η^2-ethylene)(Et)Mo(NPh)η^4-(*o*-($SiMe_3N)_2C_6H_4$)Al($CH_3)_2$] **(42b)**

Ethyl aluminum dichloride (0.352 ml, 2.92mmol) was added to a toluene solution of 25, (1.21g, 2.43mmol). The solution was allowed to stir for one hour and toluene was removed in vacuo yield a brown solid. The brown solid was washed several times with pentane to yield **42b** in 63.7% yield. ^{1}H NMR (C_6D_6): δ 6.20 (overlapping mulitiplet, 5H phenyl imido) 5.59 (td, 1H, J =7.2 Hz, 1.9 Hz *o*-pda) 5.39 (td, 1H, J = 7.3 Hz, 2.0 Hz, *o*-pda) 5.23 (dd, 1H, J = 7.3 Hz, 1.9 Hz, *o*-pda) 4.70 (dd, 1H, J = 7.5 Hz, 1.9 Hz, *o*-pda) 3.05 (ddd, 1H, J = 14.3 Hz, 11.1 Hz, 4.2 Hz, η^2-ethylene) 2.41 (ddd, 1H, J = 13.2 Hz, 10.9 Hz, 5.5 Hz, η^2-ethylene) 2.22 (q, 2H, J = 7.4 Hz, Et) 1.94 (ddd, 1H, J = 14.0 Hz, 11.5 Hz, 5.5 Hz, η^2-ethylene) 1.85 (t, 3H, J = 7.4 Hz, Et(CH_3)) 1.21 (ddd, 1H, J = 13.4 Hz, 11.5 Hz, 4.3 Hz, η^2-ethylene) 0.32 (s, 9H, $SiMe_3$) 0.26 (s,

9H, $SiMe_3$) ^{13}C NMR (C_7D_8), δ 154.9, 153.0,150.6, 128.7, 105.7, 96.4, 95.7, 95.2, 49.7, 49.0, 27.4, 22.5, 0.0, -0.41.

Synthesis of [(η^2-styrene)(Me)Mo(NPh)η^4-(*o*-($SiMe_3N)_2C_6H_4$))Al($CH_3)_2$] **(39)**

Trimethyl aluminum (0.20 ml, 2.09mmol) was added to a toluene solution of **20c**, (0.93g, 1.72mmol). The green solution quickly turned red and was allowed to stir for one hour, and then toluene was removed in vacuo to yield a red solid. Analysis of the ^1H NMR spectrum revealed that 39 was formed as a 50:50 mixture of the two isomers **39a** and **39b** in 64.0 % yield. Recrystalization from an 80:20 mixture of pentane/ether solution afforded **39a** in 24.8 %yield. Compound **39b** was obtained in low purity. The stereochemistry of **39** was determined by gHMQC, gHMBC, and NOESY spectroscopy. ^1H NMR (C_6D_6): (**39a**) δ 7.00-6.84(10H aromatic protons overlapping), 5.60 (3H *o*-pda protons overlapping with **39b**), 4.75 (dd, 1H J = 6.7, 2.6 Hz, o-pda proton), 4.35 (dd 1H J = 6.5 2.5 Hz o-pda proton), 3.38 (dd 1H J = 13.8 5.7 Hz η^2 styrene proton), 2.90 (dd 1H J =13.6 11.2 Hz η^2 styrene proton), 1.69 (d 1H J = 10.9 5.5 Hz η^2 styrene proton), 1.33 (s 3H (CH_3)), 0.25 (s 9H $SiMe_3$) 0.19 (s 9H $SiMe_3$) –0.03 (s 3H (CH_3)), -0.33 (s 3H (CH_3)), ^{13}C NMR (C_7D_8) chemical shifts were determined by gHMQC and gHMBC (see Figures 5-7 for details). **(39b)** δ 7.00 (10H aromatic protons overlapping), 5.89 (tt 3H J= 7.1 1.9 Hz *o*-pda proton) 5.53 (3H *o*-pda protons overlapping with **39a**), 5.00 (dd, 1H J = 7.1, 1.6 Hz, o-pda proton), 3.80 (dd 1H J = 7.2 2.2 Hz *o*-pda proton), 3.65 (dd 1H J = 12 9 11.0 Hz η^2 styrene proton), 3.06 (dd 1H J =13.1 6.9 Hz η^2 styrene proton), 2.21 (d 1H J = 10.9 5.5 Hz η^2 styrene proton), 1.41 (s 3H (CH_3)), 0.30 (s 9H $SiMe_3$) 0.12 (s 9H $SiMe_3$) 0.01 (s 3H (CH_3)), -0.31 (s 3H (CH_3)) ^{13}C NMR (C_7D_8) chemical shifts were determined by gHMQC and gHMBC (see Figures 5-9 for details).

Synthesis of [(η^2-styrene)(Me)Mo(NPh)η^4-(*o*-($SiMe_3N)_2C_6H_4$)}$Al(Cl)_2$] **(40)**

Methyl aluminum dichloride (2.66ml of a 1.0M solution in hexanes) was added to a green toluene solution of **20c**, (1.20g, 2.22mmol). The solution was allowed to stir for one hour and toluene was removed in vacuo yield a reddish brown solid. The red solid was washed with pentane and excess solvent was removed in vacuo to yield **40** as a mixture of two isomers. The stereochemistry of **40** was determined by gHMQC, gHMBC, and NOESY spectroscopy.

40a

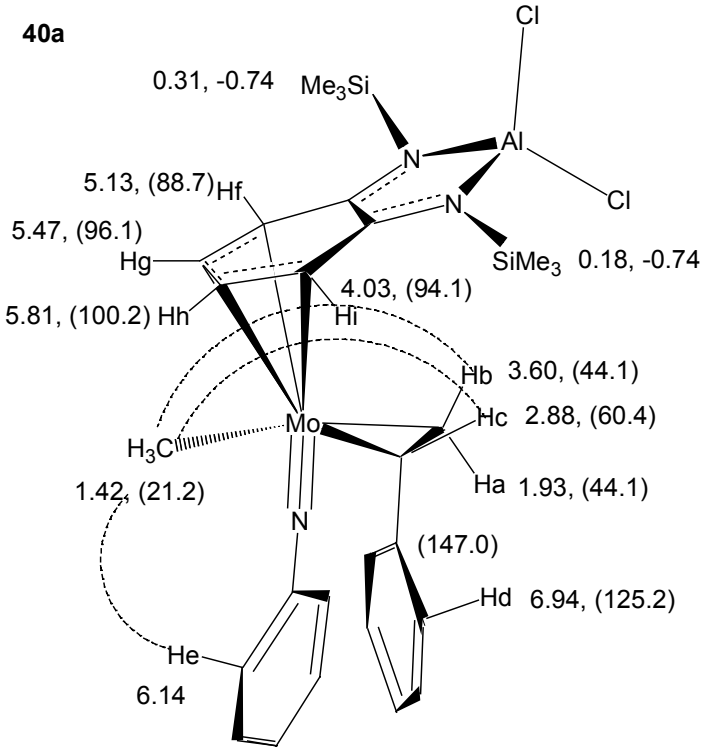

^{13}C NMR shifts are in parentheses
Dashed lines represent NOE's

gHMBC
Methyl proton (1.42ppm) shows 3 bond correlations to the methylene carbon at 44.1ppm
Metallcycle proton 2.88 shows 2-bond correlations to the methylene carbon at 44.1 and 3-bond correlations to the phenylene carbon at 147.0ppm

40b

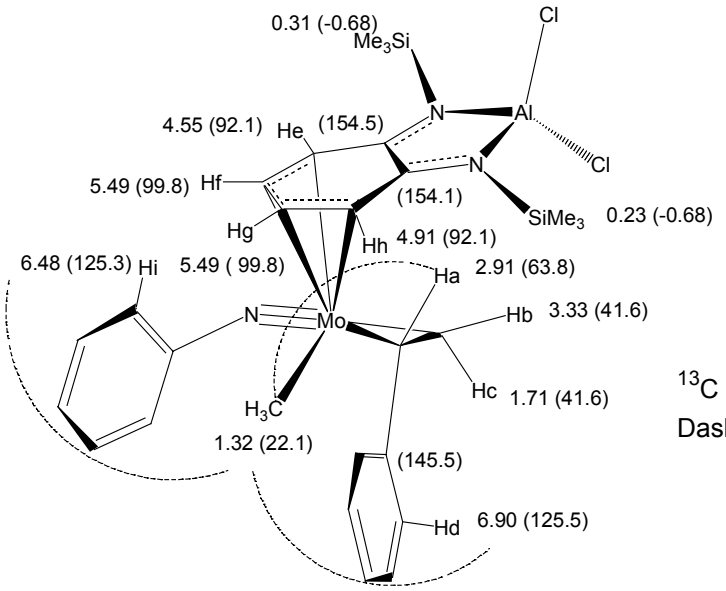

^{13}C NMR shifts are in parentheses
Dashed lines represent NOE's

gHMBC
Methyl proton (1.32ppm) shows 3 bond correlations to the methylene carbon at 41.6ppm
Metallcycle proton 2.91 shows 2-bond correlations to the methylene carbon at 41.6 and to the phenylene carbon at 145.5ppm

Synthesis of $[(\mu^2\ NPh)Mo(Cl)(\eta^4\text{-}(Cl_2Al((o\text{-}(Me_3SiN)_2\text{-}C_6H_4))]_2$, **(41)**

Ethyl aluminum dichloride (0.352 ml, 2.92mmol) was added to a green pentane solution of **20a**, (1.65g, 2.43mmol). The solution was allowed to stir overnight, during which time a green powder precipitated. The suspension was filtered and washed several times with pentane. Excess pentane was then removed in vacuo. The green powder was redissolved in CH_2Cl_2, the solution concentrated and pentane added to precipitate **41**, in 30% yield. The ^{1}H NMR spectrum of **41** revealed that this compound exists as a mixture of 3 isomers (see text for details). ^{1}H NMR ($CDCl_3$) δ 7.49, 7.39, 7.17, 5.58, 4.14, 0.97, 0.27, 0.26, 0.25. ^{13}C NMR ($CDCl_3$) δ 129.7, 119.2, 95.6, 91.0, 9.6, 6.8, 4.8, 3.4, 0.4, -

0.07, -4.20, -4.50. Anal. Calcd. $C_{41}H_{88}Al_2Cl_6Mo_2N_6Si_4$ C 40.50, H 5.64, N 6.91 Found C 41.08, H 5.91, N 7.02 .

Kinetic Study

NMR tube samples were prepared by dissolving **25** (*ca*. 10mg, 0.020mmol) and mesitylene (13.88μl), added as an internal standard, in 1.0ml of C_7D_8 in the glove box and . Diethyl acetylene dicarboxylate was then added to the NMR tube, the tube was then capped. The concentration of DEAD was obtained by plotting the values of the integral for the (DEAD) ethyl group for known concentrations DEAD versus the integrals for the (CH_3) protons of mesitylene. The NMR probe was equilibrated to the desired temperature and the sample was then loaded into the probe. Approximately 120 spectra were recorded over the duration of three half-lives. The value of the integral for the $SiMe_3$ protons of the starting material was recorded for each spectrum. The observed rate constants were obtained by plotting the Ln(integral) vs time. Three samples were performed at each temperature and the rate constants reported were the average of three runs. Activation parameters were obtained by measuring the rate constants at four different temperatures. A plot of Ln(k/T) vs (1/T (K)), results in a line of with a slope of $-\Delta H^{\ddagger}/R$ and an intercept of $[(\Delta S^{\ddagger}/R) + 23.76]$. Reported errors in the rate constants represent the standard deviation from the least squares fit of the experimental data. Reported errors in the activation parameters are obtained from all experimental data (12 points in the Eyring plot), using 2σ.

Table 6-1. Kinetic analysis for the reaction of DEAD with **25**

T(K)	k(run#1)* 10^4	k(run#1) * 10^4	k(run#1) * 10^4
355.8	9.81	10.6	11.9
349.5	5.78	7.02	7.72
342.5	3.79	3.49	2.73
334.8	1.67	1.67	1.74

Eyring Plot Analysis: $\Delta S^{\ddagger}$ = -14.7 +/-3.0 cal/K.mol; $\Delta H^{\ddagger}$ = 20.5 +/- 1.0 Kcal/mol

Computational Studies.

All Density functional theory (DFT) calculations were performed using the Gaussian 98W program package.[143] In most cases molecules were optimized using Becke's hybrid three-parameter functional (B3LYP). The Los Alamos effective core potential, (ECP), plus a standard double-zeta basis set (LANL2DZ)[67] was used to describe the molybdenum center. The Dunning/Huzinaga[66] full double zeta basis set (D95) was used to describe all other atoms. Molecules were visualized with the MOLDEN program.[131]

Alkyne complexes **22** and **23**. Model compound **22** and **TS 22** were optimized at the B3LYP/LANL2DZ level. Using the same level of theory and basis set, vibrational frequency calculations and NBO population analyses were performed on the stationary points to confirm their existence as minima (number of imaginary frequencies =0 or maxima (transition structures) # imaginary frequencies =1, and to analyze (MOs). An IRC calculation was performed to confirm that the transition state is linked to the minima on the potential energy surface. Single-point energies were calculated using the B3LYP level of theory and the LANL2DZ+P basis set, where +P stands for the addition of polarization functions to the D95 basis set as implemented in the Gaussian 98W program. Energy differences (ΔE) are electronic energies i.e. they are taken straight off of the potential energy surface and do not include zero point corrections.

Complex **23** and **TS 23** were optimized with the two-layer ONIOM method developed by Morokuma et al.[8-12] Using this method the inner layer consisted of **22** and was modeled with the LANL2DZ basis set. The outer layer consisted of **23** and was comprised of the entire (complete) system and was modeled with the LANL2MB method. The LANL2MB[144,145] basis set consists of the The Los Alamos effective core potential (ECP) plus a standard double-zeta basis set (LANL2DZ) on the Molybdenum atom and the STO-3G basis set on all other atoms. Single-point energies were calculated using the B3LYP level of theory and the LANL2DZ basis set. Using the same level of theory and basis set, vibrational frequency calculations, NBO population analyses were performed on the stationary points to confirm there existence as minima (number of imaginary frequencies =0 or maxima (transition structures) # imaginary frequencies =1, and to analyze (MOs). IRC calculations are not possible within the current implementation of the ONIOM program, however, confirmation that the transition state is linked to the minima on the potential energy surface, was obtained by visualization of the imaginary frequency using the MOLDEN program.

Single-point energies were calculated using the B3LYP level of theory and the LANL2DZ basis set. Energy differences (ΔE) are electronic energies i.e. they are taken straight off of the potential energy surface and do not include zero point corrections.

Complex **20c** and **24**. These complexes were optimized in an analogous fashion to **23**.

Metallacyclopentane complex **25.** Model compounds **25, 25b, 25c** and **TS 25-25b** and **TS 25b-25c** were optimized at the mPW1K/LANL2DZ level. In the model system, the *o*-phenylene group (o-C_6H_4) that links the two N atoms of the diamido ligand was

simplified to a –CH=CH- carbon chain. The organic groups on the nitrogen atoms, ($SiMe_3$ of the amido and phenyl group of the imido), were replaced by hydrogen atoms for simplicity. The mPW1K method that has been recently developed by Truhlar and co-workers has been recently shown to give more reliable barrier heights than other functionals.[146] Using the same level of theory and basis set, vibrational frequency calculations, were performed on the stationary points to confirm their existence as minima (number of imaginary frequencies =0 or maxima (transition structures) # imaginary frequencies =1, and to analyze (MOs) and to calculate zero point energies. An IRC calculation was performed to confirm that the transition state is linked to the minima on the potential energy surface. Single-point energies were calculated using the B3LYP level of theory and Dunning's Aug-cc-pVDZ basis set.[66,147,148] Relative free energy differences reported (ΔG^0_{298}) include the effects of zero point energy corrections...

For ONIOM calculations the inner layer was optimized with the mPW1K/LANL2DZ level. The outer layer was optimized with the mPW1K/LANL2MB level of theory.

Molecules **37** and **38**. The molecules were optimized with the B3LYP/LANL2DZ method. The $SiMe_3$ substituents on the diamide ligand were replaced by (CH_3) and the substituents on the phenyl imido ligand with H for simplicity.

X-ray Experimental

X-ray Experimental for Complex **26b**.

Single crystals of **26b** were obtaimed from slow evaporation of a diethyl ether solution. Data were collected at 173 K on a Siemens SMART PLATFORM equipped with A CCD area detector and a graphite monochromator utilizing MoK_α radiation (λ =

0.71073 Å). Cell parameters were refined using 6673 reflections. A hemisphere of data (1381 frames) was collected using the ω-scan method (0.3° frame width). The first 50 frames were remeasured at the end of data collection to monitor instrument and crystal stability (maximum correction on I was < 1 %). Absorption corrections by integration were applied based on measured indexed crystal faces.

The structure was solved by the Direct Methods in *SHELXTL5*[149], and refined using full-matrix least squares. The non-H atoms were treated anisotropically, whereas the hydrogen atoms were calculated in ideal positions and were riding on their respective carbon atoms. A total of 313 parameters were refined in the final cycle of refinement using 5684 reflections with $I > 2\sigma(I)$ to yield R_1 and wR_2 of 3.03% and 7.23%, respectively. Refinement was done using F^2.

Table 6-2. Crystal data and structure refinement for **26b**.

Identification code	ei01	
Empirical formula	C28 H37 Mo N3 Si2	
Formula weight	567.73	
Temperature	173(2) K	
Wavelength	0.71073 Å	
Crystal system	Monoclinic	
Space group	P2(1)/n	
Unit cell dimensions	a = 11.2646(5) Å	α= 90°.
	b = 9.7968(4) Å	β= 92.659(1)°.
	c = 25.675(1) Å	γ = 90°.
Volume	2830.4(2) $Å^3$	
Z	4	
Density (calculated)	1.332 Mg/m^3	
Absorption coefficient	0.569 mm^{-1}	
F(000) 1184		
Crystal size	0.20 x 0.17 x 0.17 mm^3	
Theta range for data collection	1.59 to 27.50°.	
Index ranges	$-14 \le h \le 14$, $-11 \le k \le 12$, $-33 \le l \le 28$	
Reflections collected	18462	
Independent reflections	6460 [R(int) = 0.0547]	
Completeness to theta = 27.50°	99.4 %	
Absorption correction Integration		
Max. and min. transmission	0.9191 and 0.8987	
Refinement method	Full-matrix least-squares on F^2	
Data / restraints / parameters	6460 / 0 / 313	
Goodness-of-fit on F^2 1.058		
Final R indices [I>2sigma(I)] R1 = 0.0303, wR2 = 0.0723 [5684]		
R indices (all data)	R1 = 0.0361, wR2 = 0.0766	
Largest diff. peak and hole	0.382 and -0.525 $e.Å^{-3}$	

$R1 = \Sigma(||F_o| - |F_c||) / \Sigma|F_o|$

$wR2 = [\Sigma[w(F_o^2 - F_c^2)^2] / \Sigma[w(F_o^2)^2]]^{1/2}$

$S = [\Sigma[w(F_o^2 - F_c^2)^2] / (n-p)]^{1/2}$ $w= 1/[\sigma^2(F_o^2)+(0.0370*p)^2+0.31*p]$, $p = [\max(F_o^2,0)+ 2* F_c^2]/3$

X-ray Experimental for Complex **29**

Single crystals were obtained by slow evaporation of a diethl ether solution of **29**. Data were collected at 173 K on a Siemens SMART PLATFORM equipped with A CCD area detector and a graphite monochromator utilizing MoK_α radiation ($\lambda = 0.71073$ Å). Cell parameters were refined using 7620 reflections. A hemisphere of data (1381 frames) was collected using the ω-scan method (0.3° frame width). The first 50 frames were remeasured at the end of data collection to monitor instrument and crystal stability (maximum correction on I was < 1 %). Absorption corrections by integration were applied based on measured indexed crystal faces.

The structure was solved by the Direct Methods in *SHELXTL5,* and refined using full-matrix least squares. The non-H atoms were treated anisotropically, whereas the hydrogen atoms were calculated in ideal positions and were riding on their respective carbon atoms. The asymmetric unit consists of two chemically equivalent but crystallographically independent molecules. A total of 733 parameters were refined in the final cycle of refinement using 10788 reflections with $I > 2\sigma(I)$ to yield R_1 and wR_2 of 3.55% and 6.87%, respectively. Refinement was done using F^2.

Table 6-3. Crystal data and structure refinement for **29**.

Identification code	ei02	
Empirical formula	C34 H39 Mo N3 Si2	
Formula weight	641.80	
Temperature	193(2) K	
Wavelength	0.71073 Å	
Crystal system	Orthorhombic	
Space group	Pbcn	
Unit cell dimensions	a = 25.544(1) Å	α= 90°.
	b = 18.7420(8) Å	β= 90°.
	c = 27.641(1) Å	γ = 90°.
Volume	13233.4(9) Å^3	
Z	16	
Density (calculated)	1.289 Mg/m^3	
Absorption coefficient	0.495 mm^{-1}	
F(000)	5344	
Crystal size .	07 x .05 x .04 mm^3	
Theta range for data collection	1.54 to 27.50°.	
Index ranges	$-32 \le h \le 33$, $-24 \le k \le 24$, $-35 \le l \le 35$	
Reflections collected	112367	
Independent reflections	15199 [R(int) = 0.0776]	
Completeness to theta = 27.50°	100.0 %	
Absorption correction	Empirical	
Min. & Max. Transmission	0.966, 0.980	
Refinement method	Full-matrix least-squares on F^2	
Data / restraints / parameters	15199 / 0 / 733	
Goodness-of-fit on F^2	1.076	
Final R indices [I>2sigma(I)]	R1 = 0.0355, wR2 = 0.0687 [10788]	
R indices (all data)	R1 = 0.0681, wR2 = 0.0836	
Largest diff. peak and hole	0.372 and -0.607 e.Å^{-3}	

$R1 = \Sigma(||F_o| - |F_c||) / \Sigma|F_o|$

$wR2 = [\Sigma[w(F_o^2 - F_c^2)^2] / \Sigma[w(F_o^2)^2]]^{1/2}$

$S = [\Sigma[w(F_o^2 - F_c^2)^2] / (n-p)]^{1/2}$

$w= 1/[\sigma^2(F_o^2)+(0.020*p)^2+11.94*p]$, $p = [\max(F_o^2,0)+ 2* F_c^2]/3$

X-ray Experimental for Complex **25**

Single crystals of **25** were obtained by cooling a concentrated pentane solution of this complex at -30^0C. Data were collected at 173 K on a Siemens SMART PLATFORM equipped with A CCD area detector and a graphite monochromator utilizing MoK_α radiation (λ = 0.71073 Å). Cell parameters were refined using up to 8192 reflections. A full sphere of data (1850 frames) was collected using the ω-scan method (0.3° frame width). The first 50 frames were remeasured at the end of data collection to monitor instrument and crystal stability (maximum correction on I was < 1 %). Absorption corrections by integration were applied based on measured indexed crystal faces.

The structure was solved by the Direct Methods in *SHELXTL6,* and refined using full-matrix least squares. The non-H atoms were treated anisotropically, whereas the hydrogen atoms were calculated in ideal positions and were riding on their respective carbon atoms. The C14-C15 moiety is disordered and was refined in two parts with their site occupation factors dependently refined. A total of 278 parameters were refined in the final cycle of refinement using 4876 reflections with $I > 2\sigma(I)$ to yield R_1 and wR_2 of 3.07 % and 7.33%, respectively. Refinement was done using F^2.

Table 6-4. Crystal data and structure refinement for **29**.

Identification code	ei11	
Empirical formula	C22 H35 Mo N3 Si2	
Formula weight	493.65	
Temperature	173(2) K	
Wavelength	0.71073 Å	
Crystal system	Monoclinic	
Space group	P2(1)/n	
Unit cell dimensions	a = 10.2921(6) Å	α= 90°.
	b = 18.1227(11) Å	β= 103.385(2)°.
	c = 13.8423(8) Å	γ = 90°.
Volume	2511.7(3) $Å^3$	
Z	4	
Density (calculated)	1.305 Mg/m^3	
Absorption coefficient	0.630 mm^{-1}	
F(000)	1032	
Crystal size	0.34 x 0.19 x 0.11 mm^3	
Theta range for data collection	1.88 to 27.50°.	
Index ranges	$-13 \le h \le 13$, $-23 \le k \le 18$, $-14 \le l \le 17$	
Reflections collected	16103	
Independent reflections	5669 [R(int) = 0.0460]	
Completeness to theta = 27.50°	98.3 %	
Absorption correction	Integration	
Max. and min. transmission	0.9397 and 0.8176	
Refinement method	Full-matrix least-squares on F^2	
Data / restraints / parameters	5669 / 0 / 278	
Goodness-of-fit on F^2	1.054	
Final R indices [I>2sigma(I)]	R1 = 0.0307, wR2 = 0.0733 [4876]	
R indices (all data)	R1 = 0.0384, wR2 = 0.0767	
Largest diff. peak and hole	0.376 and -0.476 $e.Å^{-3}$	

$R1 = \Sigma(||F_o| - |F_c||) / \Sigma|F_o|$

$wR2 = [\Sigma[w(F_o^2 - F_c^2)^2] / \Sigma[w(F_o^2)^2]]^{1/2}$

$S = [\Sigma[w(F_o^2 - F_c^2)^2] / (n-p)]^{1/2}$

$w= 1/[\sigma^2(F_o^2)+(m*p)^2+n*p]$, $p = [\max(F_o^2,0)+ 2* F_c^2]/3$, m & n are constants.

X-ray Experimental for Complex **30b**

Single crystals of **30b** were obtained by slow diffusion of pentane into a concentrated toluene solution of **30b**.Data were collected at 173 K on a Siemens SMART PLATFORM equipped with A CCD area detector and a graphite monochromator utilizing MoK_α radiation ($\lambda = 0.71073$ Å). Cell parameters were refined using up to 8192 reflections. A full sphere of data (1850 frames) was collected using the ω-scan method (0.3° frame width). The first 50 frames were re-measured at the end of data collection to monitor instrument and crystal stability (maximum correction on I was < 1 %). Absorption corrections by integration were applied based on measured indexed crystal faces.

The structure was solved by the Direct Methods in *SHELXTL6,* and refined using full-matrix least squares. The non-H atoms were treated anisotropically, whereas the hydrogen atoms were calculated in ideal positions and were riding on their respective carbon atoms. In addition to the complex, the asymmetric unit has a half toluene molecule located on an inversion center. Its methyl group is thus disordered over two equivalent positions (The center of the phenyl group lies on the inversion center. A total of 444 parameters were refined in the final cycle of refinement using 6271 reflections with $I > 2\sigma(I)$ to yield R_1 and wR_2 of 3.49% and 7.58%, respectively. Refinement was done using F^2.

Table 6-5. Crystal data and structure refinement for **30b**.

Identification code	ei19	
Empirical formula	C39.50 H49 Mo N5 Si2	
Formula weight	745.96	
Temperature	173(2) K	
Wavelength	0.71073 Å	
Crystal system	Triclinic	
Space group	P-1	
Unit cell dimensions	a = 11.5484(9) Å	α= 102.802(2)°.
	b = 11.8609(9) Å	β= 93.928(2)°.
	c = 14.8731(12) Å	γ = 94.868(2)°.
Volume	1971.4(3) Å3	
Z	2	
Density (calculated)	1.257 Mg/m3	
Absorption coefficient	0.426 mm-1	
F(000)	782	
Crystal size	0.27 x 0.26 x 0.11 mm3	
Theta range for data collection	1.41 to 27.50°.	
Index ranges	-14 ≤ h ≤11, -15 ≤ k ≤13, -19 ≤ l ≤ 19	
Reflections collected	12375	
Independent reflections	8614 [R(int) = 0.0441]	
Completeness to theta = 27.50°	95.1 %	
Absorption correction	Integration	
Max. and min. transmission	0.9542 and 0.9004	
Refinement method	Full-matrix least-squares on F2	
Data / restraints / parameters	8614 / 0 / 444	
Goodness-of-fit on F2	0.915	
Final R indices [I>2sigma(I)]	R1 = 0.0349, wR2 = 0.0758 [6271]	
R indices (all data)	R1 = 0.0520, wR2 = 0.0788	
Largest diff. peak and hole	0.615 and -0.644 e.Å-3	

R1 = ∑(||Fo| - |Fc||) / □|Fo|
wR2 = [∑[w(Fo2 - Fc2)2] / □□ẉFo2̣2]]1/2
S = [∑[w(Fo2 - Fc2)2] / (n-p)]1/2
w= 1/[σ2(Fo2)+(m*p)2+n*p], p = [max(Fo2,0)+ 2* Fc2]/3, m & n are constants.

X-ray Experimental for Complex **33**

Single crystals of 33 were obtained by cooling a petane solution of this complex to -30^0C. Data were collected at 173 K on a Siemens SMART PLATFORM equipped with A CCD area detector and a graphite monochromator utilizing MoK_α radiation (λ = 0.71073 Å). Cell parameters were refined using up to 8192 reflections. A full sphere of data (1850 frames) was collected using the ω-scan method (0.3° frame width). The first 50 frames were re-measured at the end of data collection to monitor instrument and crystal stability (maximum correction on I was < 1 %). Absorption corrections by integration were applied based on measured indexed crystal faces.

The structure was solved by the Direct Methods in *SHELXTL6,* and refined using full-matrix least squares. The non-H atoms were treated anisotropically, whereas the hydrogen atoms were calculated in ideal positions and were riding on their respective carbon atoms. The asymmetric unit consists of the Mo complex and two ½ ether molecules (all ether molecules are located on inversion centers). The latter were disordered and could not be modeled properly, thus program SQUEEZE, a part of the PLATON package of crystallographic software, was used to calculate the solvent disorder area and remove its contribution to the overall intensity data. One of the Si atoms is disordered in two positions, Si2 and Si3. Accordingly, their methyl groups and the dimethylphenyl moiety are also disordered and were refined in two parts, with their site occupation factors dependently refined. A total of 621 parameters (with 36 restraints) were refined in the final cycle of refinement using 6995 reflections with $I > 2\sigma(I)$ to yield R_1 and wR_2 of 4.84% and 9.81%, respectively. Refinement was done using F^2.

Table 6-6. Crystal data and structure refinement for **33**.

Identification code	ei17	
Empirical formula	C58 H73 Mo N7 O Si2	
Formula weight	1036.35	
Temperature	173(2) K	
Wavelength	0.71073 Å	
Crystal system	Triclinic	
Space group	P-1	
Unit cell dimensions	a = 11.4653(12) Å	α= 90.006(2)°.
	b = 13.7990(14) Å	β= 100.229(2)°.
	c = 20.264(2) Å	γ = 112.571(2)°.
Volume	2905.1(5) Å^3	
Z	2	
Density (calculated)	1.185 Mg/m^3	
Absorption coefficient	0.310 mm^{-1}	
F(000)	1096	
Crystal size	0.33 x 0.18 x 0.14 mm^3	
Theta range for data collection	1.02 to 27.50°.	
Index ranges	$-14 \le h \le 14$, $-17 \le k \le 14$, $-24 \le l \le 26$	
Reflections collected	18326	
Independent reflections	12774 [R(int) = 0.0823]	
Completeness to theta = 27.50°	95.7 %	
Absorption correction	Integration	
Max. and min. transmission	0.9629 and 0.8726	
Refinement method	Full-matrix least-squares on F^2	
Data / restraints / parameters	12774 / 36 / 621	
Goodness-of-fit on F^2	0.814	
Final R indices [I>2sigma(I)]	R1 = 0.0484, wR2 = 0.0981 [6995]	
R indices (all data)	R1 = 0.0868, wR2 = 0.1038	
Largest diff. peak and hole	0.653 and -0.813 e.Å^{-3}	

$R1 = \Sigma(||F_o| - |F_c||) / \Sigma|F_o|$

$wR2 = [\Sigma[w(F_o^2 - F_c^2)^2] / \Sigma[w(F_o^2)^2]]^{1/2}$

$S = [\Sigma[w(F_o^2 - F_c^2)^2] / (n-p)]^{1/2}$

$w = 1/[\sigma^2(F_o^2)+(m*p)^2+n*p]$, $p = [\max(F_o^2,0)+ 2* F_c^2]/3$, m & n are constants.

X-ray Experimental for Complex **34**

Data were collected at 173 K on a Siemens SMART PLATFORM equipped with A CCD area detector and a graphite monochromator utilizing MoK_α radiation ($\lambda = 0.71073$ Å). Cell parameters were refined using up to 8192 reflections. A full sphere of data (1850 frames) was collected using the ω-scan method (0.3° frame width). The first 50 frames were remeasured at the end of data collection to monitor instrument and crystal stability (maximum correction on I was < 1 %). Absorption corrections by integration were applied based on measured indexed crystal faces.

The structure was solved by the Direct Methods in *SHELXTL5,* and refined using full-matrix least squares. The non-H atoms were treated anisotropically, whereas the hydrogen atoms were calculated in ideal positions and were riding on their respective carbon atoms. By interchanging their positions, ligands CH3 and C4H8 are disordered where atoms C21, C24 and C25 have full occupancy while atoms C22 and C23 on one hand are disordered and were refined in a second part as C22' C23'. Their site occupation factors were dependently refined to 0.66(1) fro the major part, and consequently 0.34(1) for the minor part. C22 and C23' are refined with isotropic thermal parameters only and were constrained to maintain a similar geometry to the C22-C23 unit. A total of 306 parameters were refined in the final cycle of refinement using 4097 reflections with $I > 2\sigma(I)$ to yield R_1 and wR_2 of 4.09% and 9.66%, respectively. Refinement was done using F^2.

Table 6-7. Crystal data and structure refinement for **34**.

Identification code	ei08	
Empirical formula	C25 H44 Al Mo N3 Si2	
Formula weight	565.73	
Temperature	193(2) K	
Wavelength	0.71073 Å	
Crystal system	Triclinic	
Space group	P-1	
Unit cell dimensions	a = 11.1574(7) Å	α= 68.598(2)°.
	b = 11.4579(7) Å	β= 80.593(2)°.
	c = 12.7057(8) Å	γ = 79.021(2)°.
Volume	1476.75(16) $Å^3$	
Z	2	
Density (calculated)	1.272 Mg/m^3	
Absorption coefficient	0.572 mm^{-1}	
F(000)	596	
Crystal size	0.11 x 0.11 x 0.05 mm^3	
Theta range for data collection	1.73 to 27.50°.	
Index ranges	$-14 \le h \le 14$, $-14 \le k \le 14$, $-16 \le l \le 16$	
Reflections collected	13438	
Independent reflections	6642 [R(int) = 0.0500]	
Completeness to theta = 27.50°	98.0 %	
Absorption correction	Integration	
Max. and min. transmission	0.9720 and 0.9325	
Refinement method	Full-matrix least-squares on F^2	
Data / restraints / parameters	6642 / 4 / 306	
Goodness-of-fit on F^2	0.913	
Final R indices [I>2sigma(I)]	R1 = 0.0409, wR2 = 0.0966 [4097]	
R indices (all data)	R1 = 0.0751, wR2 = 0.1038	
Largest diff. peak and hole	0.918 and -0.609 $e.Å^{-3}$	

$R1 = \Sigma(||F_o| - |F_c||) / \Sigma|F_o|$

$wR2 = [\Sigma[w(F_o^2 - F_c^2)^2] / \Sigma[w(F_o^2)^2]]^{1/2}$

$S = [\Sigma[w(F_o^2 - F_c^2)^2] / (n-p)]^{1/2}$

$w= 1/[\sigma^2(F_o^2)+(0.047*p)^2]$, $p = [\max(F_o^2,0)+ 2* F_c^2]/3$

X-ray Experimental for Complex **36**

Crystals of **36** were obtained by slow evaporation of a diethyl ether solution of the compound. Data were collected at 173 K on a Siemens SMART PLATFORM equipped with A CCD area detector and a graphite monochromator utilizing MoK_α radiation (λ = 0.71073 Å). Cell parameters were refined using up to 8192 reflections. A full sphere of data (1850 frames) was collected using the ω-scan method (0.3° frame width). The first 50 frames were remeasured at the end of data collection to monitor instrument and crystal stability (maximum correction on I was < 1 %). Absorption corrections by integration were applied based on measured indexed crystal faces.

The structure was solved by the Direct Methods in *SHELXTL5,* and refined using full-matrix least squares. The non-H atoms were treated anisotropically, whereas the hydrogen atoms were calculated in ideal positions and were riding on their respective carbon atoms. A total of 404 parameters were refined in the final cycle of refinement using 31376 reflections with $I > 2\sigma(I)$ to yield R_1 and wR_2 of 3.68% and 8.84%, respectively. Refinement was done using F^2.

Table 6-8. Crystal data and structure refinement for **36**.

Identification code	ei10	
Empirical formula	C35 H46 Al Mo N3 Si2	
Formula weight	687.85	
Temperature	173(2) K	
Wavelength	0.71073 Å	
Crystal system	Monoclinic	
Space group	P2(1)/n	
Unit cell dimensions	a = 14.1426(8) Å	α= 90°.
	b = 11.3076(7) Å	β= 107.361(2)°.
	c = 23.6743(16) Å	γ = 90°.
Volume	3613.5(4) $Å^3$	
Z	4	
Density (calculated)	1.264 Mg/m^3	
Absorption coefficient	0.480 mm^{-1}	
F(000)	1440	
Crystal size	0.23 x 0.15 x 0.05 mm^3	
Theta range for data collection	1.80 to 27.50°.	
Index ranges	$-18 \le h \le 18$, $-14 \le k \le 14$, $-30 \le l \le 30$	
Reflections collected	31376	
Independent reflections	8249 [R(int) = 0.0645]	
Completeness to theta = 27.50°	99.2 %	
Absorption correction	Integration	
Max. and min. transmission	0.9761 and 0.9082	
Refinement method	Full-matrix least-squares on F^2	
Data / restraints / parameters	8249 / 0 / 404	
Goodness-of-fit on F^2	1.002	
Final R indices [I>2sigma(I)]	R1 = 0.0368, wR2 = 0.0884 [5840]	
R indices (all data)	R1 = 0.0644, wR2 = 0.0988	
Largest diff. peak and hole	1.007 and -0.692 $e.Å^{-3}$	

$R1 = \Sigma(||F_o| - |F_c||) / \Sigma|F_o|$

$wR2 = [\Sigma[w(F_o^2 - F_c^2)^2] / \Sigma[w(F_o^2)^2]]^{1/2}$

$S = [\Sigma[w(F_o^2 - F_c^2)^2] / (n-p)]^{1/2}$

$w= 1/[\sigma^2(F_o^2)+(m*p)^2+n*p]$, $p = [\max(F_o^2,0)+ 2* F_c^2]/3$, m & n are constants.

X-ray Experimental for Complex **41**

Data were collected at 173 K on a Siemens SMART PLATFORM equipped with A CCD area detector and a graphite monochromator utilizing MoK_α radiation ($\lambda = 0.71073$ Å). Cell parameters were refined using up to 8192 reflections. A full sphere of data (1850 frames) was collected using the ω-scan method (0.3° frame width). The first 50 frames were remeasured at the end of data collection to monitor instrument and crystal stability (maximum correction on I was < 1 %). Absorption corrections by integration were applied based on measured indexed crystal faces.

The structure was solved by the Direct Methods in *SHELXTL5,* and refined using full-matrix least squares. The non-H atoms were treated anisotropically, whereas the hydrogen atoms were calculated in ideal positions and were riding on their respective carbon atoms. The systematic absences could not differentiate between space groups C2, Cm and C2/m. In fact the structure was solved and refined in all three and the same disorders were observed in all of them. Space group C2/m provided the best refinement and thus it was used to fully refine the structure. The asymmetric unit consists of ¼ of the dimer and ¼ of a toluene solvent molecule. Each of which is located on a 2/m symmetry site. The toluene molecule could not be modeled properly, thus program SQUEEZE, a part of the PLATON package of crystallographic software, was used to calculate the solvent disorder area and remove its contribution to the overall intensity data. The Al(Cl)(C2H5) moiety is disordered and is refined in two parts. Their site occupation factors were dependently refined to 0.29(1) for the major part, and consequently 0.21(1) for the minor part. These moieties lay on the mirror plane thus the site occupation factors site above add up to 50%. A total of 160 parameters were refined

in the final cycle of refinement using 2795 reflections with $I > 2\sigma(I)$ to yield R_1 and wR_2 of 3.05% and 7.91%, respectively. Refinement was done using F^2.

Table 6-9. Crystal data and structure refinement for **41**.

Identification code	ei07	
Empirical formula	C40 H66 Al2 Cl4 Mo2 N6 Si4	
Formula weight	1130.99	
Temperature	193(2) K	
Wavelength	0.71073 Å	
Crystal system	Monoclinic	
Space group	C2/m	
Unit cell dimensions	a = 20.6565(9) Å	α= 90°.
	b = 15.0381(7) Å	β= 107.917(2)°.
	c = 9.7848(4) Å	γ = 90°.
Volume	2892.1(2) $Å^3$	
Z	2	
Density (calculated)	1.299 Mg/m^3	
Absorption coefficient	0.763 mm^{-1}	
F(000)	1164	
Crystal size	0.13 x 0.12 x 0.04 mm^3	
Theta range for data collection	1.71 to 27.50°.	
Index ranges	$-26 \le h \le 26$, $-19 \le k \le 19$, $-12 \le l \le 12$	
Reflections collected	13047	
Independent reflections	3444 [R(int) = 0.0400]	
Completeness to theta = 27.50°	99.4 %	
Absorption correction	Integration	
Max. and min. transmission	0.9694 and 0.8663	
Refinement method	Full-matrix least-squares on F^2	
Data / restraints / parameters	3444 / 0 / 160	
Goodness-of-fit on F^2	1.013	
Final R indices [I>2sigma(I)]	R1 = 0.0305, wR2 = 0.0791 [2795]	
R indices (all data)	R1 = 0.0390, wR2 = 0.0807	
Largest diff. peak and hole	1.014 and -0.543 $e.Å^{-3}$	

$R1 = \Sigma(||F_o| - |F_c||) / \Sigma|F_o|$

$wR2 = [\Sigma[w(F_o^2 - F_c^2)^2] / \Sigma[w(F_o^2)^2]]^{1/2}$

$S = [\Sigma[w(F_o^2 - F_c^2)^2] / (n-p)]^{1/2}$

$w= 1/[\sigma^2(F_o^2)+(0.0469*p)^2]$, $p = [\max(F_o^2,0)+ 2* F_c^2]/3$

LIST OF REFERENCES

1. Crabtree RH. *The Organometallic Chemistry of the Transition Metals*; John Wiley & Sons, Inc.: New York, Toronto, 2001.

2. Frenking, G. *J. Organomet. Chem.* **2001**, *635*(1-2), 9-23.

3. Frenking, G.; Pidun, U. *J. Chem. Soc., Dalton Trans.* **1997**, (10), 1653-&.

4. Cramer C.J. *Essentials of Computational Chemistry: Theories and Models*; Wiley Interscience: New York, 2002.

5. Foresman J.; Frisch E. *Exploring Chemistry With Electronic Structure Methods*; Gaussian Inc.: Pittsburgh, PA, 1993.

6. Young D.C. *Computation Chemistry: A Practcal Guide for Applying Techniques to Real World Problems*; Wiley Interscience: New York, Toronto, 2001.

7. Webster, C. E.; Hall, M. B. *Coord. Chem. Rev.* **2003**, *238*, 315-331.

8. Dapprich, S.; Komaromi, I.; Byun, K. S.; Morokuma, K.; Frisch, M. J. *J.Mol.Struct. - Theo* **1999**, *462*, 1-21.

9. Vreven, T.; Morokuma, K. *J. Comput. Chem.* **2000**, *21*(16), 1419-1432.

10. Vreven, T.; Morokuma, K. *J. Chem. Phys.* **2000**, *113*(8), 2969-2975.

11. Karadakov, P. B.; Morokuma, K. *Chem. Phys. Lett.* **2000**, *317*(6), 589-596.

12. Vreven, T.; Morokuma, K. *J. Chem. Phys.* **1999**, *111*(19), 8799-8803.

13. Cohen R; Rybtchinski B; Gandelman M; Rozenberg H; Martin J.M.L; Milstein D *J.Am.Chem. Soc.* **2003**, *125* , 6532.

14. Rybtchinski B.; Revital C.; Yehoshoa B-D..; Martin J.M.L.; Milstein D *J.Am.Chem.Soc.* **2003**, *125*(11041).

15. Feldgus, S.; Landis, C. R. *Organometallics* **2001**, *20*(11), 2374-2386.

16. Feldgus, S.; Landis, C. R. *J. Am. Chem. Soc.* **2000**, *122*(51), 12714-12727.

17. Nugent W.A; Mayer J.M. *Metal-Ligand Multiple Bonds*; Wiley and Sons Inc.: New York, 1988.

18. Wigley D.E. *Prog.Inorg.Chem* **1994**, *42*, 239.

19. Eikey R.A.; Abu-Omar M.M. *Coord.Chem.Rev* **2003**, *243*, 83.

20. Morrison, D. L.; Wigley, D. E. *Inorg. Chem.* **1995**, *34*(10), 2610-2616.

21. Morrison, D. L.; Wigley, D. E. *J. Chem. Soc., Chem. Commun.* **1995**, (1), 79-80.

22. Smith, D. P.; Allen, K. D.; Carducci, M. D.; Wigley, D. E. *Inorg. Chem.* **1992**, *31*(8), 1319-1320.

23. Chao, Y. W.; Rodgers, P. M.; Wigley, D. E.; Alexander, S. J.; Rheingold, A. L. *J. Am. Chem. Soc.* **1991**, *113*(16), 6326-6328.

24. Chao, Y. W.; Wexler, P. A.; Wigley, D. E. *Inorg. Chem.* **1989**, *28*(20), 3860-3868.

25. Cundari, T. R. *Chemical Reviews* **2000**, *100*(2), 807-818.

26. Benson, M. T.; Bryan, J. C.; Burrell, A. K.; Cundari, T. R. *Inorg. Chem.* **1995**, *34*(9), 2348-2355.

27. Cundari, T. R. *J. Am. Chem. Soc.* **1992**, *114*(20), 7879-7888.

28. Haymore B.L.; Maata E.A.; Wentworth R.A.D. *J. Am.Chem. Soc.* **1979**, *101*, 2063.

29. Schofield M.H.; Kee T.P.; Anhaus J.T.; Schrock R.R. *Inorg.Chem* **1991**, *30*(3595).

30. Ortiz, C. G.; Abboud, K. A.; Boncella, J. M. *Organometallics* **1999**, *18*(21), 4253-4260.

31. Boncella, J. M.; Wang, S. Y. S.; Vanderlende, D. D.; Huff, R. L.; Abboud, K. A.; Vaughn, W. M. *J. Organomet. Chem.* **1997**, *530*(1-2), 59-70.

32. Wang, S. Y. S.; Abboud, K. A.; Boncella, J. M. *J. Am. Chem. Soc.* **1997**, *119*(49), 11990-11991.

33. Del Rio, D.; Galindo, A. *J. Organomet. Chem.* **2002**, *655*(1-2), 16-22.

34. Wang, S. Y. S.; Vanderlende, D. D.; Abboud, K. A.; Boncella, J. M. *Organometallics* **1998**, *17*(12), 2628-2635.

35. Hoveyda, A. H.; Schrock, R. R. *Chem.-A* **2001**, *7*(5), 945-950 .

36. Robbins, J.; Bazan, G. C.; Murdzek, J. S.; Oregan, M. B.; Schrock, R. R. *Organometallics* **1991**, *10*(8), 2902-2907.

37. Schrock, R. R.; Duval-Lungulescu, M.; Tsang, W. C. P.; Hoveyda, A. H. *J. Am. Chem. Soc.* **2004**, *126*(7), 1948-1949.

38. Schrock, R. R.; Hoveyda, A. H. *Angew. Chem., Int. Ed. Engl.* **2003**, *42*(38), 4592-4633.

39. Tsang, W. C. P.; Hultzsch, K. C.; Alexander, J. B.; Bonitatebus, P. J.; Schrock, R. R.; Hoveyda, A. H. *J. Am. Chem. Soc.* **2003**, *125*(20), 6337.

40. Teng, X.; Cefalo, D. R.; Schrock, R. R.; Hoveyda, A. H. *J. Am. Chem. Soc.* **2002**, *124*(36), 10779-10784.

41. Schrock, R. R.; Jamieson, J. Y.; Dolman, S. J.; Miller, S. A.; Bonitatebus, P. J.; Hoveyda, A. H. *Organometallics* **2002**, *21*(2), 409-417.

42. Tsang, W. C. P.; Schrock, R. R.; Hoveyda, A. H. *Organometallics* **2001**, *20*(26), 5658-5669.

43. Schrock, R. R. *Polyhedron* **1995**, *14*(22), 3177-3195.

44. Huff, R. L.; Wang, S. Y. S.; Abboud, K. A.; Boncella, J. M. *Organometallics* **1997**, *16*(8), 1779-1785.

45. Durfee, L. D.; Rothwell, I. P. *Chemical Reviews* **1988**, *88*(7), 1059-1079.

46. Cameron, T. M.; Ortiz, C. G.; Ghiviriga, I.; Abboud, K. A.; Boncella, J. M. *Organometallics* **2001**, *20*(10), 2032-2039.

47. Cameron, T. M.; Ortiz, C. G.; Abboud, K. A.; Boncella, J. M.; Baker, R. T.; Scott, B. L. *J. Chem. Soc., Chem. Commun.* **2000**, (7), 573-574.

48. Cameron, T. M.; Ghiviriga, I.; Abboud, K. A.; Boncella, J. M. *Organometallics* **2001**, *20*(21), 4378-4383.

49. Cameron, T. M.; Abboud, K. A.; Boncella, J. M. *J. Chem. Soc., Chem. Commun.* **2001**, (13), 1224-1225.

50. Copley, R. C. B.; Dyer, P. W.; Gibson, V. C.; Howard, J. A. K.; Marshall, E. L.; Wang, W. Y.; Whittle, B. *Polyhedron* **1996**, *15*(18), 3001-3008.

51. Barrie, P.; Coffey, T. A.; Forster, G. D.; Hogarth, G. *J. Chem. Soc., Dalton Trans.* **1999**, (24), 4519-4528.

52. Del Rio, D.; Montilla, F.; Pastor, A.; Galindo, A.; Monge, A.; Gutierrez-Puebla, E. *J. Chem. Soc., Dalton Trans.* **2000**, (14), 2433-2437.

53. Del Rio, D.; Montilla, F.; Pastor, A.; Galindo, A.; Monge, A.; Gutierrez-Puebla, E. *J. Chem. Soc., Dalton Trans.* **2000**, (14), 2433-2437.

54. Crane, T. W.; White, P. S.; Templeton, J. L. *Inorg. Chem.* **2000**, *39*(6), 1081-1091.

55. Crane, T. W.; White, P. S.; Templeton, J. L. *Organometallics* **1999**, *18*(10), 1897-1903.

56. Templeton, J. L. *Adv. Organomet. Chem.* **1989**, *29*, 1-100.

57. Birdwhistell, K. R.; Tonker, T. L.; Templeton, J. L. *J. Am. Chem. Soc.* **1987**, *109*(5), 1401-1407.

58. Templeton, J. L.; Herrick, R. S.; Morrow, J. R. *Organometallics* **1984**, *3* (4), 535-541.

59. Herrick, R. S.; Templeton, J. L. *Organometallics* **1982**, *1*(6), 842-851.

60. Tatsumi, K.; Hoffmann, R.; Templeton, J. L. *Inorg. Chem.* **1982**, *21*(1), 466-468 .

61. Cameron T.M. PhD Dissertation, University of Florida, 2002.

62. Galindo, A.; Ienco, A.; Mealli, C. *New J. Chem.* **2000**, *24*(2), 73-75.

63. Sandstrom J. *Dynamic NMR Spectroscopy*; Academic Press: London//New York, 1982.

64. Becke, A. D. *J. Chem. Phys.* **1993**, *98*(2), 1372-1377.

65. Lee, C. T.; Yang, W. T.; Parr, R. G. *Phys. Rev. B* **1988**, *37*(2), 785-789.

66. *Modern Theoretical Chemistry*; T. H. Dunning Jr.; P.J. Hay; Plenum: New York, 1976; Vol. 3,1.

67. Hay, P. J.; Wadt, W. R. *J. Chem. Phys.* **1985**, *82*(1), 270-283.

68. E.D. Glendening; A.E. Reed; J.E.Carpenter; F.Weinhold *NBO Version 3.1* .

69. Weinhold, F. *J. Chem. Educ.* **1999**, *76*(8), 1141-1146.

70. Reed, A. E.; Curtiss, L. A.; Weinhold, F. *Chemical Reviews* **1988**, *88*(6), 899-926.

71. *Orbital Interactions in Chemistry*; Albright T.A.; Burdett J.K.; Whangbo M; John Wiley & Sons: NY , 1985; p 383.

72. Takahashi, T.; Tsai, F. Y.; Li, Y. Z.; Wang, H.; Kondo, Y.; Yamanaka, M.; Nakajima, K.; Kotora, M. *J. Am. Chem. Soc.* **2002**, *124*(18), 5059-5067.

73. Morrison, D. L.; Wigley, D. E. *Inorg. Chem.* **1995**, *34*(10), 2610-2616.

74. Ortiz CG PhD Dissertation, University of Florida, 1999.

75. Dapprich, S.; Komaromi, I.; Byun, K. S.; Morokuma, K.; Frisch, M. J. *J.Mol.Struct. - Theo* **1999**, *462*, 1-21.

76. Nielson, A. J.; Glenny, M. W.; Rickard, C. E. F.; Waters, J. M. *J. Chem. Soc., Dalton Trans.* **2000**, (24), 4569-4578.

77. Pidun, U.; Frenking, G. *J. Organomet. Chem.* **1996**, *525*(1-2), 269-278.

78. Xi, Z. F.; Hara, R.; Takahashi, T. *J. Org. Chem.* **1995**, *60*(14), 4444-4448.

79. Barnes, C. L. *J. Appl. Crystallogr.* **1997** , *30*(1), 568.

80. Bianchini, C.; Caulton, K. G.; Chardon, C.; Eisenstein, O.; Folting, K.; Johnson, T. J.; Meli, A.; Peruzzini, M.; Rauscher, D. J.; Streib, W. E.; Vizza, F. *J. Am. Chem. Soc.* **1991**, *113*(13), 5127-5129.

81. Takahashi, T.; Kotora, M.; Hara, R.; Xi, Z. F. *Bull. Chem. Soc. Jpn.* **1999**, *72*(12), 2591-2602.

82. Takahashi, T.; Tsai, F. Y.; Li, Y. Z.; Nakajima, K.; Kotora, M. *J. Am. Chem. Soc.* **1999**, *121*(48), 11093-11100.

83. Takahashi, T.; Xi, C. J.; Xi, Z. F.; Kageyama, M.; Fischer, R.; Nakajima, K.; Negishi, E. *J. Org. Chem.* **1998**, *63*(20), 6802-6806.

84. Takahashi, T.; Xi, Z. F.; Yamazaki, A.; Liu, Y. H.; Nakajima, K.; Kotora, M. *J. Am. Chem. Soc.* **1998**, *120*(8), 1672-1680.

85. Ozerov, O. V.; Patrick, B. O.; Ladipo, F. T. *J. Am. Chem. Soc.* **2000**, *122*(27), 6423-6431.

86. Ozerov, O. V.; Ladipo, F. T.; Patrick, B. O. *J. Am. Chem. Soc.* **1999**, *121*(34), 7941-7942.

87. Holland, P. L.; Andersen, R. A.; Bergman, R. G. *J. Am. Chem. Soc.* **1996**, *118*(5), 1092-1104.

88. Takahashi, T.; Fischer, R.; Xi, Z. F.; Nakajima, K. *Chem. Lett.* **1996**, (5), 357-358.

89. Mclain, S. J.; Wood, C. D.; Schrock, R. R. *J. Am. Chem. Soc.* **1979**, *101*(16), 4558-4570.

90. Mclain, S. J.; Schrock, R. R. *J. Am. Chem. Soc.* **1978**, *100*(4), 1315-1317.

91. Grubbs, R. H.; Miyashita, A. *J. Am. Chem. Soc.* **1978**, *100*(23), 7416-7418.

92. Grubbs, R. H.; Miyashita, A. *J. Am. Chem. Soc.* **1978**, *100*(4), 1300-1302.

93. Lynch, B. J.; Truhlar, D. G. *J. Phys. Chem.* **2001**, *105*(13), 2936-2941.

94. Lynch, B. J.; Fast, P. L.; Harris, M.; Truhlar, D. G. *J. Phys. Chem.* **2000**, *104*(21), 4811-4815.

95. Laaksonen, L. *Journal of Molecular Graphics* **1992**, *10*(1), 33-&.

96. Shibata, T.; Yamashita, K.; Katayama, E.; Takagi, A. *Tetrahedron* **2002**, *58*(43), 8661-8667.

97. Martins, A. M.; Ascenso, J. R.; De Azevedo, C. G.; Dias, A. R.; Duarte, M. T.; Da Silva, J. F.; Veiros, L. F.; Rodrigues, S. S. *Organometallics* **2003**, *22*(21), 4218-4228.

98. Sanchez-Nieves, J.; Royo, P.; Pellinghelli, M. A.; Tiripicchio, A. *Organometallics* **2000**, *19*(16), 3161-3169.

99. Wu, Z. Z.; Diminnie, J. B.; Xue, Z. L. *Organometallics* **1999**, *18*(6), 1002-1010.

100. Mills, R. C.; Abboud, K. A.; Boncella, J. M. *Organometallics* **2000**, *19*(16), 2953-2955.

101. Cundari, T. R. *Chemical Reviews* **2000**, *100*(2), 807-818.

102. Li, X. Y.; Schopf, M.; Stephan, J.; Harms, M.; Sundermeyer, J. *Organometallics* **2002**, *21*(12), 2356-2358.

103. Brummond, K. M.; Kent, J. L. *Tetrahedron* **2000**, *56*(21), 3263-3283.

104. Templeton, J. L.; Ward, B. C. *J. Am. Chem. Soc.* **1980**, *102*(9), 3288-3290.

105. Moock, K. H.; Macgregor, S. A.; Heath, G. A.; Derrick, S.; Boere, R. T. *J. Chem. Soc., Dalton Trans.* **1996**, (10), 2067-2076.

106. Aghatabay, N. M.; Carlton, L.; Davidson, J. L.; Douglas, G.; Muir, K. W. *J. Chem. Soc., Dalton Trans.* **1996**, (6), 999-1011.

107. Frenking, G.; Pidun, U. *J. Chem. Soc., Dalton Trans.* **1997**, (10), 1653-&.

108. Aghatabay, N. M.; Davidson, J. L.; Muir, K. W. *J. Chem. Soc., Chem. Commun.* **1990**, (20), 1399-1401.

109. Eisch J.J. *Aluminum;* Comprehensive Organometallic Chemistry II 1; Elsevier: Oxford, UK, 1995.

110. Hagen, H.; Boersma, J.; Van Koten, G. *Chem. Soc. Rev.* **2002**, *31*(6), 357-364.

111. Hendriksen D.E USP 5,059,739, 1989.

112. Lawson G.W USP 3,813,453 , 1975.

113. Menapace H.R.; Benner G.S.; Maly N.A. USP 3,903,193.

114. Brown, M.; Menapace H.R.; Maly N. A USP 3,897,512, 1972.

115. Klooster, W. T.; Lu, R. S.; Anwander, R.; Evans, W. J.; Koetzle, T. F.; Bau, R. *Angew. Chem., Int. Ed. Engl.* **1998**, *37*(9), 1268-1270.

116. Evans, W. J.; Ansari, M. A.; Ziller, J. W.; Khan, S. I. *Inorg. Chem.* **1996**, *35*(19), 5435-5444.

117. Evans, W. J.; Anwander, R.; Ziller, J. W. *Inorg. Chem.* **1995**, *34*(23), 5927-& .

118. Klimpel, M. G.; Anwander, R.; Tafipolsky, M.; Scherer, W. *Organometallics* **2001**, *20*(19), 3983-3992.

119. Dapprich, S.; Komaromi, I.; Byun, K. S.; Morokuma, K.; Frisch, M. J. *J.Mol.Struct. -Theo* **1999**, *462*, 1-21.

120. Nielson, A. J.; Glenny, M. W.; Rickard, C. E. F.; Waters, J. M. *J. Chem. Soc., Dalton Trans.* **2000**, (24), 4569-4578.

121. Klimpel, M. G.; Sirsch, P.; Scherer, W.; Anwander, R. *Angew. Chem., Int. Ed. Engl.* **2003**, *42*(5), 574-+.

122. Aoyagi, K.; Gantzel, P. K.; Kalai, K.; Tilley, T. D. *Organometallics* **1996**, *15*(3), 923-927.

123. Van Koten G.; Vrieze K. *Adv. Organomet. Chem.* **1982**, *21*, 153.

124. **Molecular Orbital Calculations:**
All molecular orbital calculations were performed with the Gaussian 98W software package. Calculated structures generally are in agreement with the structural parameters.

125. Gibson, V. C.; Spitzmesser, S. K. *Chemical Reviews* **2003**, *103*(1), 283-315.

126. Daniele, S.; Hitchcock, P. B.; Lappert, M. F.; Merle, P. G. *J. Chem. Soc., Dalton Trans.* **2001**, (1), 13-19.

127. Britovsek, G. J. P.; Gibson, V. C.; Wass, D. F. *Angew. Chem., Int. Ed. Engl.* **1999**, *38*(4), 428-447.

128. Cossee, P. *J. Catal.* **1964**, *3*(1), 80-88.

129. Strazisar, S. A.; Wolczanski, P. T. *J. Am. Chem. Soc.* **2001**, *123*(20), 4728-4740.

130. Montilla, F.; Pastor, A.; Galindo, A. *J. Organomet. Chem.* **1999**, *590*(2), 202-207 .

131. Bergman, D. L.; Laaksonen, L.; Laaksonen, A. *J. Mol. Graph. & Mod.* **1997**, *15*(5), 301-+.

132. Dias, E. L.; Brookhart, M.; White, P. S. *Organometallics* **2000**, *19*(24), 4995-5004.

133. Del Rio, D.; Galindo, A. *J. Organomet. Chem.* **2002**, *655*(1-2), 16-22.

134. Ison E.A.; Abboud K.A.; Ghiviriga I.; Boncella J.M. *Organometallics* **2004**, *23*(5), 929-931.

135. Boncella, J. M.; Andersen, R. A. *Organometallics* **1985**, *4*(1), 205-206.

136. Anillo, A.; Diaz, M. R.; Garcia-Granda, S.; Obeso-Rosete, R.; Galindo, A.; Ienco, A.; Mealli, C. *Organometallics* **2004**, *23*(3), 471-481.

137. Ward, M. D.; Mccleverty, J. A. *J. Chem. Soc., Dalton Trans.* **2002**, (3), 275-288.

138. Herebian, D.; Bothe, E.; Neese, F.; Weyhermuller, T.; Wieghardt, K. *J. Am. Chem. Soc.* **2003**, *125*(30), 9116-9128.

139. Justel, T.; Bendix, J.; Metzler-Nolte, N.; Weyhermuller, T.; Nuber, B.; Wieghardt, K. *Inorg. Chem.* **1998**, *37*(1), 35-43.

140. Anillo, A.; Garcia-Granda, S.; Obeso-Rosete, R.; Galindo, A.; Ienco, A.; Mealli, C. *Inorg. Chim. Acta* **2003**, *350*, 557-567.

141. Galindo, A.; Gomez, M.; Del Rio, D.; Sanchez, F. *Eur.J.Inorg.Chem* **2002**, (6), 1326-1335.

142. Mills R. C. PhD Dissertation, University of Florida, 2001.

143. M. J. Frisch; G. W. Trucks; H. B. Schlegel; G. E. Scuseria; M. A. Robb; J. R. Cheeseman; V. G. Zakrzewski; J. A. Montgomery, Jr.; R. E. Stratmann; J. C. Burant; S. Dapprich; J. M. Millam; A. D. Daniels; K. N. Kudin; M. C. Strain; O. Farkas; J. Tomasi; V. Barone; M. Cossi; R. Cammi; B. Mennucci; C. Pomelli; C. Adamo; S. Clifford; J. Ochterski; G. A. Petersson; P. Y. Ayala; Q. Cui; K. Morokuma; N. Rega; P. Salvador; J. J. Dannenberg; D. K. Malick; A. D. Rabuck; K. Raghavachari; J. B. Foresman; J. Cioslowski; J. V. Ortiz; A. G. Baboul; B. B. Stefanov; G. Liu; A. Liashenko; P. Piskorz; I. Komaromi; R. Gomperts; R. L. Martin; D. J. Fox; T. Keith; M. A. Al-Laham; C. Y. Peng; A. Nanayakkara; M. Challacombe; P. M. W. Gill; B. Johnson; W. Chen; M. W. Wong; J. L. Andres; C. Gonzalez; M. Head-Gordon; E. S. Replogle; and J. A. Pople *Gaussian 98W* Gaussian, Inc.: Pittsburgh PA, 2001.

144. Hehre W.J.; Stewart R.F.; Pople J.A. *J. Chem. Phys.* **1969**, *51*, 2657.

145. Collins J.B.; Schler P.V.R.; Binkley J.S.; Pople J.A. *J. Chem. Phys.* **1976**, *64*, 5142.

146. Lynch, B. J.; Fast, P. L.; Harris, M.; Truhlar, D. G. *Journal of Physical Chemistry a* **2000**, *104*(21), 4811-4815.

147. Kendall R.A.; Dunning T.H. Jr.; Harrison R.J. *J. Chem. Phys.* **1992**, *96*, 6796.

148. Dunning T.H. Jr. *J. Chem. Phys.* **1989**, *90*, 1007.

149. Sheldrick G.M. *SHELLXT* Madison, WI: 1986.

BIOGRAPHICAL SKETCH

Elon Ison was born on February 2nd ,1974, in San Fernando, Trinidad and Tobago. The first of two children of Walter and Patricia Ison, he spent his first 19 years in his native country. In 1995 he came to the United States to pursue a degree in chemistry at Kean University in New Jersey. His hard work and determination paid off when he received his baccalaureate degree with honors in 1999. The following summer he married Ana Bitanga and together they enrolled into the graduate school at the University of Florida. In December of the same year his daughter Mya was born. Elon joined the group of Dr. James Boncella in 2000 and pursued research in organometallic chemistry. This dissertation summarizes his five years of research in the Boncella labs. Elon graduated with a Ph.D. in the summer of 2004. He looks forward to a long and challenging career in scientific research.